SEQUENCE STRATIGRAPHY, DIAGENESIS, AND DEPOSITIONAL FACIES OF AN EXPOSED MEGAFLAP: PENNSYLVANIAN HERMOSA GROUP, GYPSUM VALLEY SALT WALL, PARADOX BASIN, COLORADO

KYLE THOMAS DEATRICK

Master's Program in Geological Sciences

APPROVED:

Katherine A. Giles, Ph.D., Chair

Richard P. Langford, Ph.D.

Gary L. Gianniny, Ph.D.

Stephen Crites, Ph. D.
Dean of the Graduate School

Dedication

I wish to dedicate this work to my family and friends, especially my parents Julie and Dennis Deatrick for their unwavering support and encouragement.

SEQUENCE STRATIGRAPHY, DIAGENESIS, AND DEPOSITIONAL FACIES OF AN EXPOSED MEGAFLAP: PENNSYLVANIAN HERMOSA GROUP, GYPSUM VALLEY SALT WALL, PARADOX BASIN, COLORADO

by

KYLE THOMAS DEATRICK, B.S. Geology

THESIS

Presented to the Faculty of the Graduate School of

The University of Texas at El Paso

in Partial Fulfillment

of the Requirements

for the Degree of

MASTER OF SCIENCE

Department of Geological Sciences

THE UNIVERSITY OF TEXAS AT EL PASO

December 2019

Acknowledgements

I wish to thank my committee members whose time and support provided tremendous input into my research. I would like to especially thank Dr. Katherine Giles, my thesis advisor, who provided guidance and endless support and encouragement throughout my research when I needed it the most. I would also like to thank the industry professionals who took the time to enthusiastically hike through the megaflap to discuss my research in the field.

I would like to thank the sponsors of the Institute of Tectonic Studies and the Salt-Sediment Interaction Research Consortium at the University of Texas at El Paso who have provided funding and critical guidance on many of the research objectives.

I would also like to acknowledge and thank the Geological Society of America-ExxonMobil research grant program for funding much of the research. I am also grateful for tuition scholarships from Marathon Oil and ConocoPhillips, as well as the E. Russell Lloyd scholarship from the West Texas Geological Foundation and the Vernon G. & Joy Hunt Award from UTEP; with each being critical in supporting my research.

Abstract

Outcrop exposures mostly of the Pennsylvanian Honaker Trail Formation provide a 2 km strike-oriented view of a megaflap on the southwestern flank of the Gypsum Valley salt wall, Paradox Basin, Colorado that serves as an outcrop analog for megaflaps recently drilled unexpectedly in the Gulf of Mexico and other salt basins worldwide. The near vertical (80-90°) stratal panel comprises a 60 m thick succession of non-evaporite facies of the Pennsylvanian upper Paradox Formation, overlain by a 117 m section of cyclic shallow marine carbonates and siliciclastics of the Honaker Trail Formation. Near vertical upper Paradox and Honaker Trail strata are onlapped by steeply dipping (70°) Permian lower Cutler Formation siliciclastics. Only 156 m of Cutler strata are exposed in an erosional window beneath a second angular unconformity. Above this unconformity, the Cutler and Honaker Trail Formations are onlapped by the Jurassic Entrada Formation to form a large-scale halokinetic growth package referred to here as the "onlap wedge." The megaflap and onlap wedge were subsequently beveled at a third angular unconformity beneath the overlying Upper Jurassic Summerville and Morrison formations, which form the "overlap wedge." Laterally, the Honaker trail strata in the megaflap gradually shallow to 50-60° on the southern flank where it is abruptly terminated at radial faults that bound a large graben. Jurassic Summerville and Morrison Formation strata overlap and cover the megaflap on its northern end. The shallow marine facies architecture and diagenesis of the Pennsylvanian carbonates and siliciclastics as well as the laterally concordant behavior of the stratal architecture are interpreted to represent a pre-kinematic roof over an incipient passive diapir. Jurassic aged marine diagenesis overprints Pennsylvanian carbonates during incipient marine transgression of the Summerville Formation.

Table of Contents

List of Tables

List of Figures

Chapter 1: Introduction

Megaflaps are geometrically defined as steep to overturned, relatively conformable deep minibasin strata that extend long distances (several kilometers) up the margins of salt diapirs or their equivalent welds (Figure 1.1)(Giles and Rowan, 2012; Rowan et al., 2016). Megaflap strata typically either thin towards the diapir or retain a constant thickness and are unconformably onlapped by growth stratal wedges of younger minibasin fill (Giles and Rowan, 2012; Rowan et al., 2016). These structures, first documented on seismic and well log data sets in the Gulf of Mexico, are thought to form by one or a combination of two end-member processes: (1) shortening, in which strata of one minibasin are thrust over the other as the diapir narrows or welds out or (2) drape folding by gravitational downbuilding, whereby the megaflap represents the initial conformable overburden of a laterally extensive salt body with a subhorizontal top that steepens as the salt body transitions from an initial pillow geometry to near vertical passive rise (Giles and Rowan, 2012; Rowan et al., 2016).

Megaflaps have been inadvertently penetrated during drilling in petroleum-bearing salt basins such as the Gulf of Mexico and South Atlantic conjugate margins, due to the misinterpretation of seismic data sets along the poorly imaged, steeply dipping salt-sediment interface. Pre-drill identification of megaflaps reduces the drilling hazards associated with encountering older, steeply dipping strata and impacts risk assessment of trap, reservoir, and seal. This outcrop analog study in the Paradox Basin provides high-resolution documentation of the depositional facies, stratal geometries, sequence stratigraphic framework, diagenesis, and structural deformation within a megaflap panel, providing additional data critical for successful pre-drill prediction and characterization of analogous salt-flank traps.

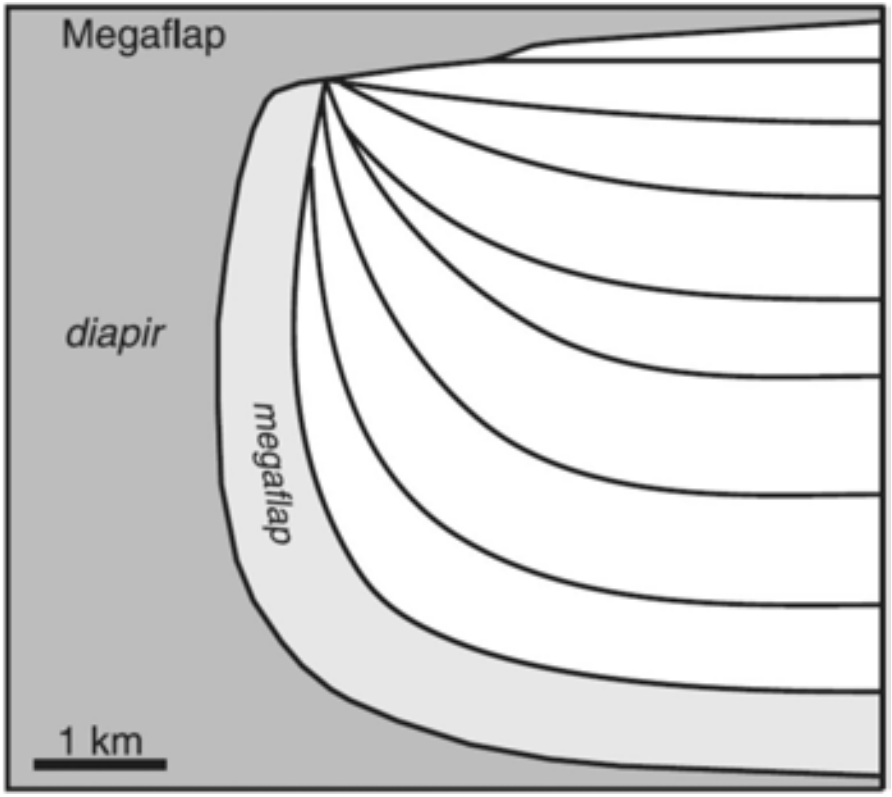

Figure 1.1- Schematic diagram showing a megaflap flanking a salt diapir. The image shows a vertical salt diapir and allochthonous canopy. The megaflap extends over several kilometers up the margins of the diapir to a vertical to overturned position. The megaflap is subsequently onlapped by minibasin strata forming growth stratal wedges that progressively onlap, erode, and overlap the vertical stratal panel of the megaflap (Rowan et al, 2016).

Outcrop scale salt-sediment interaction studies offer comparative analogues to seismically resolvable structures in the petroleum bearing salt-basins of the Gulf of Mexico, the North Sea, and South Atlantic margins of offshore Brazil and West Africa (Giles and Lawton, 1999; F. Lawton et al., 2001; Rowan et al., 2003, 2012; Aschoff and Giles, 2005; Lawton and Buck, 2006; Andrie et al., 2012; Giles and Rowan, 2012; Gannaway, 2014; Poprawski et al., 2014; Hearon et al., 2015; Ribes et al., 2015). At the Gypsum Valley salt wall in the southeastern Paradox Basin the Upper Pennsylvanian to lower most Permian strata form a partially exposed megaflap. The preserved transverse cross section provides an excellent opportunity to examine the internal

depositional facies and stratal architecture as well as the structural deformation within and at the margins of a megaflap. Understanding the internal stratal architecture of the megaflap panel will address questions relating to timing and origin of the megaflap, as well as offer key insights into the early formation of the Gypsum Valley salt wall and fluid flow associated with diapir flanking, steeply dipping stratigraphy. Utilizing standard field techniques (Brunton, Jacob's Staff, and measuring tape) combined with recent advances in digital field mapping technology, the interplay of depositional systems, salt tectonics and diagenesis associated with the megaflap was assessed in this study. Using these sedimentological tools to advance the previous work established by geophysicists and structural geologists, this study enhances our understanding of the formational history of steeply dipping diapir-flanking strata in the Paradox Basin.

1.2 Objectives

This study aims to further our understanding of the Paradox Basin salt tectonism through undertaking a sedimentological and stratigraphic analyses of exposed Pennsylvanian and Permian strata that form the megaflap panel along the southeastern flank of the Gypsum Valley salt wall. Geological investigations of Gypsum Valley began in the mid-1940s defining the broad structural relationships of the conspicuous salt structure for the purpose of locating local uranium enrichment and economically viable mineral deposits (Stokes and Phoenix, 1948). Significant research of the valley peaked in the early-60's to 70's through investigations of the diapir proximal structures and potential economically significant ore deposits in the Pennsylvanian strata (Stokes and Phoenix, 1948; Shoemaker et al., 1958; Vogel, 1960; Elston et al., 1962). Since this preliminary research the geologic community has seen a considerable evolution in the understanding of salt tectonics in light of the extensive exploration and production efforts in the deep water Gulf of Mexico, North Sea, and the conjugate margins of South America and Africa.

The primary objectives of this research are to assess the Pennsylvanian and Permian stratigraphy of the megaflap through common tools associated with basin analysis including: (1) Lithofacies and petrographic analysis, (2) Determination of the depositional environments through process interpretation, (3) Sequence stratigraphic analysis, and (4) Assessment of diagenesis. In order to meet these broad goals the field area was: (1) analyzed for sedimentary characteristics including texture, lithology, bedding style, and stratal relationships through measuring of stratigraphic sections, (2) partitioned measured sections into facies based on modern and ancient depositional environments described in literature and finally (3) integrated data to gain further insight into the depositional, diagenetic and structural characteristics of the megaflap.

Chapter 2: Geologic Setting of Study Area

2.1 The Paradox Basin

The late Paleozoic age Paradox Basin is the largest and one of twenty North American intracratonic basins that developed adjacent to basement-cored uplifts during the Ancestral Rocky Mountains (ARM) orogeny (Kluth, 1986; DeCelles and Giles, 1996; Barbeau, 2003; Dickinson and Lawton, 2003) (Figure 2.1). The Paradox Basin is 190km across and 265km long and bounded by the Uncompahgre uplift to the northeast and San Luis Uplift to the east (Figure 2.2). The Uncompahgre Uplift is a structural high of thrusted Precambrian crystalline basement, 50km wide and trending NW-SE for 150 km across southwestern Colorado and part of eastern Utah (Shoemaker et al., 1958; Elston et al., 1962; Baars and Stevenson, 1981; Nuccio and Condon, 1996; Barbeau, 2003). The uplift is bounded on the southwest and northeast by 200-300km long steeply dipping fault zones, developing structural relief of the uplift in excess of 5km (Shoemaker et al., 1958; Elston et al., 1962; Baars and Stevenson, 1981; Barbeau, 2003). The Paradox Basin has been interpreted as forming as a foreland basin, with flexural subsidence of the footwall derived from progressive thrust sheet loading along the western margin of the Uncompahgre Uplift (Barbeau, 2003). In cross-section the Paradox Basin exemplifies typical foreland basin structural characteristics derived from contractional orogenic events; with distinct foredeep and forebulge geometry (Giles and Dickinson, 1995; DeCelles and Giles, 1996; Barbeau, 2003) (Figure 2.3). The development of the foredeep, an asymmetric trough adjacent to the uplift, accommodated a thick, (5km) cyclic succession of Pennsylvanian - Permian strata (Cater and Craig, 1970; Nuccio and Condon, 1996; Barbeau, 2003). These facies laterally transition and thin to the southwest into prolific petroleum bearing shelf carbonates containing phylloid algal mounds along the basin forebulge at Aneth, Utah (Hite and Buckner, 1981). The geographic limit of the Paradox Basin is

defined by the map-view extent of the evaporite cycles within the Paradox Formation (Condon, 1997).

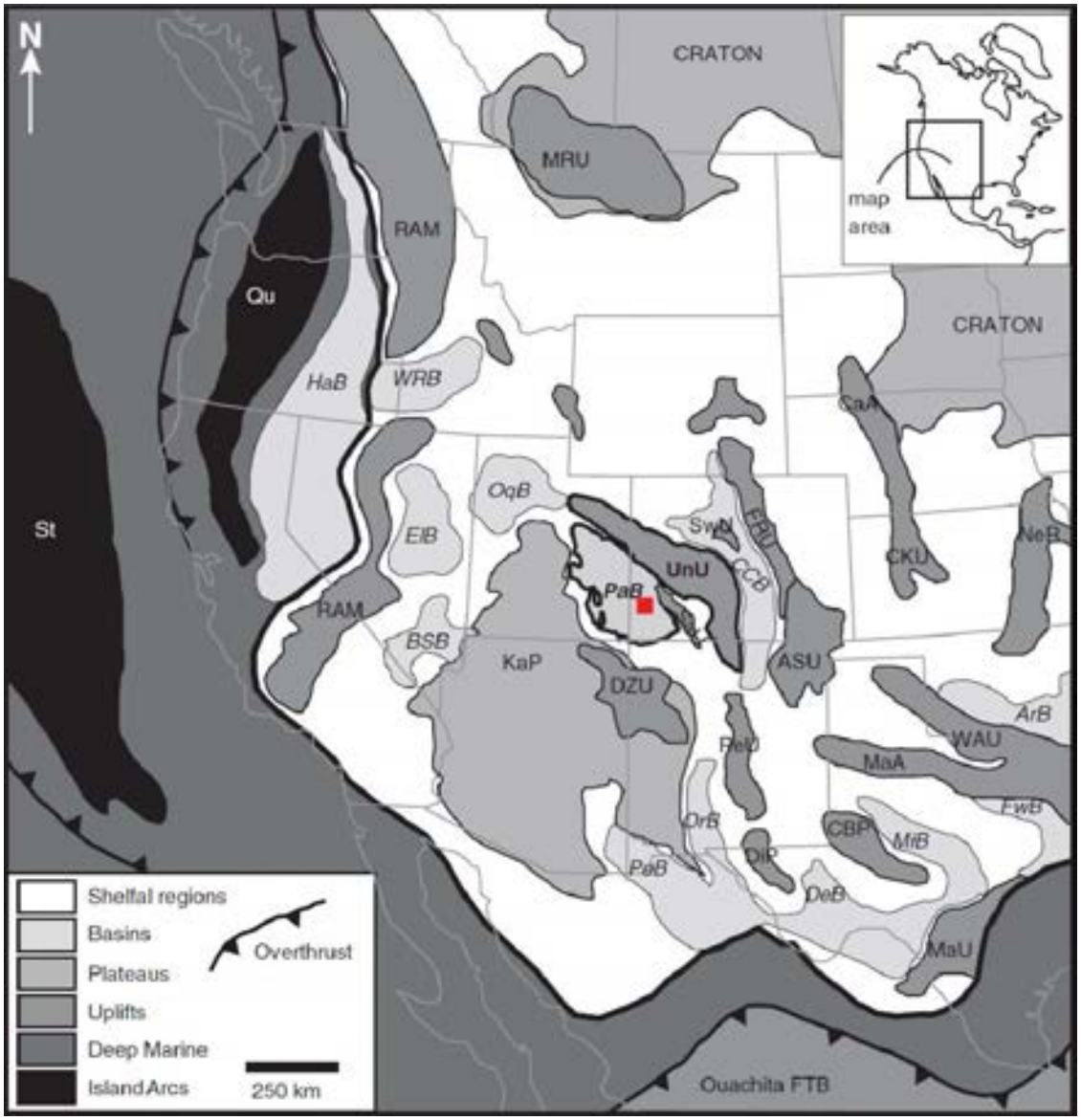

Figure 2.1- Tectonic setting and paleogeographic interpretation of the western North American craton (middle Pennsylvanian, 310 Ma). The tectonic system shows a tripartite boundary with the North American craton with subduction and collision along the western edge and progressive development of the Ouachita Fold Thrust Belt to the south. Intercontinental compression derived from the tectonic boundaries produced uplift of the Ancestral Rocky Mountains and flanking foreland basins. The Uncompahgre (initialed UnU) and Paradox Basin (initial PaB) are shown outlined above. The red box denotes the position of the study area. (Trudgill, 2011).

The Paradox Basin fore-deep is characterized by widespread salt diapirism in the form of NW-SE trending elongate salt-walls roughly parallel to the long axis of the Uncompahgre Uplift, which are fed by the Paradox Formation layered evaporites. This region has been variably referred to as the "Paradox Fold and Fault Belt" (Doelling, 1988); "Deep Fold and Fault Belt" (DFFB) (Rasmussen and Rasmussen, 2009), or the "Northern Paradox Basin" (NPB) (Trudgill, 2011). This study refers to this region as the Paradox Basin foredeep, tying the region to a specific tectonic process of basin development and utilizing established nomenclature of foreland basin characteristics (Giles and Dickinson, 1995; DeCelles and Giles, 1996). During Pennsylvanian ARM shortening, contemporaneous basement uplifts formed along linear fault trends in the Paradox Basin foredeep, parallel to the Uncompahgre Uplift (Baars, 1966; Cater and Craig, 1970; Baars and Stevenson, 1981; Kluth, 1986; Barbeau, 2003; Trudgill, 2011). The basement faults formed the buttresses deflecting mobilized salt into salt swells and eventually salt-cored anticlines and diapiric salt walls (Barbeau, 2003; Rasmussen and Rasmussen, 2009; Trudgill, 2011). Seismic imaging and borehole analysis reveals that most of the basement fault trends are southwest and northeast dipping *en echelon* reverse faults parallel to the thrust bounded Uncompahgre front (Barbeau, 2003; Trudgill, 2011; Rasmussen, 2014). It is widely accepted that salt walls in the Paradox Basin form over these pre-existing basement structures (Baars, 1966; Baars and Stevenson, 1981; Ge et al., 1997; Ge and Jackson, 1998; Trudgill, 2011). The geometry of linear basement fault trends in the Paradox Basin foredeep forms a polygonal framework of dominantly northwest-southeast fault trends that are dipping northeast and parallel to the Uncompahgre Uplift (likely forming as a result of crustal flexure of the forebulge and foredeep as the basin subsided) as well as a subordinate northeast-southwest fault trend (Trudgill, 2011). Prominent structural relief is evident over small lateral distances across numerous basement fault trends in the Paradox

Basin foredeep (Baars, 1966; Warner, 1978). The Paradox Formation inherited this basement paleotopographic relief, which controlled the lateral and vertical facies architecture and thickness trends of the formation. Faults forming localized depocenters ultimately controlled lateral changes in the formation thus controlling the three-dimensional architecture of the salt-budget (Trudgill, 2011). Resultant unroofing of the Uncompahgre Uplift is thought to have initiated diapirism through differential loading caused by prograding asymmetrical wedges of Cutler Group alluvial megafans and fluvial systems flanking the Uncompahgre (Ge et al., 1997; Ge and Jackson, 1998; Hudec et al., 2009; Trudgill, 2011).

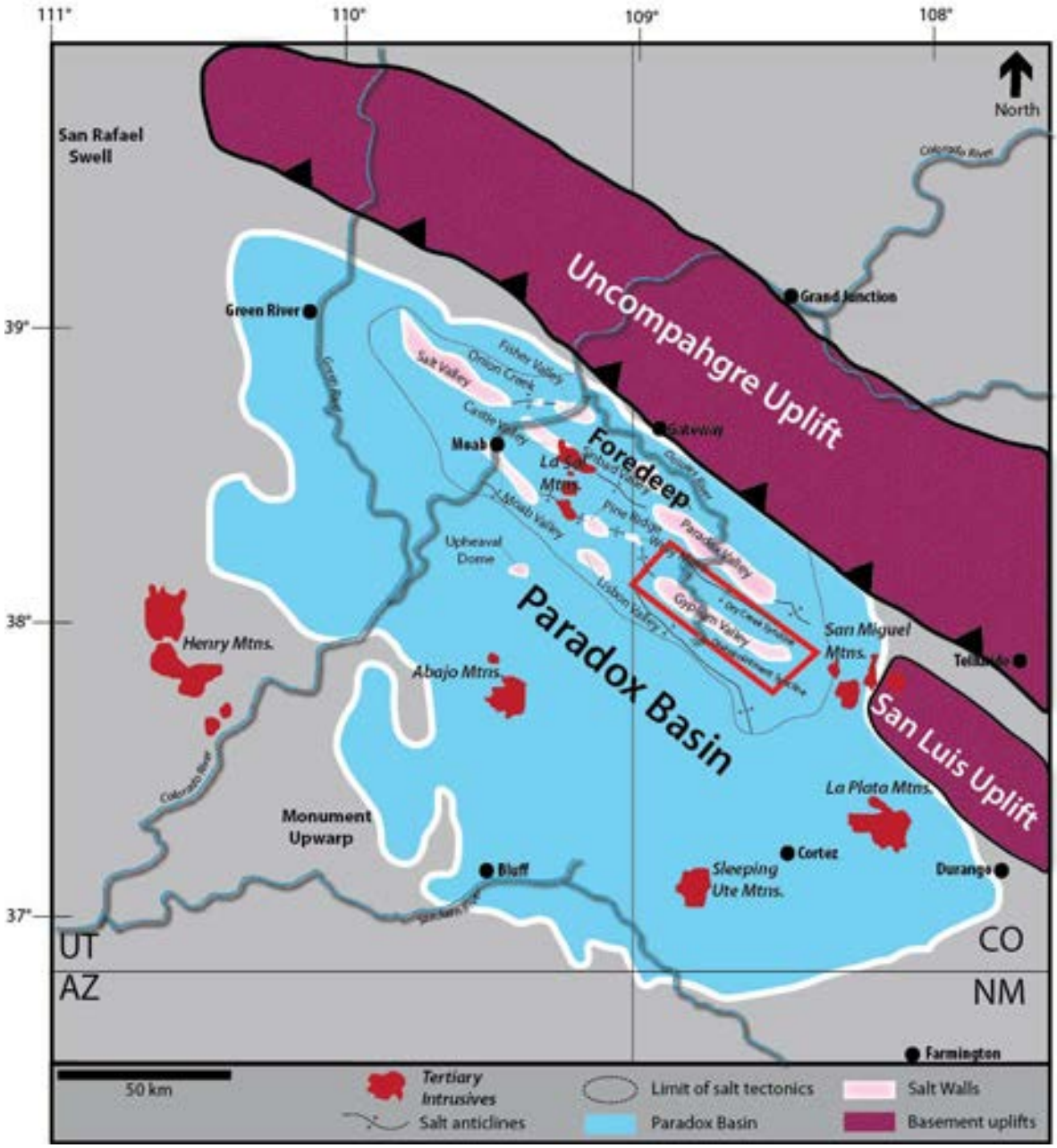

Figure 2.2 - Map view of the Paradox Basin and flanking Uncompahgre and San Luis Uplifts (purple) within the four-corners region of Colorado, New Mexico, Arizona, and Utah. The map details locations of salt wall structures (drawn in pink) and map view extent salt tectonic features within the foredeep of the basin (dotted line). The map view boundary of the basin in blue is drawn as the depositional extent of the evaporite facies of the Paradox Formation (white line). Notable Tertiary volcanic intrusives are drawn in red. The red box outlines the Gypsum Valley salt wall, the principle salt tectonic feature of the study area. (Figure modified after Trudgill, 2011).

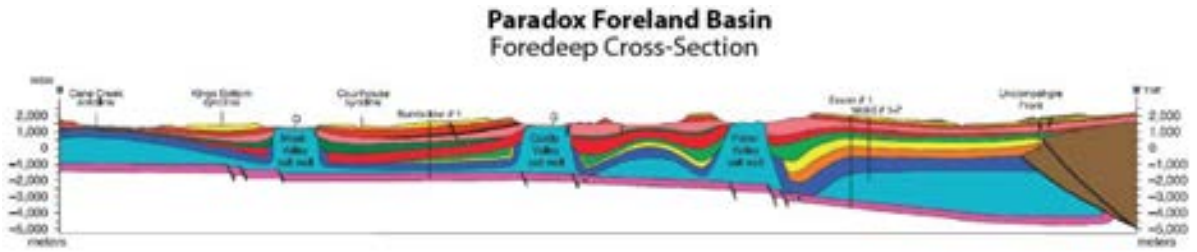

Figure 2.3 - Cross-section showing propagating thrust sheets of the Uncompaghre Uplift (Brown) to the right, and characteristic geometry typical of foreland basins, showing distinct foredeep and forebulge. The salt walls drawn in blue are flanked by mini-basin strata forming an asymmetric depositional framework, and lateral thickness variations. The oldest salt walls develop proximal to the Uncompaghre, and decrease in age and height away from the uplift (Trudgill, 2010).

2.2 Stratigraphy of the Paradox Basin

The Paradox Basin fill contains thick sequences of Pennsylvanian through Permian aged strata subdivided into three regional stratigraphic units: the Pennsylvanian Paradox and Honaker Trail formations of the Hermosa Group, and the Permian Cutler Group (Figure 2.4) (Wengerd and Strickland, 1954; Wengerd and Matheny, 1958; Pray and Wray, 1963; Baars et al., 1967; Weber et al., 1995; Condon, 1997). The Hermosa Group comprises strata of the Molas, Pinkerton Trail, Paradox and time correlative Lower Hermosa formations (i.e., subdivisions of the Paradox Formation from the western shelf in ascending order: Alkali Gulch, Barker Creek, Akah, Desert Creek, and the Ismay zones), and the Honaker Trail Formation. The Permian Cutler Group contains all correlative strata previously incorporated into the type Cutler, lower Cutler, as well as the Halgaito, Cedar Mesa Sandstone, Organ Rock Formation, and the White Rim Sandstone. The significant aspects of the Hermosa Group and Cutler Group are the bounding angular unconformities defined by the top regional Leonardian angular unconformity at the top of the Organ Rock or White Rim formations and the basal regional Pennsylvanian Morrowan angular

unconformity capping Mississippian rocks (Wengerd and Matheny, 1958; Baars et al., 1967; Weber et al., 1995; Condon, 1997; Rasmussen and Rasmussen, 2009). Thus, the defining characteristics of the Hermosa Group and Cutler Group are the bounding angular unconformities and the incorporated glacioeustatic cycles of carbonates, evaporites, siliciclastics, and orogenic conglomerates (Baars et al., 1967; Hite and Buckner, 1981; Weber et al., 1995; Rasmussen and Rasmussen, 2009). The basal unit discussed here initially is the Atokan-Desmoinesian (313-306 Ma) Hermosa Group, Paradox Formation, which is up to 2500m thick in the fore-deep and characterized by 29 high-frequency glacio-eustatic sea-level cycles (Peterson and Hite, 1969; Hite and Buckner, 1981). The cycles average 45-60m thick and contain heterogeneous strata of nodular to laminated anhydrite, silty dolomite, black calcareous shale, biohermal carbonates, and capping halite grading into potash salts (Peterson and Hite, 1969; Hite and Buckner, 1981). The Paradox Formation cyclothems thin and pinch out towards correlative petroleum-bearing, biohermal shelf carbonates along the southwest margin of the basin (Figure 2.5) (Peterson and Hite, 1969; Hite and Buckner, 1981).

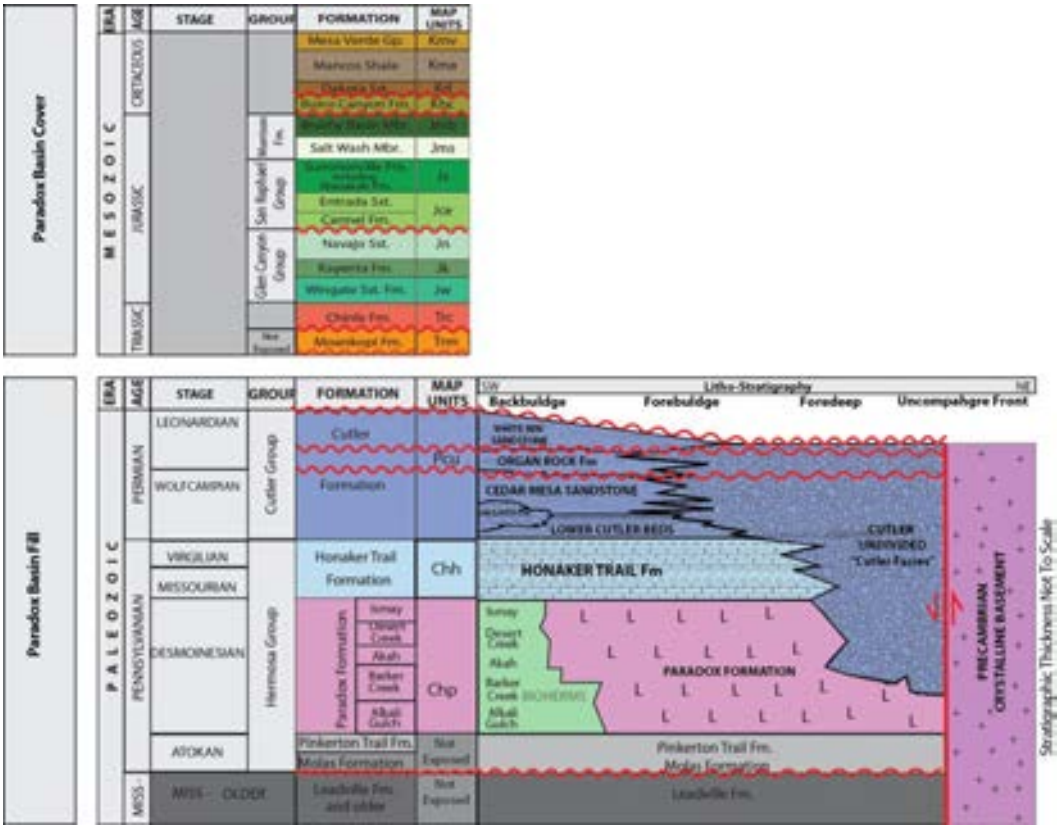

Figure 2.4 - Composite Stratigraphic column and schematic lithostratigraphic variations across the Paradox Basin. Stratigraphy is partitioned into primary Paradox Basin fill defined by Pennsylvanian and Permian strata, and Regional cover defined by Mesozoic sediments. Modified after Stokes and Phoenix (1948); Werngerd, (1954); and Trudgill (2011).

2.2.1 Pennsylvanian Hermosa Group

Paradox Formation

The Paradox Formation is a layered evaporite sequence, composed primarily of halite, that extends over 11,000 square miles in southeastern Utah and southwest Colorado, with the greatest accumulation occurring in the fore-deep or Uncompahgre Trough directly adjacent to the Uncompahgre Uplift (Peterson and Hite, 1969; Hite and Buckner, 1981). The original salt-budget for the region is difficult to estimate due to wide spread post-depositional mobilization of salt and

formation of diapiric salt walls. However, in areas of less deformation the original evaporite sequence is estimated at 1500m to 2500m thick (Peterson and Hite, 1969; Hite and Buckner, 1981). The evaporite cyclothems form the middle unit of the Hermosa Group called the Paradox Formation. Where the evaporite cycles are present the Hermosa Group can be subdivided into the Honaker Trail Formation above the evaporites and the Pinkerton Trail Formation below the evaporite sequence (Wengerd and Strickland, 1954; Hite and Buckner, 1981). The Paradox Formation demonstrates remarkable cyclic depositional sequences derived from glacio-eustatic sea-level fluctuations during the Pennsylvanian. Each of the 29 cycles can be correlated to an equivalent cycle of the biohermal carbonates of the southwestern shelf (Peterson and Hite, 1969; Hite and Buckner, 1981). Due to the existence of petroleum reservoirs in these shelf carbonates, exploration and development of the Aneth Petroleum Field, Utah, has spurred the partitioning of the Paradox Formation (Figre 2.4) into the Ismay, Desert Creek, Akah, Barker Creek, and Alkali Gulch zones (in descending order) based on petroleum occurrence alone, as many of these zones span several depositional cycles (Peterson and Hite, 1969; Hite and Buckner, 1981; Matheny and Longman, 1996) (Figures 2.5, 2.6).

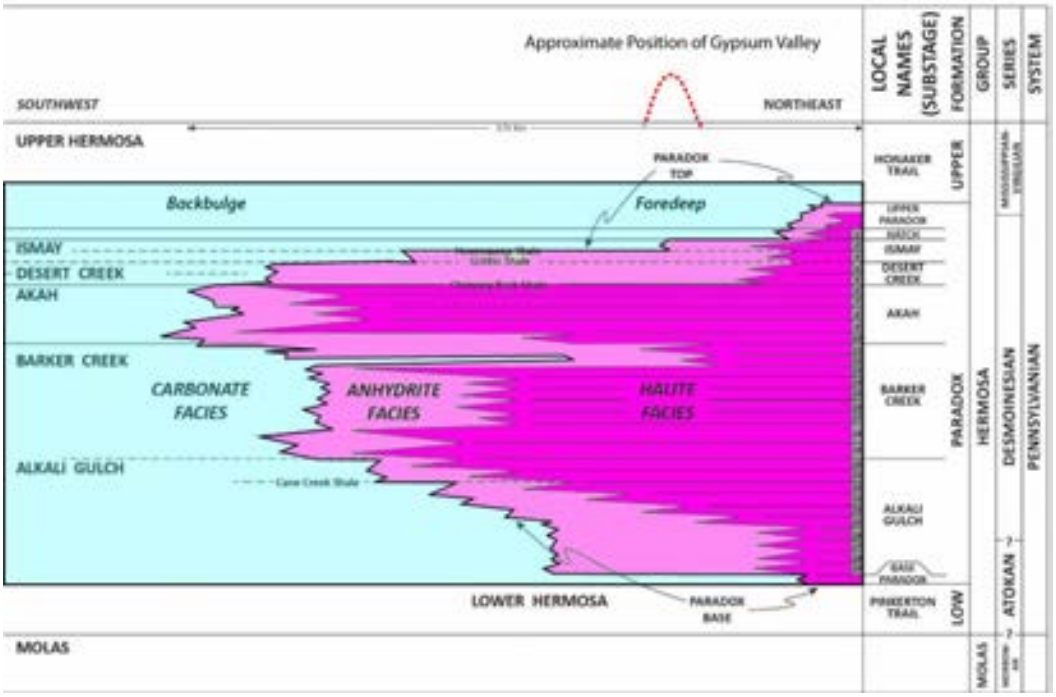

Figure 2.5 - Schematic diagram showing a NE-SW cross section through Paradox Basin showing the lateral distribution of lithofacies and stratigraphic nomenclature of the Paradox Formation. Numbered units correspond to the 29 evaporitic cycles described by Hite (1972). Red dashed line represents approximate location of Gypsum Valley (Modified after Matheny et al., 2009).

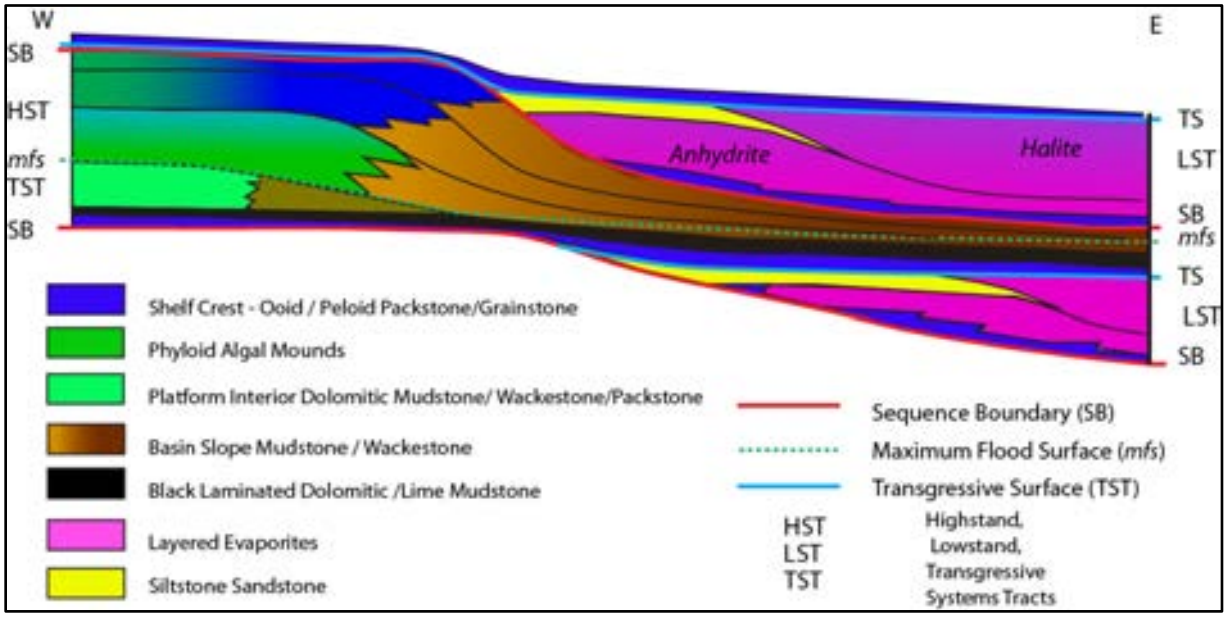

Figure 2.6 - Schematic diagram showing the sequence stratigraphic framework of shallow marine shelf carbonates (left) and the evaporitic basin evaporites (right) of the Paradox Formation cycles (modified after Weber et al., 1995).

Honaker Trail Formation

The Missourian-Virgilian (307-298 Ma) Honaker Trail Formation, named by Wengerd and Matheny 1958, overlies the Paradox Formation and comprises mixed lithology cycles of peritidal carbonates interbedded with silty maroon/gray/green shale, red siltstone, and coarse-grained arkosic and micaceous fluvial siliciclastics. The formation ranges from 200-1500m trending northeast from the western shelf to the Paradox Basin foredeep (Wengerd and Strickland, 1954; Baars et al., 1967; Trudgill, 2011). The top Honaker Trail Formation is placed at the base of a transitional sequence (grading from dominantly carbonates to sandstones and siltstones with subordinate carbonates) that is formally referred to locally as the Rico Formation (Wengerd and Strickland, 1954; Baars et al., 1967). Because the "Rico" terminology was abandoned by Baars (1962), the Honaker Trail Formation was redefined to include the Rico strata with formation top defined as the highest or last limestone (termed the "Rico" bed) in the Honaker Trail type section at Honaker Trail, San Juan County, Utah (Baars et al., 1967). Thus, the redefined Honaker Trail Formation contains all lithologies between the top Paradox Formation evaporites and the Pennsylvanian-Permian disconformity (Baars et al., 1967). Transgressive and regressive migration of the shoreline driven by glacio-eustatic sea-level fluctuations produced rapid vertical facies changes in this shallow marine system (Wengerd and Strickland, 1954; Baars et al., 1967; Condon, 1997; Trudgill, 2011). Unlike the open marine, low gradient carbonate-dominated shelf of the southwest basin margin, the northern margin, which is adjacent to the Uncompahgre Uplift and now exhumed salt walls, shows highly variable regional lateral thickness and facies changes within the Honaker Trail Fm. (Gianniny and Miskell-Gerhardt, 2009; Trudgill, 2011). Characteristic thicknesses and facies of the Honaker Trail Formation deviate from the regional trend at the northern margin as a result of the proximity to the prograding siliciclastic alluvial fan and fluvial systems sourced from the Uncompahgre Uplift. The transgressive shallow marine carbonates

subsequently onlapped the irregular paleotopography created by the prograding coarse-grained siliciclastics resulting in complex stratal relationships generated by repetitive sea-level fluctuations (Condon, 1997). Although rapid thickness and lateral facies changes can be accounted for through proximity to the Uncompahgre alluvial fan system, incipient diapirism or salt swells from onset mobilization of the Paradox Formation evaporites may have also influenced the local depositional architecture.

2.2.2 Cutler Group

Cutler Formation

The Virgilian-Wolfcampian (298-280 Ma), type Cutler Formation at Cutler Creek in Ouray County, Colorado, was first described by Cross et al. (1905), as a non-fossiliferous Pennsylvanian red bed overlying the Rico Formation. However, upon re-examination Cross (1907) redefined the Cutler as probable Permian-aged strata based solely on the absence of fossils (Cross and Howe, 1905; Cross, 1907). Since this definition was proposed, later researchers have unfortunately used the name Cutler for all the red coarse-grained strata present between the overlying Triassic Moenkopi and Chinle formations and the first underlying Pennsylvanian limestone beds (Wengerd and Strickland, 1954; Wengerd and Matheny, 1958). The first marine limestone beds encountered at the base of the Cutler Type section in Ouray, Colorado, via an oil and gas test well, contain fossils of Late Desmoinesian age, placing the limestone close to the Ismay-Desert Creek interval of the Paradox Formation (Rasmussen, 2014). This date suggests that the Cutler undifferentiated strata encountered in the borehole and the overlying exposure of the Type Cutler section are locally correlative to the Desmoinesian Paradox Formation and Missourian Honaker Trail Formation (Rasmussen, 2014). The Cutler Group overlies the Hermosa Group and forms a thick depositional

wedge of primarily coarse-grained arkosic sandstones and conglomerates sourced from the Uncompahgre Uplift. On the southwest distal margin of the basin the Cutler Group siliciclastics are subdivided into the lower Cutler, Cedar Mesa Sandstone, Organ Rock Formation, and White Rim Sandstone (Condon, 1997). On the northeast proximal margin, near the salt wall region and Uncompahgre Uplift the Cutler Formation is typically undifferentiated and consists of a heterogenous sequence of fluvial/alluvial arkosic conglomerates and sandstone that interfinger with eolian and shallow marine siltstone and mudstone (Condon, 1997). The Cutler Formation shows the most dramatic thickness variation across the foredeep of the post-salt stratigraphic intervals, with a range of <1-2500m (Trudgill, 2011).

2.2.3 Moenkopi Formation

Unconformably overlying the Cutler Group is the Moenkopi Formation, a typically chocolate brown silty unit consisting of shallow marine shoreface depositional environments as well as tidal flats, fluvial systems, and flood plains (Doelling et al., 2002; Foster, 2015). The formations maximum observed thickness is 762m in central Utah, an aspect attributed to its extensive cover throughout Colorado Plateau (Doelling et al., 2002). Locally the formation is absent on the Uncompahgre Uplift and drastically thins or is completely eroded at proximal positions to several salt walls in the Uncompahgre foredeep including Gypsum Valley (Trudgill, 2011). When present along salt walls in the foredeep, the Moenkopi Formation is characterized by gypsic paleosols and contains a basal meter scale to centimeter thick gypsum bed (Doelling et al., 2002; Foster, 2015).

2.2.4 Chinle Formation

The Triassic Chinle Formation is a red siltstone and sandstone unit containing primarily fluvial channel and flood plain facies with well-developed soil horizons. Thickness ranges from 60-250m with depositional architecture heavily influenced by salt movement in the Paradox Basin foredeep (Trudgill 2011). The Chinle Formation is the first unit to onlap and overlap the Uncompahgre Uplift, resting nonconformably on the Precambrian crystalline basement (Trudgil 2011). Paleosols of the Chinle Formation are inceptisols and alfisols, indicating a warm, semiarid to monsoonal climate of deposition (Prochnow et al., 2006).

2.2.5 San Raphael Group and Morrison Formation: Salt Wash Member

Jurassic stratigraphy exposed within the field area consists primarily of the San Raphael Group (Entrada Sandstone and Summerville formations) and the Morrison Formation with no exposures of The Glen Canyon Group. The Glen Canyon Group is composed of the Wingate, Kayenta, and Navajo sandstones and is exposed to the north in Little Gypsum Valley. The San Raphael Group is the first Mesozoic strata observed to come into contact with Paleozoic strata in the field area. Within the field area the basal sequence of exposed Jurassic stratigraphy is composed of the Entrada Sandstone, which is the upper member of the San Raphael Group. The Entrada Sandstone is a white to buff, very-mature, well-sorted, well-rounded, fine-grained eolian quartz sandstone. Diagnostic sedimentary fabrics are wind-ripple to dune-cross stratification with minor amounts of abraded chert lag deposits (Robeck, 1960). Regional thickness of the unit ranges from 30m to 100m with the most drastic changes occurring at the margins of diapiric salt-walls where the unit thins to <5m at Gypsum Valley, and unconformably onlaps older steeply dipping Permian Cutler Group and Hermosa Group strata (Vogel, 1960). The Summerville Formation is

characterized by red silty mudstones, shales, and well-rounded mature quartzose sandstones that are interpreted as marginal marine to flood-plain depositional environments with periodic thin lacustrine carbonates (Anderson and Lucas, 1994). Thickness of the Jurassic unit ranges from 60 m thick and thins towards the eastern margin of the basin to approximately 8 m where it can be absent at the margins of steeply dipping salt-walls (Stokes and Phoenix, 1948; Vogel, 1960; Trudgill, 2011).

The Jurassic Morrison Formation is composed of the Salt Wash Member and Brushy Basin Member. The Salt Wash Member is the only unit of the Morrison represented in the field area that is in contact with the Pennsylvanian and Permian stratigraphy and locally contains abundant and often large petrified wood debris. The Salt Wash Member is a thick to medium bedded light gray to buff white, fine- to medium-grained, well-sorted fluvial sandstone with minor pebble conglomerate proximal channel fills, thin lacustrine flood-plain carbonates and red to green mudstones and shales. The Morrison Formation is approximately 245 m thick to the southwest and thins to the northeast. Regionally the Salt Wash member is 155 m with significant thinning as it onlaps the topographic highs of the salt-walls (Stokes and Phoenix, 1948; Vogel, 1960; Turner and Peterson, 2004).

2.3 Gypsum Valley Salt Wall

The Gypsum Valley salt wall is 48 km long, 3 km wide, and is located in the fore deep of the Paradox Basin with the axial trace of the anticlinal structure parallel to the strike of the Uncompahgre uplift (Figure 2.7). The Gypsum Valley salt wall is the southernmost salt wall in a distal position from the Uncompahgre at approximately 50 km away (Shoemaker et al., 1958; Elston et al., 1962; Cater and Craig, 1970). Generally, the salt walls become younger and shorter, with respect to subsurface relief, away from the Uncompahgre, making Gypsum Valley one of the youngest and last salt walls to develop (Shoemaker et al., 1958; Elston et al., 1962; Trudgill, 2011). The salt wall is physiographically partitioned into Little Gypsum Valley (northeast end starting north of the Dolores River) and Big Gypsum Valley (southeast end of the salt wall, south of the Dolores River) through a conspicuous narrowing of the diapir width (Stokes and Phoenix, 1948). Big Gypsum Valley is flanked by the Disappointment minibasin to the southwest and the Dry Creek minibasin to the northeast and the salt-sediment interface forms a map-view arcuate structure at the southern termination. Much of the evaporite facies of the Paradox Formation has been eroded out of the core of the anticline forming numerous collapse structures of the overburden and Jurassic-age solution growth synclines throughout the axis of the salt wall (Vogel, 1960). The exhumed diapir forms a collapsed structure with a floor composed primarily of Tertiary alluvium and volcanic gravels, gypsum, and collapsed roof blocks of Late Paleozoic through mid-Mesozoic strata. The modern Dolores River cuts across the breached diapir, with locations in Little Gypsum Valley showing modern fluvial sediments capping the Paradox Formation.

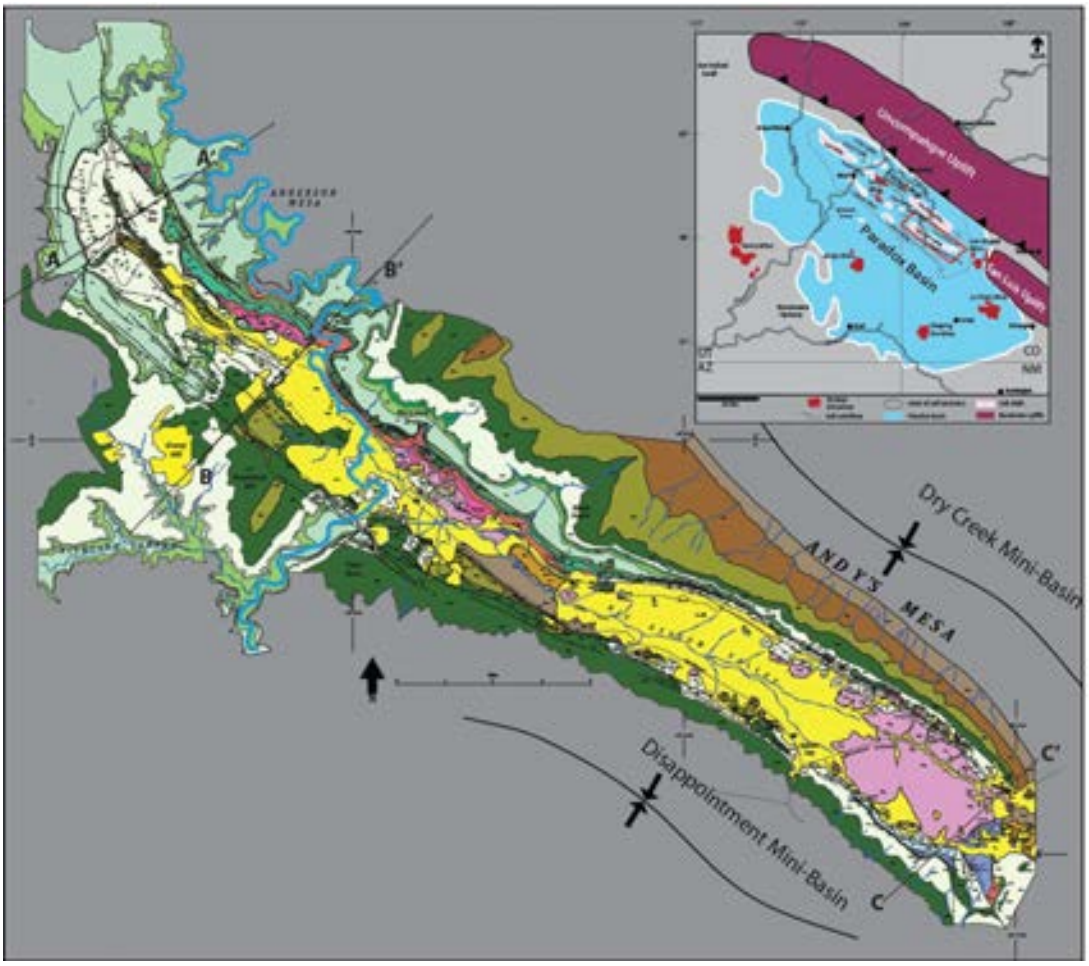

Figure 2.7 - Geologic map of the Gypsum Valley Salt Wall with formation colors defined by stratigraphic chart of figure 2.4. The structure is bounded by the Disappointment mini-basin to the south and the Dry Creek mini-basin to the north. Much of the core of the salt wall shows exposure of the Paradox Formation as a modern gypsum cap and Quaternary cover. The modern Dolores River is shown cutting across the width of the diapir to the north. The red box along the southern termination of the salt wall delineates the primary study area and outcropping vertical Pennsylvanian and Permian strata. Modified after (Stokes and Phoenix, 1948)

A large gas field named Andy's Mesa flanks the northeastern perimeter of Gypsum Valley within the Dry Creek minibasin, with wells producing from the Pennsylvanian Honaker Trail Formation and Permian lower Cutler at approximately 1.7 km in depth. Well control in the gas field indicates that the Honaker Trail Formation is approximately 737 m thick in the mini-basin and dips roughly 22 degrees away from the diapir (Amador et al., 2009; DuChene et al., 2009; Coalson, 2014). On the southwestern flank of Big Gypsum Valley, less than 3km away, and in notable structural difference, the vertical Pennsylvanian strata are exposed forming a 2km strike-oriented outcrop of a relatively conformable succession of non-evaporite facies of the Paradox Formation and mixed lithology cycles of the Honaker Trail and lower Cutler formations. The Honaker Trail Formation, from its sub-horizontal position within the axial trace of the Disappointment minibasin is gradually folded over 4.6 km to its outcropping vertical position, forming pronounced subsurface structural relief of 2.6 km (Escosa et al., 2018). The top of the vertical Pennsylvanian strata are terminated by a well exposed angular unconformity overlain by sub-horizontal Jurassic strata.

The primary study area is located on the southeastern end of the salt wall in Big Gypsum Valley and flanks the southwest margin of the diapir where it begins to terminate at the map view arcuate termination of the plunging salt wall. The study area comprises the vertical to sub vertical exposures of Pennsylvanian-Permian aged strata, and the onlapping stratal wedges of the Mesozoic Entrada and Summerville formations, and the Jurassic-aged Morrison Formation. A more detailed map and cross-section (Figure 2.8; 2.10) shows the diapir-flanking Pennsylvanian strata and onlapping younger units of the Disappointment minibasin. The field area contains a conformable succession of vertical non-evaporite facies of the Paradox Formation and mixed lithology cycles of peritidal and shallow marine limestones of the Honaker Trail Formation. The Lower Cutler here,

marks a lithologic and structural transition to predominately terrigenous siliciclastics at progressively shallower dips and is the last exposure of Paleozoic strata in the study area before being onlapped and subsequently covered by shallowly dipping Jurassic strata. The Lower Cutler is capped by the low angle Jurassic Summerville and Entrada formations forming a pronounced angular unconformity that extends along strike of the field area and down section into the Honaker Trail Formation. Up section from the Lower Cutler the field area is dominated by successively lower dips of stratal wedges of the Morrison Formation.

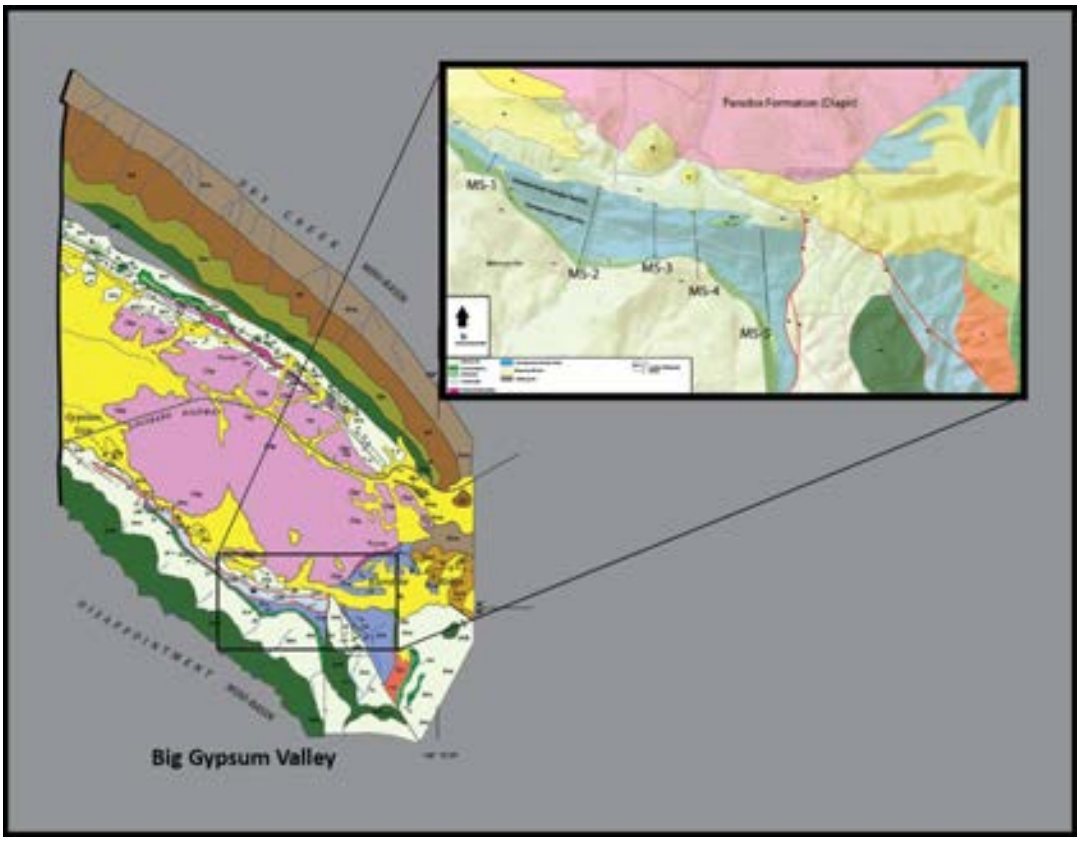

Figure 2.8 - Geologic map of the southern termination of the Gypsum Valley Salt Wall with black box outlining primary study area. The zoomed in area shows in blue, vertical Paleozoic strata and locations of measured sections, used as the primary tool to assess the geometry of the stratigraphic framework of megaflap stratigraphy. White dashed line within the megaflap panel shows the lithologic and structural partitioning into the Pennsylvanian and Permian. Modified after (Stokes and Phoenix, 1948)

Gypsum Valley currently represents a breached salt wall with much of the Jurassic Morrison Formation that formed the diapir roof erosionally removed. Breaching and exhumation of the diapir exposed the Paradox Formation, the salt sediment interface, and exposed halokinetic stratigraphy ranging from Late Pennsylvanian through the Cretaceous. In map view, the salt wall is partitioned into Little Gypsum Valley and Big Gypsum Valley primarily through pronounced necking of the diapir width near the central axis of the wall (Figure 2.9).

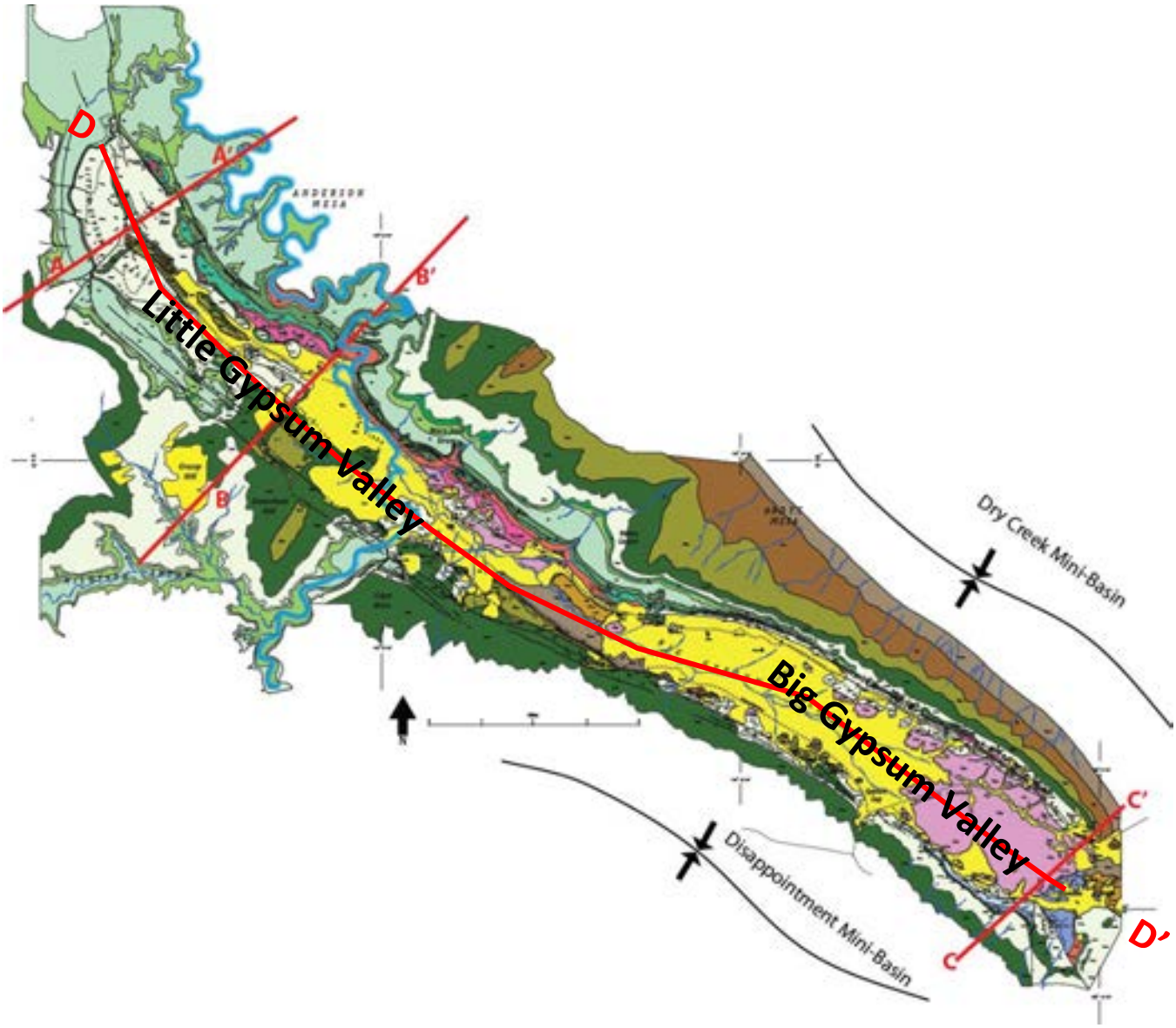

Figure 2.9: Geologic map of Gypsum Valley, dashed line shows structural partitioning of the salt-wall into two distinct regions primarily through pronounced necking of the diapir width at the central axis of the diapir. Structure cross-sections are denoted by red lines A-A', B-B', C-C', and elevation profile D-D'. Flanking mini-basins, Disappointment and Dry-Creek bound the southern termination of the salt-wall the south and north respectively. Modified after (Stokes and Phoenix, 1948)

Several cross sections generated along strike of the salt wall axis reveal the salt core, stratigraphy thinning towards the diapir generating the flanks of the local mini-basin geometries, as well as complex structural and sedimentary heterogeneity; the most prominent of which in Little Gypsum Valley is the preserved Jurassic Morrison roof forming a synclinal geometry above the diapir seen in cross-sections A and B (Figure 2.10). Moving along strike towards Big Gypsum Valley and the principal study area, marked elevation increase is observed along with simultaneous increase in diapir width, increased exposure of the Paradox Formation gypsum caprock, and gradual steepening of Pennsylvanian strata to an exposed vertical position within the principal study area (Figure 2.10; 2.11; 3.1). Cross-section D-D' (Figure 2.9; 2.11) documents this elevation increase from Little Gypsum Valley to Big Gypsum Valley to be roughly 500 m in elevation gain with the highest elevation being the southern termination of the salt wall and the location of near vertical Pennsylvanian Paradox Formation shales and the Honaker Trail Formation forming the megaflap (Figure 2.8).

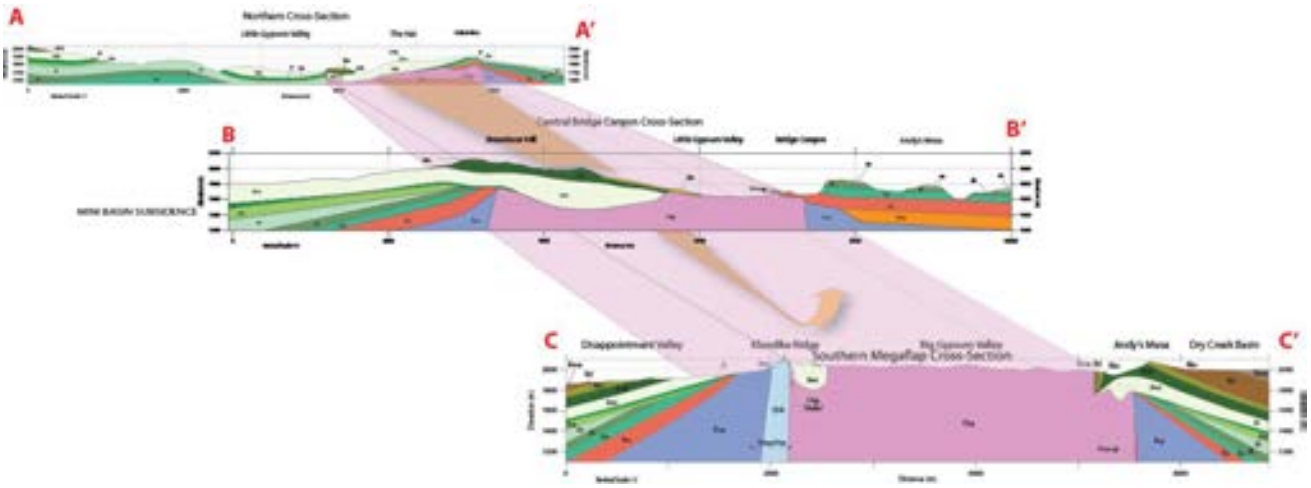

Figure 2.10: Structural cross-sections A-A', B-B', C-C', moving along strike from Little Gypsum Valley to Big Gypsum Valley. Cross-sections show along strike structural heterogeneity characteristic of diapir flanking strata. Cross-sections A-A' and B-B' depict Jurassic strata forming synclinal geometries on the diapir roof and exposed salt shoulder of Little Gypsum Valley (McFarland, 2016). Moving along strike of the salt-wall towards Big Gypsum Valley, progressive rotation of Pennsylvanian and Permian strata is observed with cross-section C-C' revealing the gypsum valley megaflap in light blue. Flanking the diapir are large scale growth stratal wedges forming pronounced angular unconformities at the edges of local mini-basins. Modified after (Stokes and Phoenix, 1948)

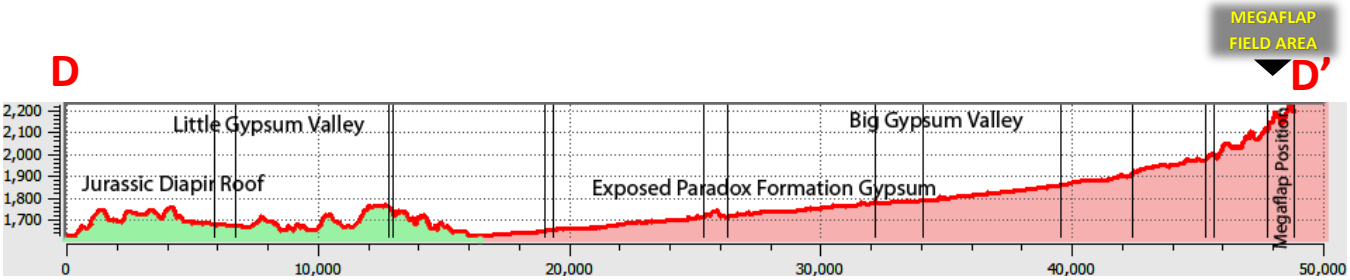

Figure 2.11 - Elevation profile D-D' showing elevation distinction of Little Gypsum Valley and Big Gypsum Valley. Moving along strike of the salt wall towards Big Gypsum Valley, coincident with increased elevation of 500 m, is the increased diapir width and the presence of vertical Pennsylvanian and Permian strata forming the megflap.

2.4 Gypsum Valley Megaflap

The exposed vertical Pennsylvanian and lower Permian strata on the southwest margin of the Gypsum Valley salt wall is interpreted by Rowan et al. (2016) to be the exposed upper reaches of a megaflap that is gradually folded over 5 km and thickens as it decreases dip towards its regional near horizontal basal position within the Disappointment minibasin (Figure 2.14). From the basal horizontal position to the outcropping vertical panel, the megaflap is estimated to have 2.5 km of vertical relief (Rowan et al. 2016).

Following the map view curvature of the southern termination from Andy's Mesa towards the primary study area, the Pennsylvanian stratigraphy interpreted at 2000m depth crosses several radial faults and drastically steepens and outcrops to a near vertical position at the salt-wall nose and finally to vertical at the southern flank bound by the Disappointment mini-basin. The most significant line of evidence for defining the outcropping vertical Pennsylvanian strata as a megaflap comes from the interpretation of regional seismic line drawings as no other subsurface datasets are available within the Disappointment mini-basin (Rowan et al., 2016) (Figure 2.13; 2.14). Seismic line drawings show interpreted and annotated characteristics of seismic data sets across Little Gypsum Valley and Big Gypsum Valley as well as the most proximal salt wall Paradox Valley and the Uncompahgre. Pennsylvanian stratal packages on the seismic line drawings are delineated with a dark purple, and are identified based on well-log formation top

picks within the local diapir flanking mini-basins and seismic facies characteristics of top Honaker Trail Fm., and the Permian Cutler Formation (Figure 2.14).

The nature of this structure fits the definition and observed characteristics of megaflaps identified on well-log data sets and seismic lines throughout many of the world's salt basins.

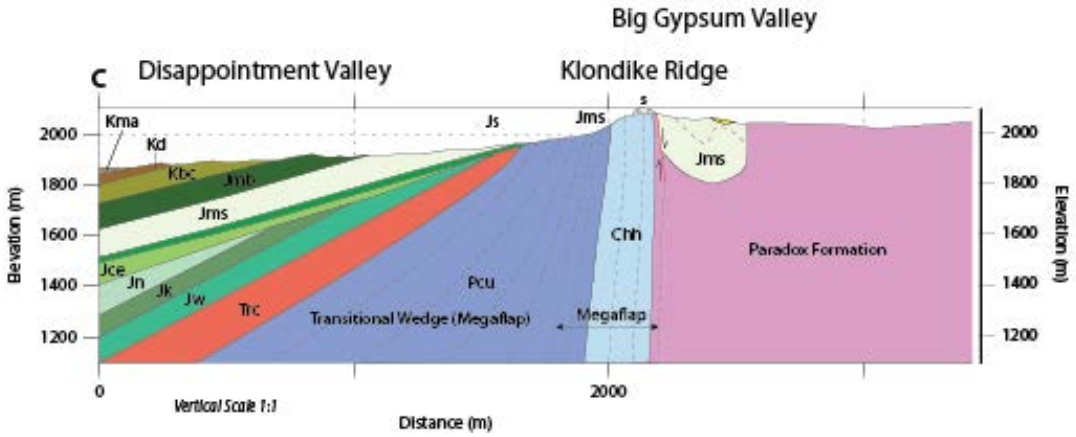

Figure 2.12: Structure Cross section through the megaflap. Cross-section shows Paradox Fm. in pink, Vertical Honaker Trail Fm. in light blue, megaflap transitional wedge in purple, outcropping Jurassic strata (Jce= Jurassic Entrada, Jms=Jurassic Salt Wash, Jmb=Jurassic Brushy Basin) in various shades of green. Subsurface onlapping strata of the Triassic Chinle Formation, and Jurassic Windagate, Kayenta, and Navajo of the Glen Canyon group are inferred. Modified after (Stokes and Phoenix, 1948)

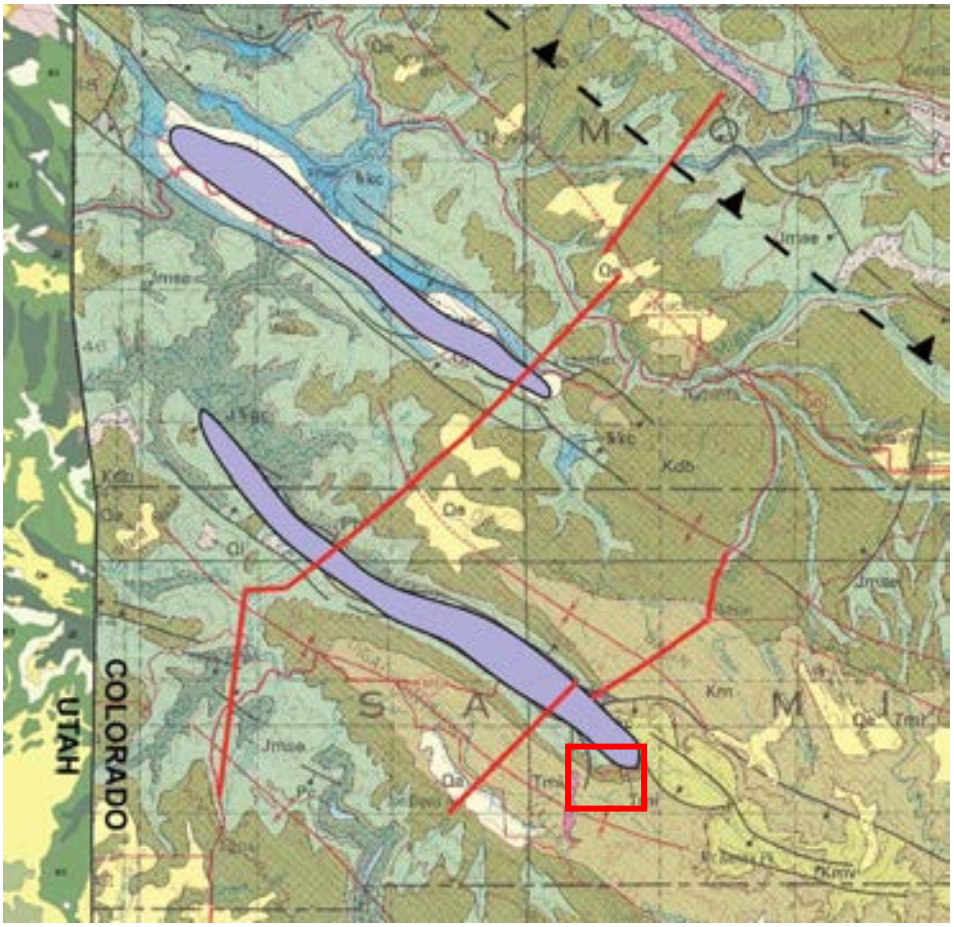

Figure 2.13 - Regional geologic map with Paradox Valley (north) and Gypsum Valley (south) with subsurface salt highlighted in purple and red lines indicating location of annotated seismic line drawings as well as red outlined box denoting the field area. (Modifed after Rowan et al, 2016).

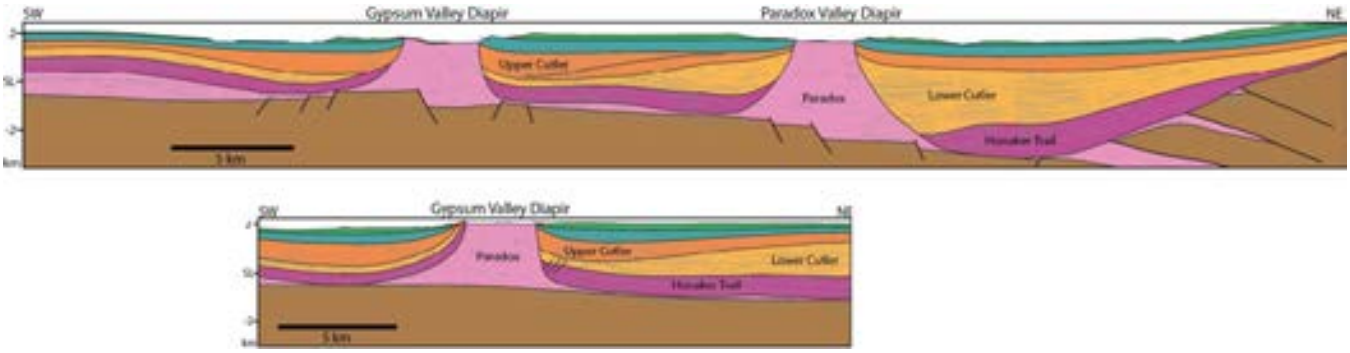

Figure 2.14 - Annotated seismic line drawings A and B showing subsurface structure interpreted from seismic facies, and formation top picks from local well data. Megaflap forming strata of the Honaker Trail Formation and Lower Cutler Formation highlighted in purple and yellow respectively. Upper Cutler Formation and superjacent Triassic strata in Orange and Green respectively (Rowan et al., 2016).

2.5 Megaflap Formation

Differential sediment loading produced by progradational clastic wedges of alluvial megafans and fluvial systems flanking the Uncompahgre triggered salt movement during the Late Pennsylvanian to Early Permian (Ge et al., 1997; Ge and Jackson, 1998; Trudgill, 2010). Rowan et al. (2016) model the evolution of the Gypsum Valley megaflap as starting as conformable near-horizontal roof strata on top of a broad salt pillow that transitions to an asymetric single-flap active diapir (Schultz-Ela et al., 1993) with a thinned roof. From 2D seismic data from the north side of the diapir Rowan et al. (2016) suggest that significant erosion associated with the regional mid-Cutler unconformtity (not-exposed in the study area) thinned the roof of the single flap active diapir, triggering salt breakthrough and initiation of passive diapirism that continued until the Late Jurassic when the Morrison Formation fluvial siliciclastics overlapped and covered the diapir crest (Rowan et al., 2016, Escosa et. al., 2018).

Chapter 3: Methods

3.1 Measured Sections & Outcrop Data

Five measured sections capturing uppermost Paradox Formation through Lower Cutler Formation stratigraphy of the megaflap and transitional wedge (Figure 3.1) were acquired along the southwest margin of the Big Gypsum Valley salt wall. Measured sections were chosen based on exposure quality, accessibility, and represent the principal data sets of this study. Of particular interest is measured section MS-2, which provides the longest continuous stratigraphic section through vertical Paradox Formation to Lower Cutler Formation stratigraphy. Measured section locations and details are located on Figures 3.1 and 3.2. Utilizing recent advances in digital mapping techniques, detailed mapping of depositional contacts, lateral facies changes, and faults are documented with a GPS enabled Asus tablet, running QGIS software in order to view satellite imagery and location in real time. Using QGIS software, assessment of the overall geometry and depositional relationships of the study area was accomplished continuously in the field. To aid digital field mapping, field photos and photo-panoramas were generated and annotated in Adobe Illustrator and finalized in Adobe Photoshop to delineate large scale structural and stratigraphic features of the study area. 100 hand samples were collected, slabbed and polished in order to more accurately determine lithofacies characteristics and to describe depositional and diagenetic fabrics of the stratigraphic sections. Of the 100 hand samples, 43 thin sections were generated for the purpose of identifying depositional and diagenetic micro-fabrics, porosity characterization, as well as standard petrographic analysis. Thin section manufacturing was completed by Spectrum Petrographics Inc., to a standard 30μm thickness and 27x46mm dimension. All thin sections are imbedded with blue dye epoxy to highlight pore space and stained with Alizarin Red-S and potassium ferricyanide to distinguish dolomite/ferrous dolomite from calcite/ferrous calcite. This

information formed the basis for depositional facies partitioning and sequence stratigraphic analysis. Locations of measured sections, hand samples, field photographs, structural orientations, depositional contacts, and faults are all georeferenced and plotted on the tablet PC running the digital field mapping platform QGIS. Utilizing well data, specifically well top information from the Andy's Mesa Gas Field located on the northeast side of Big Gypsum Valley, structural cross-sections were generated in *Midland Valley Move* to highlight structural relationships and megaflap geometry across the Big Gypsum Valley Diapir and redrawn in Adobe Illustrator. Field data, stratigraphic sections, and structural cross-sections were then compiled into an accurate and high resolution geologic map of the megaflap panel (Figure 3.2).

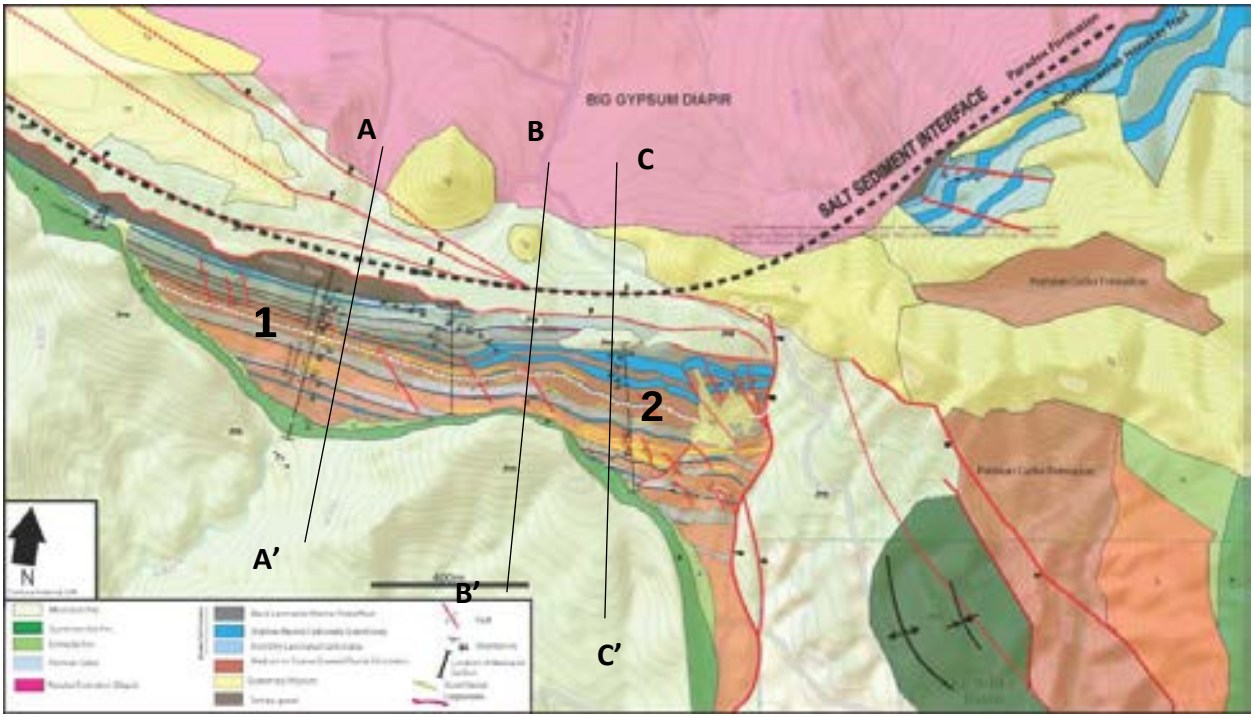

Figure 3.1- simplified geologic map of Big Gypsum Valley diapir and megaflap at the southwest termination. Map shows labels 1 and 2 identifying the 1) Vertical zone comprising vertical Pennsylvanian strata and the transitional wedge of 70° dipping strata of the Lower Cutler Formation 2) The lower dip zone of progressive shallowing of structural dip to 50° moving along strike from zone 1, as well as increased internal faults in the megaflap and the bounding radial fault down dropping Jurassic strata.

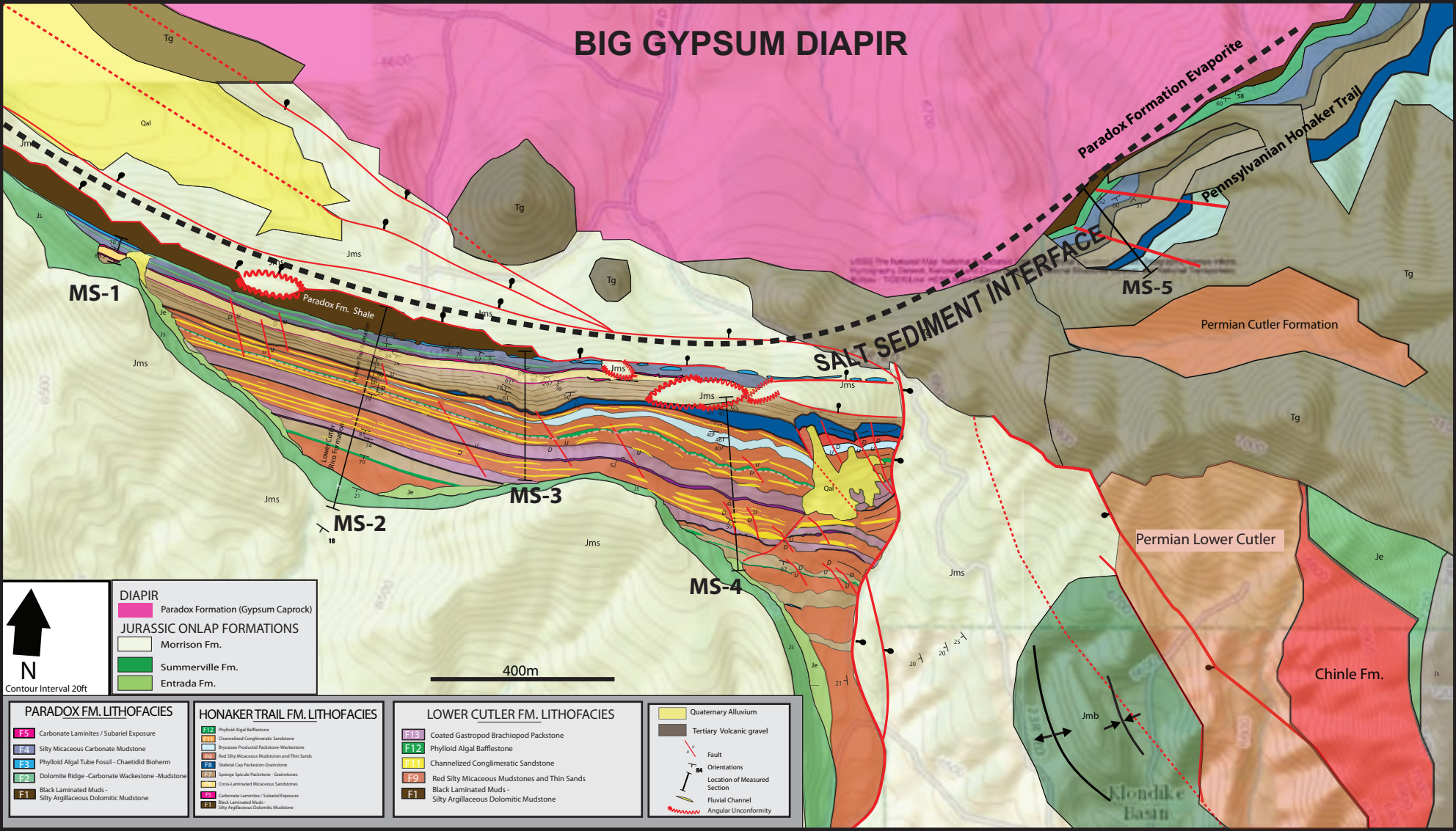
BIG GYPSUM DIAPIR
Paradox Formation Evaporite
Pennsylvanian Honaker Trail
SALT SEDIMENT INTERFACE
MS-1
MS-2
MS-3
MS-4
MS-5
Paradox Fm. Shale
Permian Cutler Formation
Permian Lower Cutler
Chinle Fm.
Klondike Basin
Tg
Qal
Jms
Je
Js
Jmb
N
Contour Interval 20ft
400m
DIAPIR
Paradox Formation (Gypsum Caprock)
JURASSIC ONLAP FORMATIONS
Morrison Fm.
Summerville Fm.
Entrada Fm.
PARADOX FM. LITHOFACIES
F5 Carbonate Laminites / Subariel Exposure
F4 Silty Micaceous Carbonate Mudstone
F3 Phylloid Algal Tube Fossil - Chaetidid Bioherm
F2 Dolomite Ridge -Carbonate Wackestone -Mudstone
F1 Black Laminated Muds - Silty Argillaceous Dolomitic Mudstone
HONAKER TRAIL FM. LITHOFACIES
F12 Phylloid Algal Bafflestone
F11 Channelized Conglimeratic Sandstone
F10 Bryozoan Productid Packstone-Wackestone
F9 Red Silty Micaceous Mudstones and Thin Sands
F8 Skeletal Cap Packeston-Grainstone
F7 Sponge Spicule Packstone - Grainstones
F6 Cross-Laminated Micaceous Sandstones
F5 Carbonate Laminites / Subariel Exposure
F1 Black Laminated Muds - Silty Argillaceous Dolomitic Mudstone
LOWER CUTLER FM. LITHOFACIES
F13 Coated Gastropod Brachiopod Packstone
F12 Phylloid Algal Bafflestone
F11 Channelized Conglimeratic Sandstone
F9 Red Silty Micaceous Mudstones and Thin Sands
F1 Black Laminated Muds - Silty Argillaceous Dolomitic Mudstone
Quaternary Alluvium
Tertiary Volcanic gravel
Fault
Orientations
Location of Measured Section
Fluvial Channel
Angular Unconformity

Figure 3.2: Geologic map constructed using QGIS, GPS and high resolution satellite imagery. Depositional facies, locations of measured sections, hand samples, field photographs, structural orientations, depositional contacts, and faults are all georeferenced and plotted on the tablet PC running the digital field mapping platform and then constructed in Adobe Illustrator.

Chapter 4: Results and Lithofacies

4.1 Megaflap Characteristics

The Big Gypsum Valley megaflap is observed to have several prominent characteristics. The structure itself is heterogenous in terms of structural orientation, style and ages of bounding unconformities, internal radial faults, bounding graben forming radial faults, and progressively shallowing dips away from the diapir edge and along strike. When moving along strike of the exposed Pennsylvanian strata from east to west to the diapir nose, two zones are distinguished on the basis of structural characteristics. These zones are 1) The structurally vertical zone and 2) The lower dip zone of approximately 50-60° proximal to the large bounding radial fault. The vertical zone comprises structurally concordant stratigraphy of the Paradox Formation, Honaker Trail Formation, and lower Cutler Formation in terms of strike orientation and limited faulting (Figure 3.1, 4.1 and Cross-section A-A' on 4.2). The lower dip zone shows gradual strike and dip deviation (from 90° to 50°) trending towards the radial fault along with increased faulting within the megaflap stratigraphy (Cross-section C-C', D-D' Figure 4.2; 4.4). Two more zones are distinguished based on structural properties trending away from the diapir edge, and are simply termed the vertical megaflap described in the vertical zone and the transitional wedge of shallowing dips of the lower Cutler Fm. forming an onlapping asymmetrical clastic wedge (Figure 2.12; 4.1, 4.2).

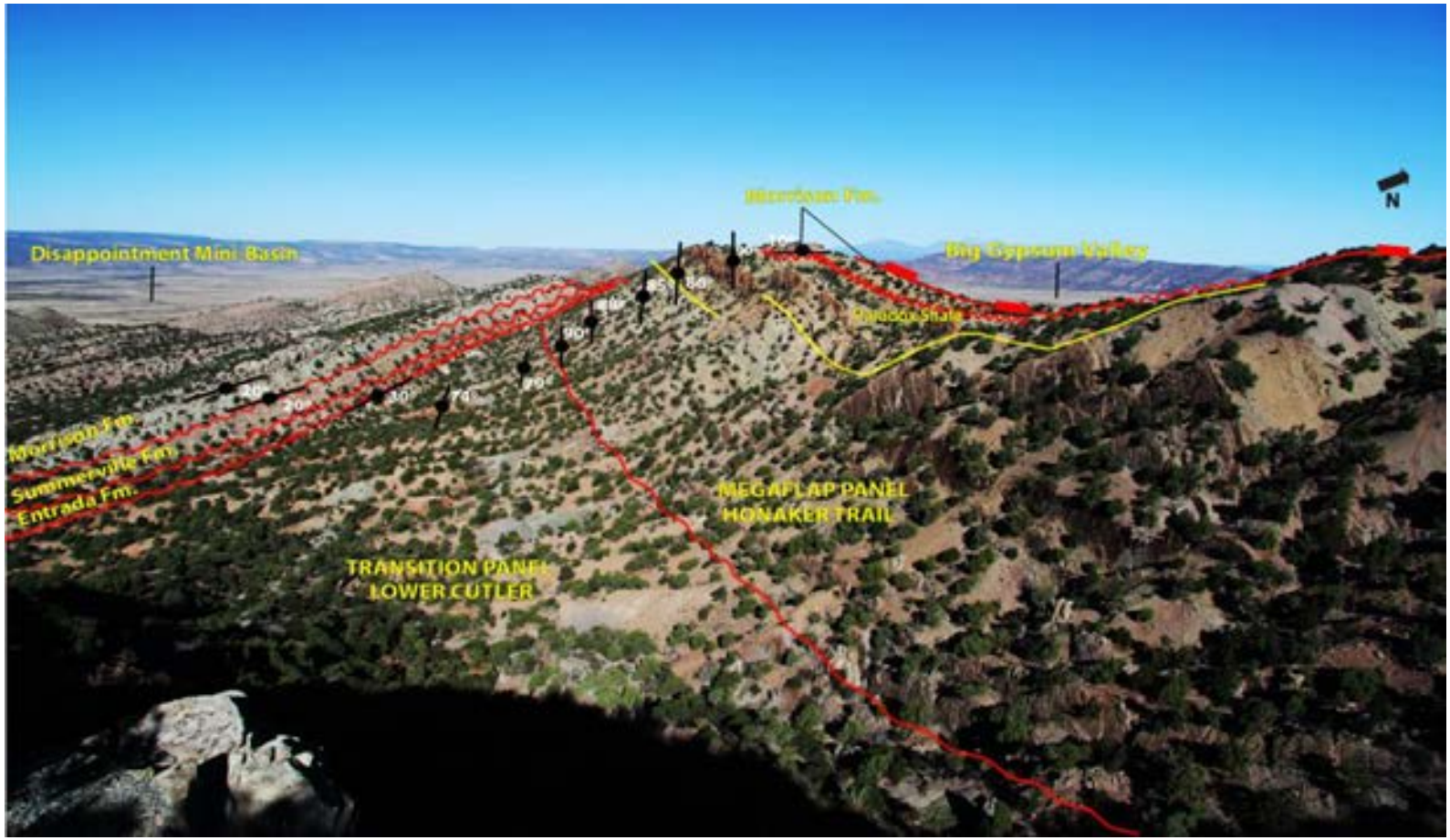

Figure 4.1- Field photograph documenting from right to left: Big Gypsum Valley forming the exhumed core of the diapir, normal fault down dropping Jurassic Morrison Formation siliciclastics and 90 degree angular unconformity bounding vertical Paradox Formation shales and flat lying Morrison overlap strata, dip orientations progressively shallowing to Jurassic onlapping strata, transitional dips and internal megaflap angular unconformity with Honaker Trail and Lower Cutler Formation, and the Disappointment mini-basin in the distance

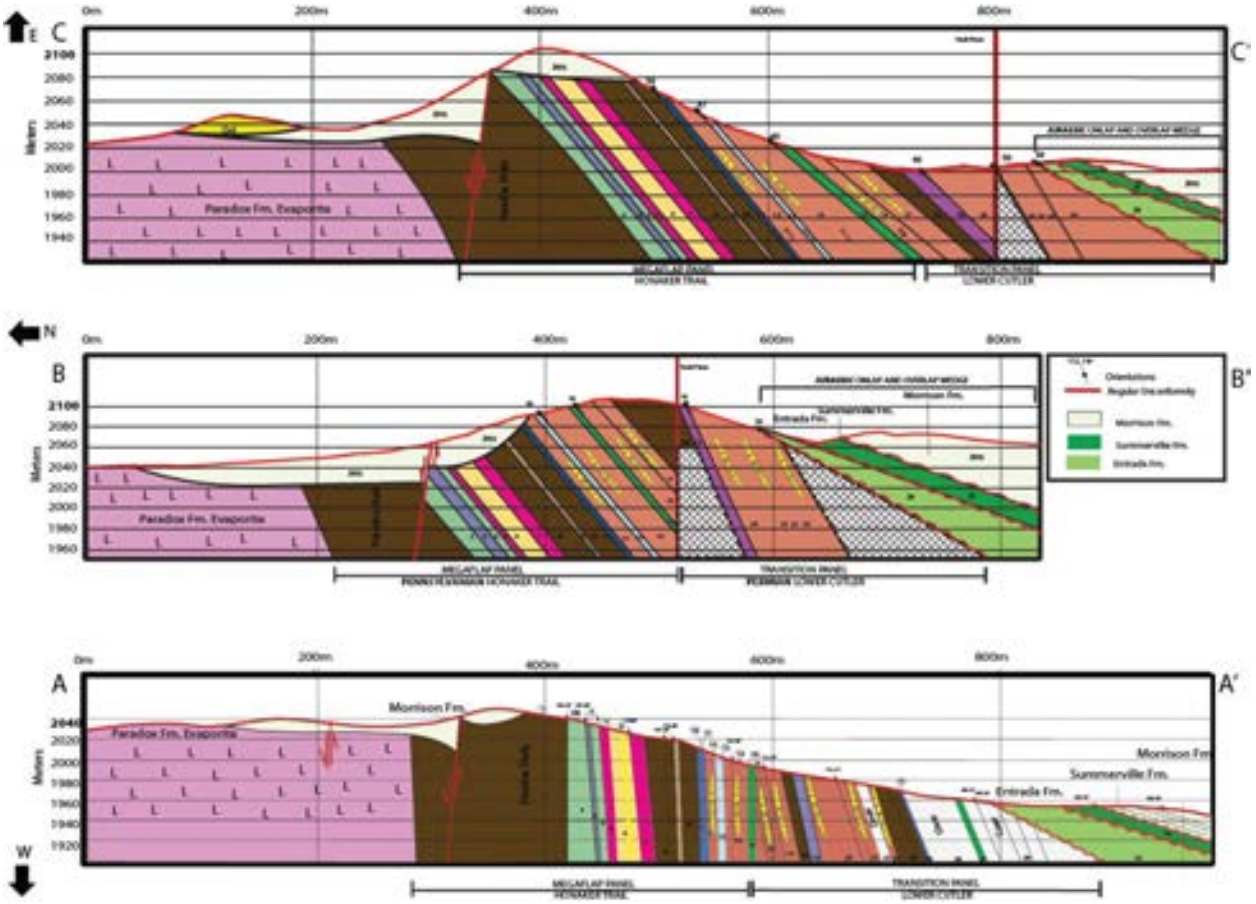

Figure 4.2 - Structure cross-sections A, B, and C trending from the vertical megaflap to progressivley shallowing dips of cross-section C located proximal to the radial fault. The facies color scheme of the megaflap can be found in the lithofacies chapter.

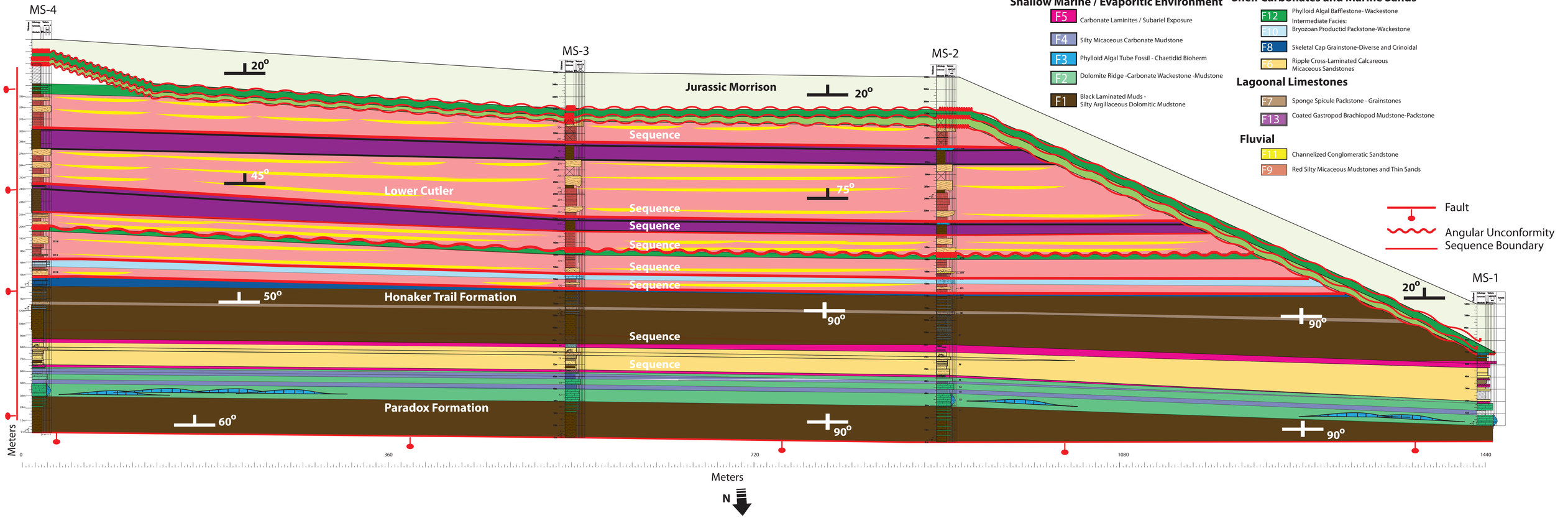
MS-4
MS-3
MS-2
MS-1
20°
45°
50°
60°
20°
75°
90°
90°
90°
20°
90°
90°
Jurassic Morrison
Lower Cutler
Honaker Trail Formation
Paradox Formation
Sequence
Sequence
Sequence
Sequence
Sequence
Sequence
Sequence
Sequence
Sabkha to
Shallow Marine / Evaporitic Environment
F5 Carbonate Laminites / Subariel Exposure
F4 Silty Micaceous Carbonate Mudstone
F3 Phylloid Algal Tube Fossil - Chaetidid Bioherm
F2 Dolomite Ridge -Carbonate Wackestone -Mudstone
F1 Black Laminated Muds -
Silty Argillaceous Dolomitic Mudstone
Shelf Carbonates and Marine Sands
F12 Phylloid Algal Bafflestone- Wackestone
F10 Intermediate Facies:
Bryozoan Productid Packstone-Wackestone
F8 Skeletal Cap Grainstone-Diverse and Crinoidal
F6 Ripple Cross-Laminated Calcareous
Micaceous Sandstones
Lagoonal Limestones
F7 Sponge Spicule Packstone - Grainstones
F13 Coated Gastropod Brachiopod Mudstone-Packstone
Fluvial
F11 Channelized Conglomeratic Sandstone
F9 Red Silty Micaceous Mudstones and Thin Sands
Fault
Angular Unconformity
Sequence Boundary
Meters
0
360
720
1080
1440
Meters
N

Figure 4.3 – Facies correlation of measured sections MS-1 (Far right) through MS-4 (Far left) across the megaflap forming a map-view cross-section of the field area. North is to the bottom beginning with the fault bound Paradox Formation adjacent to the diapir and top shows on-lapping Jurassic unconformities dipping away.

4.1.1 Transitional Wedge

Along with documenting the sedimentological characteristics of the exposed megaflap, measured sections throughout the panel also document structural orientations up-section away from the diapir edge. Sections encountering Permian lower Cutler Formation stratigraphy document a pronounced structural change in the form of progressively shallowing dips from 79° to 70°, in marked contrast from the vertical Paradox Fm. and Honaker Trail Fm. This structural change is noted on the geologic maps of the megaflap as a white dashed line. The dashed line denotes top Honaker Trail Fm., the structural transition from vertical to near vertical as well as a lithologic transition from predominately marine sedimentation to dominantly terrigenous siliciclastics. The structural deviation is referred to as the transition wedge, an asymmetrical wedge of siliciclastics and carbonates of the lower Cutler Fm. onlapping the inclined megaflap panel

4.1.2 Radial Faults

In map view of Big Gypsum Valley at the southern termination of the salt wall the megaflap outcrops and shows map-view curvature related to the diapir edge. When moving along strike of the exposed Pennsylvanian strata from the vertical zone to lower dip zone, numerous faults are noted within the megaflap panel as well as a large megaflap bounding radial fault. Trending from the vertical zone to the lower dip zone, the megaflap is bound to the east by a radial fault down dropping Morrison Formation siliciclastics against Pennsylvanian strata. Trending towards the radial fault from the vertical zone, concomitant with shallowing dips of the megaflap, is observed rotation of the strike of the structure to a more north-south orientation, in contrast to the near east-west strike observed in the vertical zone of the megaflap (Figure 4.4).

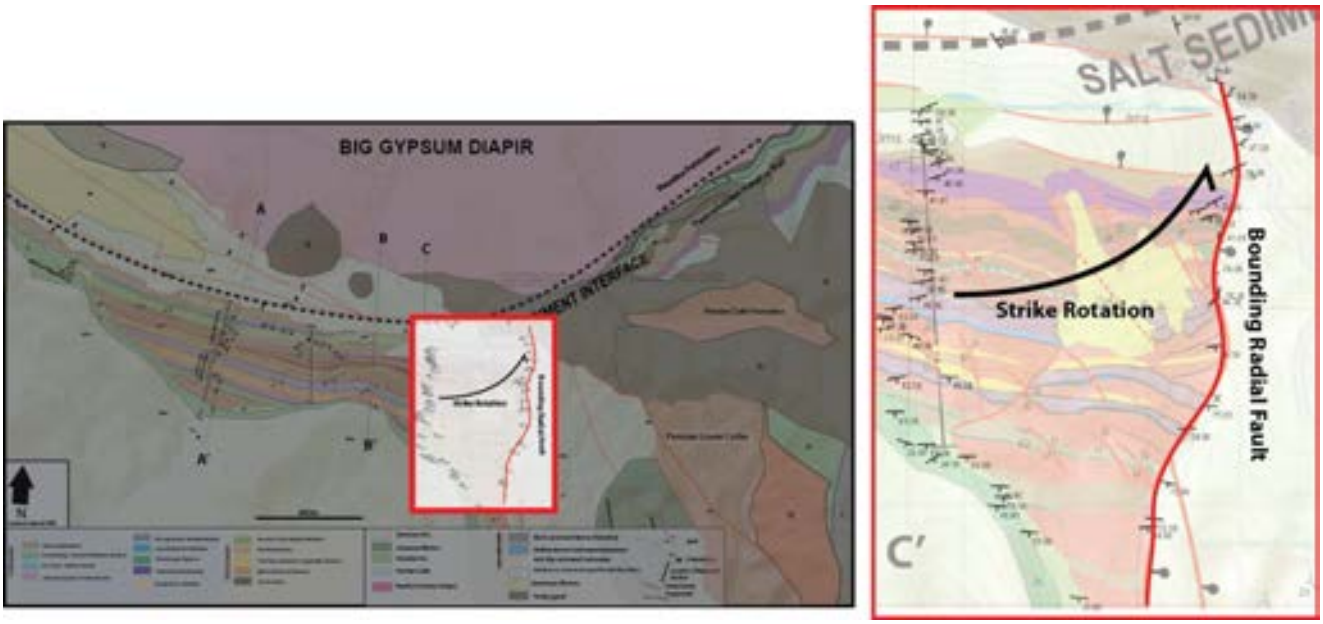

Figure 4.4 - Geologic map of the southwest termination of Big Gypsum Valley diapir with structural orientations of the discordant zone and bounding radial fault highlighted. To the right the zone is shown enlarged with strike orientations clearly showing roation at the radial fault.

4.1.3 Unconformities

Preserved unconformities bound the megaflap in several styles, ages, and at various positions within the megaflap stratigraphy. Specifically the megaflap is in unconformable contact with the Jurassic Morrison Formation, The Jurassic Entrada Formation, The Jurassic Summerville Formation as well as the stratal wedge of onlapping lower cutler siliciclastics.

4.1.4 Jurassic Morrison Formation Unconformity

The Jurassic Morison Formation is preserved in unconformable contact with the megaflap in several locations along strike. Pods of the Jurassic Morrison Formation are in a near horizontal orientation on top of the vertical Pennsylvanian Paradox Formation shales and bioherms of the dolomite ridge (Figure 4.5). The Morrison Formation on top of the Paradox Formation forms

synclinal geometries that gently dip northward towards the Big Gypsum Valley salt wall, while the onlapping Morrison Formation near the lower Cutler dips southward away at approximately 20°. The Morrison Formation capping the megaflap is white-gray, cross-bedded, well-sorted, medium-grained sandstone, and contains large clasts of petrified Jurassic tree limbs, however contains no evidence of recycled Paradox Formation shales.

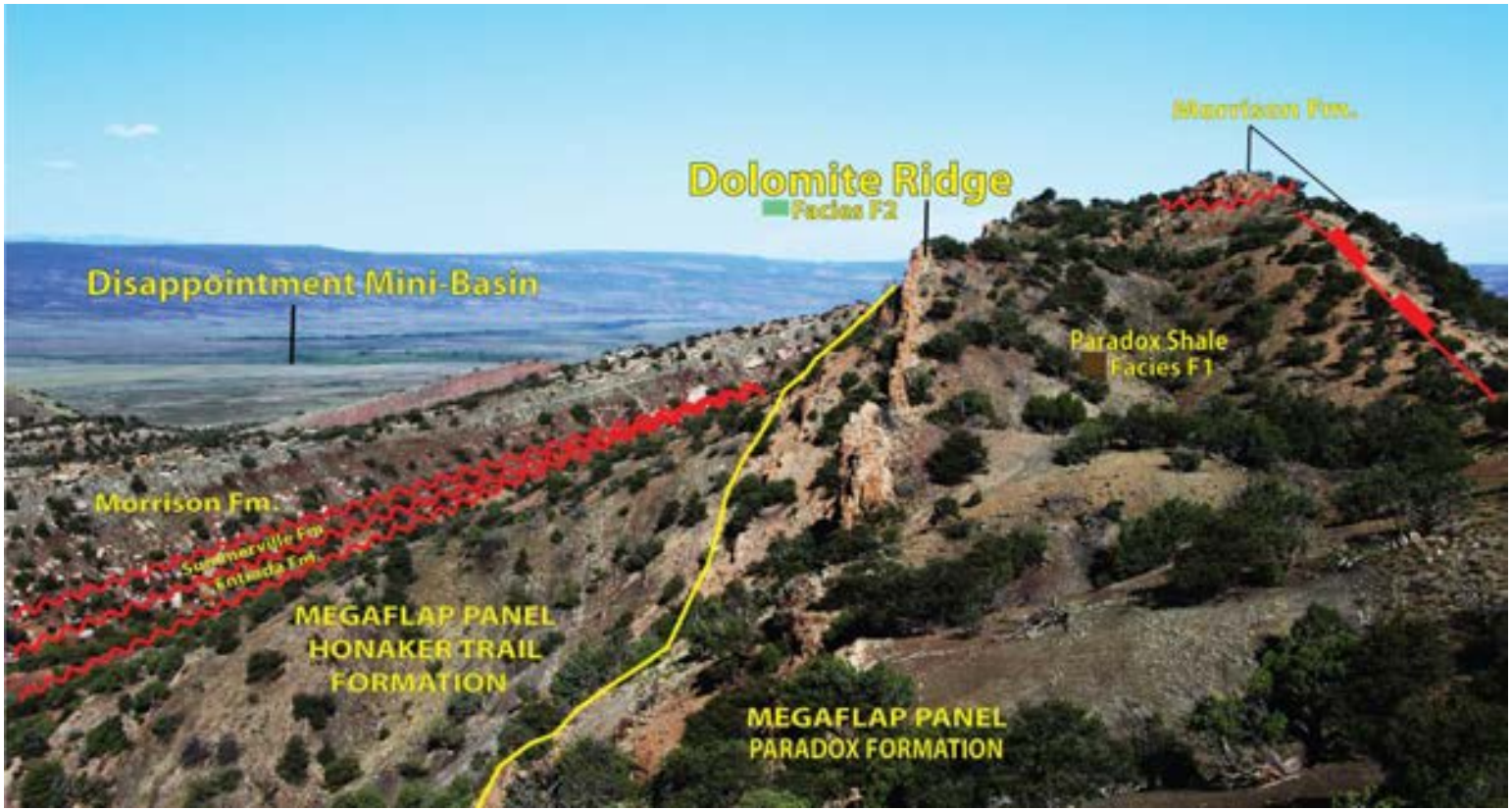

Figure 4.5- Outcrop photograph of the megaflap panel showing vertical units of the Paradox Formation and Honaker Trail Formation as well as progressive angular unconformities of onlapping Jurassic Entrada Fm., Summerville Fm., and Morrison Fm. Facies F-1 is at an angular unconformity and/or basal fault contact with Jurassic Morrison fluvial siliciclastics. The resistant ridge forming carbonate wackestone-mudstone of facies F-2 is shown as a prominent laterally extensive feature with sharp basal contact with facies F-1.

4.1.5 Jurassic Summerville Formation Unconformity

The Summerville Formation exposure in map view is preserved above the lithofacies of the Honaker Trail and lower Cutler Formation as a continuous boundary throughout much of the field area. The Summerville is observed to be a conglomeratic unit consisting of chert and carbonate black-pebble conglomerates and well-rounded, fine- to medium-grained, well-sorted orange-red sandstone within a mudstone matrix. The chert pebble conglomerates within the Summerville Formation are interpreted to be derived from the exposed steeply dipping Pennsylvanian carbonates of the Paradox and Honaker Trail formations. When the Summerville is restored to horizontal, the now vertical Pennsylvanian carbonate would still be generating prominent relief as the megaflap structure would be steeply dipping (approximately 70 degrees) in the Jurassic.

4.1.6 Jurassic Entrada Formation Unconformity

The Jurassic Entrada Formation is in contact with the Gypsum Valley megaflap along much of the exposed width only thinning and overlapped by the Jurassic Summerville Formation in a few locations. The Entrada Sandstone is in angular contact with lithofacies of the Honaker Trail and many of the fluvial and marine siliciclastics units of the lower Cutler Formation. Poor exposure and preservation of the Entrada is characteristic throughout the field area, however no carbonate clasts or detritus from the steeply dipping Pennsylvanian and Permian strata are observed reworked into the formation.

4.2 Lithofacies and Depositional Process Interpretation

The primary focus of this study is to characterize the depositional and diagenetic setting as well as the sequence stratigraphic framework of the megaflap through analysis of measured sections, petrographic data, and geologic mapping. Interpretation of field observations and

measured sections MS-1, MS-2, MS-3 MS-4 and MS-5 (Figure 3.1, 3.2) are the primary dataset used to delineate the depositional lithofacies and stratigraphic architecture of the megaflap panel.

The megaflap stratigraphic units comprise, in ascending order the: uppermost Paradox Formation Honaker Trail Formation and the Lower Cutler Formation. The basal position of the stratigraphic sections are bound by either an angular unconformity of Jurassic Morrison fluvial siliciclastics or bound by a normal fault down-dropping Morrison Formation siliciclastics (Figure 4.3). The megaflap units are vertical to near vertical (80°-90°) with stratigraphic sections terminated by an angular unconformity (approximately 20°) with the overlying Jurassic Entrada or Jurassic Summerville formations. However, the stratigraphy present beneath the unconformity varies along the outcrop trace of the unconformity. Nowhere in the study area is the megaflap to salt wall contact exposed.

Outcrop analysis and interpretations are derived from observations of various sedimentological attributes including color, lithology, grain size, type and sorting, sedimentary structures, and stratigraphic surfaces. The field area contains a continuous upper Paleozoic stratigraphic section extending from the black shales of the Paradox Formation, through the carbonate-dominated Honaker Trail Formation and ending in the transitional unit of siliciclastics and subordinate carbonates of the Lower Cutler Formation. Thirteen distinct lithofacies are documented including: 1) black silty argillaceous dolomitic mudstone, 2) echinoderm brachiopod mudstone-wackestone containing local 3) phylloid algal - tube fossil - chaetitid bioherm, 4) silty micaceous dolomitic mudstone, 5) laminated dolomite, 6) ripple cross-laminated calcareous micaceous sandstone, 7) sponge spicule packstone-grainstone, 8) diverse skeletal packstone-grainstone, 9) red silty, micaceous mudstone and thin-bedded sandstone 10) bryozoan, productid brachiopod wackestone-packstone, 11) channelized conglomeratic

sandstone, 12) phylloid algal bafflestone -wackestone, 13) coated grain, gastropod brachiopod mudstone – packstone.

The lithofacies represent depositional settings ranging from non-marine fluvial siliciclastics to offshore marine mudstones and shallow marine carbonates (Figure 4.6). The following lithofacies analysis is organized by stratigraphic occurrence for each formation in the megaflap, however some lithofacies are also present in the other formations as documented on stratigraphic sections. The composite stratigraphic section trends from the inferred salt-sediment interface, marked by a normal fault, to the angular unconformity with the overlying, onlapping Jurassic strata. The basal laterally continuous dolomite ridge was used as a datum for measured sections and correlation purposes (Figure 4.5 and 4.7). Tables 1, 2 and 3 provide lithofacies descriptions and color scheme used to represent particular facies on the stratigraphic sections and geologic maps for each formation.

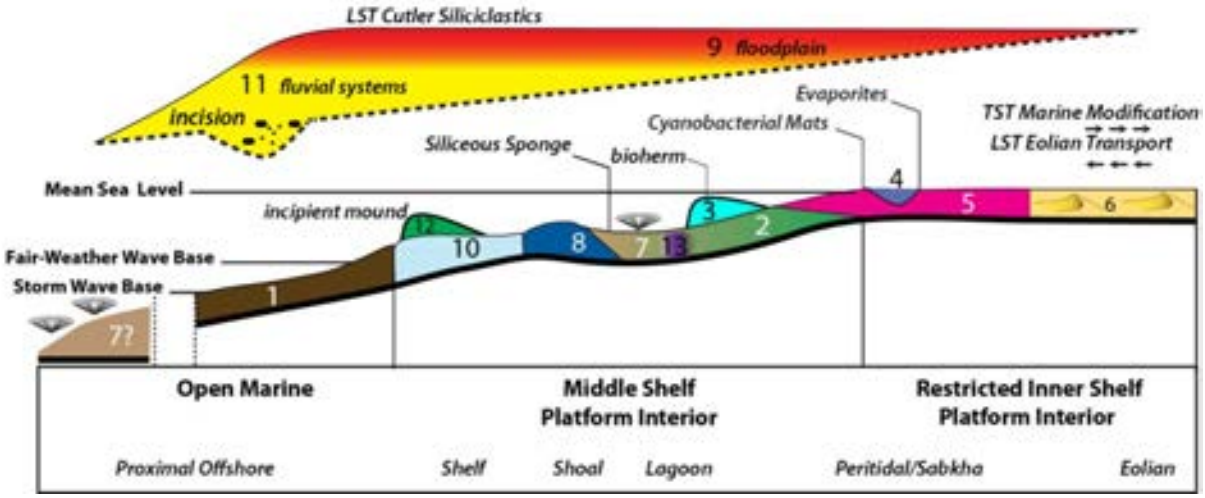

Figure 4.6 – Schematic facies model of the Paradox, Honaker Trail and lower Cutler Formation stratigraphy.

Table 1 - Lithofacies descriptions of the Paradox Formation

Fm.	Facies Number	Rock Type (Dunham, 1962)	Bedding	Grain Type, Sizes	Sedimentary Fabric	Fossils	Diagenesis	Depositional Environment
Paradox Formation	Carbonate Laminites / Subariel Exposure F5	Boundstone and mm Mudstone interbeds with local auto-breccia (Light Tan)	Medium bedded	Rare of pellioids, fine rip-up clasts and silt	Mm scale Bacterial/Algal binding, breccias	Rare Ostracods	Solution breccia	Supratidal to intertidal mudflats or shallow lagoons
	Silty Micaceous Carbonate Mudstone F4	Silty Argillaceous Carbonate mudstone (Light Gray, White)	Medium bedded	Muscovite, Biotite, Glauconite, Qtz Silt, Zircons, Suronic Dolomite Matrix	Burrow Mottled	Plant Debris	Dolomitization	Pro-delta?
	Phylloid Algal Tube Fossil - Chaetetid Bioherm F3	Phylloidal Bafflestone (Dark Brown, Tan)	No apparent bedding	Phylloid Algae, Micrite, Unknow oncoidal grains, Chaetetids	Massive no apparent fabric, Chaotic	Phylloid Algae, Chaetetid Sponge	Hydrothermal Dolomitization and Silicification	Open Marine, Tidal to Subtidal, within photic zone at fair weather wavebase
	Dolomite Ridge - Carbonate Wackestone - Mudstone F2	Skeletal Wackestone (Tan, Rusty Red interbeds)	Medium Bedded	Qtz Silt, reworked insitu skeletal grains	Wavy medium bedded, silicified sponge debris, re-worked skeletal grains	Chain Coral Debris, Productid Brachiopod Fragments, and echinoderm plates	Hydrothermal Dolomitization and Silicification	Open Carbonate Shelf
	Black Laminated Muds - Silty Argillaceous Dolomitic Mudstone F1	Silty Mudstone (Dark Gray)	Fine to thinly bedded, Fissile	Argillaceous, Silty quartz grains dolomitic micrite	Fissile Shale interbedded discontinuous competent lenses. Moderately Burrowed	Brachiopod and Brachiopod spines, Rare Echinoderm Plates	Matrix Dolomitization. Skeletal Grain Silicification	Offshore Marine

Table 2 - Lithofacies descriptions of the Honaker Trail Formation

Fm.	Facies Number	Rock Type (Dunham, 1962)	Bedding	Grain Type, Sizes	Sedimentary Fabric	Fossils	Diagenesis	Depositional Environment
Honaker Trail Formation	Phylloid Algal Bafflestone-Wackestone F12	Phylloid Bafflestone-Grainstone	Medium bedded	Neomorphosed phylloid agal plates	Medium bedded, brecciated appearance	Phylloid algae, forams	Neomorphism	Shallow marine within photic zone
	Channelized Conglomeratic Sandstone F11	Pebble to cobbles of arkosics, carbonates, black chert, and mudstone clasts. Medium-grained well-sorted sub-angular arkosic matrix	Channel geometry, maximum 10-20m thickness.	Arkosic matrix. Pebble to robbles of arkosics, carbonates, black chert mudstone rip-up clasts	Trough cross beds, planar tabular beds, l ateral accretion sets	None	Porosity development kaolinitization of feldspar grains	Fluvial, channel proximal and associated fluvial overbank.
	Intermediate Facies: Bryozoan Productid Packstone-Wackestone F10	Crinoidal Bryozoan Wackestone	Medium wavy bedded	Qtz Silt, reworked insitu skeletal grains	Wavy medium bedded, silicified sponge debris, re-worked skeletal grains	Chain Coral Debris, Productid Brachiopod echinoderm plates	Silicification	Open Carbonate Shelf
	Skeletal Cap Grainstone-Rhyolite and Crinoidal F8	Intraclastic Grainstone	Medium wavy beds	Fine- to medium-grained rounded intraclasts	Low angle laminations, trough geometry, dessication cracks	Crinoids, Echinoderms bryozoa	Pervasive Poikilotopic cements	Subtidal or Shoreface
	Sponge Spicule Packstone - Grainstones F7	Spicule Mudstone (Dark Gray, Black)	Thinly Bedded	Sponge Spicule Debris	Thinly bedded with carbonate mud drapes. Beds thicken upwards.	Sponge Spicules	Calcification	Lagoon
	Black Laminated Muds - Silty Argillaceous Dolomitic Mudstone F1	Silty Mudstone (Dark Gray)	Fine to thinly bedded, Fissile	Argillaceous, Silty quartz grains dolomitic micrite.	Fissile Shale interbedded discontinuous competent lenses. Moderately Burrowed	Brachiopod and Brachiopod spines, Rare Echinoderm Plates	Matrix Dolomitization. Skeletal Grain Silicification	Offshore Marine
	Dolomite Laminites / Subariel Exposure F5	Boundstone and mm Mudstone interbeds with local auto-breccia (Light Tan)	Medium bedded	Rare of pellioids, fine rip-up clasts and silt	Mm scale Bacterial/Algal binding, breccias	Rare Ostracods	Solution breccia	Supratidal to intertidal mudflats or shallow lagoons
	Red Silty Micaceous Mudstones and Thin Sands F9	Red Silty Micaceous Mudstones and Thin Sands	cm scale to 10s of meters.	Medium to fine dominantly quartz silt and argillaceous material, reddish brown, sometimes maroon.	Massive, often no apparent bedding to planar. Rooted	None	Oxidation/ Reduction of organic matter	Fluvial Overbank
	Ripple Cross-Laminated Calcareous Micaceous Sandstones F6	Ripple Cross-Laminated Calcareous Micaceous Sandstones	1m thick amalgamated 10-30cm beds	Siliciclastic	Cross-laminated to planar. Interbeds rooted	None	Porosity development through kaolinitization of Feldspar grains	Shallow Marine - Shoreface

Table 3 - Lithofacies descriptions of the Lower Cutler Formation

Fm.	Facies Number	Rock Type (Dunham, 1962)	Bedding	Grain Type, Sizes	Sedimentary Fabric	Fossils	Diagenesis	Depositional Environment
Lower Cutler	Coated Gastropod Brachiopod Mudstone-Packstone F12	Gastropod Wackestone	Wavy heavily bioturbated	Gastropods, Phylloid Algae Brachiopod Shells	Burrow mottled, carbonate nodules with fissile mud interbeds	Gastropods, Phylloid Algae Brachiopod Shells	Silicification	Lagoon
	Black Laminated Muds – Silty Argillaceous Dolomitic Mudstone F3	Silty Mudstone (Dark Gray)	Fine to thinly bedded, Fissile	Argillaceous, Silty quartz grains dolomitic micrite.	Fissile Shale Interbedded discontinuous competent lenses. Moderately Burrowed	Brachiopod and Brachiopod spines, Rare Echinoderm Plates	Matrix Dolomitization. Skeletal Grain Silicification	Offshore Marine
	Channelized Conglomeratic Sandstone F11	Pebble to cobbles of arkosics, carbonates, black chert, and mudstone clasts. Medium grained well-sorted sub-angular arkosic matrix	Channel geometry, maximum 10 -20m thickness.	Arkosic matrix. Pebble to ccobbles of arkosics, carbonates, black chert mudstone rip-up clasts	Trough cross beds, planar tabular beds, l ateral accretion sets	None	Porosity development kaolinitization of feldspar grains	Fluvial, channel proximal and associated fluvial overbank.
	Red Silty Micaceous Mudstones and Thin Sands F10	Red Silty Micaceous Mudstones and Thin Sands	cm scale to 10s of meters.	Medium to fine dominantly quartz silt and argillaceous material, reddish brown, sometimes maroon.	Massive, often no apparent bedding to planar. Rooted	None	Oxidation/ Reduction of organic matter	Fluvial Overbank

4.2.1 Paradox Formation Lithofacies Description and Interpretation

The Paradox Formation lithofacies (Figure 4.7, Table 1) observed in the study area consists entirely of the non-evaporite bearing facies of the uppermost Paradox Formation and represent primarily dysaerobic offshore (approx. >35m water depth) to a shallow water photic zone facies assemblages. The exposure of the Paradox Formation within the megaflap in total is 66 m with a basal unit of black laminated shales interbedded with competent lenses of silty argillaceous dolomitic mudstone (Figures 4.7 and 4.3). The uppermost beds form the dolomite ridge datum unit, which represents one of the most prominent visual features of the Paradox Formation in this area. The ridge contains several cycles of laterally continuous, resistant, ridge forming echinoderm brachiopod carbonate mudstone to wackestones with local accumulations of unknown tube fossil-phylloid algal-chaetedid sponge bioherms, silty micaceous carbonate mudstone and capping laminated dolomite. The laterally extensive dolomite ridge is used as a datum for measured section correlation throughout the field area. The Paradox Formation stratigraphic column (Figure 4.7) is a composite section of measured sections 1-5 providing a detailed composite section of the encountered lithofacies succession.

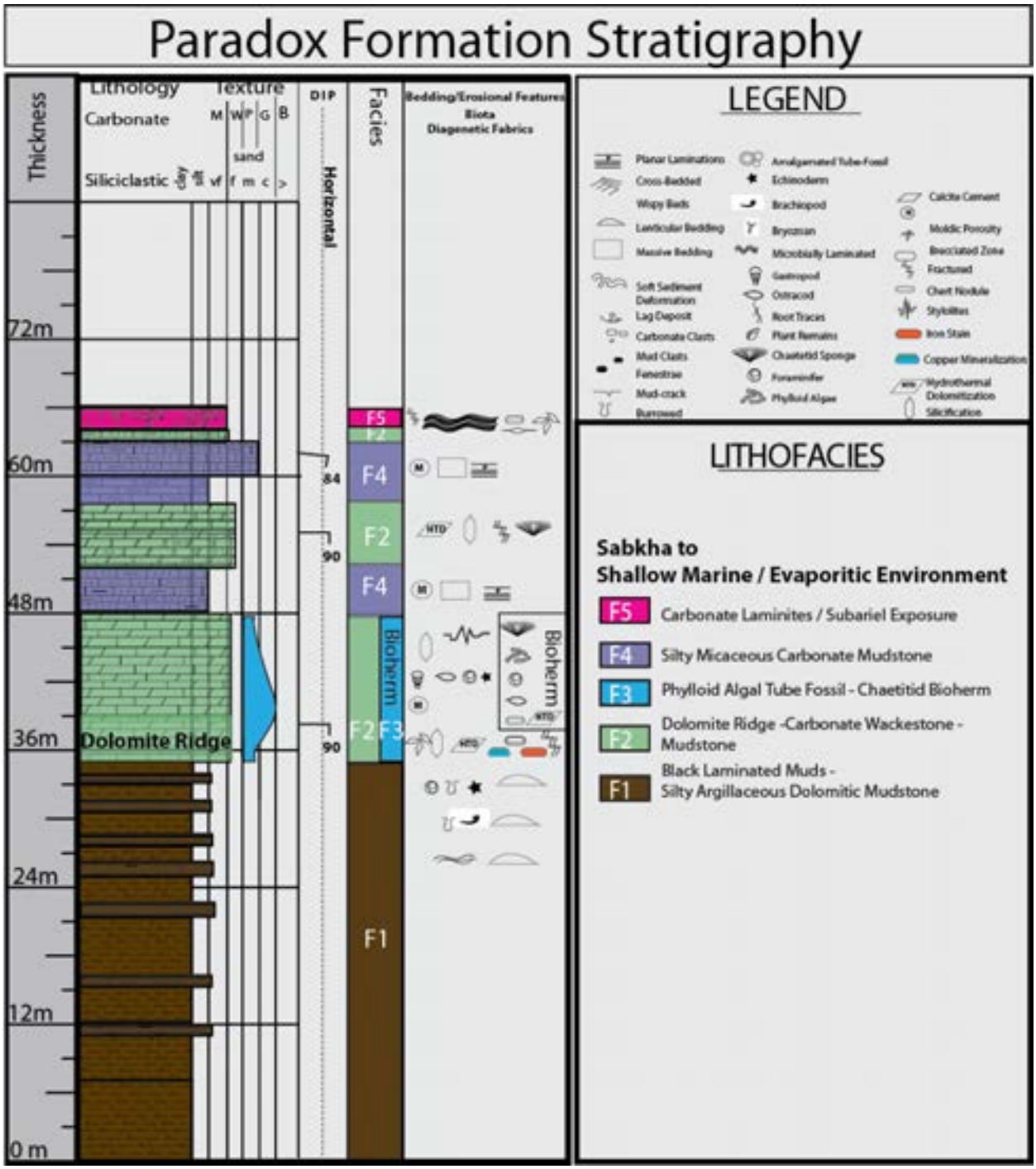

Figure 4.7- Composite stratigraphic column of the Paradox Formation lithofacies assemblage exposed within the first 66 meters of the megaflap panel. Column shows from right to left; thickness, carbonate rock type, average dip, facies color and alphanumeric classification used in text, bedding features, biota, and diagenetic fabrics. The basal facies F-1 shows Jurassic Morrison fluvial siliciclastics in either fault contact or angular unconformity with the adjacent vertical Paradox Formation.

Facies F-1: Black Silty Argillaceous Dolomitic Mudstone

Description

Facies F-1 forms the basal unit of the Paradox Formation within the megaflap and is exposed within measured sections MS-1, MS-2, and MS-3, and MS-5. The basal contact is either a normal fault or angular unconformity with the Jurassic Morrison Formation. Facies F-1 thickness is isopachous across the megaflap at approximately 36m. The lithology is a black (unweathered) to gray (weathered) silty mudstone, composed predominately of argillaceous material, subangular quartz, orthoclase and plagioclase silt (20-30%) within a dolomitic micrite and peloidal matrix. The facies consists of interbedded laminated and fissile silty argillaceous dolomitic mudstone with thin to medium bedded laterally discontinuous more competent beds of burrow-mottled dolomitic mudstones (Figure 4.8). The burrowed mudstone contains sparse skeletal fragments of normal marine invertebrates such as brachiopod shells and spines, trilobite fragments, and echinoderm plates. The interbedded clay-rich shales are highly fissile forming shale partings and disintegrate readily. The competent discontinuous lenses were sampled for the purpose of generating polished slabs and thin-sections (Figure 4.9). This facies description, stratigraphic location and age are similar to the black laminated mud (BLM) facies described by Goldhammer et al. (1991) along the western shelf of the Paradox Basin at the Honaker Trail locality. The laterally discontinuous more competent silty carbonate lenses increase in frequency of occurrence up-section towards one of the most prominent features of the vertical stratigraphic panel, a laterally continuous dolomitized and silicified dolomite ridge formed of Facies F-2 and F-3.

Figure 4.8- Outcrop photograph of facies F-1 of the fissile black silty argillaceous dolomitic mudstones interbedded with thin to medium bedded (10-20cm) laterally discontinuous more competent beds of burrow-mottled mudstones containing very rare skeletal fragments of normal marine invertebrates. The unit is vertical at 90 degrees with stratigraphic up direction to the left in this photo. Shale content increases downward (right) with cycles of competent medium-thin bedded units increasing in abundance to the left.

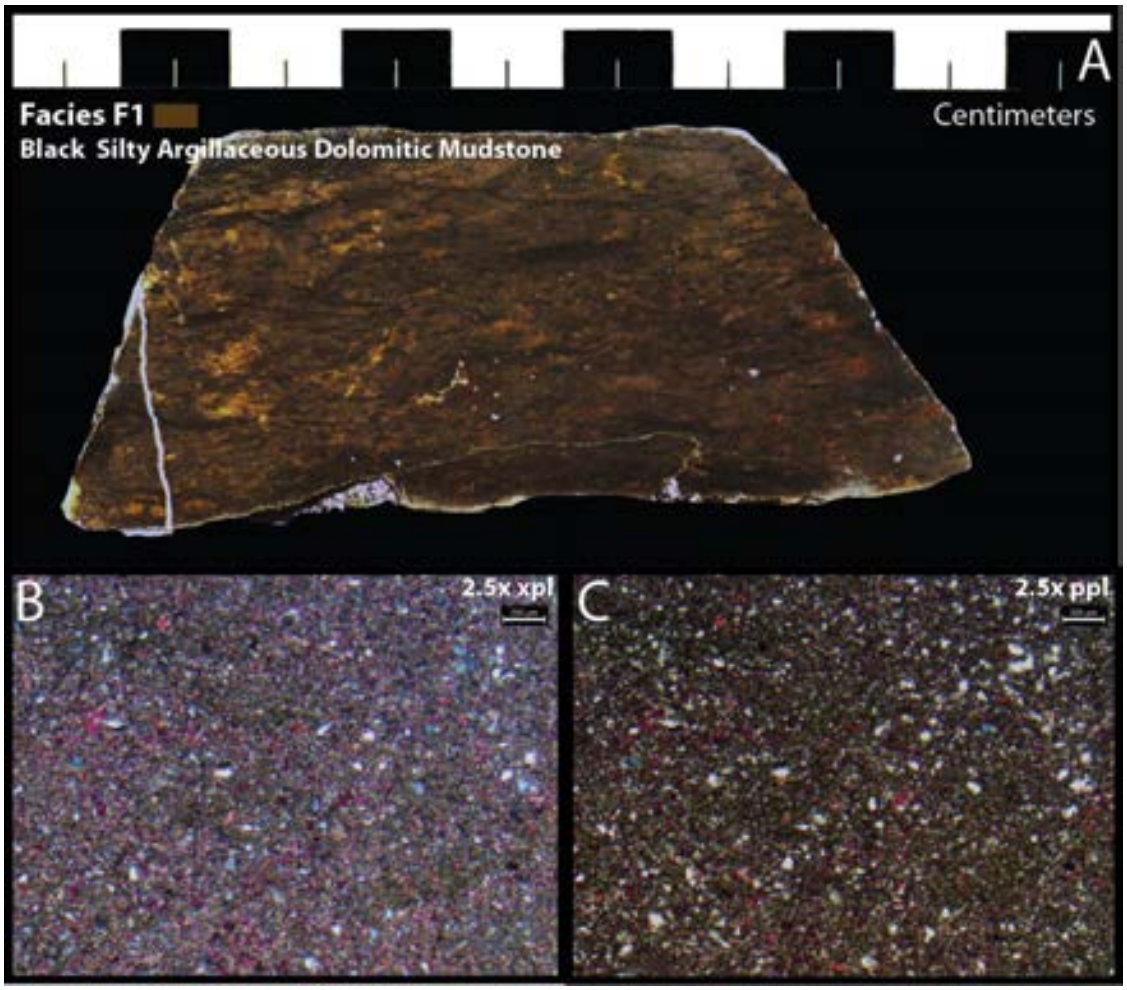

Figure 4.9- Polished hand sample and photomicrographs of facies F-1. (A) Polished hand sample of the more competent medium to thin bedded units showing burrow mottled fabric with dark wispy bands of argillaceous material. (B) and (C) are photomicrographs of thin-sections from the hand sample (A) and are shown under crossed polarized and plain light respectively. Thin-sections show dolomitic peloidal matrix with admixed silty subangular siliciclastic grains. Fossil fragments are rare and consist of normal marine invertebrates such as brachiopods and echinoderm plates. Thin-section was stained with Alizarin Red S to differentiate dolomite and calcite. Although dolomitic late dissolution of labile potassium feldspar grains enhanced pore space and was subsequently infilled and occluded with calcite.

Interpretation: Offshore dysaerobic shallow marine

The exposure of facies F-1 represents an initial offshore marine facies characteristic of shales of the Paradox Formation. The BLM facies described by Goldhammer (1994), and Facies F-1 described here are the lateral up-dip equivalents of the deep water (>150m) black sapropelic shales forming the source rock and regionally correlative 29 shale-evaporite cycles of the Paradox Formation (Peterson and Hite, 1969; Hite and Buckner, 1981; Goldhammer et al., 1994). The facies is devoid of fossils and suggest a restricted-marine origin and deep water (>150m) anaerobic conditions suitable for the preservation of organic matter (Goldhamer et al., 1994). However, anaerobic bottom conditions within an evaporite basin will persist at much shallower depths (≥35m) due to the development of a density-salinity gradient produced by intense evaporation of seawater during lowstands, generating dense bottom water hypersaline brines (Peterson and Hite, 1969; Hite and Buckner, 1981). Subsequent marine transgression will reflux toxic hypersaline brines onto the shelf developing anaerobic conditions in a shallow water setting (Byers, 1977; Hite and Buckner, 1981). Fissile and laminated mudstones of facies F-1 lack observable skeletal grains on outcrop and are extremely rare in thin-section. Fissile laminated intervals lack diverse marine fauna, which supports the interpretation of hypersaline and toxic marine conditions not suitable for a diverse array of organisms (Goldhammer et al, 1994). Though obscured by the fault contact at the base, the facies overlies the evaporite facies of the Paradox Formation suggesting lateral proximity to a restricted marine environment where evaporation concentrated dissolved solids and precipitation of halite and sulfate minerals such as gypsum and anhydrite (Peterson and Hite, 1969; Hite and Buckner, 1981). The competent well-cemented interbeds of burrow-mottled mudstones increasing in frequency up section suggest an increase in dissolved oxygen content in the waters (Goldhammer et al., 1994), which may be related to a shallowing upward trend, facilitating the

colonization by a more diverse array of normal marine invertebrates. An increase in normal marine fauna suggests an influx of normal marine conditions up-section and supports an offshore shallow marine environment below storm and fair weather wave base (Wengerd and Matheny, 1958; Hite and Buckner, 1981; Goldhammer et al., 1994; Weber et al., 1995; Grammer et al., 1996; Gianniny and Miskell-Gerhardt, 2009).

Facies F-2: Echinoderm Brachiopod Mudstone- Wackestone

Description

Near the top of the exposed Paradox Formation is a prominent laterally extensive feature referred to as the dolomite ridge (Figure 4.5, 4.10) The base of the dolomite ridge contains an isopachous, 3m thick, echinoderm-brachiopod mudstone to wackestone bed trending along strike across the entire exposed megaflap. The ridge weathers into an interbedded wavy rusty brown and light tan fabric, with the fresh surface exposing a light pink and gray coarse-crystalline dolomitized and silicified carbonate. The unit contains dark to light-colored, elongated, bed-parallel chert nodules containing silicified sponge debris, coarse-grained sand to gravel-sized skeletal grains of crinoids, undifferentiated echinoderm plates, brachiopod shells, foraminifera, rare ostracods, gastropods and rare phylloid algae detritus as well as other undifferentiated dolomitized shell fragments. Rip-up, coated micritic intraclasts are common. Admixed subangular quartz silt comprises approximately 20% of the recrystallized micritic matrix. Skeletal grains are rare and recrystallized due to intense dolomitization, and are only recognizable through characteristic geometries of shell fragments and petrographic properties such as the unit-extinction of ghost geometries of echinoderm plates (Figure 4.10). The initial 3m thick unit displays massive to wavy bedding with a sharp basal contact with facies F-1 and an interbedded gradational upper contact with facies F-4.

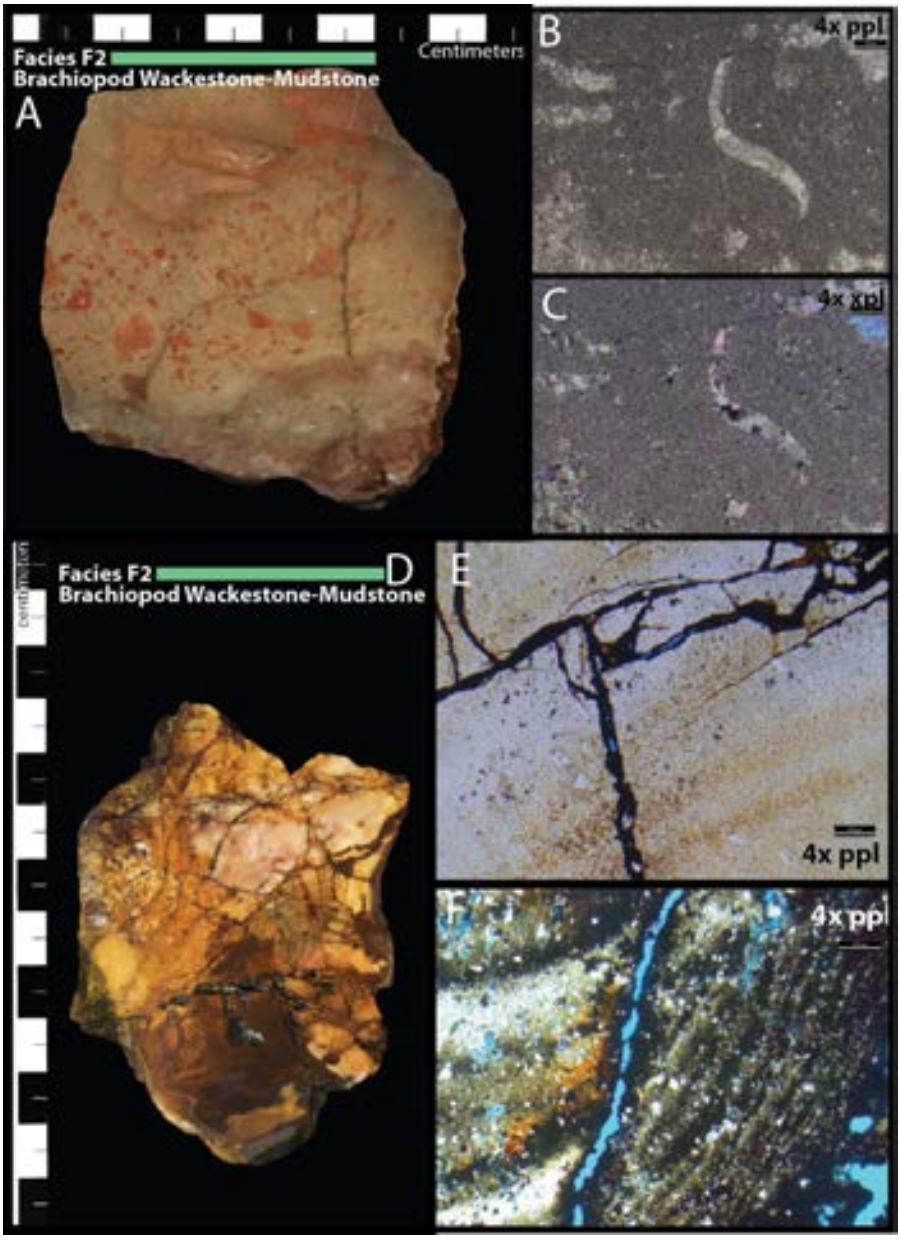

Figure 4.10- Hand sample photo and photomicrographs of facies F-2. (A) Polished handsample with centimeter scale bar showing depositional fabrics of angular recrystallized grains of echinoderm plates and phylloid algal detritus dispersed within a silty micritic matrix. Photomicrographs of thin-sections (B) and (C) shown under plain and crossed polarized light respectively reveal a recrystallized micritic matrix, brachiopod shells, phylloid algal detritus and the unit extinction of echinoderm plates. Images (D), (E) and (F) are polished handsample and photomicrographs of thin-sections under plain and crossed polarized light respectively. The sample is taken from a fault proximal position and show a highly fractured fabric, silicification, lisegag banding, and dark iron oxide cement lining fracture network.

Interpretation: Shallow marine-subtidal

Abundant normal marine fauna, light (unweathered) color, and phylloid algal detritus indicate a shallow water-subtidal (approx. 5-15m), well oxygenated depositional environment within the photic zone. Lateral association with biohermal facies F-3 further support a shallow water setting under normal marine conditions (Figure 4.11, 4.12).

Facies F-3: Phylloid Algal, Tube Fossil - Chaetitid Bioherm

Trending along strike of facies F-2, facies F-3 occurs as pods of a porous and permeable globular dolomitized carbonate outcrop adjacent to the vertical beds of the dolomitized ridge (Figure 4.11). The deformed carbonates outcrop as isolated patches of columnar growths 5 meters wide and 3-4 meters in thickness or as laterally continuous pods for 10's of meters. The outcrop is lichen covered, weathers a dark brown to white-unweathered, and has no apparent bedding. The facies is observed to have a highly porous and permeable framework with a variety of stromatolitic fabrics, abundant phylloid algal plates, unknown amalgamated tubular fossils (Figure 4.12), and fully articulated domal to hemispherical *chaetetes* heads (< .3 m) (Figure 4.12). Abundant chert nodules with an observable microporous fabric and radial structure are found within the biohermal carbonates. Many of the nodules are disarticulated coralline sponge fragments however some are whole *chaetetes* heads (Figure 4.12). Other fabrics are obscured through overprinting by hydrothermal dolomitization (Figure 4.13). Facies F-3 overlies Facies F-1 or is fault bounded at the base by down dropped Jurassic Morrison fluvial siliciclastics.

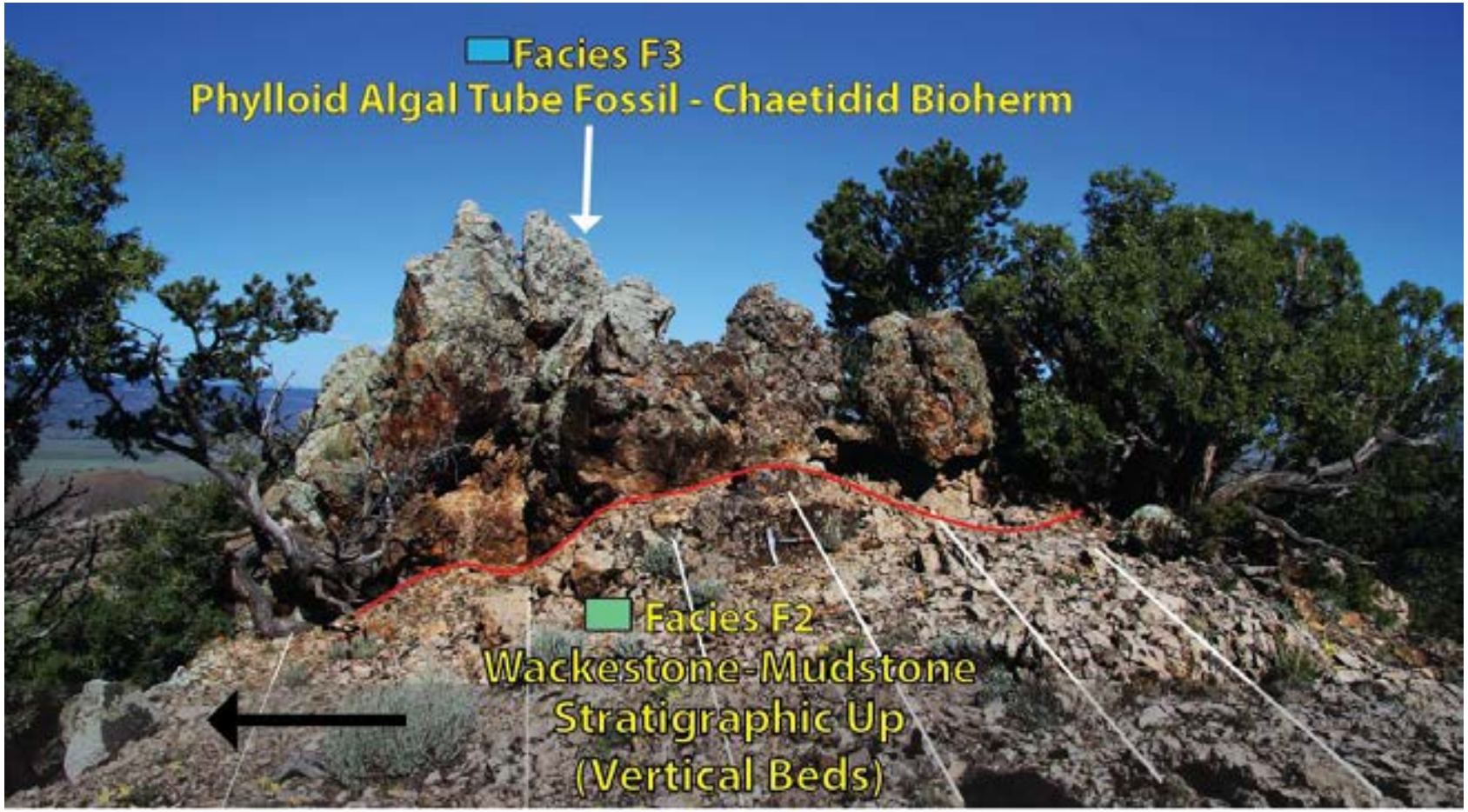

Figure 4.11- Outcrop photograph of the phylloid algal tube fossil-chaetedid bioherm of facies F-3, with black arrow showing stratigraphic up direction of the vertical unit and red line showing distinct separation of the two facies. Moving along depositional strike of the dolomite ridge of facies F-2 these globular biohermal structures are encountered as 4 meter tall and 5 meter wide columnar structures within facies F-2 or more laterally continuous assemblages restricted to the depositional thickness of facies F-2.

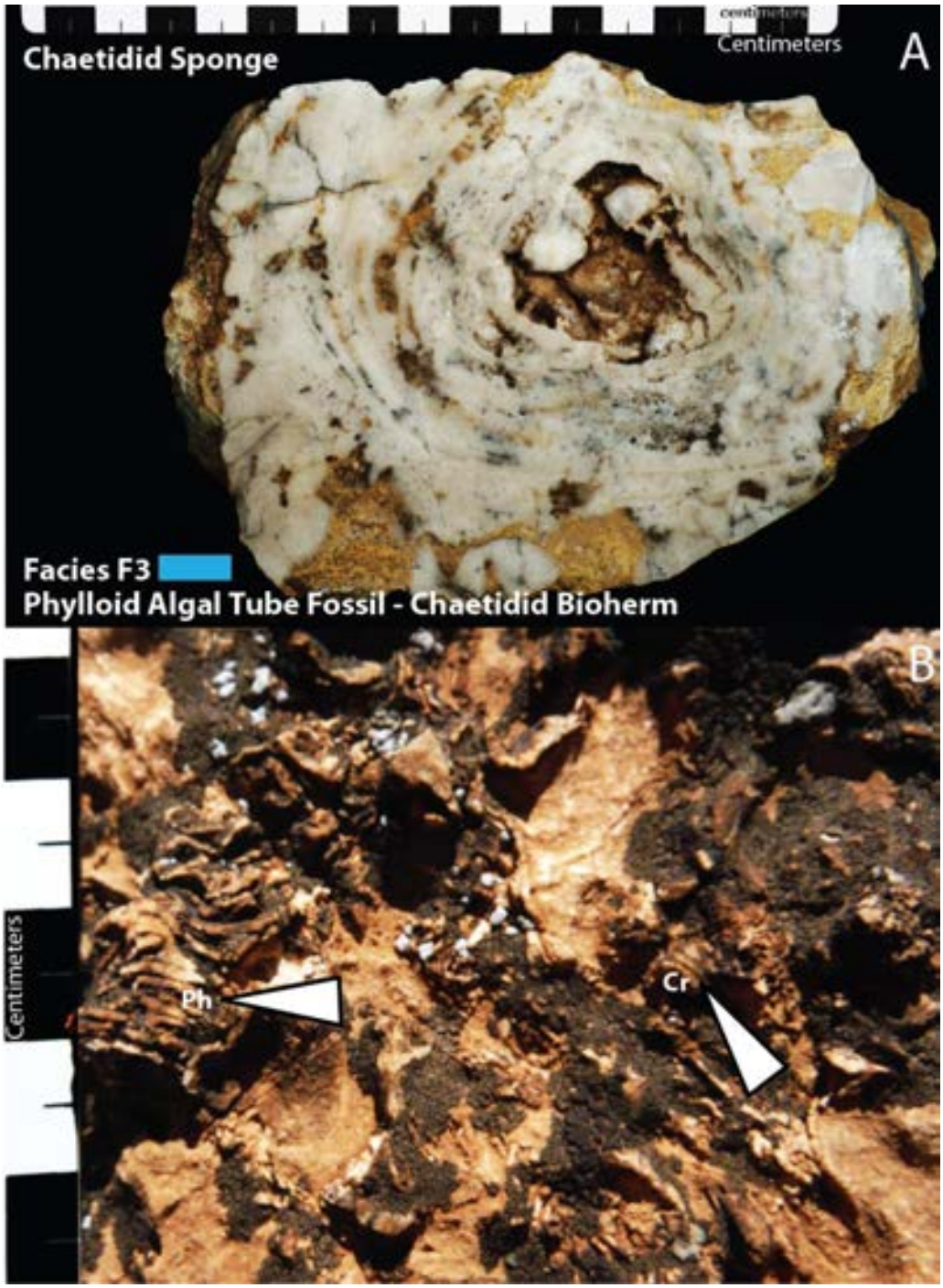

Figure 4.12- Polished fossil specimen of a fully articulated chaetidid sponge with centimeter scale bar (A) and outcrop photograph of facies F-3 (B) with white arrows pointing to stacked phylloid algal detritus (Ph) and crinoid stems (Cr). The outcrop is lichen covered (black areas) and golden brown with a distorted fabric typical of accumulations of colonizing marine organisms.

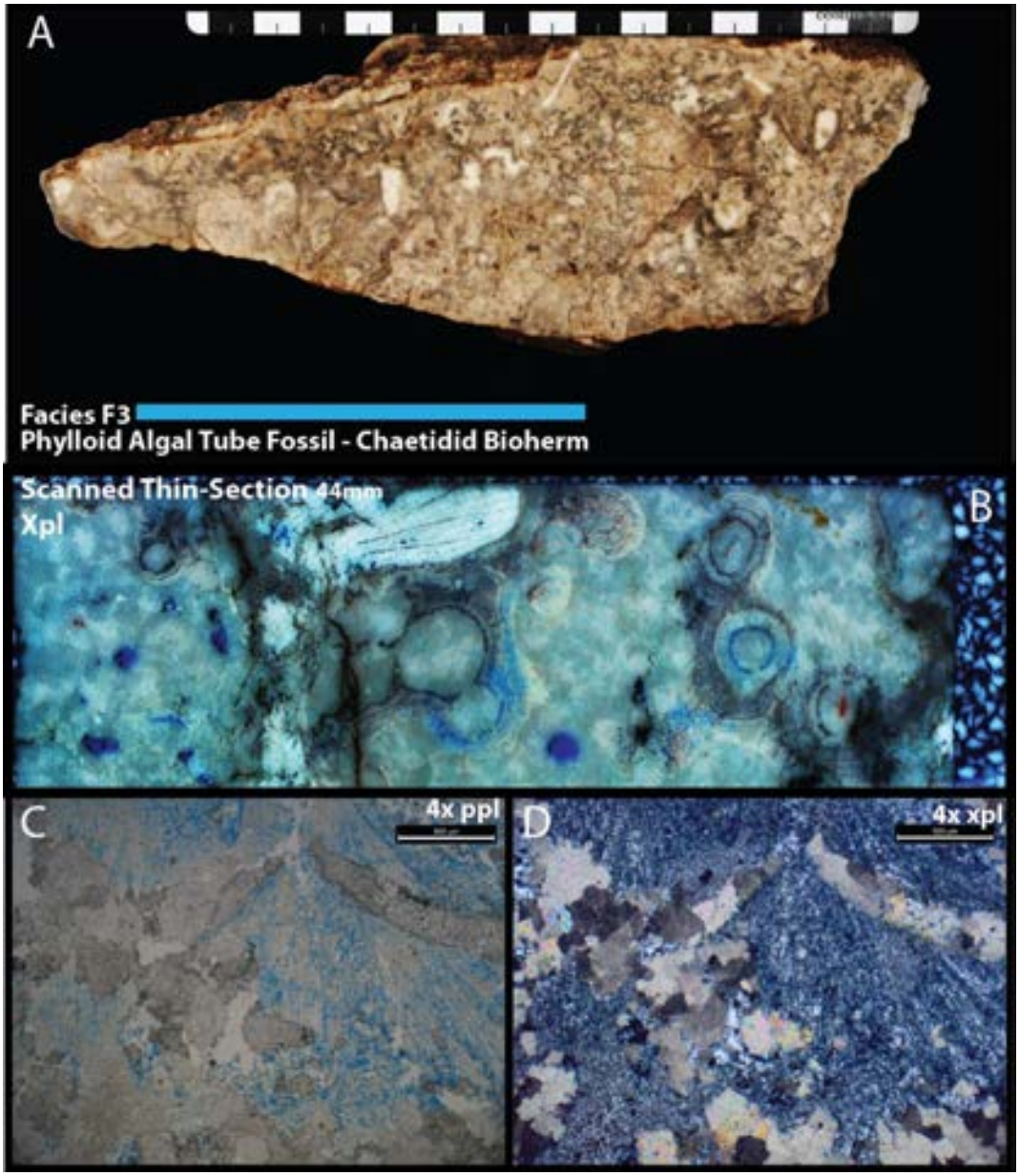

Figure 4.13- Polished hand sample of the phylloid algal tube fossil – chaetidid bioherm of facies F-3 (A) with centimeter scale bar of facies F-3 showing brown to white unweathered color with a variety of stromatolitic fabrics, tube fossil, and phylloid algal plates. Image (B) is a scanned thin-section 44mm across under crossed polarized light showing abundant amalgamated tube fossils of unknown origin. Photomirographs (C) and (D) under plain and crossed polarized light respectively, show dolomitized elongated rectangular curved shapes typical of phylloid plates within silicified radial fibrous cements.

Interpretation: Subtidal Bioherm

Local biohermal accumulations of calcareous chaetitid sponges, amalgamated tubular fossils and phylloid algae likely existed as patch reefs along a broad open well-circulated carbonate shelf with low turbidity, normal marine salinity, and within the photic zone at fair-weather wave base or near surface (0-15m below sea-level). Chaetitids are principally noticeable in Carboniferous stratigraphy and are present throughout North America, Eurasia, and South American locations (Suchy and West, 2001). These coralline sponges are commonly the dominant frame-building organisms of small bioherms in relatively shallow water of the Carboniferous (Connolly et al., 1989). Modern day analogues are common in shallow water reef environments in the Bahamas and western Pacific (Hartman and Goreau, 1975). Although modern coralline sponges show low tolerance to light and turbidity, ancient chaetitid sponge facies assemblages appear to thrive within the photic zone and even within wave base or near sea level environments in high energy conditions (West, 1988). Furthermore, along the western shelf of the Paradox Basin, the up-dip equivalents to transgressive sapropelic organic rich black shales of the Paradox Formation are abundant phylloid algal mounds interpreted to be deposited within well circulated, shallow, oxygenated, normal marine waters within the photic zone and at or below fair-weather wave base, further supporting this shallow water interpretation (Peterson and Hite, 1969; Goldhammer et al., 1994)

Facies F-4: Silty, Micaceous Dolomitic Mudstone

Above the dolomite ridge contact, silty micaceous dolostones are interbedded with cycles of facies F-2. These dolostones are a greenish gray (weathered) to light gray (unweathered) in

color. The sequence is a 3-4m thick, heavily bioturbated unit with 10 cm to 30 cm thick beds or is locally massive with no apparent bedding. Thin interbeds, <10 cm, of micaceous dark gray. clay-rich shales are abundant. The facies is primarily dolomitized carbonate mud (50%-70%) with increasing amounts upsection to approximately 50-60%, subangular quartz and potassium-feldspar silt with remaining volume containing abundant micaceous and argillaceous debris, glauconite, siderite, rare sponge spicules, and rare echinoderm plates. The facies contains distinct burrows, macerated plant debris, black organic material lining moldic pores, and abundant argillaceous material within a coarsely-crystalline dolomitized carbonate mud matrix. Burrows are infilled with dolomite mud, and lined with argillaceous and micaceous debris, forming dark wispy bands across the face of the sample (Figure 4.14a). The unit also contains abundant abraded detrital zircons (Figure 4.14c)

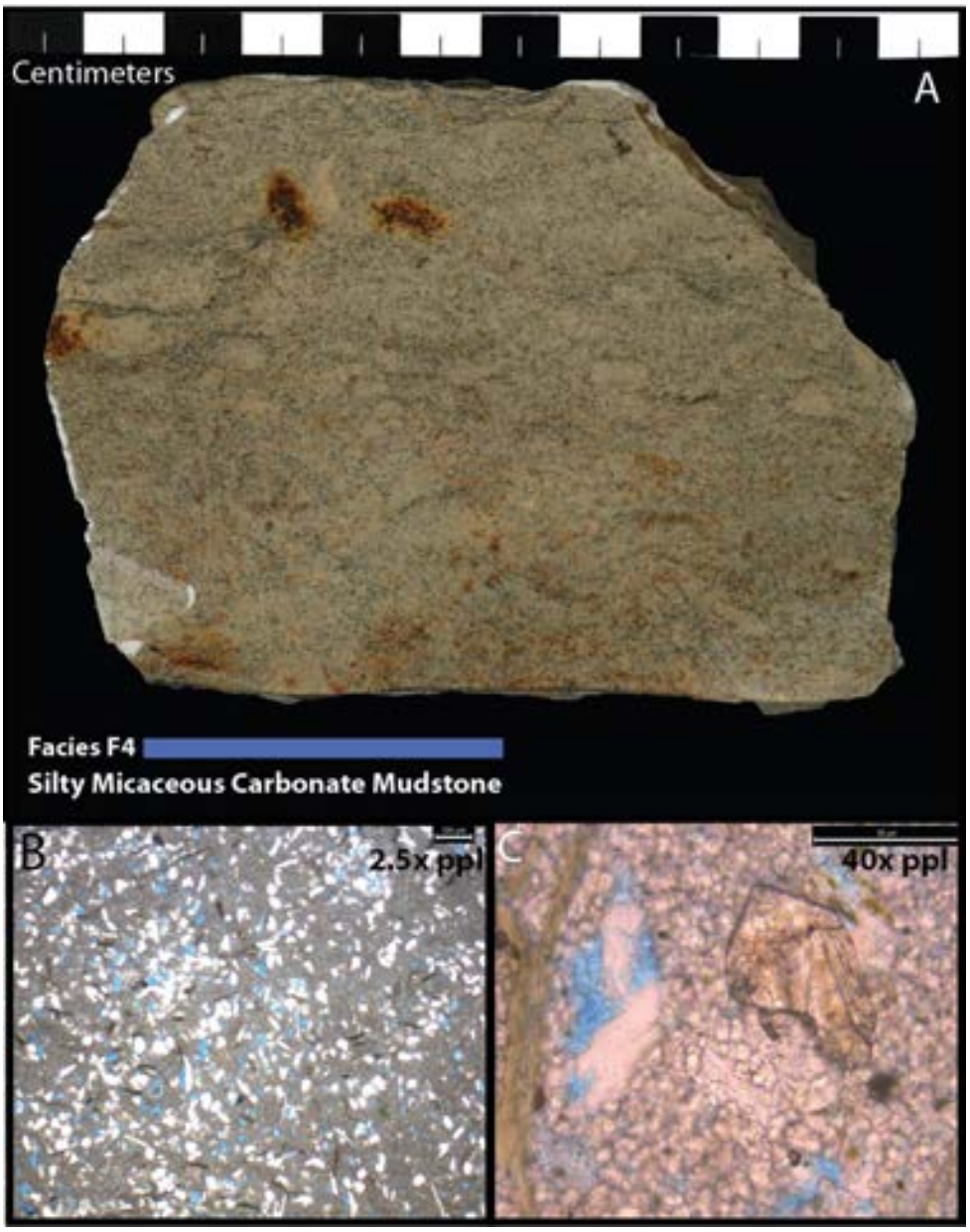

Figure 4.14- Photo of polished hand sample of the silty micaceous carbonate mudstone facies F-4 (A) with centimeter scale bar. Sample contains abundant elliptical burrows infilled with carbonate mud matrix, red oxidation fabrics of reduced plant debris, and dark wispy bands of micaceous and argillaceous material. Photomicrographs of thin sections (B) and (C) under plane and crossed polarized light respectively show a near 50% split between carbonate mud matrix and silty subangular quartz silt. Sample contains abundant gluaconite, mica, plant debris, high relief brown crystals of siderite, and abundant detrital zircons (C). Photomicrograph (C) shows euhedral pore space once occupied by labile potassium feldspar grains now kaolinitized.

Interpretation: near shore tidal to coastal marine

The presence of abundant plant debris, and low normal marine invertebrate diversity and abundance indicates a proximity to continental detrital influx in a marginal marine environment.

Facies F-5: Laminated Dolomite

Description

Overlying facies F-4 are laminated dolomites in .- 1 m, which are laterally continuous across the field area providing excellent marker beds for correlation. The laminites locally transition laterally to auto-brecciated fabrics. The dolomitic lithofacies consists of laminated to stromatolitic fabrics, containing fenestrae, mudcracks, and lack normal marine fauna (Figure 4.15). Locally along strike the beds become brecciated with fractures filled with coarsely-crystalline calcite cement. The unit is capped by planar laminated dolomite beds cross-cut by calcite-filled, centimeter scale downward narrowing fissures interpreted as mudcracks, which marks the top of the Paradox Formation in the megaflap study area.

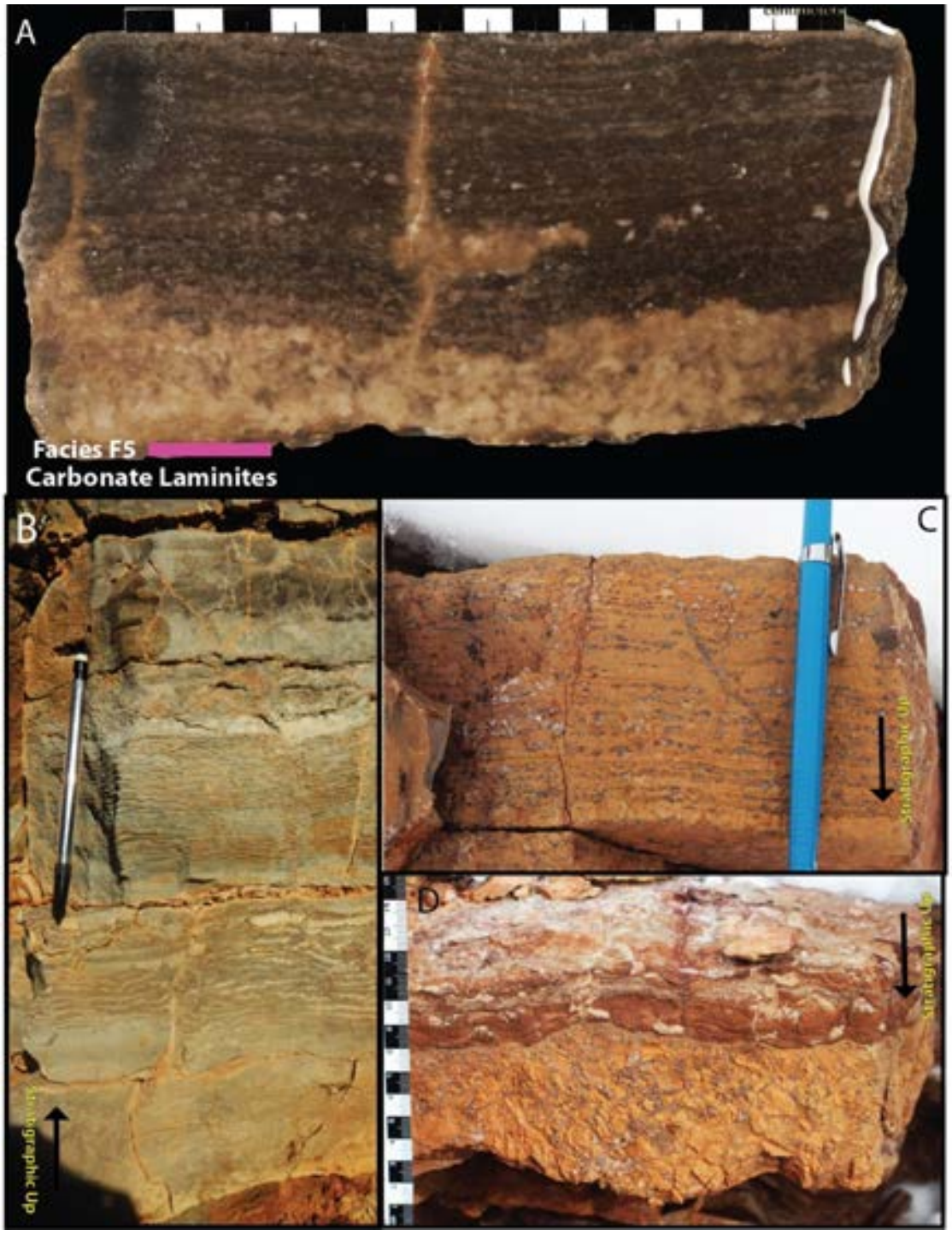

Figure 4.15- Photo of polished hand sample (A) of dolomitic laminite facies F-5 showing crinkly laminated fabric common of cyanobacterial mats found in tidal flat depositional environments. Outcrop photograph (B) and (C) with black arrows indicating stratigraphic up directions shows brecciated cap a common fabric associated with subaerial exposure of this facies. Outcrop photograph (C) shows occluded vuggular porosity developed from the trapping of gas bubbles from decaying progressively layered cyanobacterial accumulations.

Interpretation: peritidal/karst

Laminated fabrics observed in the field are interpreted to be of microbial origin most likely resulting from photosynthetic cyanobacterial mats and contain similar features discussed by (Riding, 2000). These biogenic fabrics are most commonly found in supratidal environments in modern arid climates (Shinn, 1983). The observation of elongated vugs, interpreted as fenestrae are indicative of microbialite deposition and resulting decay and degassing of organic material (Shinn, 1968). Fenestrae typically undergo immediate early marine cementation preserving the initial geometry of these voids (Figure 4.15c). Mudcracks, as well as other desiccation features are commonly observed as the result of sub-aerial exposure in intertidal zones; observed as vertical tapering down fissures occluded with calcite or overlying sediments (Shinn, 1968). Dispersed silt-sized quartz grains observed in thin-section are indicative of an environment proximal to a clastic source and are commonly brought in through eolian processes or washed into the depositional environment and bound and trapped by encrusting cyanobacterial mats (Shinn, 1968).

Brecciation of depositional laminites may form in response to: (1) repeated exposure and desiccation of carbonate sediments, which often form soils in modern carbonate environments in subaerial exposure settings (Esteban and Wilson, 1993). These systems however have poor preservation potential throughout the geologic record, often only preserving underlying caliche and karst fabric (Esteban and Wilson, 1993), or (2) the influx of meteoric water resulting in the dissolution and diagenetic modification of carbonate material or evaporites such as anhydrite and halite resulting in collapse. Brecciation, dissolution, and laterally disrupted laminations common of facies F-5 indicate periods of sub-aerial exposure in a semi-arid environment (Esteban and Wilson, 1993). Karst features are derived from a diagenetic process that results in the dissolution of calcium carbonate, irregular topography generated from subsurface caves and fissures, as well as reprecipitation of dissolved calcium carbonate. Laminations, collapse features, and keystone vugs, are typical of peritidal carbonate depositional environments (Shinn, 1968, 1983).

4.2.2 Lithofacies of the Honaker Trail Formation

The Honaker Trail Formation conformably overlies the Paradox Formation in the study area and is in turn overlain with angular unconformity by the Lower Cutler Formation. The Honaker Trail contains 3 dominantly siliciclastic lithofacies including: (F-6) ripple cross-laminated calcareous micaceous sandstone; (F-9) red, silty, micaceous mudstone and thin bedded sandstone; (F-11) channelized conglomeratic sandstone; and 5 dominantly carbonate lithofacies including: (F-5) laminated dolomite (described under Paradox Formation lithofacies), (F-7) sponge spicule packstone – grainstone, (F-8) skeletal packstone to grainstone), (F-10) bryozoan, brachiopod (productid) wackestone to packstone, and (F-12) phylloid algal bafflestone to wackestone, (Figure 4.16). The depositional setting of the siliciclastic facies range from fluvial to marine shoreface depositional settings. The carbonate lithofacies range from restricted lagoon to open marine shelf depositional settings.

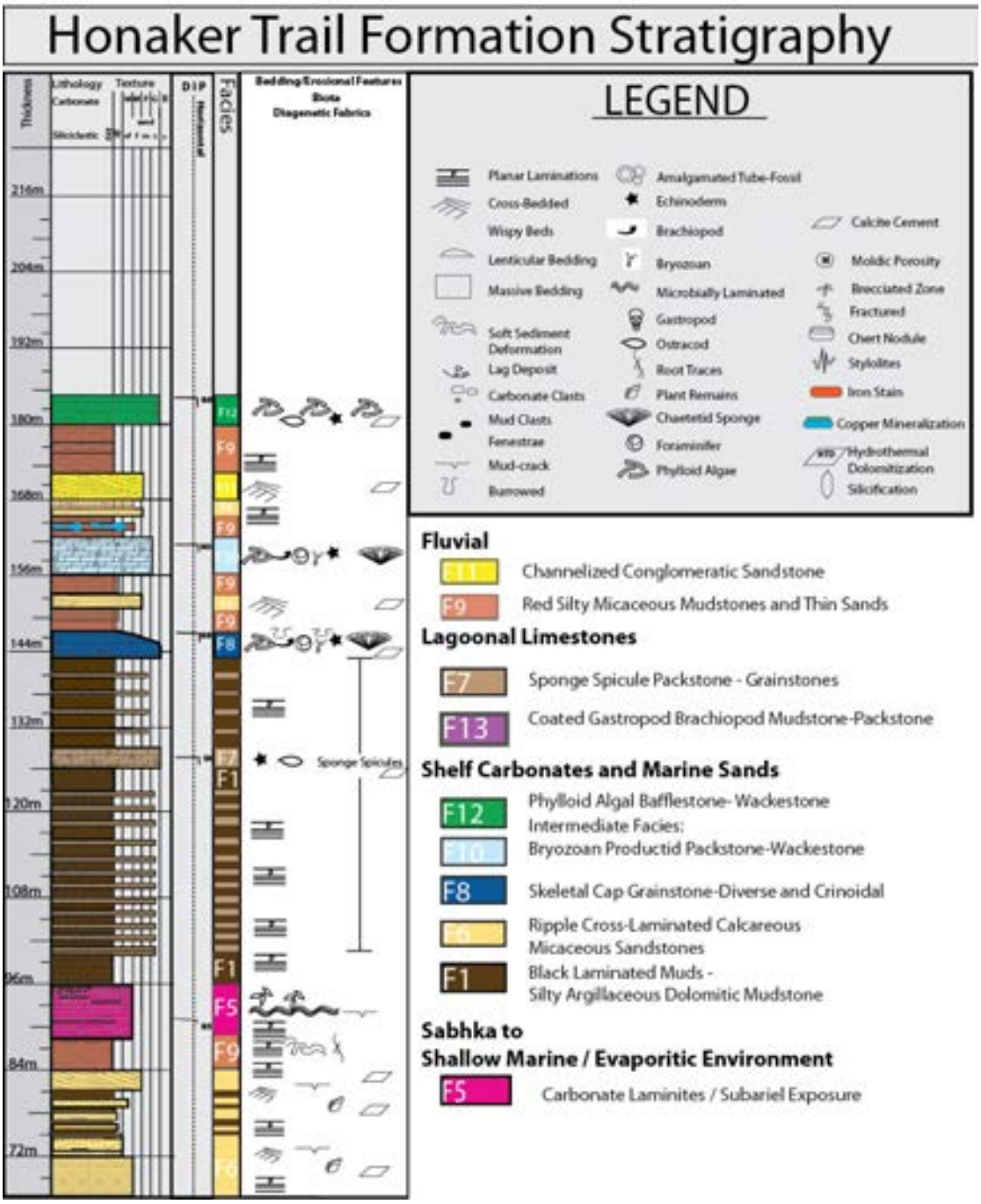

Figure 4.16: Composite stratigraphic column from measured sections 1-5 of the exposed Honaker Trail Formation. The column shows from left to right, thickness, lithology, facies type, diagenetic and sedimentary fabrics and faunal assemblage.

Facies F-6: Ripple Cross-Laminated Calcareous Micaceous Sandstone

Description

The basal succession of the exposed Honaker Trail Formation is composed of light gray and tan calcareous siltstones and sandstones similar to the quartz sandstone facies (QSF1 and QSF2) described by Goldhammer et al. (1994) along the western shelf of the Paradox Basin at the Honaker Trail Type locality. The basal succession of this facies is approximately 25m thick with an erosional base and gradational top. The unit contains thin 1-5cm dark gray calcareous siltstones interbedded with either 2-10cm thin bedded asymmetric rippled and cross-laminated micaceous fine-grained sandstone or thick bedded 10-20cm planar laminated tabular siltstone to fine-grained calcareous sandstone beds. The weathered surface of the outcrop is tan to brownish red, with the fresh surface showing greenish brown or red coloration. Sandstone intervals form laterally discontinuous cross-bedded lenses or laterally continuous sand sheets with planar tabular surfaces. Small-scale low-angle ripple-cross stratification is very common amongst discontinuous sand lenses and form asymmetric current ripples or wave ripples on the bed tops. Polished hand samples taken from this lithofacies show a heterolithic fabric with darker micaceous drapes capping the ripple cross-laminae (Figure 4.18). Other fabrics within this unit are polygonal centimeter scale networks of mudcracks with upturned edges and mud filled tapering down fissures, rain imprints, and salt hoppers (Figure 4.17d). Burrows and burrow mottled fabrics are very rare within this lithofacies. Petrography shows abundant muscovite (10-15%) disseminated or concentrated as preferentially aligned masses along bedding planes, and minor amounts of glauconite, chlorite and plant debris (<1-2%) and no clay fraction (Figure 4.19). The sandstones are well-sorted, silt to fine-grained, sub-angular micaceous quartz arenites with peloidal micrite (30-50%). Petrographic analyses shows a moderately compacted fabric with no signs of chemical compaction such as

interpenetrating quartz grain contacts. Much of the micaceous debris and micrite facilitate grain rotation and mechanical compaction, thus limiting grain contacts to mostly planar and significantly preserving porosity.

Figure 4.17: Outcrop photographs from the ripple cross-laminated calcareous and micaceous sandstones. A) stacked laterally continuous sand sheets and discontinuous ripple cross laminated thin sand interbedded with siltstones. B) Planar tabular to massive bedded sandstone. C) Ripple cross-laminated micaceous sandstone and D) polygonal network of mudcracks bounded by thinly laminated wave rippled siltstones.

Figure 4.18: Polished hand-sample of facies F-6. Sample shows heterolithic ripple cross-laminations with cross-strata capped by darker micaceous sediments with increasing abundance towards the top. The sample shows the variation is color observed in outcrop from gray-green-tan to red.

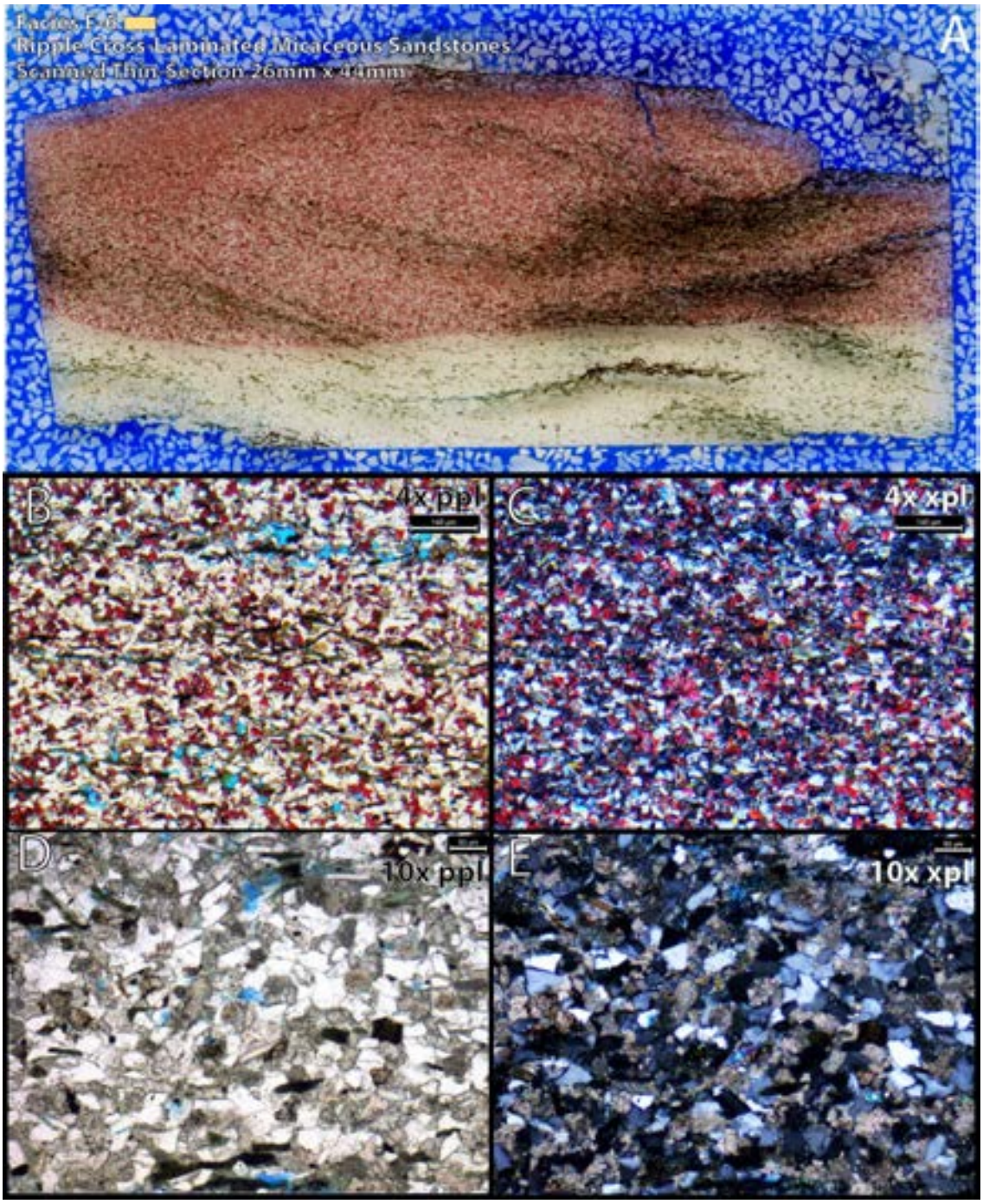

Figure 4.19: Scanned thin section (A) and photomicrographs (B,C, D,E) of facies F-6. The scanned thin-section is standard 26mm by 44mm and is shown under plain light to highlight micaceous debris capping the ripple cross-laminated fabric. Photomicrographs under plain and crossed polarized light show siliciclastic material dominated by micrite and monocrystalline quartz and admixed to preferentially aligned micaceous debris. The sands have rare macerated plant debris and lack intergranular clay.

Interpretation: Transitional Marine High Energy Shoreface to Intertidal (5-15m water depth)

Quartz sandstone and siltstone facies of the Paradox Basin are commonly interpreted as having an eolian provenance with subsequent marine modification and share similar fabrics with other fine-grained quartz sandstones of upper Paleozoic mixed clastic and shallow marine carbonate systems such as in the Delaware Basin of West Texas (Driese and Dott 1984; Borer and Harris, 1989; Goldhammer et al., 1994). Evidence supporting a subaqueous depositional system include: (1) the presence of detrital muscovite preferentially aligned to bedding planes indicative of water-lain sedimentation, as these minerals are readily winnowed from wind-blown sands (Borer and Harris 1989); (2) lack of large scale high-angle crossbedding with slipface avalanche laminae or inverse grading (Borer and Harris, 1989)and other diagnostic eolian sedimentary structures that would suggest aqueous interdune environments; (3) Low-angle ripple cross-stratification and planar to tabular cross bedded fabrics are common sedimentary fabrics found in high-energy zones of nearshore environments (Miall, 2013); (4) Thinly bedded rippled and mudcracked heterolithic beds with mudrapes are further interpreted as shallow subtidal to intertidal deposits based upon modern analogs of sandy tidal flats (Reineck and Singh, 1980). Although some workers interpret rippled and mudcracked mixed clastics sandstones described here as interdune environments, demonstrable eolian sedimentary fabrics however are missing in this unit; (5) drusy calcite cement typical of early marine cementation.

Numerous researchers of the Paleozoic Delaware Basin, for instance, interpret sandstones within the analogous mixed clastic systems of the Yates Formation as eolian depositional systems tied to sea-level lowstands and subsequent progradation of dune complexes across an exposed shelf (Silver and Todd, 1969). However, the siliciclastics of the Yates Formation have also been interpreted as being transported across the shelf during relative sea-level rise as described by

Candelaria (1989). Borer and Harris (1989) however invoke both processes, eolian transport during sea-level lowstands and subsequent marine reworking during relative sea-level rise. This two stage origin best explains the clay-free well-sorted silt-sized quartz sands of the Honaker Trail Formation, as they are bound at the base by subaerial exposure of facies F-5 and transition into deeper water facies upward. Thus facies F-6 occupies the boundary between an exposed shelf and relative sea-level rise supporting the interpretation that these sands may have an initial eolian provenance and were subsequently reworked along a high-energy shoreface to intertidal depositional system. Numerous modern analogues exist for a mixed clastic depositional system such as this, the most notable and well documented example of laterally adjacent eolian siliciclastics and shallow marine carbonates is described from the Persian Gulf by Shinn (1973) along the leeward margin of the Qatar peninsula.

Facies F-7: Sponge Spicule Packstone to Grainstone

Description

The sponge spicule packstone to grainstone facies described here is equivalent to the description of the sponge facies named by Pray and Wray (1963) and descriptions by Goldhammer et al. (1994), at the Honaker Trail Type locality along the western shelf of the Paradox Basin. Facies F-7 gradationally overlies facies F-1(black, silty, argillaceous dolomitic mudstone, but has a sharp upper contact with overlying facies (similar in depositional style to facies F-1) (Figure 4.20). The competent carbonate beds are about 10-20cm thick and increase in thickness and abundance upward towards a 3m thick prominent ridge of wavy bedded, laminated limestone interbedded with thinly bedded, <1cm silty argillaceous and micaceous mudstone drapes. The competent limestone beds weather to a brownish tan with fresh surface showing a dark gray almost

black shale appearance with abundant black and dark gray chert nodules. Initial outcrop observations interpreted the carbonate succession as silty mudstones of facies F-1 due to lack of observable skeletal grains and similar depositional style. However, upon thin-section analysis, the competent carbonate beds interbedded with argillaceous mudstones are observed to be sponge spicule packstones to grainstones (Figure 4.21). Needle-like siliceous sponge spicules (now calcified) form wispy laminated fabrics of preferentially aligned masses parallel to their long axis. The primary skeletal grain type observed are siliceous sponge spicules (>50%) with rare ostracods and echinoderm spines (<1%), disseminated sub-angular quartz silt (<5%), and minor amounts of pyrite (<1%) with the remainder dominated by argillaceous material and a micrite mud matrix often silicified.

Figure 4.20 – Bedding style of facies F-1

Figure 4.21 - Outcrop photograph of the sponge spicule grainstone of facies F-7. The unit is bound on the right by a gradational contact with Facies F-1. The competent beds are dominantly spiculitic and interbedded with wispy micaceous laminations that form shaley partings.

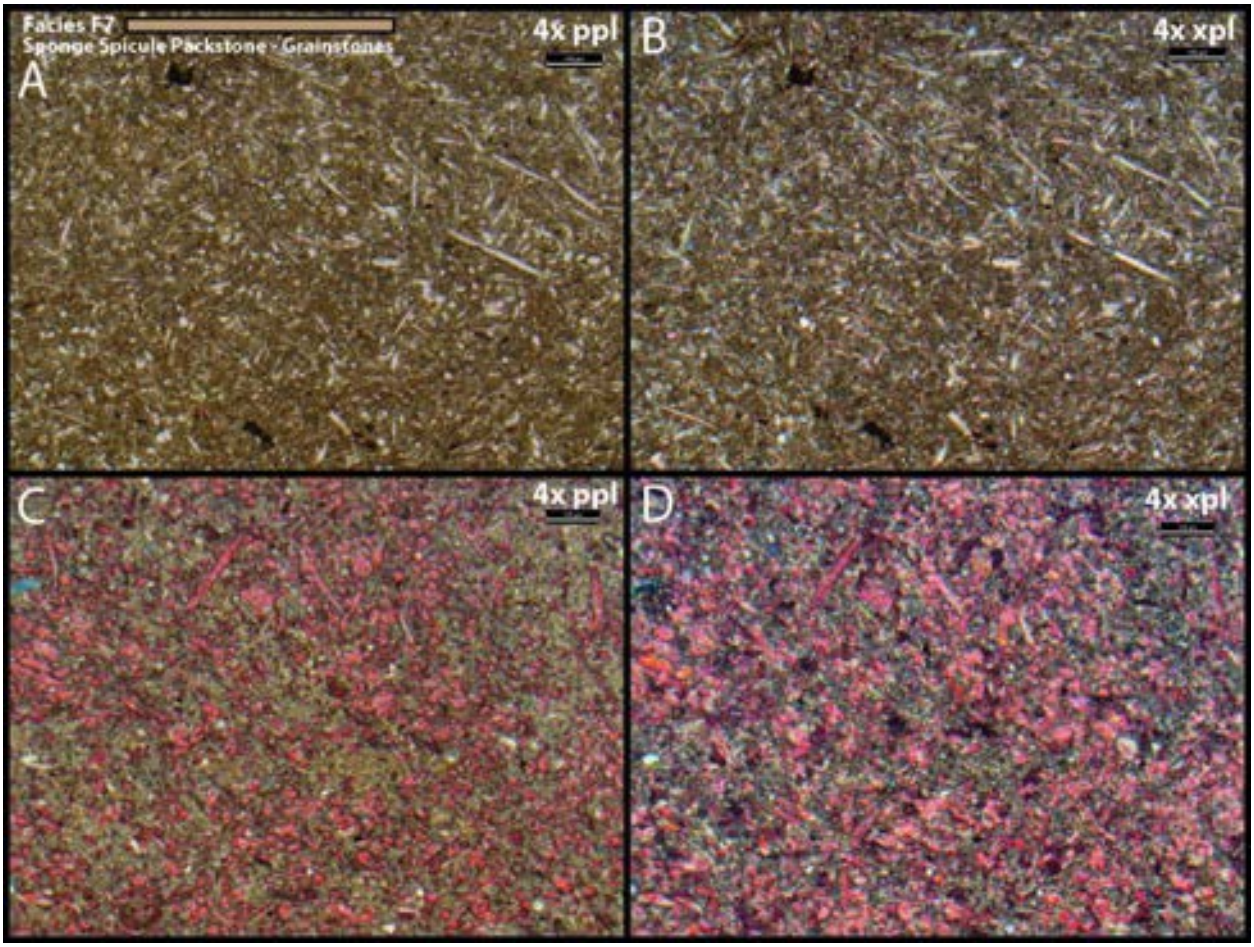

Figure 4.22 - Photomicrographs of facies F-7 of the sponge spicule grainstone. Sponge spicules are calcified and form a grain supported framework of needle-like spicules.

Interpretation: Restricted Low Energy Siliceous Sponge Lagoon (<10m water depth)

Lack of burrowing, dark color, thin laminations, occurrence of pyrite and the presence of a low diversity fauna are characteristics of marine conditions not suitable for a diverse array of marine invertebrates (Peterson and Hite, 1969; Hite and Buckner, 1981). Because sponges can tolerate extreme environmental conditions relative to normal marine fauna, they may become pervasive under marine conditions that favor minimal competition (Pray and Wray, 1963; Suchy et al., 2001). Environmental conditions supporting a low diversity fauna likely resulted from the circulation of hypersaline stagnant basinal waters onto the shelf during relative sea-level rise (Pray and Wray,

1963; Grammer et al., 1996) resulting in the deposition of facies F-1 at the base of this facies. Marine conditions likely improved enough to allow for subsequent colonization by a single faunal assemblage of soft-bodied organisms under dysaerobic conditions (Pray and Wray, 1963; Goldhammer et al., 1994; Grammer et al., 1996). Hypersaline dysaerobic marine conditions such as these would preserve organic matter resulting in the dark color of the unweathered surface as well as significantly decreasing abundance of normal marine invertebrates, limiting burrowing and preserving a thinly laminated sedimentary fabric. This facies specific depositional environment, specifically regarding water depth, is difficult to ascertain as many of the sedimentary features exhibit deep water as well as proximal marine conditions (Pray and Wray, 1963; Goldhammer et al., 1994; Grammer et al., 1996).

Facies F-8: Diverse Skeletal Packstone - Grainstone

Description

Facies F-8 is similar in description to the cap facies described by Pray and Wray (1963) and the Skeletal Cap facies descriptions by Goldhammer et al (1991) at the Honaker Trail Type locality along the western shelf of the Paradox Basin. Grammer et al. (1996) at the San Juan goose necks of the western shelf of the basin, further subdivided this facies into the Skeletal Capping Facies-Diverse and Skeletal Capping Facies-Crinoidal; SC-D and SC-C respectively, allowing for the differentiation of low to higher energy environments of deposition.

Facies F-8 is composed of a basal packstone to grainstone of medium to very coarse-grained material of predominately crinoidal debris as well as extremely abraded, rounded and broken debris of brachiopods, fusulinids, encrusting forams, bryozoans, trilobites, phylloid algae, and gastropods with well-developed micrite envelopes (equivalent to SC-C from Grammer, 1996) (Figure 4.24). The outcrop weathers a maroon to light gray with fresh surface composed of maroon

mudstone where present and light gray to tan color grainstone (Figure 4.23 & Figure 4.24). The basal grainstone has sharp lower and upper contacts (Figure 4.23a), is medium to thick bedded (2m in total) and is trough cross-bedded with low angle laminations (Figure 4.23c) and is devoid of siliciclastic material at the base. Vertically the facies is partitioned by <1m thick brachiopod wackestone beds and is overlain by a more diverse marine assemblage referred to as the skeletal cap facies–diverse as described by Grammer et al (1996). The overlying unit is composed of an unweathered light gray wackestone to grainstone containing a diverse array of normal marine invertebrates of crinoids, brachiopods (productid and spiriferids), bryozoans, trilobite fragments, fusulinids as well as encrusting, uniserial, biserial and opthalmidid foraminifera, and whole coralline sponges. The unit becomes increasingly silty (5-50%) upward with the bed top composed of nearly 50% siliciclastics where it is highly burrow-mottled with vertical and horizontal traces (Figure 4.23b).

Figure 4.23 - Outcrop photograph of the skeletal cap facies F-8. Field photo (A) shows the sharp contact with the underlying interbedded sequence of facies F-1 and F-7. The ridge forming limestone (A) is the basal crinoidal grainstone composed of low angle laminations (C) vertically separated by wackestones. Upsection the facies transitions into the skeletal cap-diverse facies with an increase in siliciclastic content to near 50% (B) where it becomes intensely bioturbated.

Figure 4.24: Polished hand samples from the skeletal cap facies F-8 showing low-angle laminations within an overall crinoidal skeletal grainstone (A) and (B) showing an increase in micritic mud of the diverse facies as dark maroon areas.

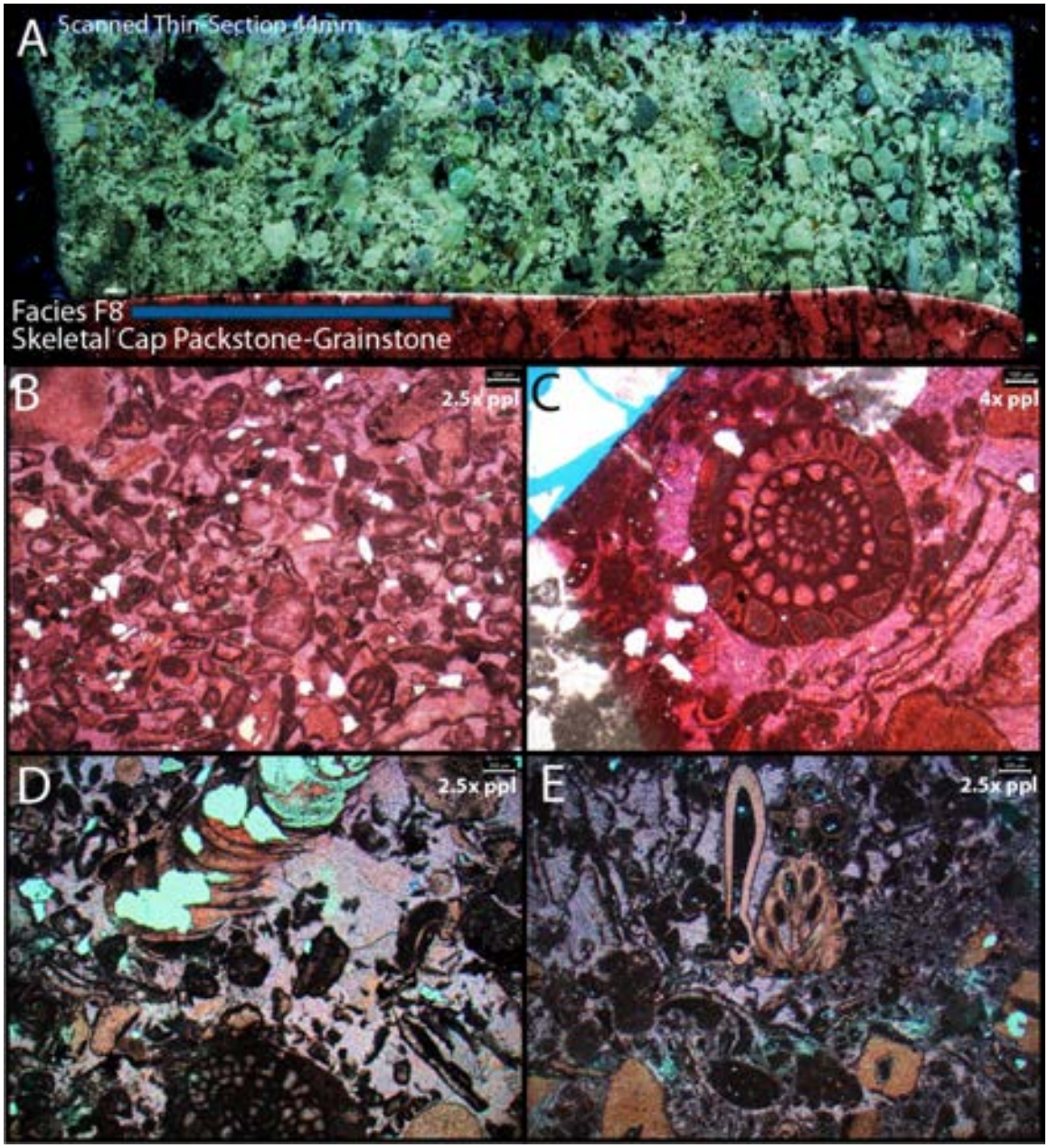

Figure 4.25: Scanned thin-section and photomicrographs of the skeletal cap facies F-8. (A) Scanned thin-section under crossed polarized light showing a grainstone fabric with a dominate echinoderm skeletal grain component. (B) Rounded, broken and abraded skeletal debris composing the basal crinoidal grainstone of skeletal cap-crinoidal, and micrite envelopes. (C, D & E) Show the transition to the faunal diversity of skeletal cap-diverse.

Interpretation: high-energy channelized to skeletal sand shoals of a shallow open marine shelf (1-5m water depth)

Abraded, rounded and micritized skeletal debris of the diverse skeletal packstone - grainstones of facies F-8 are interpreted as high-energy, shallow platform skeletal sand shoals and channels between topographic highs. The high faunal diversity of the unit, low matrix content, and rounded, broken, and abraded material within trough and low-angle laminations are indicative of deposition under moderate to high-energy wave dominated conditions on a shallow open marine shelf under normal marine conditions. Abundant foraminifers up section along with increasing siliciclastic content and bioturbation is interpreted as a decrease in energy to a moderate to low energy shallow subtidal environment with an increase in windblown terrigenous siliciclastic input.

Facies F-9: Red Silty Micaceous Mudstone and Thin-bedded Sandstone

Description

Facies F-9 is one of the most abundant facies types in the Honaker Trail and Lower Cutler exposures and is typically found with sharp basal contacts above limestone units and interbedded with coarse-grained, channelized conglomeratic sands of facies F-11. The facies is composed of thin bedded (2-10cm) red to green mudstones to siltstones (Figure 4.25, 4.27) with abundant white bleached root traces and small centimeter scale beds of dark clay-rich mudstones (Figure 4.28). The red siltstones typically lack bedding but are otherwise planar to laminated with abundant root traces or ripple cross-laminated and devoid of marine fossils. Some intervals contain Stage II caliche soil horizons containing nodular carbonate (Figure 4.26b). The facies is commonly scoured and eroded by facies F-11 forming cut and fill geometries above, as well as signs of soft-sediment

deformation in the form slump features interpreted as cut bank collapse of partially lithified sediment.

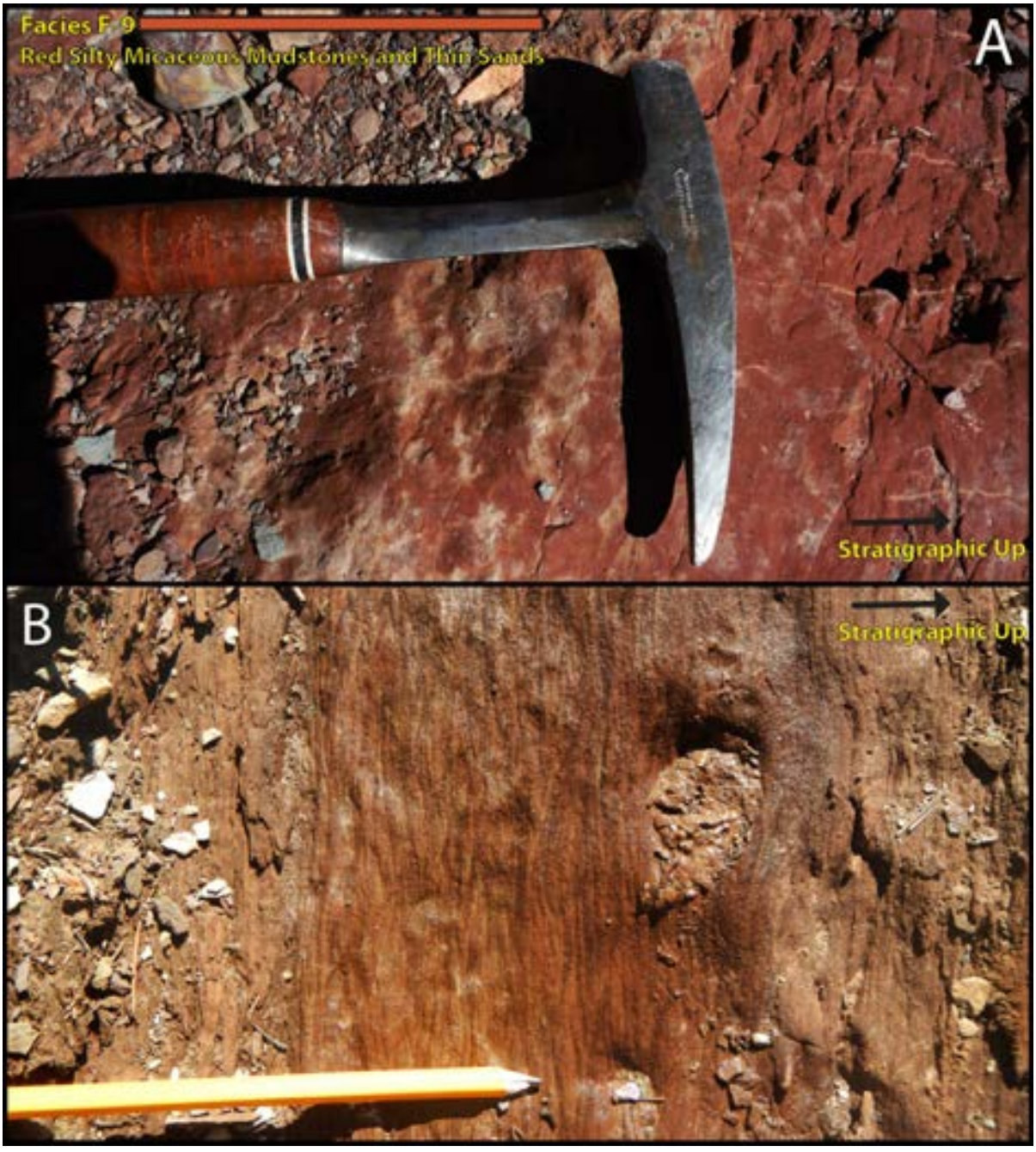

Figure 4.26: Outcrop photographs of the red silty micaceous mudstones and thin sands of facies F-9. (A) Field photograph showing a common root mottled fabric with a massive red mudstone typical of this facies. (B) Ripple laminated fabric with common carbonate nodules forming an interpreted caliche horizon.

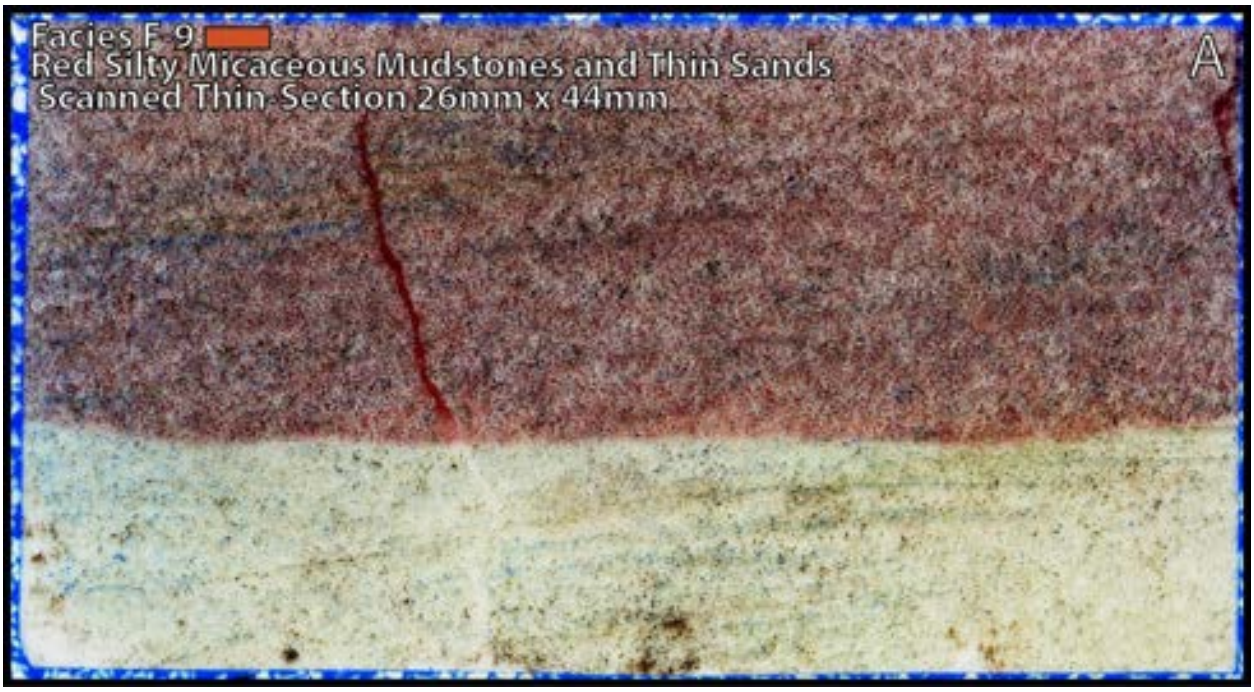

Figure 4.27: Scanned thin-section 26mm x 44mm under plain light showing the overall silty laminated and calcite cemented composition of the thin sands found within facies F-9.

Interpretation: Fluvial Overbank and Floodplain Environments

Facies F-9 is interpreted to be the overbank floodplain environments of meandering fluvial systems, with caliche horizons observed as nodular limestone within red rooted mudstones, suggesting this environment developed throughout depositional hiatuses. Caliche observed in the field area, as well as other ancient analogues are interpreted to be the result of periodic wetting and drying in an arid climate (Estaban and Klappa, 1983). Caliche may form either directly from carbonate pedogenesis and soil formation or by cementation in the phreatic zone (Flügel, 2010). Abundant root traces are interpreted to be sign of a terrigenous flora indicating proximity to a terrigenous or transitional marine environment.

Facies F-10: Bryozoan Productid Brachiopod Wackestone to Packstone

Description

This facies description closely fits the characterization of the "*intermediate facies"* defined by Pray and Wray (1963) for carbonate strata located between the sponge facies and algal facies of the Ismay interval of the Paradox Formation along the western shelf of the Paradox Basin. Goldhammer et al. (1991) further characterized this facies as greenish mudstones to wackestones composed of robust marine fauna consisting of large crinoids, intact brachiopods specifically spiriferids, bryozoans, fusulinids, coralline sponges, minor foraminifers and phylloid algae.

Facies F-10 is a greenish gray to maroon weathered to light gray green maroon unweathered. The facies is 6m thick, consisting of wavy bedded crinoidal bryozoan wackestone with cm scale mud drapes and sharply bounded by terrigenous siliciclastics at its upper and lower contacts. The unit is a heavily burrow- mottled with beds dominated by articulated bed parallel productid and spiriferid brachiopods, prismopora and branching bryozoans, crinoid plates, and whole coraline sponges (Syringopora, Favosites, and Chaetitid approximately 10cm across) (Figure 4.28). Hand samples are composed of a burrow mottled carbonate mud fabric with burrows infilled giving the appearance of darker mud clasts (Figure 4.29). The sample is fetid with thin-sections showing kerogen occluding porosity and restricted to burrows. Further thin section analysis reveals a carbonate (partially silicified) mud matrix dominated by calcified siliceous sponge spicules and approximately 5-10% admixed quartz silt (Figure 2.29)

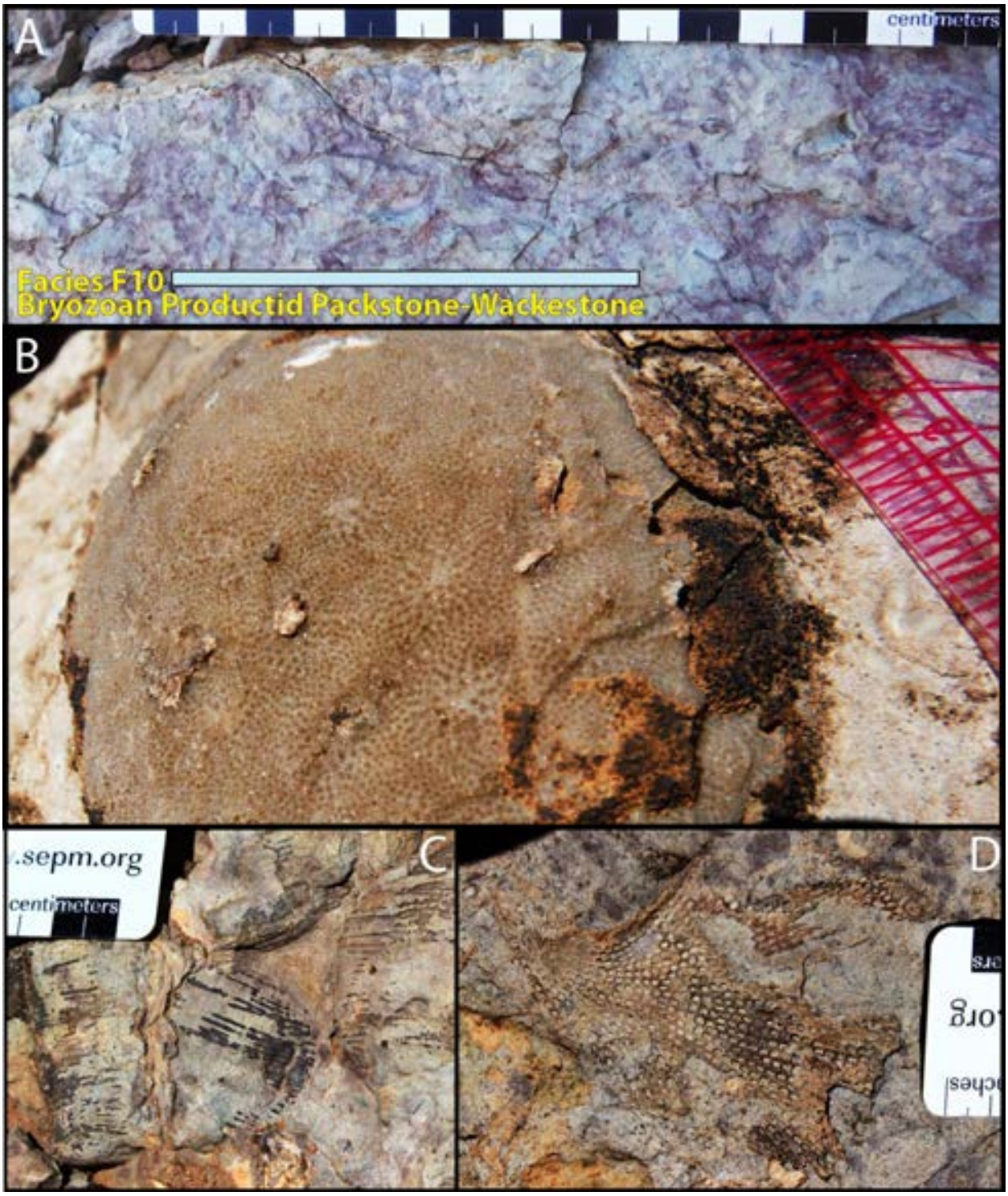

Figure 4.28: Field photograph of facies F-10 of the intermediate bryozoan productid packstone-wackestone facies. (A) outcrop photograph showing the diagnostic green/maroon mottled fabric common of the weathered surface of this facies. (B) Favosites? Abundant articulated corraline sponges and (C) bed parallel articulated productid brachiopods as well as abundant branching bryozoans.

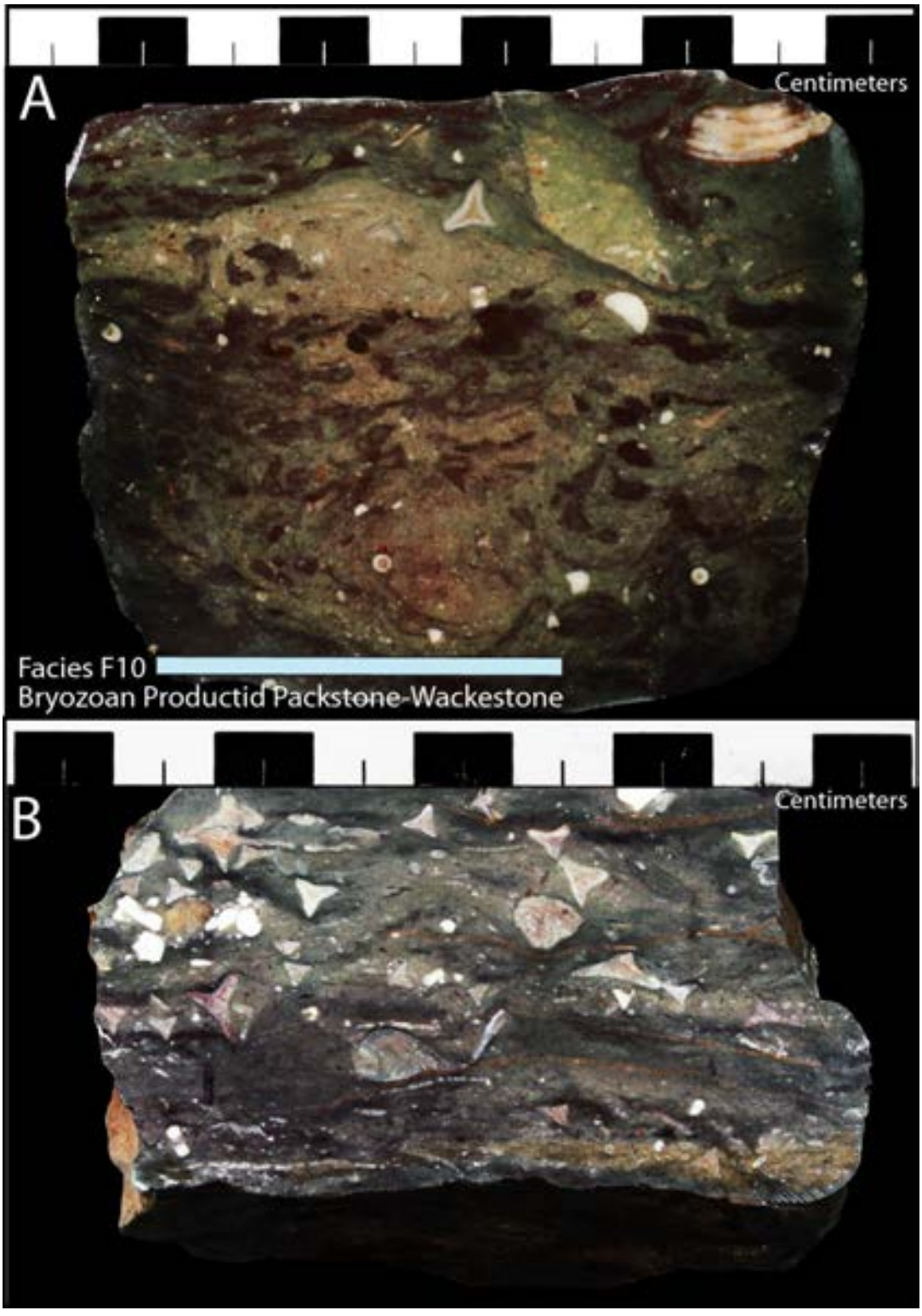

Figure 4.29: Polished hand sample from facies F-10 of the intermediate bryozoan-productid packstone-wackstone. Photographs (A) and (B) show green/maroon weathered color as well as darker mudfilled burrows. The facies is dominated by prismopora bryozoans as well as productid brachiopods and crinoid debris aligned preferentially to the bedding plane.

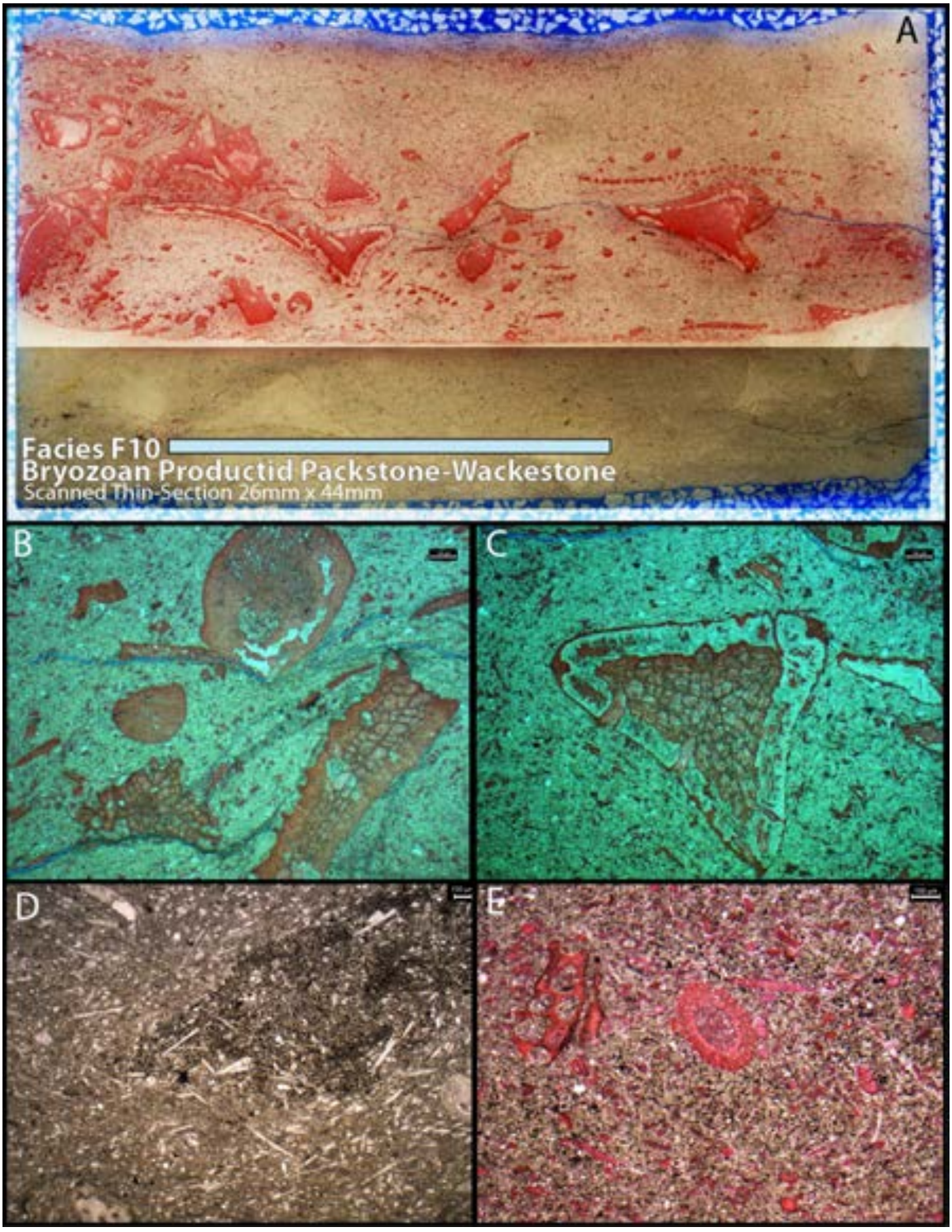

Figure 4.30: Scanned thin-section and photomicrographs of facies F10. Scanned thin-section is 26mm x 44mm and is shown under plain light highlighting bed parallel dispersal of skeletal debris and mud supported framework. Photomicrographs (A & B) show the primary skeletal component of prismopora bryozoans. Photomicrographs (D & E) show an abundance of siliceous sponge spicules that forming an abundant skeletal component of the micritic matrix.

Interpretation: Low energy open platform (5-10m water depth)

The principal characteristics of lithofacies F-10 are abundant normal marine fauna, mud-supported framework, burrow mottled fabric, green, gray and maroon color, and lack of primary organic material indicating deposition under shallow, well-circulated normal marine conditions(Scholle et al., 1983; Tucker and Wright, 1991). The facies was likely deposited on a moderate to low energy open marine shelf due to the abundance of articulated bed parallel marine fauna (Scholle et al., 1983; Tucker and Wright, 1991).

Facies F-11: Channelized Conglomeratic Sandstone

Description

Facies F-11 does not have a western shelf equivalent based on descriptions from Pray and Wray, 1963, and Goldhammer et al. (1994). However, this facies does fit descriptions by Gianniny and Miskell-Gerhardt (2009), of coarse-grained conglomeratic sands along the eastern margin of the Paradox Basin. Facies F-11 is predominately found in the Lower Cutler section of the exposed megaflap. The facies, combined with associated facies F-9 consists of 60m cycles of coarse-grained fluvial channels interbedded with fluvial overbank deposits of red silty root-mottled mudstones. Typical sedimentary fabrics within the channel facies are: pebble conglomerate lag deposits, soft-sediment deformation associated with fluid escape structures and cut bank collapse, erosional scoured bases, well rounded black chert and angular red mudstone rip-up clasts, trough cross-bedding, climbing ripples, lateral accretion sets, and abundant root traces within fluvial overbank mudstones (Figure 4.31). The trough cross-bedded pebble conglomerates are commonly 10-30cm thick beds that amalgamate to 6-9m channelized structures (Figure 4.31c). This facies represents one of the first instances of Cutler-Type facies within the megaflap panel, as well as marked avulsion of up-dip carbonates evident through increased carbonate pebble rip-up clasts and

a progressive decrease in structural dip generating an onlapping clastic wedge geometry. Petrographic analyses reveals a calcite cemented predominately angular- to sub-angular moderately-sorted medium to coarse-grained to pebble sized quartzofeldspathic sandstone consisting of plagioclase, orthoclase, monocrystalline and polycrystalline quartz (Figure 4.32 & 4.33). Limited chemical compaction is observed as most clastic grain contacts are planar, with preserved euhedral outline of dissolved potassium feldspar and abundant depositional porosity.

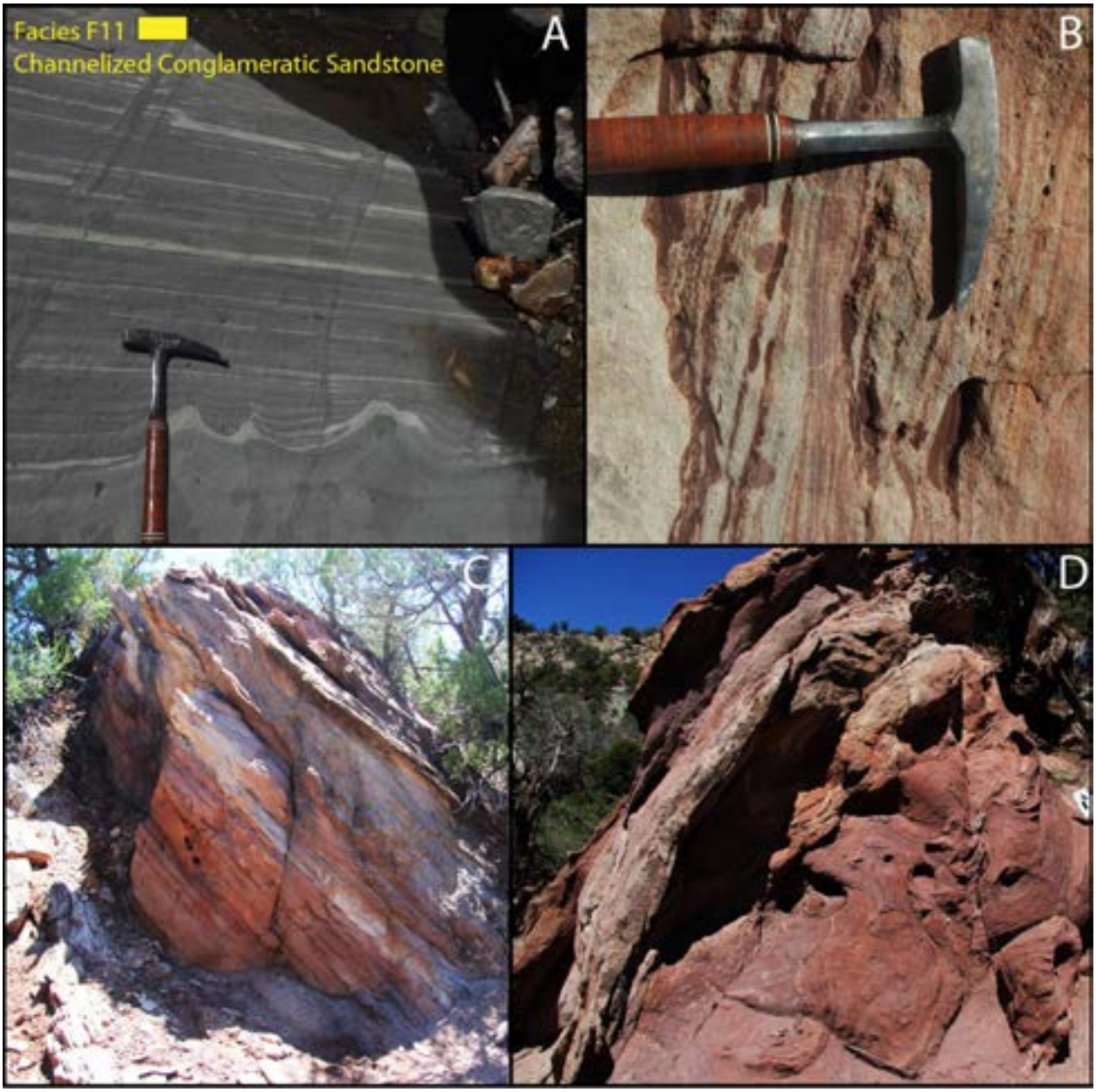

Figure 4.31: Field photographs of facie F11 of the channelized conglomeratic sandstones. Photograph (A) shows fluid escape structures as well as planar laminations of channel filling coarse sands, stratigraphic up-direction indicated by top of hammer. Photograph (B) show angular to flat pebble rip up clasts of red mudstone from facies F-9 and well as rounded black chert. Photograph (C) shows amalgamated 10-20cm beds of trough cross-bedding, climbing ripples, and planar beds with an overall finning up fabric. The amalgamated beds together form 5-9m channelized features. Photograph (D) soft sediment deformation of slumped and collapsed fabric of once partially lithified mudstone cutbank.

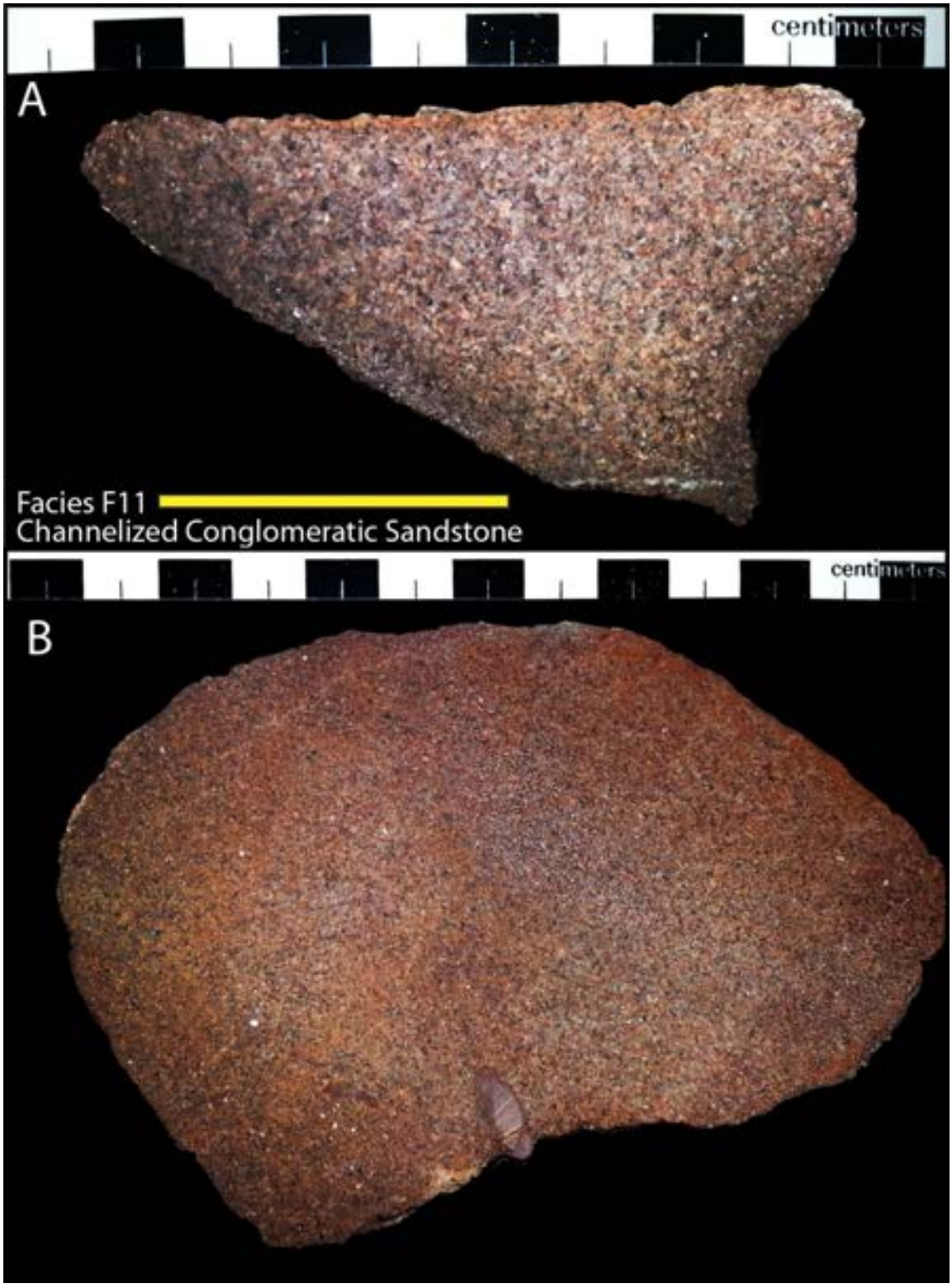

Figure 4.32: Polished handsample of facies F-11 of the channelized conglomeratic sandstone. Photographs (A & B) show coarse moderately sorted subangular arkosic sandstones

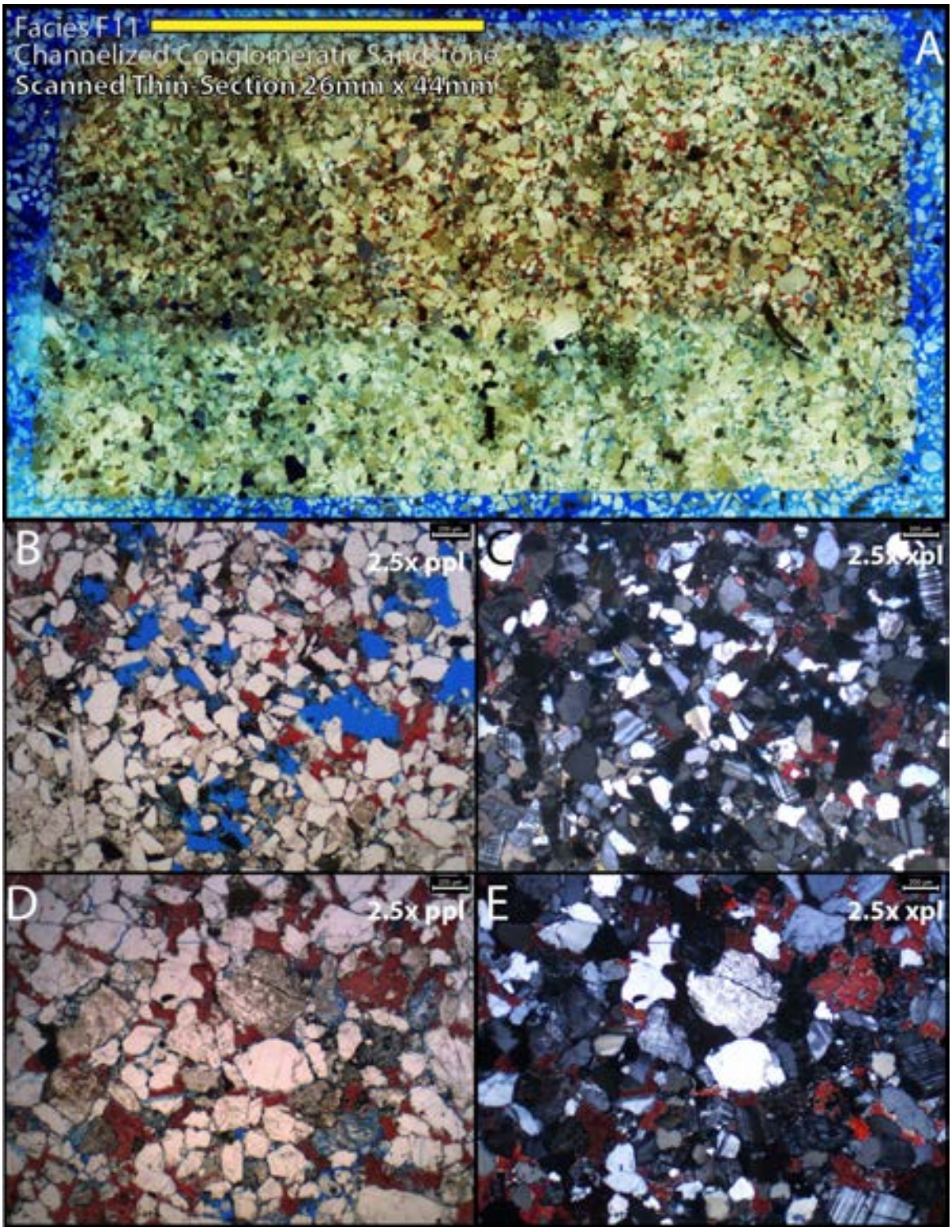

Figure 4.33: Scanned thin-section and photomicrographs of facies F-11 of the channelized conglomeratic sandstone. (A) scanned thin-section under polarized light showing overall moderately sorted subangular and arkosic fabric. Photomicrographs show calcite as the predominate cement as well as the arkosic composition of monocrystalling and polycrystalline quartz, orthoclase and plagioclase. Note the moderately compacted fabric of predominately planar

grain contacts and well preserved and solution enhanced porosity. Photomicrograph Figure 4.33(B) shows abundant opaque kerogen lining pore throats.

Interpretation: Stacked, Braided Fluvial Channels

Combined with the close association with red mudstone facies F-9, facies F-11 strongly exhibits abundant sedimentary structures found in many ancient and modern fluvial systems (Miall, 2013). Angular red mudstone clasts and rounded black chert found at the base of erosional and scoured surfaces are commonly developed at the base of high-energy fluvial channel deposits interpreted as channel lags deposits (Miall, 2013). Climbing ripple laminations are common sedimentary structures found in numerous fluvial environments as described by Ashley et al. (1982). Together lithified collapsed cut-bank deposits, lag deposits of rounded black pebble chert within an overall fining-upward succession indicate bedload and waning flow conditions within an overall traction transport regime typical of braided fluvial systems (Miall, 2013). Within the salt wall region of the Paradox Basin, proximal to the Uncompahgre Uplift, the Cutler Formation consists of a heterogenous sequence of fluvial/alluvial arkosic conglomerates and sandstone that interfinger with shallow marine siltstone and mudstone (Werner, 1974; Mack and Rasmussen, 1984; Condon, 1997). The siliciclastics described here are interpreted to be the braided fluvial systems of the distal edges of alluvial megafans shed from the Uncompahgre Uplift.

Facies F-12: Phylloid Algal Bafflestone -Wackestone

Description

The phylloid algal facies (F-12) is only present at the top of the Honaker Trail Formation in the study area and marks the boundary between the Honaker Trail and overlying Lower Cutler Formation. The phylloid algal facies described here does not form biohermal mound as described by Wray and Pray, (1963), and Goldhammer et al. (1994), along the western shelf of the Paradox

basin. Instead, the facies fits the descriptions of Grammer et al. (1996) of the "*Incipient Mound Facies (IM*)" described as a phylloid algal biostromal facies along the western shelf of the basin. The facies is characterized as a muddy phylloid algal bafflestone with a peloidal micritic matrix with admixed normal marine skeletal debris. Facies F-12 is laterally continuous and typically grades upward to the mudstones of facies F-1 or is sharply overlain by red silty mudstones of facies F-9 (Figure 4.34). The facies in the study area is floored by a thin 20cm wavy-bedded, carbonate wackestone with abundant brachiopod, articulated ostracods, and rounded clasts of black chert nodules. A thin-section taken from the basal carbonate wackestone unit shows a fabric dominated by brachiopod fragments and spines, articulated ostracods, foraminifera, and echinoderm plates. The basal carbonate wackestone grades into the phylloid algal bafflestone (Figure 4.34). The phylloid bafflestone also contains a diverse marine fauna including crinoids, brachiopods, bryozoa, and fusilinids (Figure 4.35).

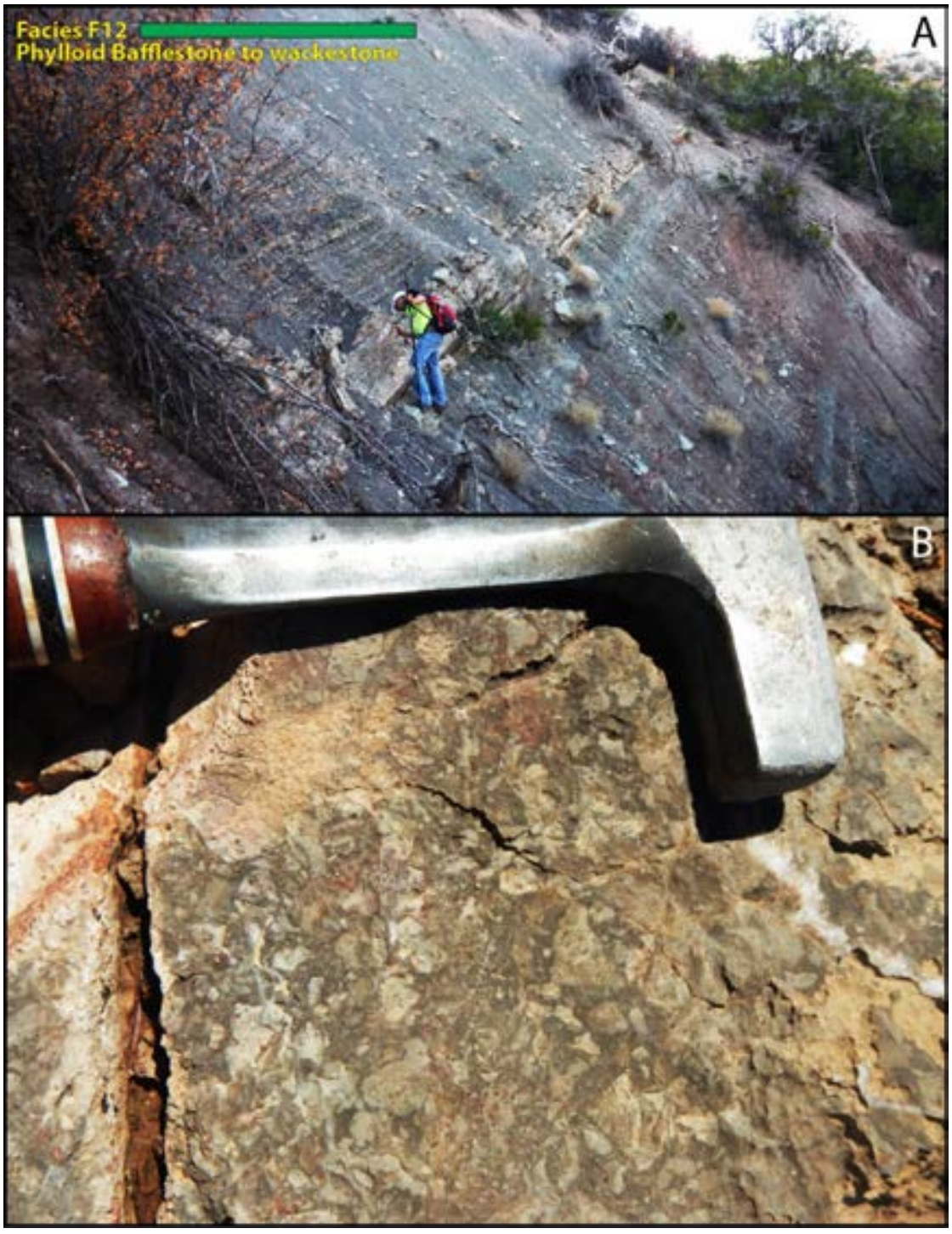

Figure 4.34: Outcrop photographs of the algal bafflestone facies F-12. Field photo (A) shows a sharp contact with underlying red terrigenous mudstones of facies F-9 and a gradational top with facies F-1. (B) Field photograph showing a bafflestone fabric of phylloid algae forming a network of shelter porosity (light gray) within a darker gray micrite.

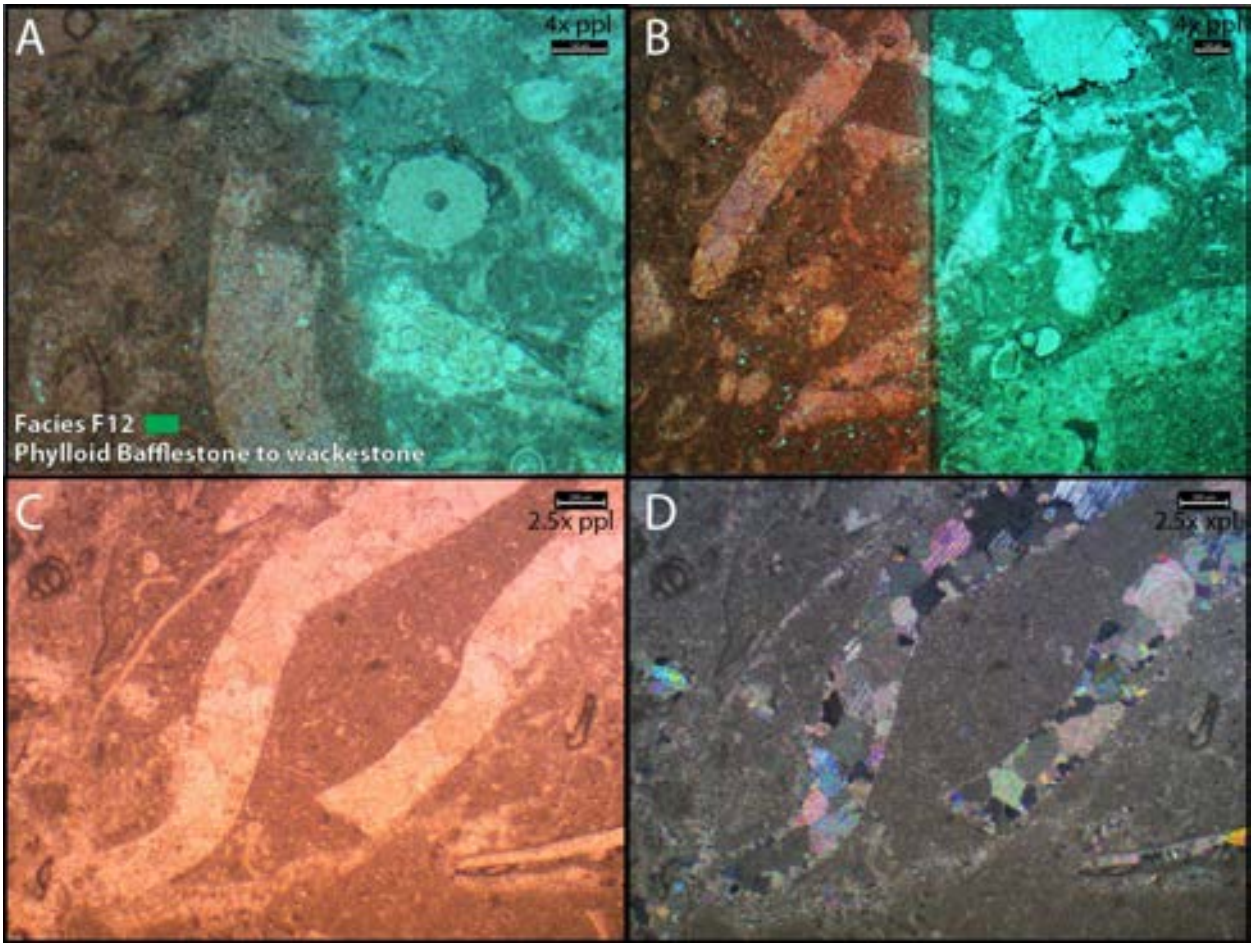

Figure 4.35: Photomicrographs of facies F-12 showing large phylloid algae plates (C & D) amd admixed normal marine fauna including crinoids, gastropods, and foraminifers (A & B).

Interpretation: Moderate Energy Open Platform, Proximal to Phylloid Algal Mounds

The presence of abundant phylloid algae, other normal marine fauna, and light color are indicative of deposition under shallow, well-circulated normal marine conditions within the photic zone . The large size of the phylloid algae plates observed indicate deposition below wave base, outside the zone of pronounced agitation that would readily disarticulate and abraded the algae into smaller fragments.

4.2.3 Lower Cutler Formation Lithofacies

The Lower Cutler Formation lithofacies (Figure 4.36, Table 3) present in the megaflap are predominately the previously described siliciclastic facies of F9 (red silty micaceous mudstone and thin sandstone) and F11 (Channelized conglomeratic sandstone). F1 (black silty argillaceous dolomitic mudstone and F12 (Phylloid algal bafflestone) are also present in subordinate amounts. A new lagoonal carbonate facies F13 (coated-grain gastropod brachiopod mudstone – packstone) is the dominate carbonate lithofacies in the study area. The exposure of the Lower Cutler Formation within the megaflap in total is 166m with a basal unit of thick ledges of braided fluvial channelized conglomeratic sandstone interbedded with red, silty micaceous floodplain mudstone.

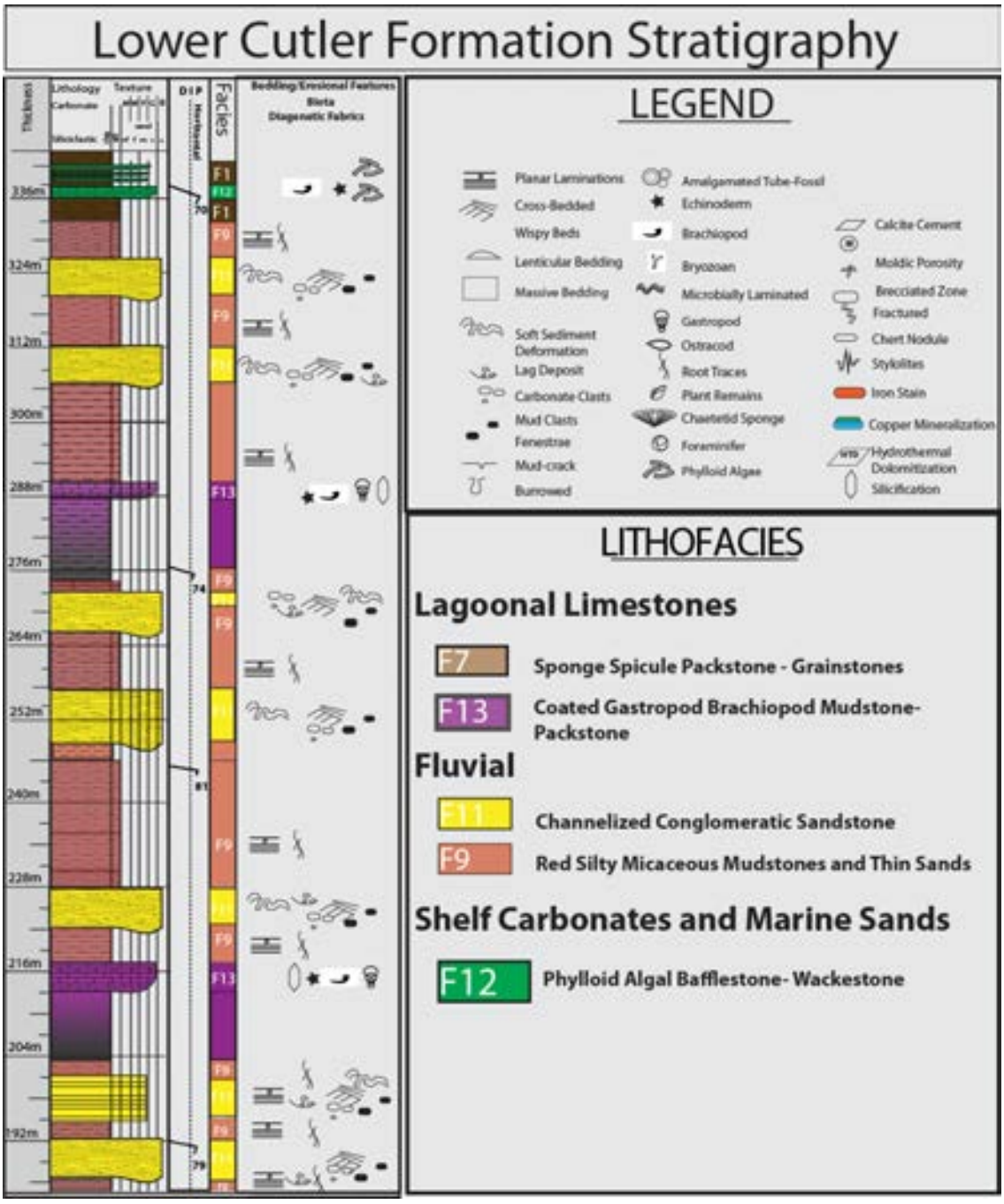

Figure 4.36: Composite stratigraphic column from measured sections 1-5 of the exposed lower Cutler Formation. The column shows from left to right, thickness, lithology, facies type, diagenetic and sedimentary fabrics and faunal assemblage.

Facies F-13: Coated-Grain Gastropod and Brachiopod Mudstone to Packstone

Description

Facies F-13 is present only in the Cutler Formation outcrops. The interval is 12m thick and contains thin 10-20cm thick carbonate beds weathered purple/green hue and burrow mottled into boudin shaped nodules interbedded with laminated muds (Figure 4.37). The beds thicken upward into a 3m thick wackestone to packstone dominated by skeletal grains of predominately gastropods, productid brachiopods, phylloid algae, bryozoans, ostrocods, and thin shelled bivalves. The skeletal grains show extensive and abundant encrusting opthalmidid foraminifera that coat the skeletal grains, that are intensely micritized, ultimatley developing thick envelopes around the skeletal grains (Figure 4.38).

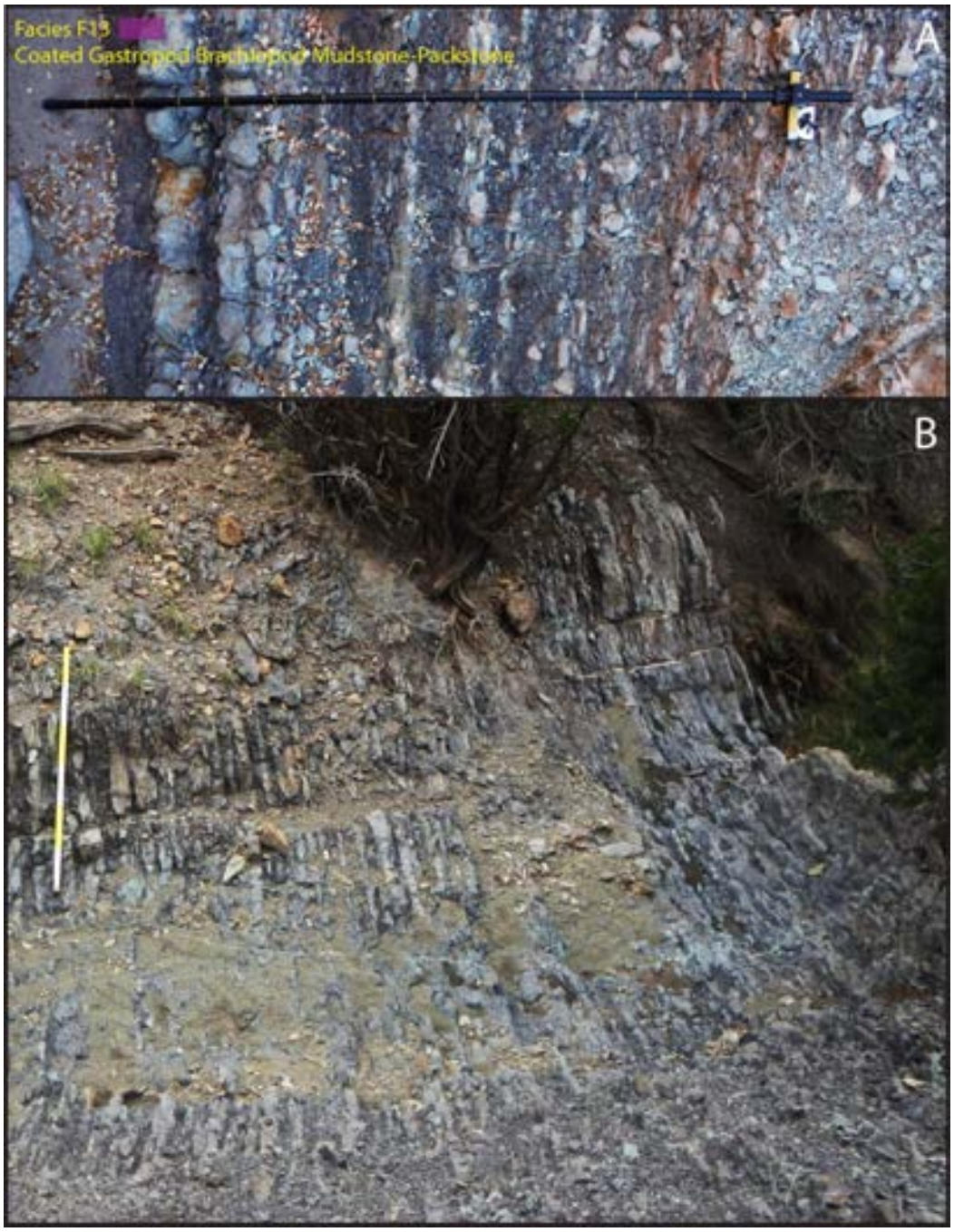

Figure 4.37: Outcrop photographs of the coated gastropod-brachiopod wackestone of facies F-13. The facies shows a thickening upwards sequence of laterally discontinuous lenses of boudin shaped carbonates and a notable purple-green hue. The limestone lenses are interbedded with black argillaceous mudstones that gradual decrease upsection towards the ridge forming limestone.

Figure 4.38: Polished hand sample and photomicrographs of facies F-13 of the coated gastropod-brachiopod mudstone-packstone. Polished hand sample (A) shows notable jasperized skeletal grains that is interpreted to form the purple/green hue of the weather surface of the outcrop across the field area. Photomicrographs (B & C) show dominant skeletal framework of gastropods and encrusting opthalmidid foraminifera as well as other normal marine invertebrates such as bryozoans, echinoderms, and ostracods.

Interpretation: Semi-restricted lagoon

The gastropod dominated wackestone to packestones is interpreted to be deposited in a moderately restricted low energy lagoon to platform interior environment. The presence of other normal marine skeletal grains such as phylloid algae, brachiopods, bryozoans, and foraminifera indicated that the environment is not restricted to the point of becoming hypersaline and promoting a low diversity fauna (Enos, 1983). However, due to abundance of gastropods, it is interpreted that competition was low enough due to environmental conditions to promote the high abundance of a single faunal type that is tolerant of large changes in environmental conditions (Enos, 1983). Slow water circulation would result in depleted nutrients or abnormal salinities that would also inhibit faunal diversity, specifically lacking phylloid algae and/or brachiopods (Enos, 1983). Copeland (1967) and Moore and Shinn (1984) documented that in arid and semi-arid regions, lagoonal depositional systems often become hypersaline, ultimately developing a low diversity facies assemblage similar to the lagoonal sponge facies. Furthermore the facies contains moderate amounts of microcrystalline calcite mud, suggesting lower wave and tidal energy, allowing for suspension deposition of fine-grained carbonate mud (Kjerfve, 1994 Copeland 1967). Higher energy environments would have winnowed the carbonate mud, subsequently leaving only a framework of skeletal debris. Based on this line of evidence the lithofacies is interpreted to be deposited in a semi-restricted lagoonal environment between the supratidal and subtidal position with low to moderate energy.

Chapter 5: Diagenesis

Because of the vast literature and understanding of primary depositional fabrics in both carbonates and siliciclastics, diagenetic modification can be qualitatively assessed through observational relationships of the primary depositional fabrics to the cross-cutting sequence of diagenetic alteration. The porosity development and occlusion related to diagenesis of carbonate lithofacies discussed here refer mainly to nomenclature developed by Choquette and Pray (1970).

5.1 Diagenesis of Depositional Carbonates

The diagenetic fabrics observed within the limestone and dolomite lithofacies of the Pennsylvanian and Permian megaflap strata are principally related to burial diagenetic processes, common early marine and meteoric phreatic to vadose diagenetic processes such as calcite cementation, dolomitization, silicification, and less common calcitization of silica. Paragenetic sequence analysis reveals multiple stages of diagenesis resulting in modifications to the primary depositional fabrics and porosity and range from early marine cementation to hydrothermal dolomitization and mineralization within highly fractured and faulted zones.

Silicification of marine limestone and dolomitic lithofacies is common throughout the megaflap. Pennsylvanian stratigraphy that contain internal sources of silica such as siliceous sponge spicules have undergone calcitization, ultimately providing a source of silica throughout the megaflap. Some silicification is observed as red chert/chalcedony replacement fabric. Red chert is often cited as a diagenetic signal that records large-scale rapid changes in sea-level throughout the Pennsylvanian (Loope and Watkins, 1989). Silicification of calcitic skeletal fossils grains commonly occurs along thin solution films, and is associated with stylolitic surfaces and anastomosing dissolution seams where calcite begins to dissolve and silica precipitates.

Carbonate replacement or calcitization of detrital quartz grains within marine lithofacies and siliceous sponge spicules is also a common diagenetic fabric observed. Etching, corrosion, embayment, and partial replacement of detrital quartz grains is common in modern reefs where elevated pH induced by biological activity progressively dissolves quartz silt grains while precipitating calcium carbonate (Friedman et al., 1976). Sedimentary rocks containing authigenic silica commonly occur in or near stratigraphy that contain partially to completely replaced silica grains, indicating a genetic relationship and suggests that silica released as a result of carbonate replacement may be a significant source of authigenic silica.

Hydrothermal dolomitization in the megaflap is a unique diagenetic process specifically as it relates to the petroleum system as it can significantly enhance reservoir quality in formations that have low primary porosity and permeability. The dolomitic fabrics commonly present are void-filling saddle dolomite and matrix-replacive. Hydrothermal void-filling saddle dolomite cements typically reduce porosity due to the large curved and irregular crystal lattice that protrude into void space. Matrix-replacive fabrics typically enhance reservoir quality through replacement of calcite and develop a sucrosic permeable fabric. Both fabrics are observed within the megaflap stratigraphy.

Development of a paragenetic sequence for the lithofacies of the megaflap relied on petrographical analysis of 43 thin-sections that were half-stained with alizarine red S and potassium ferricyanide to delineate calcium carbonate (limestone) from calcium-magnesium carbonate (dolomite) as well as ferrous iron. The thin-sections, ground to standard 30 μm, were analyzed using a Leica Compund Light Microscope with polarizing optical attachments. Thin-section photomicrographs were obtained with a Leica DFC295 digital microscope color camera. Thin-sections have also been digitally scanned using an Epson Perfection V600 Scanner to produce

large plain light images as well as polarized images by bounding the thin-sections with polarized film.

5.1.1 Diagenetic Observations

Micritization

All shallow marine facies show some level of micritization with minimal micritization affecting the shelf carbonates (F-8, F-10, F-12) and intensely altering lagoonal facies (F-13) (Figure 4.38A and C; Figure 5.1, 5.2C). F-13 is observed to have undergone intensive micritization forming thick micrite envelopes that grade into a mixture of coating foraminifera and clotted peloidal micrite. Biohermal facies of F-2 show no preservation of early marine micritization processes due to intense dolomitization, while deeper marine facies such as F-1 show moderate amounts of micritization where skeletal grains are present.

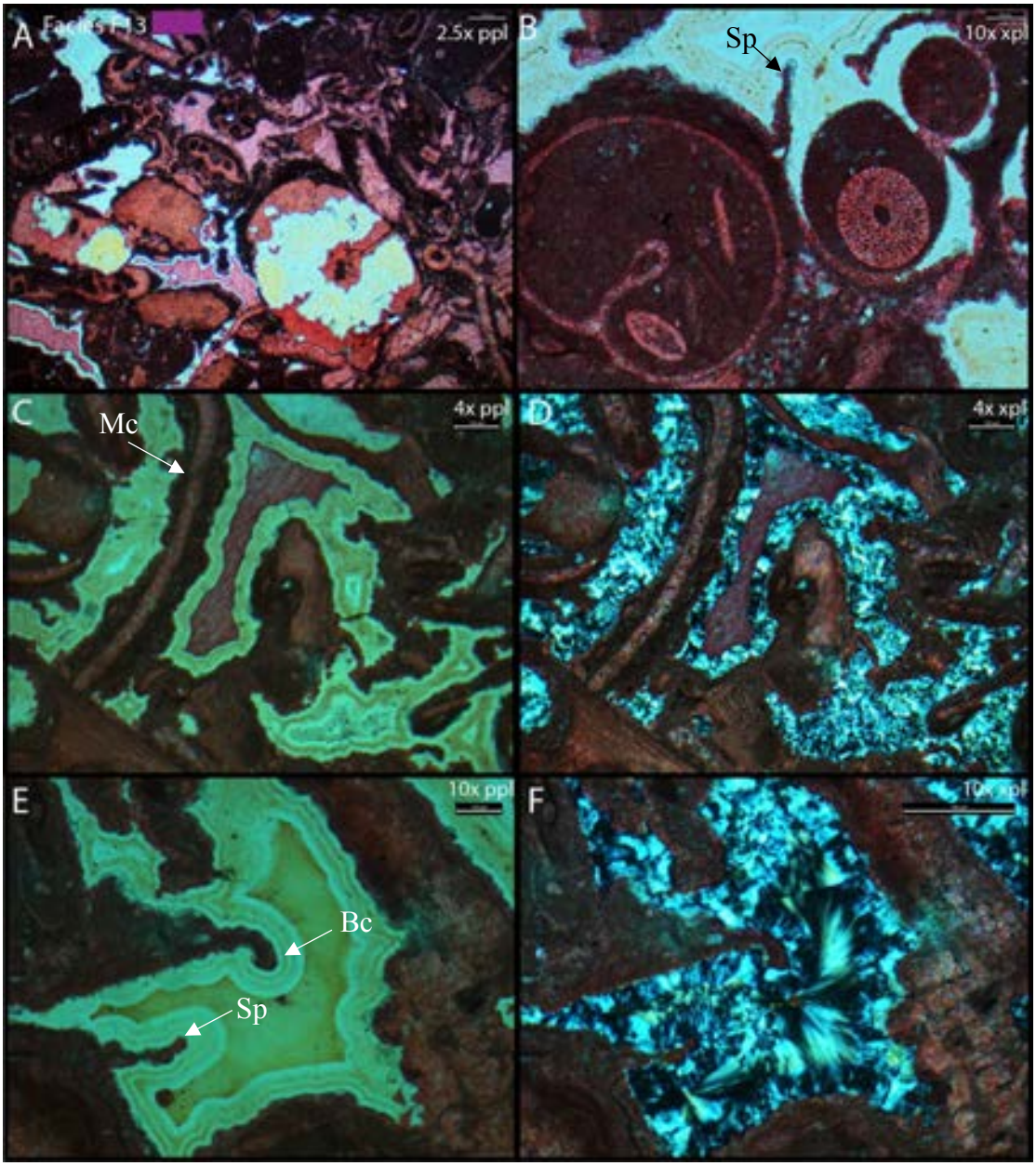

Figure 5.1- Photomicrographs of lagoonal facies F-13. A) Lagoonal facies grainstone with thick micrite envelopes and incipient silicification surrounding twinned poikilotopic calcite cement. B) micrite filled gastropod with spherical calcite nucleating off the clotted peloidal micrite envelope and coating foraminifera. C) Leached aragonitic and HMC skeletal grains and preserved brachiopod fragments with thick micrite and coating foraminifera envelopes. D) Polarized photomicrograph. E) Spherical calcite protrusions with nucleating radial fibrous fans of banded red chalcedony. F) Polarized photomicrograph. Mc = Micrite Envelope, Sp = Spherical Calcite, Bc = Banded Botryoidal Chalcedony

5.1.2 Cementation

Calcite

Observed fabrics of calcite cementation are fibrous, acicular and form isopachous rims around grains and may be cut by or overlie borings generated by endolithic microorganisms. The cement phase is commonly non-ferroan and followed by more massive sparry calcite or ferroan calcite. All shelf carbonates (Facies F-2, F-3, F-8, F-10, F-12) are observed to have developed a cement phase of thin isopachous rims of fibrous calcite where preserved (Figure 4.25, 4.36; Figure 5.12, Figure 5.2). Facies F-13 is the only facies that shows spherical calcite cements lining thick clotted micrite (Figure 5.1). All shelf carbonates except dolomite facies show ferroan calcite cross-cutting non-ferroan calcite. Biohermal facies F-3, although intensely altered, shows large centimeter scale cements of successive generations of relict now silicified radial fibrous acicular aragonite fans infilling shelter pore space (Figure 4.13C and D). More aragonitic cements are found preserved as small botryoidal fans and are found within rounded secondary dissolution cavities lining fracture walls of the Dolomite Ridge facies F-2, and nucleate off botryoidal hematitic cements (Figure 5.3). The aragonite cement phase is not isopachous and it is preferential to the ceiling of pore spaces as pendant structures where the well-developed botryoids laterally degrade into a more disorganized crystal mesh of aragonite (Figure 5.3).

5.1.3 Dolomite

Facies F-3 and F-2 of the Dolomite Ridge are the only facies observed to have diagenetic dolomite in the form of hydrothermal dolomite (HTD). HTD fabrics typically show sweeping extinction of the curved crystal lattice as a diagnostic petrographic characteristic (Davies and Jr, 2006). The cements are often observed protruding into pore spaces of facies F-2 (Figure 5.13 C & D).

5.1.4 Silica Replacement

Red chert replacement fabrics are present in all of the shelf carbonate intervals and intensely alter facies F-13 of the lagoonal facies. The fabric is observed as successive generations of banded botryoidal isopachous silica cements progressively replacing primary pore space occupied by calcite (Figure 5.1) or more commonly as anastomosing fabrics that are mechanically fractured (Figure 5.12A and B). In Facies F-13 the fabrics forms well developed and successive generations of banded botryoidal isopachous silica. The fabric is a red chert as observed in outcrop and hand samples, and is likely responsible for the formations overall purple hue (Figure 4.37, 4.38) and its red coloration and optically brown petrographic color is due to abundant inclusions of iron as hematite within the crystal lattice (Loope and Watkins, 1989). Silicification is also present in the dolomitic facies as euhedral isopachous authigenic quartz phases and is restricted to biohermal facies F-3, and replace aragonite fans. Matrix silicification is also intense especially in facies F-7 and F-10 that contain siliceous sponge spicules, where sponge spicules are always replaced by calcite or ferrous calcite and the surrounding matrix if often completely silicified (Figure 5.10 and 5.11).

5.1.5 Recrystallization

All facies show some form of recrystallization or neomorphism. Neomorphism is observed to intensely alter dolomitic facies of F-2 and F-3. Petrographic observations show dolomite crystal size was slightly enhanced through matrix neomorphism compared to unaltered micrite matrix forming a more sucrosic fabric. All carbonate intervals show some matrix neomorphism.

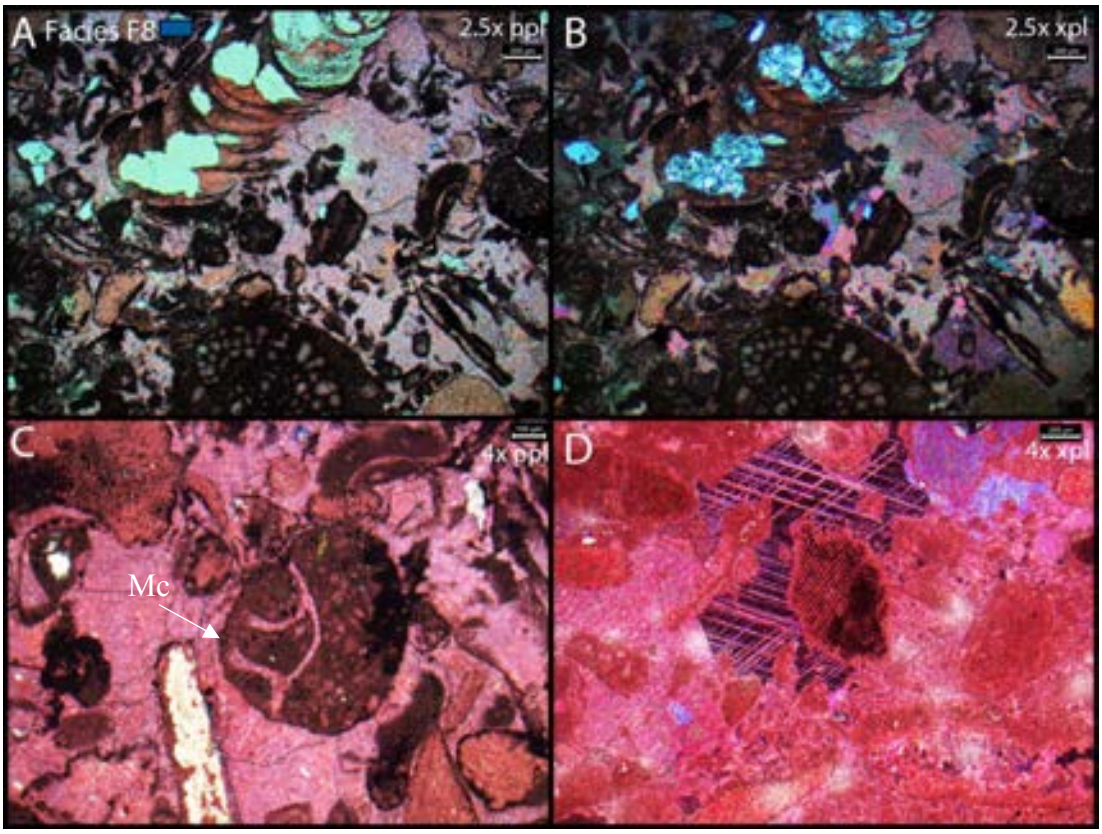

Figure 5.2- Photomicrographs from facies F-8 of the shelf limestones. The thin-sections show early marine diagenetic fabrics consisting of thin micrite rims, thin blocky isopachous calcite rims, and void filling calcite spar. Much of the calcite spar is neomorphosed into twinned poikiolotopic calcite taking a purple stain, evidence of ferroan calcite. Chalcedony and silicification is rare and restricted to grains or minor matrix alterations.

5.1.6 Dissolution and Collapse

Dissolution of carbonate and dolomite facies is a common fabric observed throughout the megaflap principally as leached skeletal grains. All shelf carbonates are observed to have leached skeletal grains often occluded with calcite (Figure 5.3). Dissolution vugs are very common within dolomite facies and less common in limestone shelf and lagoonal carbonates. Collapse features are restricted to Facies F-5 which are laterally continuous algal laminated units. Measured section MS-1, contains a large scale collapse structure 1.5m thick and approximately 100m wide, and capped by the Jurassic Summerville angular unconformity perpendicular to the bedding plane (Figure 5.4). The outcrop consists of blocks of limestone (Figure 5.5) bound by isopachous fibrous calcite cement with remaining void space occupied by large dog-tooth calcite spar. Hand samples of the limestone blocks from the collapse structure show a chaotic fabric consisting of localized collapse fabrics, pervasive lisegang banding, isopachous banded calcite cement, void filling dog-tooth calcite spar and exotic clasts of red sandstone (Figure 5.6). Petrographic observations of the red sandstone clasts reveals conspicuous well-rounded monocrystalline quartz and plagioclase grains coated with brownish red iron oxide dust rims and are entrained within a poikiolotopic calcite cement matrix (Figure 5.7). The quartz and plagioclase grain boundaries show signs of intense corrosion, etching, and embayment as many of the grains are being dissolved. The exotic red sandstone petrographically, appears to be matrix supported through intense dissolution of the originally grain supported detrital clast (Figure 5.7).

5.1.7 Mechanical and Chemical Compaction

Pressure dissolution fabrics observed in the megaflap are typically anastomosing dissolution seams and stylolites. All facies show some signs of burial deformation in the form of concavo- convex and interpenetrating contacts along grain boundaries, and mechanical fracturing of grains (Figure 5.10A and B; Figure 5.12C and D)

5.1.7 Fracture

Many faults and fractures are observed within the megaflap stratigraphy. Fracturing is observed to effect the Dolomite Ridge of the Paradox Formation pervasively with minimal fracturing affecting stratigraphy in the Honaker Trail and lower Cutler.

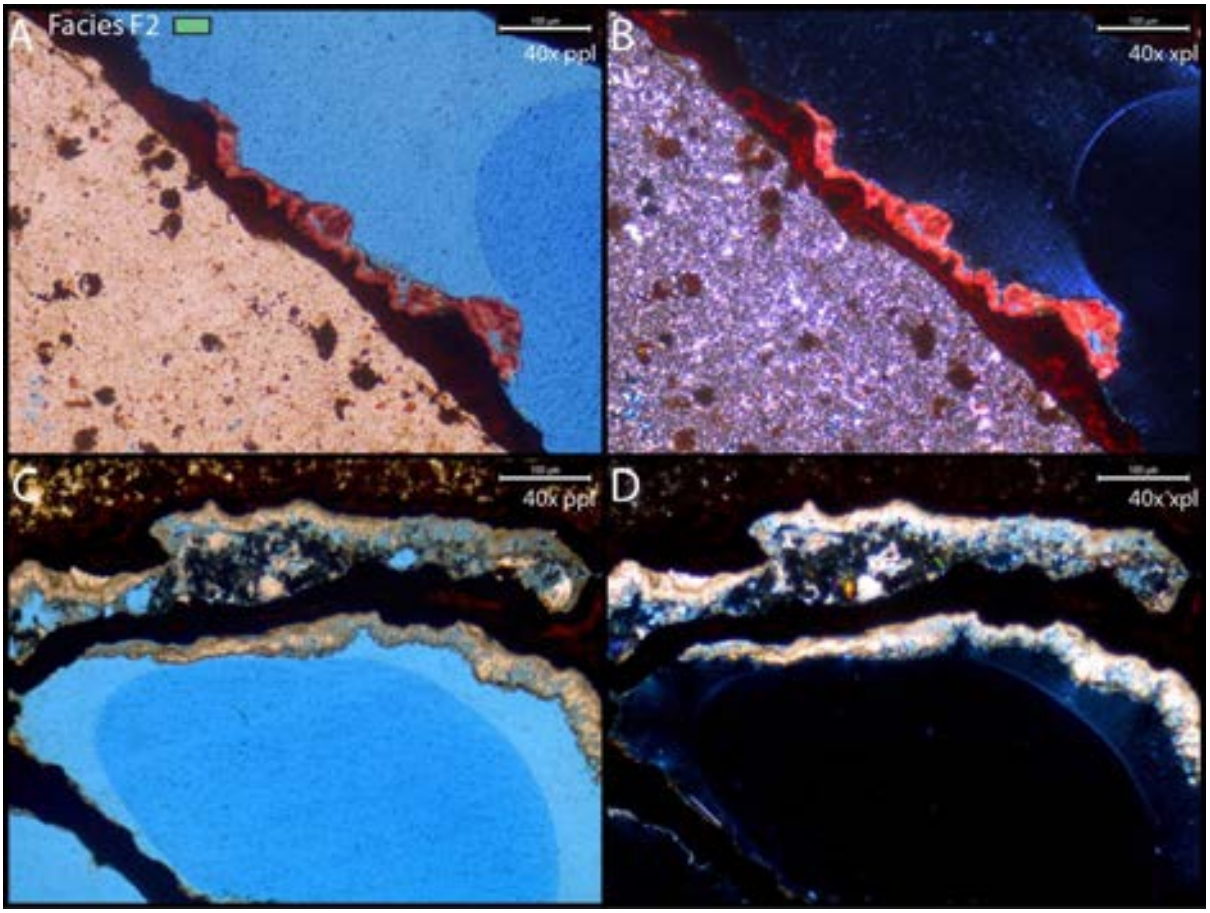

Figure 5.3- Photmicrographs of facies F-3 under 40x zoom within fractures. Photomicrographs (A&B) under plain and crossed-polarized light show well defined paragenetic sequence of the silicified carbonate host, iron saturated fluids occluding disolition vugs and lining fracture walls as botryoidal cement and finally Alizarine Red-S stain of late stage calcite cement within large rounded solution pores. Photomicrographs (C&D) of the same sample show more clearly the iron oxide cement as botryoidal masses lining rounded solution pores, with bladed botryoidal aragonite nucleating on its surface within the unstained portion of the thin-section.

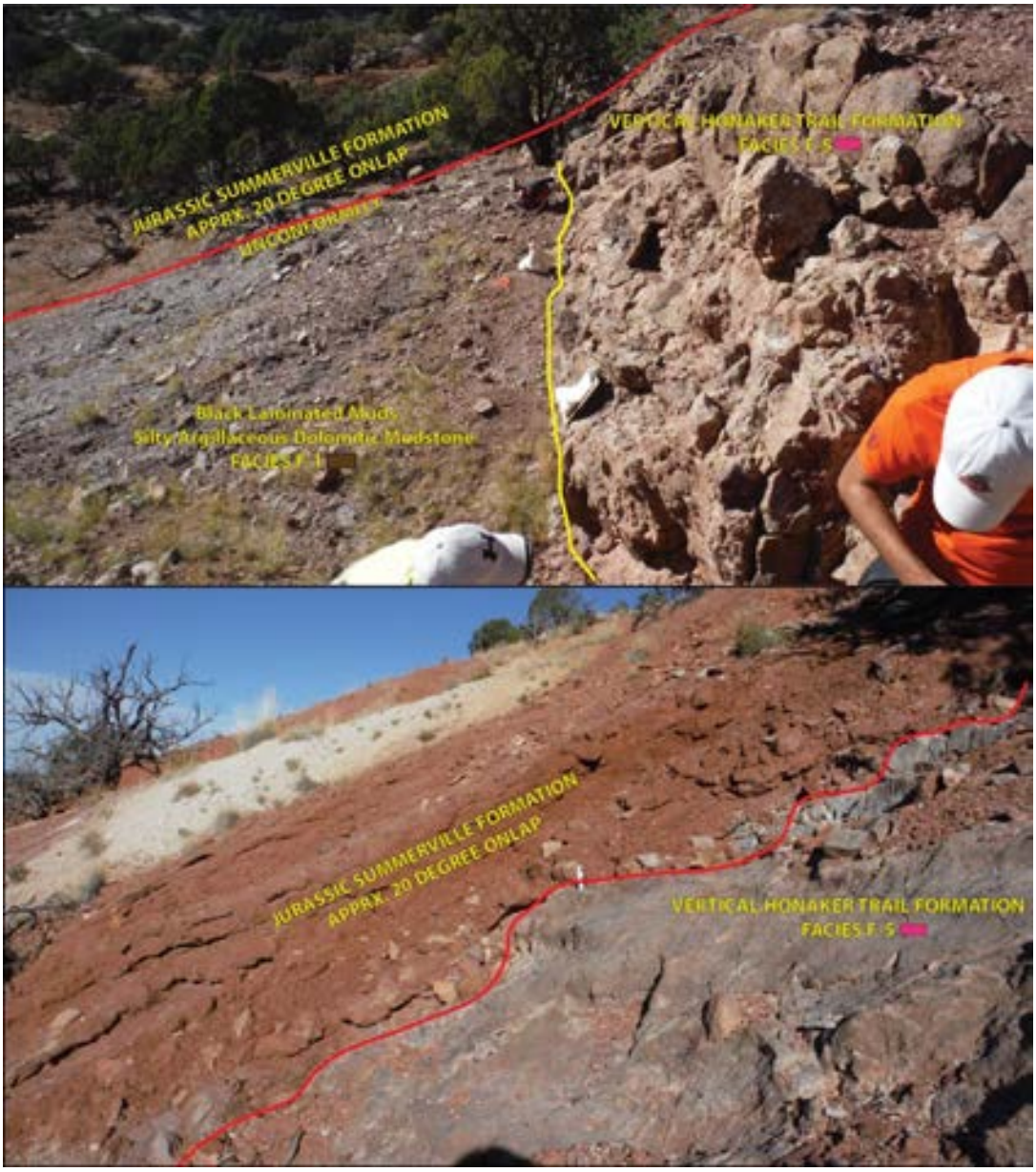

Figure 5.4- Outcrop photograph of vertical facies F-5 at an angular unconformity (approximate 20 degree onlap) with the red Jurassic Summerville Formation siliciclastics. Facies F-5 at MS-1 is a chaotic collapse structure of karsted limestone blocks 1.5 m thick and 100 meters wide with a deeply corrugated unconformity surface.

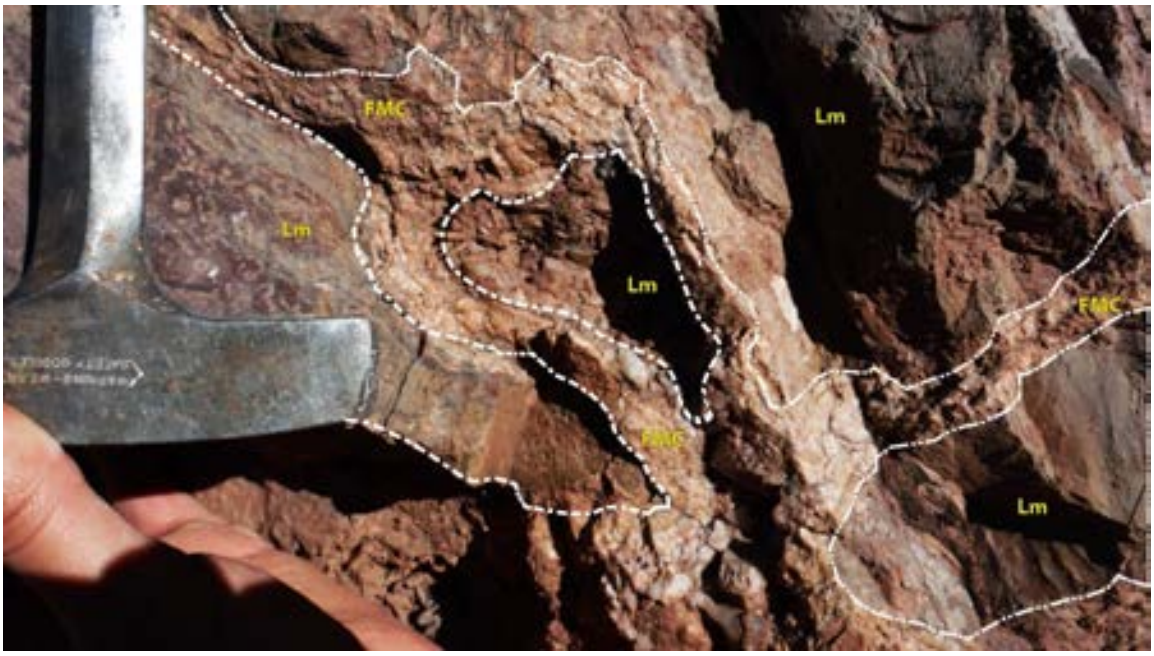

Figure 5.5- Outcrop photograph of facies F-5 at section MS-1, showing limestone blocks (Lm) bounded by isopachous fibrous marine cement (FMC) with larger void filling dog-tooth calcite spar at the edges of FMC.

Figure 5.6- Polished handsample from facies F-5 at section MS-1. These samples reveal that the limestone blocks themselves contain a chaotic fabric of collapse structures, fibrous marine cement and exotic red sandstone clasts.

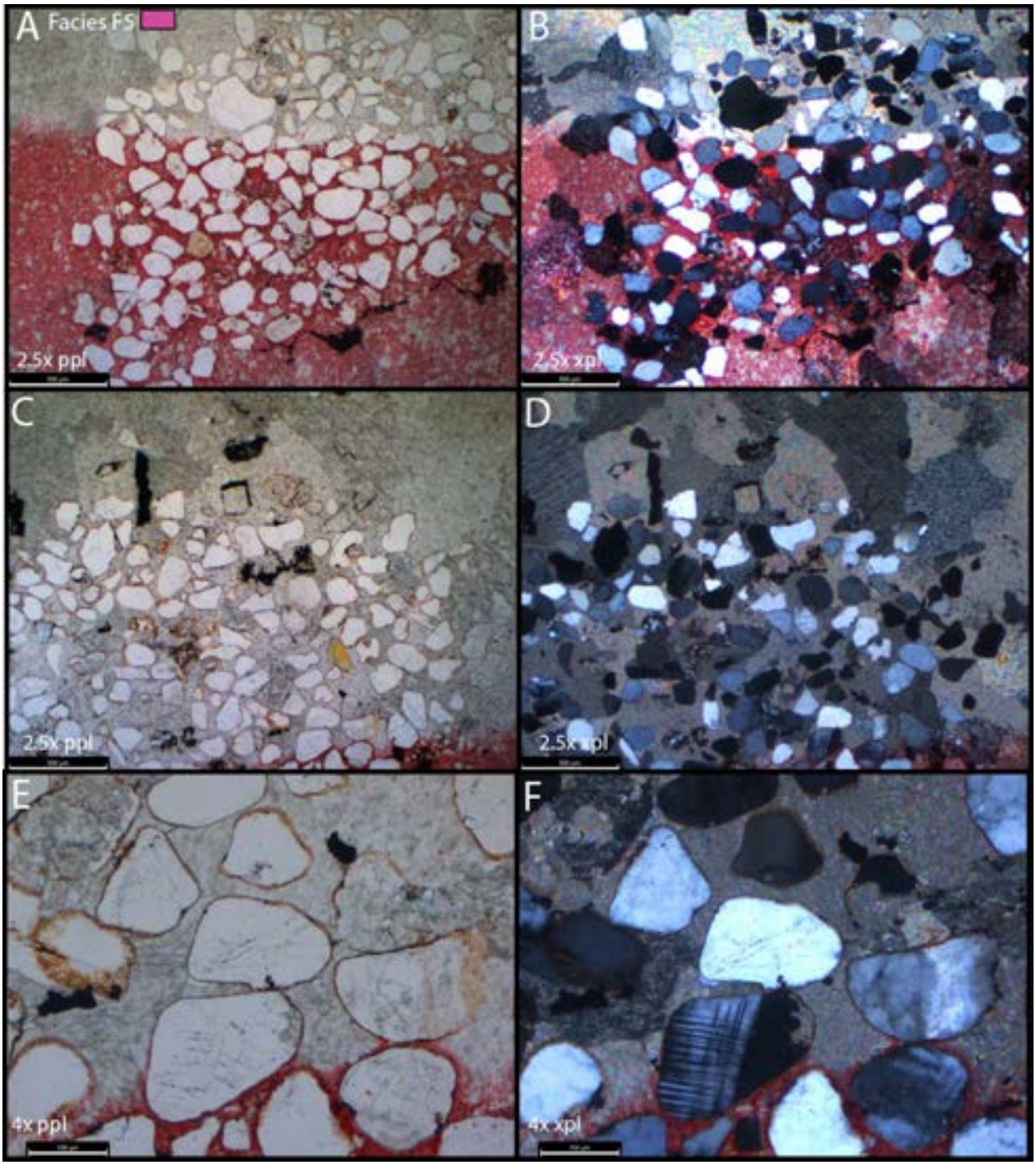

Figure 5.7- Photomicrograph from thin-sections of facies F-5 from measured section MS-1 showing rounded monocrystalline quartz and plagioclase grains with iron oxide dust rims within a poikilotopic calcite spar matrix. Calcite is observed replacing quartz and plagioclase grains with a deeply embayed and etched fabric.

5.2 Interpretation

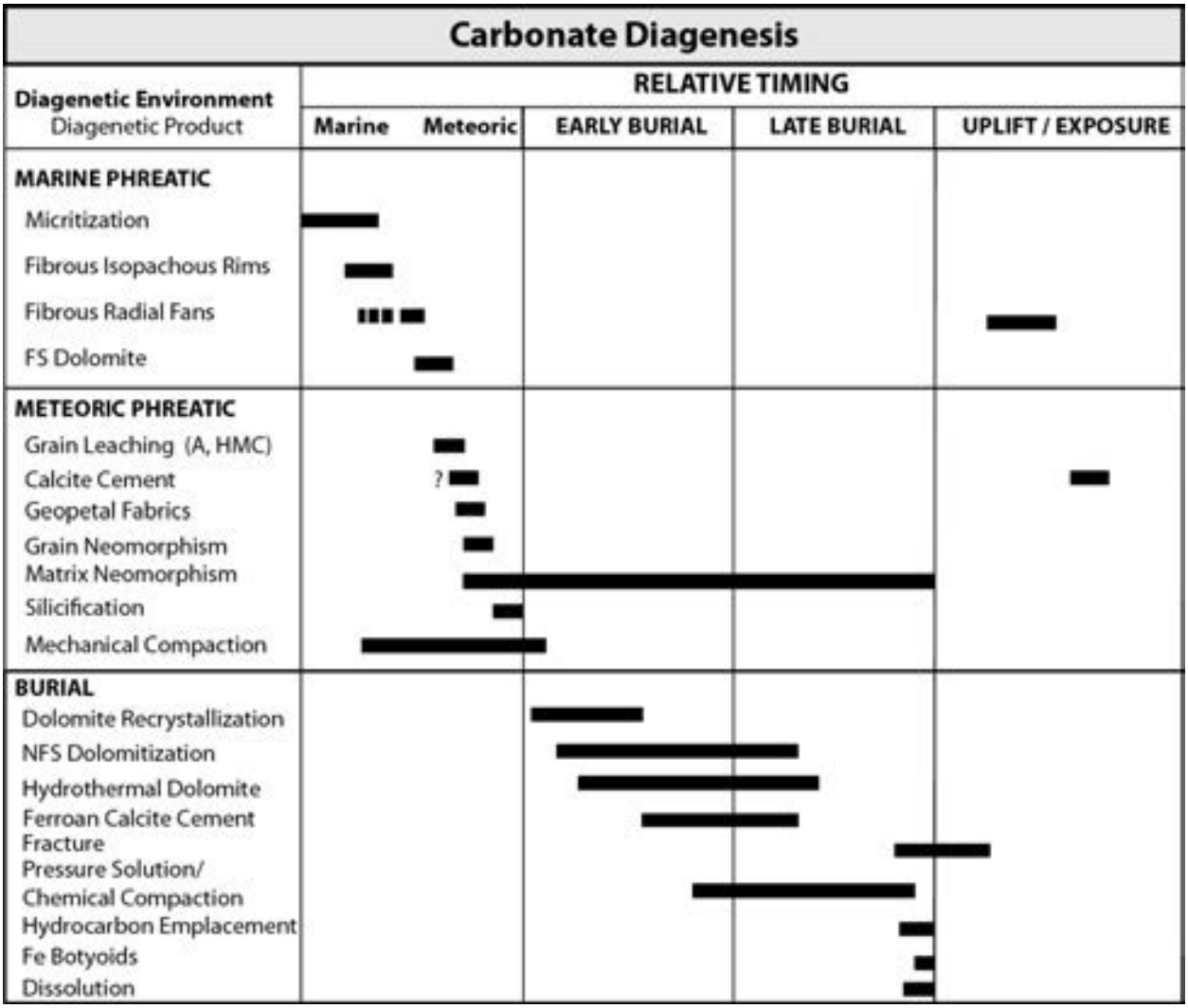

Figure 5.8 – Paragenetic sequence interpretation for carbonates

5.2.1 Stagnant Marine Phreatic – Micritization

Microbial micritization is a process within a marine environment through which endolithic microorganisms, such as algae, actively bore into the boundaries of skeletal grains, ultimately

producing cavities and fine-grained sediment or micrite. The encapsulating sediment is termed a micrite envelope and is a diagnostic fabric typical of early marine diagenesis. The earliest stage of diagenesis observed in the stratigraphic succession is recorded as micrite envelopes around skeletal grains, and is interpreted as a syndepositional fabric within a marine phreatic environment where endolithic algae are abundant. Therefore micritization will be most intense within the shallow marine shelf carbonates and becoming less pronounced in deeper water facies.

5.2.2 Active Marine Phreatic - Marine Cementation

Carbonate and dolomite beds of the megaflap are interpreted to have initially undergone early marine and syndepositional diagenetic processes ultimately generating the first generation of diagenetic cements after micritization. The precipitation of cements in carbonate sediments within marine environments occurs when pore-fluids become supersaturated with respect to calcium carbonate or the mineral phase precipitated (Tucker and Wright, 1991; Tucker and Bathurst, 2009). Cementation is also preferential to specific high-energy environments with active pumping mechanisms that force high amounts of seawater through the pore networks (Scholle et al., 1983; Tucker and Wright, 1991). Shelf margins and shorelines with intense wave, storm and tidal activity are environments commonly associated with preferential cementation (Scholle et al., 1983; Tucker and Bathurst, 2009). These initial non-ferrous cements are diagnostic characteristics indicative of early marine diagenesis and are readily identifiable based on common morphological features of the cement phase (Flügel, 2010). The early marine cement phase is commonly followed by more massive sparry calcite of meteoric origin. Biohermal facies F-3, although intensely altered, shows large centimeter scale cements of successive generations of relict now silicified radial fibrous acicular fans infilling shelter pore space. Radial fan structures such as these are similar in form to originally aragonitic radial fibrous fans typically found in Pennsylvanian-Permian bioherms of the

western Orogrande Basin, New Mexico (Soreghan et al., 2000). The radial fans are interpreted to be an early marine aragonitic cement developed within the network of shelter porosity within the bioherm (Figure 4.13).

5.2.3 Meteoric Phreatic – Vadose

Meteoric environments are extremely dynamic systems in which small-scale changes in sea-level can imprint complex diagenetic fabrics. The meteoric system refers to a zone in which groundwater derived from rainwater is in contact with the sedimentary body (Choquette and Pray, 1970; Tucker and Bathurst, 2009). This system can be partitioned into several zones based on distinctive processes that yield readily identifiable products. The major zones discussed are the vadose zone and the phreatic zone which are separated by the water table at which atmospheric and hydrostatic pressures are equal (Tucker and Wright, 1991). The major characteristics of the zones pertain to saturation in which the phreatic zone is under permanent saturation and the vadose zone is regarded as a zone of periodic saturation and drying. Groundwater movement through the sedimentary body is controlled by either diffuse flow through the primary pore network or through conduit flow through joints and fractures and is principally driven by gravitational or capillary forces (Tucker and Wright, 1991). Under mixing zone conditions vadose and phreatic waters with differing temperatures, salinities, calcite saturations and pH levels combine, often enhancing dissolution rates as ground waters rise and fall (Tucker and Bathurst, 2009). The main mechanisms operating throughout meteoric diagenesis are dissolution, cementation, and neomorphism. Similar to early marine cements overlying micrite envelopes, meteoric processes have readily identifiable fabrics based on common morphological features of the cement phase as well as cross-cutting relationships with syndepositional processes and marine cementation. Interpreted meteoric

processes affecting carbonate sediments in the megaflap are minor dissolution fabrics from diffuse flow, dissolving carbonate grains, to conduit flow developing karst fabrics such as the collapse feature of facies F-5. Collapse features, pendant cements, rounded pores, and red chert formation are observed fabrics interpreted to be products of metoric to vadose diagenesis within the megaflap. Dissolution is the most commonly observed fabric as it is readily preserved as meteoric cement phases occlude the porosity ultimately preserving the remnant pore structure.

All carbonate facies, contain some form of dissolution resulting from acidified undersaturated groundwater flowing through the pore network under diffuse flow. Under these conditions, the acidified meteoric waters will dissolve susceptible grains such as those with High-Mg calcite (HMC) or aragonitic compositions (Figure 5.1B and C). As labile grains are leached simultaneous repricipitation of stable crystal phases such as low-Mg calcite occurs (Choquette and Pray, 1970; Tucker and Bathurst, 2009). Consequently the primary pore network is occluded during meteoric diagenesis and secondary porosity is created. Dolomite ridge facies F-2 and F-3 show extensive dissolution that ranged from meteoric to vadose environments and formed large rounded secondary pore space as well as leached carbonate grains (Figure 5.3). Extensive dissolution is attributed to the facies high primary permeability and local fracturing and faulting.

Although early marine cements are defined as being the initial cement generation, these cements can occur at any point as long as the sedimentary body enters a marine or meteoric to vadose environment. Dolomite ridge facies F-2 shows a marine vadose to meteoric cementation phase developed after successive generations of burial diagenetic cements and fracturing. The aragonitic botryoidal fans found within rounded secondary dissolution cavities that line fracture walls and are interpreted to be pendant structures (Figure 5.3). The late-stage aragonite phase is

interpreted as a return to a meteoric phreatic or marine vadose environments after burial cements phases and fracturing, in which marine waters irregularly coated the pore-network.

Intense vadose fabrics are further interpreted in facies F-5 of the carbonate laminites and contain features typical of arid carbonates deposited within a peritidal setting. The facies consist of a primary dolomitic fabric of marine phreatic dolomite with primary porosity, as birdseye fenestrae, often enhanced and occlude with meteoric phreatic calcite cement. Other early syndepositional to meteoric phreatic fabrics consists of collapse features, calcite occluded keystone vugs, and entrained eolian detrital quartz grains (Scholle et al., 1983; Shinn, 1983). The most notable vadose fabric of this facies occurs within the Honaker Trail Formation at MS-1 within the large scale collapse structure capped by the Jurassic Summerville angular unconformity (Figure 5.4). The collapsed blocks of limestone would initially be interpreted as algal laminated dolomites, however the polished hand sample are extremely chaotic with regards to depositional and diagenetic fabrics (Figure 5.6). Exotic red sandstone clasts are entrained within the blocks, with very-well rounded siliciclastic grains, a characteristic not observed in any of the siliciclastic units of the Honaker Trail Fm, Paradox Formation, or Permian siliciclastics (Figure 4.19, Figure 4.32). The limestone blocks are interpreted to be the original solution collapse blocks of facies F-5 developed within a marine phreatic to vadose environment, however when the megaflap strata was exposed and onlapped by the incipient marine Jurassic Summerville Formation, this facies underwent further brecciation, collapse and cementation. The Jurassic age collapse entrained matrix material and well-rounded Jurassic-aged monocrystalline quartz silt grains and developed Jurassic aged meteoric calcite spar. The quartz and silicate grains observed showed signs of corrosion and etching at the margins and are partially to completely dissolved and replaced with calcite (Figure 5.7). Quartz etching and calcite replacement occurs at elevated pH (> pH 9),

commonly observed in modern marine vadose reef environments, especially with high evaporation rates as observed in the Red Sea (Davies and Kinsey, 1973). The Jurassic Summerville Formation overlying facies F-5 is a composed of a reddish-brown well-rounded pebble conglomerate of predominately well-rounded black chert and limestone clasts within a rounded to well-rounded red sandy to muddy matrix. Although not petrographically observed, the Jurassic Summerville Formation red color sandstone is interpreted to be attributed to iron oxide dust rims associated with syndepositional marine to vadose diagenesis of the Jurassic sandstone.

Brecciation of laminated dolomites observed in the field have several possible modes of formation: (1) cyclic exposure and desiccation of carbonate sediments, often forming soils in modern carbonate environments in subaerial exposure settings. These soils however have poor preservation potential throughout the geologic record, often only preserving underlying caliche and karst fabric (Scholle et al., 1983) (2) the influx of meteoric water resulting in the dissolution and diagenetic modification of carbonate and evaporite material resulting in collapse. Brecciation, dissolution, and laterally disrupted laminations common of facies F-5 indicate periods of sub-aerial exposure in a semi-arid environment (Tucker and Wright, 1991; Tucker and Bathurst, 2009). The collapse features observed at MS-1 are interpreted to be derived from a two-stage diagenetic process that results in the dissolution of and collapse of evaporitic layers associated with facies F-5 within the early marine vadose to meteoric phreatic environments during the Pennsylvanian, and a second dissolution event related to exposure during the Jurassic. Furthermore, the Jurassic angular unconformity surface of facies F-5 at section MS-1 is deeply corrugated and rippled (Figure 5.4), suggesting a wave-washed marine environment responsible for the dissolution and precipitation of marine phreatic isopachous cements. Late stage burial and compressional orogenic

events during the Cretaceous fractured the facies again, evident in clear meteoric calcite veins cross-cutting the chaotic fabric of the limestone blocks (Figure 5.6).

All shelf carbonates and lagoonal facies show vadose diagenesis in the form of red chert replacement fabrics. Lagoonal facies (F-13) shows extensive red chert replacement fabrics in the form of banded botryoidal chalcedony and anastomosing silicification. The spherical calcite phase present that lines the clotted peloidal micrite and thick micrite envelopes that blend into coating foraminfera is interpreted to be a meteoric phreatic to vadose cement phase. The spherical calcite phases are interpreted to be nucleation points for silicification. Silicification of calcitic fossils occurs along thin solution films at which calcite dissolves and silica precipitates. The mechanism is replacement controlled by force of crystallization, whereby the growth of the silica phase exerts pressure across the silica-carbonate contact, increasing the Gibbs free energy and hence solubility of shell calcite (Maliva and Siever, 1988). Physical evidence for force of crystallization-controlled replacement includes restriction of carbonate dissolution to the silica-carbonate contact, and euhedral quartz terminations at some quartz-calcite contacts (observed in facies F-3). Correlations among some replacement quartz types and fossil taxa indicate that shell microstructure and bulk pore water silica concentration control replacement quartz type (Maliva and Siever, 1988). Loope and Watkins (1988) observed red chert replacement fabrics in southeastern Utah within Pennsylvanian mudstones to packstones of the Honaker Trail Formation on the Western shelf of the Paradox Basin. The observed diagenetic fabric was always observed in association with desiccation cracks and other sub-aerial exposure fabrics, and were always observed within 5m of a subaerial exposure surface (Loope and Watkins, 1989). Red chert required the formation of Pyrite within anoxic burial conditions and the respiration of anerobic bacteria decomposing organic material within skeletal material (Loope and Watkins, 1989). During regression and sea-level drop

the sedimentary body would enter a vadose environment ultimately oxidizing pyrite into iron oxides (Loope and Watkins, 1989; Figure 5.9). Principal lines of evidence for silicification predating deep burial environments is the mechanical fracturing disrupting many of the observed silicified fabrics. The red chert replacement fabric observed through the marine facies of the megaflap are interpreted to be a diageneic fabric associated with subaerial exposure and requires environmental ranges from marine phreatic to vadose.

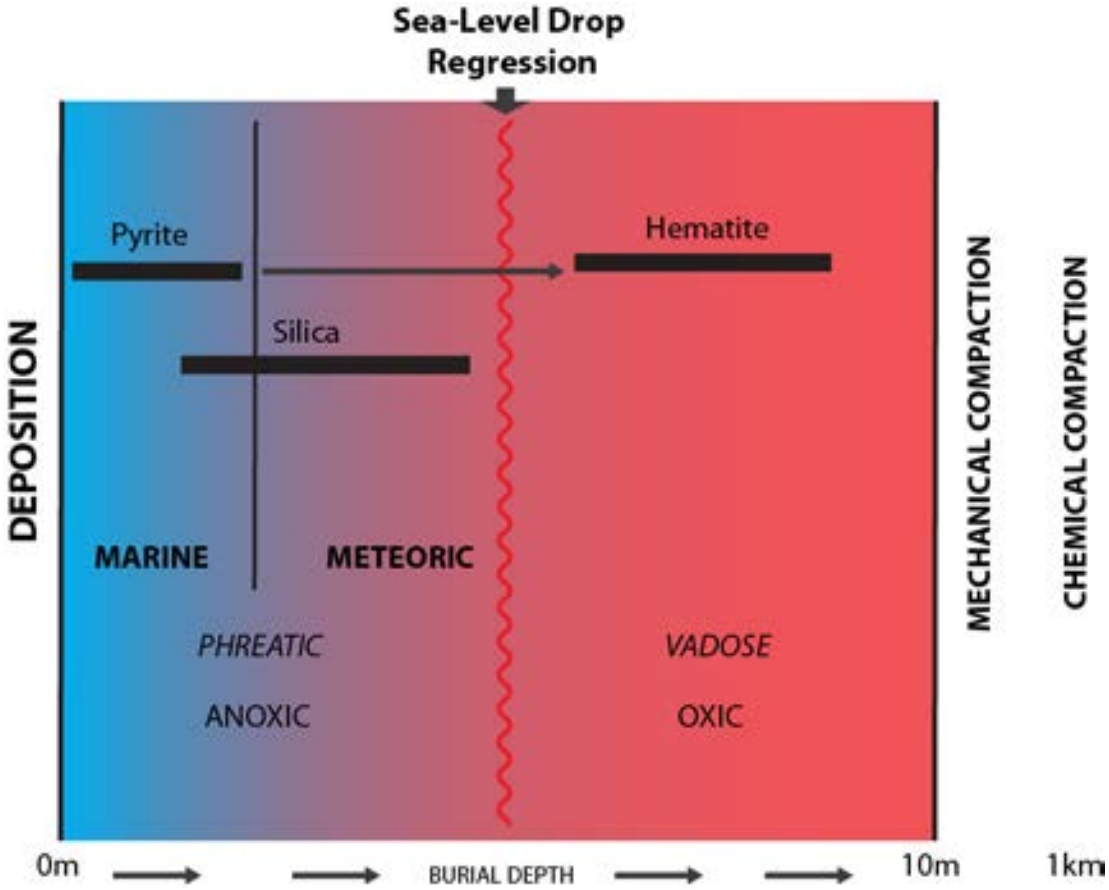

Figure 5.9. – Schematic showing possible origins of red chert formation within a phreatic to vadose environment. Modified from (Loope and Watkins, 1989).

5.2.4 Burial Environments

Burial diagenetic systems and related products such as cementation, mechanical and chemical compaction are generated over significant ranges of depth, pressures, and temperatures as well as

highly variable pore-fluid chemistries. The burial diagenetic realm is considered to occur below the zone at which sediments are altered by near surface processes within the marine phreatic to meteoric environments. Burial diagenetic effects are progressive making it difficult to discern timing as well as attempting to tie diagenetic processes to specific depth ranges. Burial diagenetic fabrics, much like early marine and meteoric diagenesis have common morphologies and crystallographic properties that are readily identifiable and specific to burial conditions.

5.2.5 Mechanical and Chemical Compaction

Mechanical processes begin soon after deposition of the overlying sediment resulting in dewatering, reorientation of grains and preferential alignment. Ductile deformation of lime mud facilitates mechanical compaction of more brittle and competent grains generating a considerable loss of thickness and porosity within the first several meters of burial. Mechanical properties of facies often dictate the severity of compactional fabrics (Choquette and Pray, 1970; Tucker and Bathurst, 2009; Flügel, 2010). Specific diagenetic processes early on such as the pervasiveness of early marine cementation will be a controlling factor in resultant burial diagenetic fabrics, as the mechanical properties of carbonates change through diagenetic environments. Carbonates with pervasive early marine cementation often preserve depositional pore architecture through progressive burial while facies with minimal cementation early on will undergo mechanical fracturing and more intense pressure dissolution and compaction (Choquette and Pray, 1970; Tucker and Bathurst, 2009). Mechanical fracturing and pressure dissolution of grains begins at approximately 3.5 to 6.5 km burial depths based on laboratory data of ooids under pressure, and quaternary-tertiary cores of shallow marine carbonates showing mechanical fracturing at several hundred meters (Choquette and Pray, 1970; Tucker and Bathurst, 2009; Flügel, 2010). Concurrent

with burial cementation and increasing overburden thickness carbonate sediments will form a range of fabrics generated from mechanical compaction as observed within megaflap stratigraphy. Deeper burial environments facilitate the generation of a range of fabrics produced from chemical compaction and pressure dissolution. Chemical compaction results in the dissolution of grains and increased solubility of carbonate material at point contacts and grain surfaces through continued applied stress and will result in the development of observed stylolite and interpenetrating contacts (Choquette and Pray, 1970; Flügel, 2010).

5.2.6 Faulting/Fracturing

Petrographic analysis of facies F-2 of the dolomite ridge is observed to have two end-members of diagenesis, the first is related to diagenesis of the dolomite host away from faulting and dominated by non-fabric and fabric selective dolomitization with preserved depositional structures (Figure 5.16a) or completely recrystallized by coarsely crystalline dolomite and silicified (Figure 5.16c). The second diagenetic fabric is proximal to faulting and brecciated fabrics and dominated by silicified (chert) carbonate, botryoidal iron oxide cement, drusy anhedral calcite and botryoidal radial fibrous aragonite (Figure 5.3). Observation of thin-sections away from faulting reveals a neomorphosed coarse- to finely crystalline dolomitized fabric and is interpreted to have been preserved by being in a distal position from fluid flow associated with faulting (Figure 5.13). The carbonate host of facies F-2 proximal to faulting and brecciated fabrics is completely silicified by microcrystalline quartz as chert, obliterating the depositional fabric with only dispersed detrital quartz recognized. Silicification replaces much of the dolomitized carbonate and was followed by secondary dissolution of the chert generating abundant vuggy porosity. Iron rich fluids then preferentially moved through the faults and fractures, further fracturing and brecciating

the host and partially infilling vuggy porosity and lining fracture walls with iron oxide cements that are botryoidal in dissolution cavities (Figure 5.3).

5.2.7 Burial Cementation

Burial cement phases are commonly void filling drusy equant calcite spar, poikilotopic calcite, syntaxial twinned calcite spar and overgrowths, ferrous calcite, as well as hydrothermal dolomite. Because calcite spar is a common fabric obtained in meteoric environments, it is difficult to address the origin of calcite spar and the extent of neomorphism or recrystallization without geochemical investigations, however burial calcite cements are typically clear, coarse, with crystal grain sizes generally increasing and terminating towards the center of void space (Tucker and Bathurst, 2009), are commonly ferrous and are penecontemporaneous with mechanical and chemical compaction fabrics (Tucker and Wright, 1991). Much of the interpretation for deep burial diagenesis within the megalflap is from observations of ferrous calcite cements and twinned poikilotopic calcite cement (Figure 5.2D, Figure 5.12E, and F). Figure 5.12E and F, of Facies 12 of the marine shelf limestones, shows shelter porosity likely preserved through marine phreatic and meteoric environments as well as preserved vadose geopetal fabric. The shelter pororisty was ultimately occluded with ferrous calcite cement (Purple Stain) developed within a burial environment. The ferrous calcite phase shows large crystal sizes compared to the fibrous marine calcite and meteoric calcite stained pink. The ferrous calcite cements also show no signs of burial compaction either mechanical or chemical, suggesting an origin contemporaneous with a burial environment. Sponge spicule facies show prominent ferrous calcite cementation within burial

environments as the siliceous sponge spicules dissolve and are occluded with meteoric calcite then finally replaced with ferrous calcite and take an overall purple stain (Figure 5.10 and Figure 5.11). Burial diagenetic cements are not facies restricted as all facies show some form of burial diagenetic cements as ferroan calcite, however facies primary depositional porosity seems to control the pervasiveness of diagenesis in all facies.

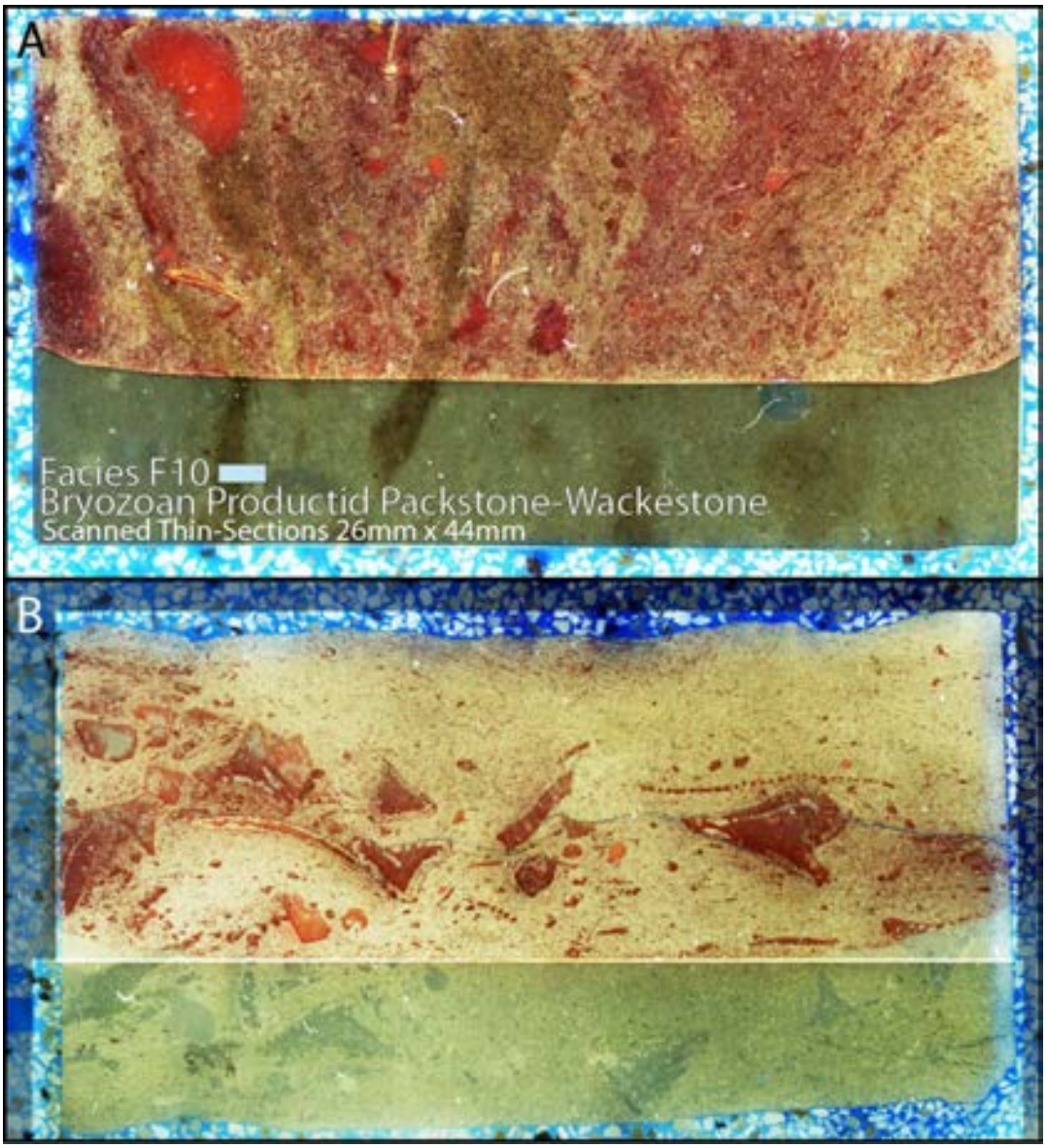

Figure 5.10-Scanned thin-section under cross-polarized light of the shelf limestone facies F-10. (A) Silicified matrix and ferrous calcite replace siliceous sponge spicules and (B) silicified matrix and moderate silicification of bryozoans, brachiopods, and echinoderm plates.

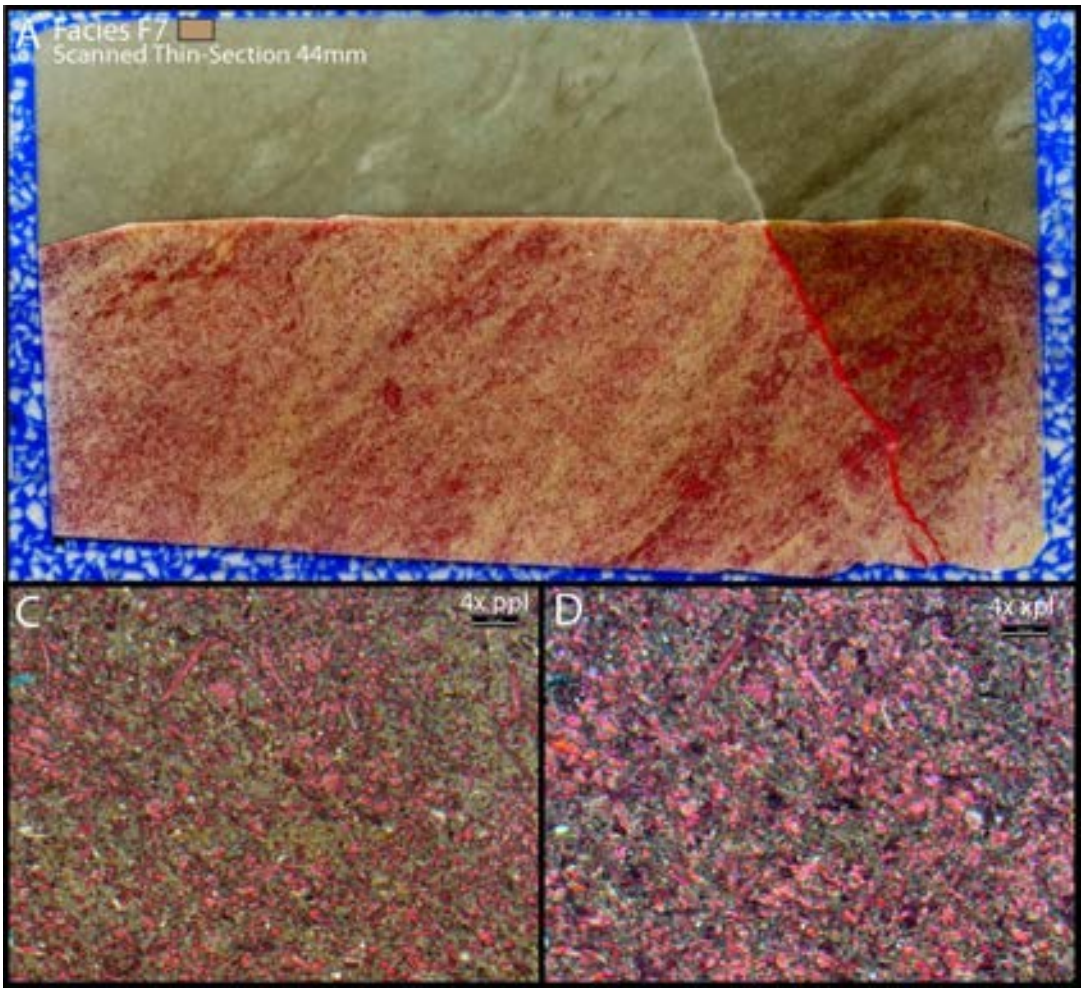

Figure 5.11- Scanned thin-section and photomicrographs from the sponge spicule lagoon facies of F-7. Siliceous sponge spicules are completely calicified while the original micritic calcite matrix is entirely silicified. Late stage fracture occlude with meteoric calcite cross-cut the samples.

5.2.8 Hydrothermal Dolomitization

Hydrothermal, is defined as any water appreciably warmer (5°C or more) than the surrounding environment, or ambient temperature (White, 1957). Hydrothermal fluids responsible for dolomitization (HTD) include mineral laden brines under burial conditions of temperature and pressure higher than that of the limestone host (Davies, 2006). Mineral saturated bines, typically Na-Ca-Mg-Cl, are the primary fluid for dolomitization. However, non-saline hydrothermal fluids with insufficient magnesium levels are also capable of dolomitization when they are sufficiently above the ambient temperature and pressure of the host (Lovering, 1969). HTD is the result of transport of hot dolomitizing fluids through a lower temperature limestone host. The definition itself implies evidence for mechanisms influencing fluid flow, and the existence of a geothermal source responsible for increased fluid temperature. Much like previously discussed diagenetic fabrics, HTD has common recognizable petrographic features such as a curved rhombohedral crystal lattice and sweeping extinction (Davies and Jr, 2006). Facies F-3 and F-2 of the Dolomite Ridge are the only facies observed to have diagenetic dolomite in the form of hydrothermal dolomite. Vuggy porosity of the Dolomite Ridge is developed through a phase of burial dissolution cross-cutting coarse neomorphosed depositional dolomite and followed by hydrothermal dolomitization (HTD) interpreted through sweeping extinction of the curved crystal lattice protruding into dissolution vugs (Figure 5.13 C & D). HTD fabrics were developed during burial (mesogenetic) diagenetic environments prior to significant mechanical fracturing of the host as the dolomitized host is cut by large fractures that are filled will hematite or ferrous minerals.

5.2.9 Neomorphism / Recrystallization

The primary composition of the components of limestone, specifically skeletal grains and lime mud, have variable mineralogy within observable modern environments and ancient limestones and is thought to control the pervasiveness of neomorphism (Tucker and Bathurst, 2009; Moore, 1989). The micrite matrix of limestones is composed of a needle like fabric of equant micrite crystals averaging 2-3 μm, creating an optically near opaque fabric. Through progressive burial diagenesis and neomorphism the fine grained micrite matrix will generate a mosaic of microspar to pseudospar with crystal sizes of 5 to over 30 μm (Moore, 1989). Although neomorphism can initiate during early meteoric diagenesis as observed in modern carbonate shelfs (Moore, 2989), burial diagenesis is interpreted through cross-cutting relationships with early marine diagenesis and a penecontemporaneous relationship with mechanical and chemical compaction. In thin-section neomorphism has optically recognizable fabrics such as; irregular and often embayed to curved crystal boundaries, irregular crystal size distribution and gradational and irregular boundaries of areas of neomorphic spar (Moore, 1989; Tucker and Bathurst, 2009). All facies show some form of matrix neomorphism with the most intense observable neomorphic fabrics occurring within the Paradox Formation of Facies 2 and 3. Facies F-2 shows dolomite crystal size was slightly enhanced through matrix neomorphism compared to unaltered micrite matrix. Circulating fluids effected much of the Paradox Fm. stratigraphy during early and late burial which moderately enhances crystal size through fabric and non-fabric selective dolomitization. Facies F-2 shows the micritic matrix is completely neomorphosed and dominated by fine- to coarsely-crystalline dolomite micro-spar with planar tosubhedral crystal boundaries with sweeping extinction (Figure 13, Figure 16a). Identifiable skeletal grains, and interpreted

intraclasts are completely neomorphosed with non-mimic fabrics of coarsely crystalline dolomite with echinoderm plates undergoing mimic replacement, preserving unit extinction.

5.2.10 Burial Dissolution

Generally limestone porosity decreases with increasing depth due to diagenetic cementation and compaction. Porosity however can also be created through burial dissolution mechanisms, as well as fracturing and faulting. Dissolution of carbonate material within burial environments is related to the development of acidified pore fluids with high Pco_2 that form during thermal decarboxylation of organic matter or through sulphate reduction (Moore, 1989; Tucker and Bathurst, 2009). The principal driver for dissolution therefore would be the presence or abundance of organic matter either within skeletal material, organic rich shales, or through circulating hydrocarbons. Burial dissolution of sulphate evaporites is another mechanism responsible for dissolution of dolomites specifically, in which pore waters are saturated with respect to Ca^{2+} creating solution collapse breccias up-dip from dissolving evaporites (Moore, 1989). Dissolution is recognizable as the creation of secondary porosity and solution vugs (Choquette and Pray, 1970). Within the megaflap stratigraphy facies F-2 and F-3 are the only carbonate lithologies to have undergone observable burial dissolution . Burial dissolution is in the form of dense clustered vugs that are either still void spaces or are filled with an optically brown iron oxide material.

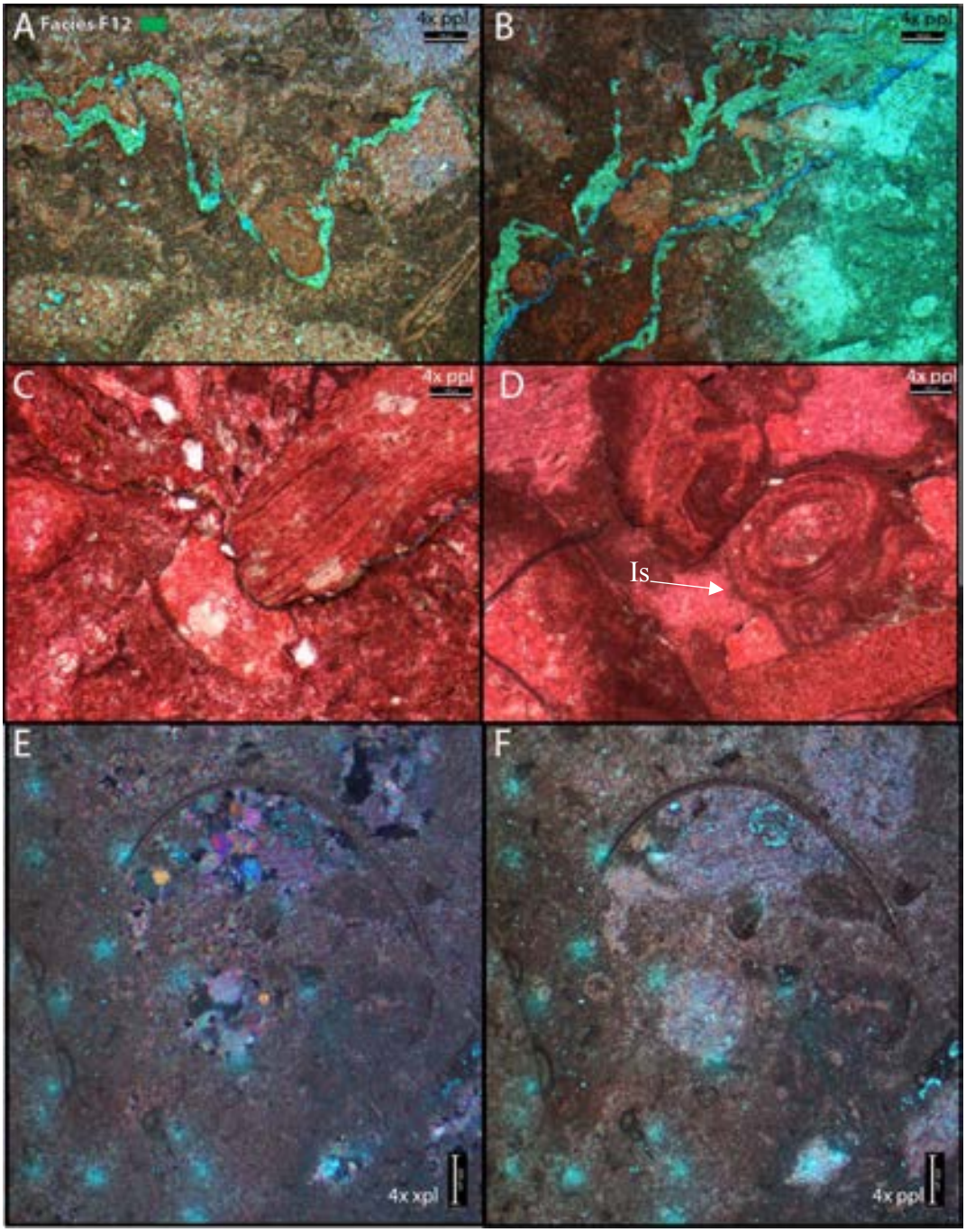

Figure 5.12- Photomicrographs of thin sections of facies F-12. The sample shows pervasive recrystallization of the micritic calcite matrix and skeletal grains. Primary porosity is commonly preserved through shelter porosity and later occluded with ferroan calcite (E & F). Non-fabric selective silicification is common in this unit. Silicification is focused along anastomosing stylolitic surfaces with selective silicification propagating along solution seams. Late stage dissolution props open solution seams and generates micro intracrystalline porosity within the microcrystalline silica cement. Is = Isopachous calcite cement

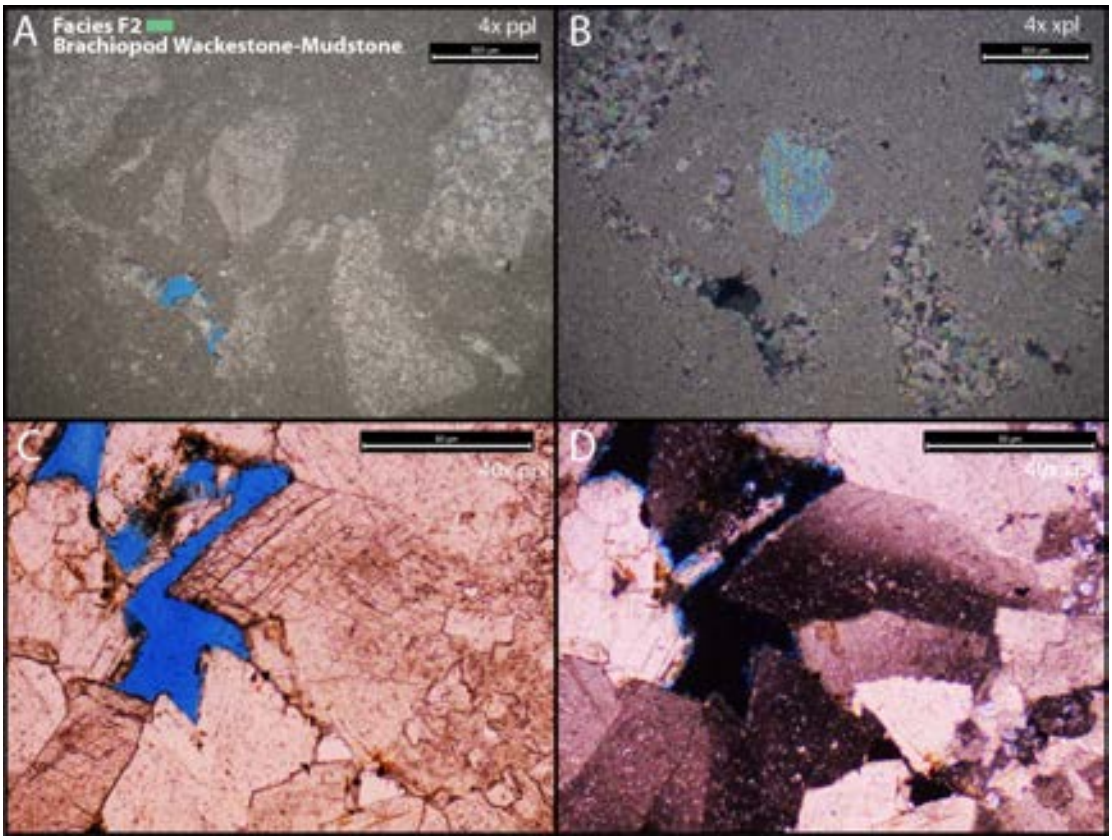

Figure 5.13- Photomicrographs from facies F-2 of the dolomite ridge (scanned thin-section Figure 5-13a). Photomicrographs (A&B) under plain light and crossed polarized respectively, show coarsely crystalline neomorphosed primary dolomite restricted to angular intraclasts, and dolomitized echinoderm plates with preserved unit-extinction within a more finely crystalline to sucrosic dolomitized matrix. Photomicrographs (C&D) under plain and crossed polarized light, showing diagnostic curved crystal lattices and sweeping extinction of hydrothermal dolomite extending into vuggular pore space shown in 5.10a.

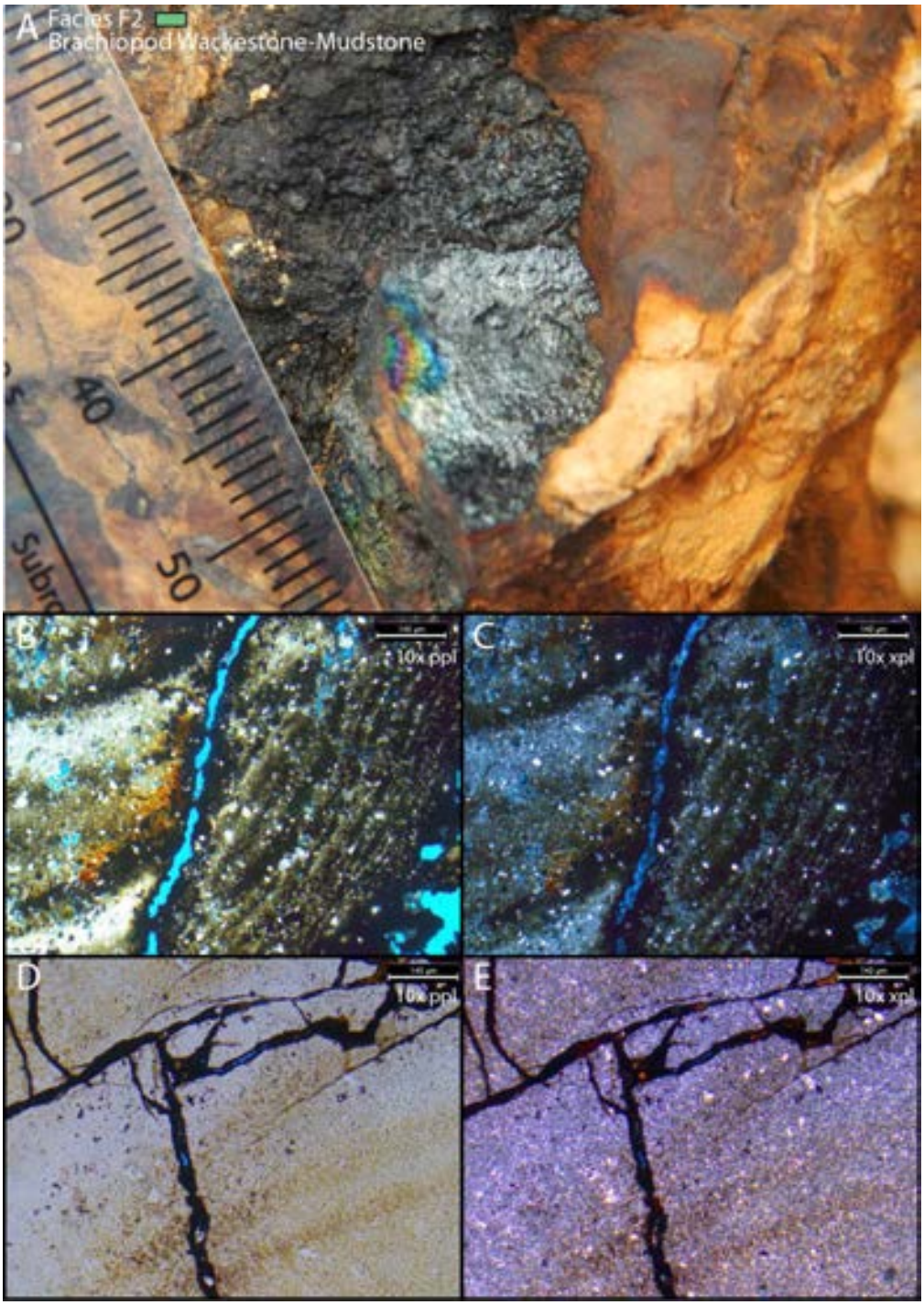

Figure 5.14 – Field photograph (A) from facies F-2 taken from a fault proximal position, and photomicrographs (B,C,D,&E) of scanned thin-section figure 5.2b. Field photograph shows black metallic and multi-colored iridescent tarnish on the weathered surface as well as red banded iron oxide staining of the overall chert host. Thin-sections (B&C) from this locality observed under plain and crossed-polarized light show intense lisegang banding of reddish to black iron oxide.

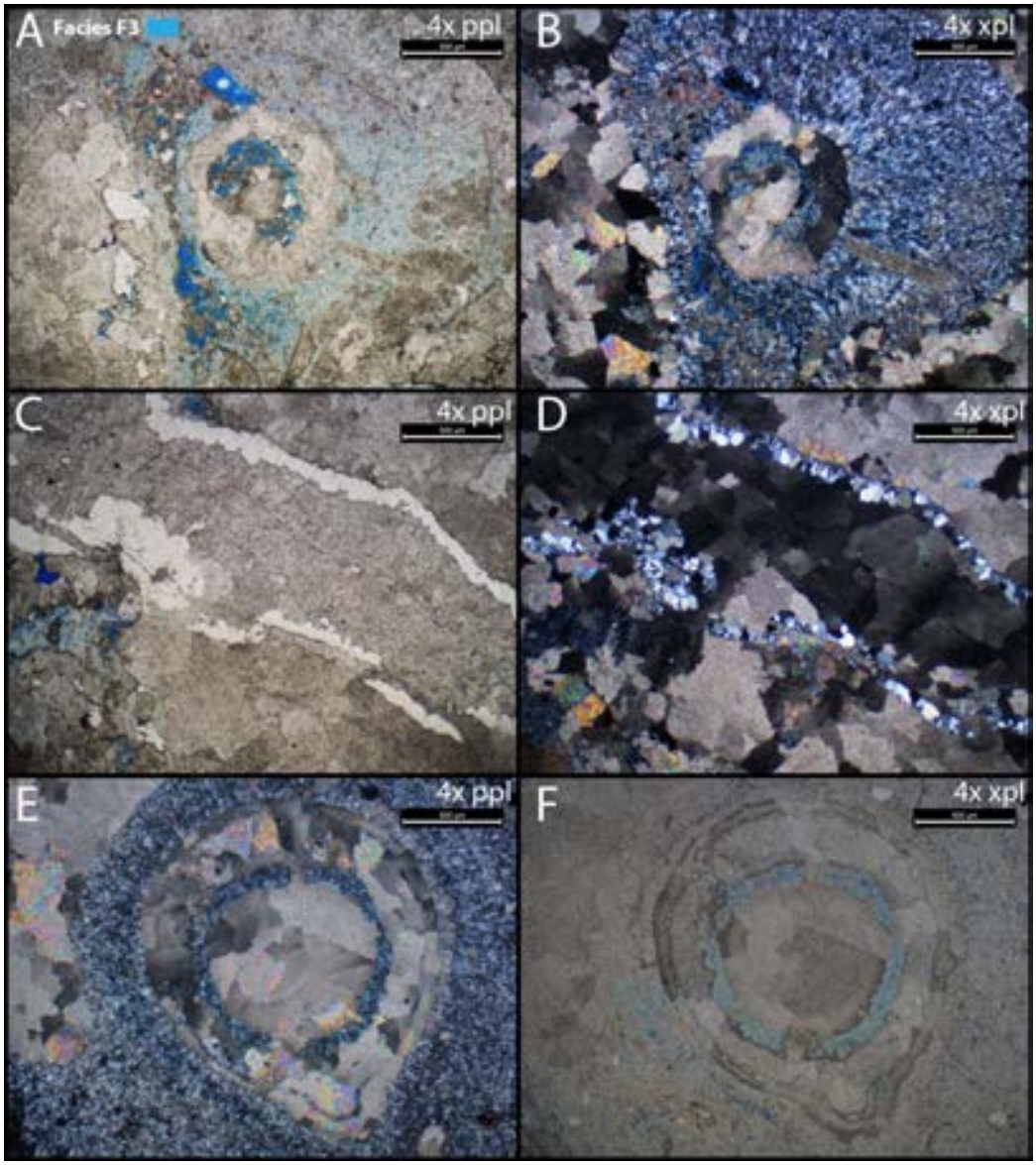

Figure 5.15- Photomicrographs of thin-sections of facies F-3. Three dominated mineralogies are present, and include hydrothermal dolomite, blocky rimming equant quartz, and radial fibrous silica cement. Oncoidal structures are skeletal tube fossil grains that dominate facies F-3.

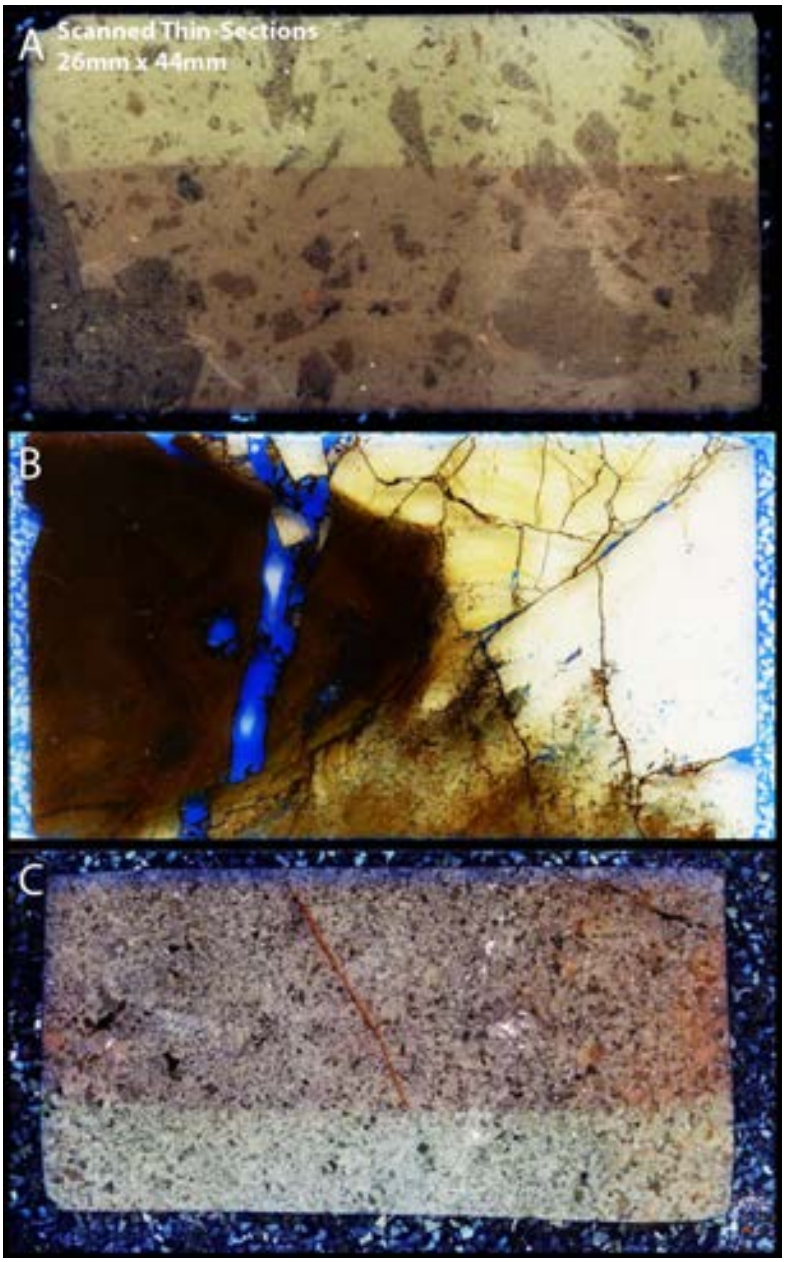

Figure 5.16- Scanned thin-sections of facies F-2 under cross-polarized light showing different diagenetic fabrics. (A) Coarsely crystalline hydrothermal dolomite developed in larger intraclasts and skeletal grains within in a neomorphosed crystalline dolomite matrix, primary depositional fabrics still observable located away from faulting. (B) Fault proximal sample showing darker brown iron oxide and silicified carbonate host and dissolution (C) a completely neomorphosed host with no preserved depositional features.

5.3 Siliciclastics

Diagenetic alteration within the siliciclastic units of the megaflap is initially controlled by the provenance of the sediment, specifically as it relates to the source terrain of the fluvial dominated lower Cutler Formation and the marine reworked eolian sands of the Honaker Trail and Paradox Formation. Variations in the overall composition of the sedimentary body are predominately influenced by the mineralogy of the source rock, but more importantly is the compositional reliance on mechanical and chemical stability of minerals (Tucker, 2001). Once minerals are exposed to environmental conditions outside of the normal temperature, pressure, and chemical regime of formation, they become chemically susceptible to weathering. The relationship between crystallization temperature and chemical weathering susceptibility can be illustrated through the Goldrich weathering stability series, or the inverse of Bowen's reaction series. Specifically, minerals of high temperature provenance; olivine, pyroxene, plagioclase are considerably less stable than that of low temperature crystallization of quartz, micas, and potassium feldspar (Goldrich, 1938; Johnsson, 1993). This relationship results in a relative increase in stable mineral composition of siliciclastic sediments through the chemical and mechanical degradation and depletion of unstable minerals (Johnsson, 1993). Furthermore, the unstable mineral assemblages of the weathering stability series are also inherently the least durable, resulting in difficulties in discerning the levels of chemical or mechanical weathering (Johnsson, 1993). Mechanical stability is reliant upon cleavage planes, and hardness; making quartz (relatively hard, no cleavage) mechanically stable in comparison to the mechanically unstable feldspar (relatively soft, showing strong cleavage), (Tucker, 2001). Though the weathering stability series produces a framework for assessing mineral degradation, severity of alteration is dependent upon intensity (primary controls: climate i.e., rainfall/temperature and

organic acids supplied through vegetation) and duration (primary controls: relief, slope, sediment storage, and sedimentation rates) of weathering (Johnsson, 1993). The fluvial dominated sands of the megaflap are principally sourced from the crystalline Precambrian basement of the Uncompaghre uplift and are primarily composed of plagioclase, potassium feldspar, monocrystalline and polycrystalline quartz, and biotite and micas while the marine reworked sands are more mature dominated by mono-crystalline quartz and micaceous material. Much of the diagenetic alteration observed in the megaflap siliclclatics therefore is related to the goldrich weathering series in that unstable compositions, principally K-feldspar become susceptible to dissolution initially during syndepositional processes and finally burial conditions that develop significant intracrystaline porosity.

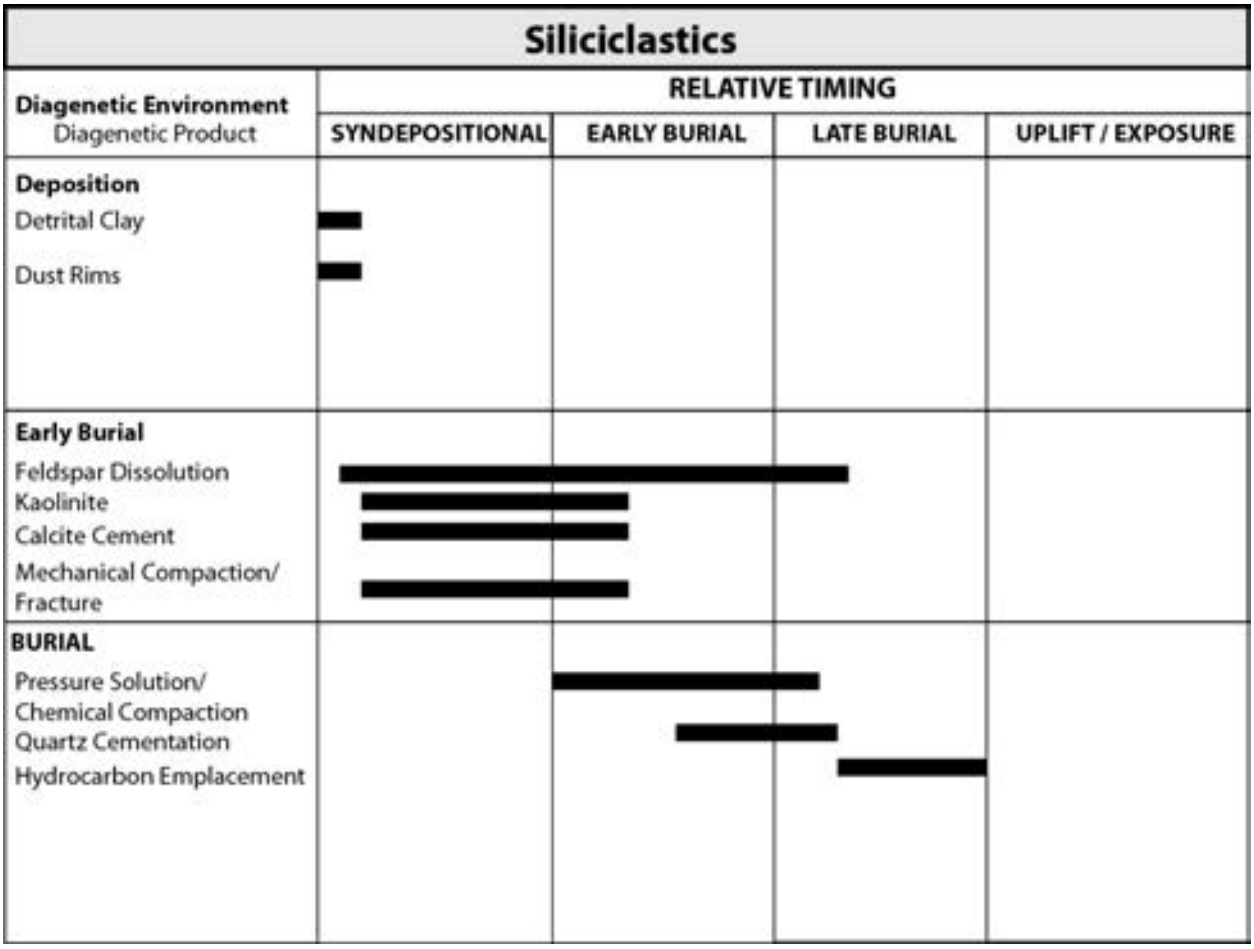

Figure 5.17 – Paragenetic Sequence showing syndepositional to uplift and exposure processes.

5.3.1 Compaction – Chemical and Mechanical

Much like the compaction observed in carbonate sediments, volume loss or severity of compactional fabrics is dependent upon the initial compositional properties of the sedimentary body and form readily identifiably features. Moderately sorted coarse-grained clastic sediments have initial depositional porosities of roughly 40% which also corresponds to the porosity of random preferential packing of uniform spheres (Burley and Worden, 2003). Therefore initial

depositional porosity values are dependent upon the initial sorting and arrangement of grains. Burial conditions result in increasing lithostatic and hydrostatic pressures with the resulting degrees of compaction are dominated by the ratio of brittle to ductile grains. Compaction therefore occurs in response to grain reorientation through plastic and ductile processes and increase in severity to dissolution and fracturing. Silicate mineral solubility generally increases with increasing temperatures and pressures generating pressure dissolution seams and increasing severity grain contacts, a diagnostic observable fabric that can be used to identify intensity of compaction. Point contacts between grains with increasing burial conditions will evolve to planar to concavo- convex to interpenetrating and ultimately sutured contacts.

All siliciclastics of the fluvial dominated facies of F-9 and F-11 as well as marine sands of F-6 show planar to concavo-convex, and minor interpenetrating contacts between siliciclastic grains (Figure 5.17). The observed compactional fabric of the siliciclastics therefore represents typical burial signatures that would develop within a sedimentary basin.

5.3.2 Dissolution

Increasing depth of burial will affect temperatures and pressures as well as composition of formation waters ultimately driving diagenetic changes of unstable mineral phases. Disolution of siliciclastic grains is readily identifiable and generally forms intracrystalline porosity in early stages to moldic porosity when only the euhedral pore space remains. Within the megaflap dissolution of detrital potassium feldspar silt is pervasive, developing significant intracrystalline porosity. K-feldspar dissolution is pervasive in all facies that contain the detrital component (F-6, F-9, F-11) as the mineral is unstable at all conditions found in sedimentary basins (Burley and Worden, 2003). Dissolution of K-Feldspar occurs over depth ranges of 1.5 to 4.5 km with

temperature ranges from 50 to 150°C (Wilkinson et al., 2001). Therefore attrition of these labile grains are interpreted to begin early until the fluid compositions change or porosity and permeability is occluded. Through the dissolution of potassium feldspar through a processes of kaolinitization, the kaolinite will begin to occlude porosity ultimately slowing the rate of dissolution (Burley and Worden, 2003). Dissolution is abundant in the Paradox Fm., Honaker Trail Formation and lower Cutler Formation, as dissolution and kaolinitization of labile arkosic detrital grains of K-feldspar is pervasive. Dissolution is only partial in many pore spaces with the remnant crystal lattice of the feldspar grains forming intracrystalline porosity with kaolinite partially occluding some pore spaces.

5.3.3 Quartz Cementation

Silica cementation of sandstones typically occurs within temperature ranges of 70 – 100°C (Burley and Worden, 2003). Quartz cementation within the megaflap typically occurs as epitaxial quartz over growths and likely occurs through formation waters saturated with silica as k-feldspars are dissolved through kaolinization as well as increased solubility of silicate matieral with increasing temperatures and pressures during burial (Burley and Worden, 2003).

5.3.4 Hydrocarbon Emplacement

Hydrocarbons within the Paradox Basin are sourced from the organic-rich source rocks of the Paradox Formation. Burial thermal history plots from Nuccio and Condon (1996) show the maximum burial depth of the Paradox Formation occurred in the Late Cretaceous to Early Tertiary time, during this period peak hydrocarbon generation and migration occurred. Much of the pore spaces of the siliciclastic units are coated with hydrocarbons as kerogen. Hydrocarbons are also observed within the euhedral pore spaces left from the dissolution of K-feldspar indicating an

emplacement much later in time as the petroleum system evolved (Figure 5.17). Oil bearing sandstones typically undergo less diagenesis compared to adjacent non-oil beating reservoirs (Burley and Worden, 2003). This cessation of significant diageneis is observed in the siliciclastic units containing oil and the hydrocarbonate emplacement is typicall the last diagenetic event (Figure 5.18).

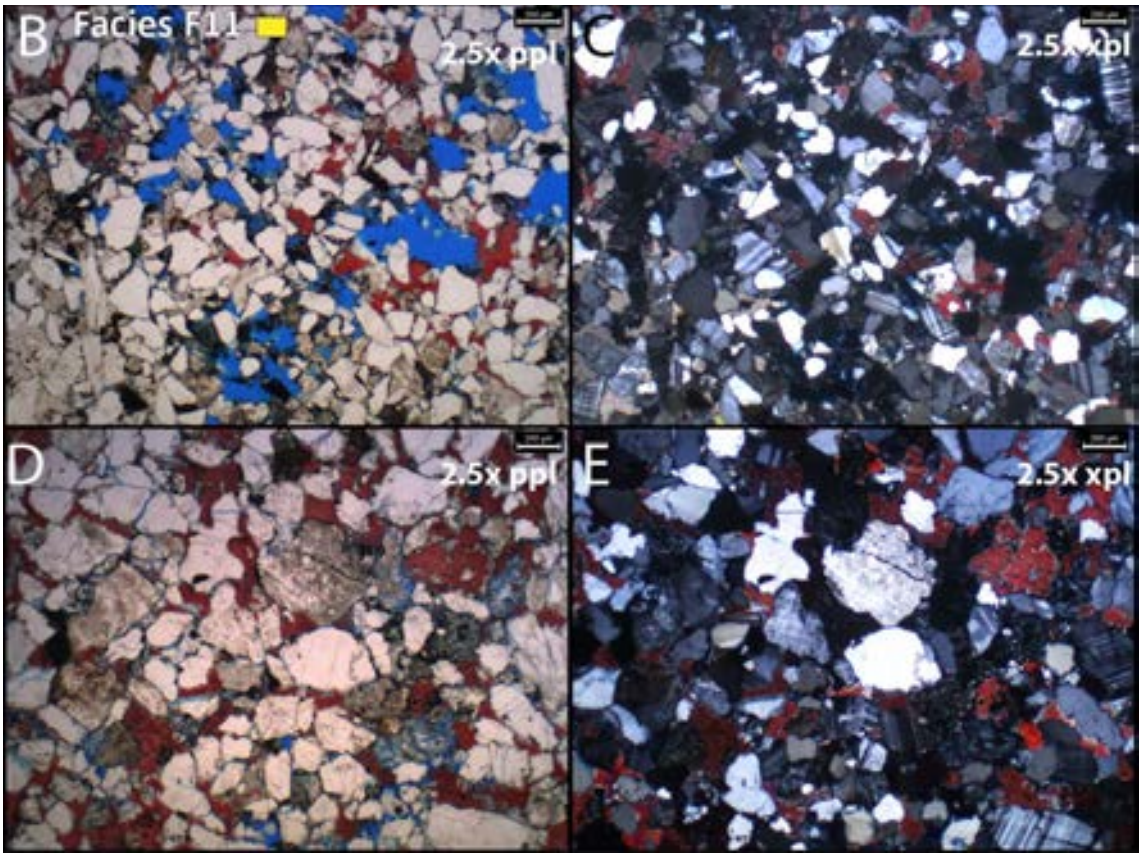

Figure 5.18 – Facies F-11 of the lower Cutler Formation. B and D with respective cross polarized view C and E showing significant dissolution as blue dyed euhedral pore space of remnant K-feldspar with hydrocarbons lining pore spaces. Meteoric calcite cement stained red.

Chapter 6: Sequence Stratigraphy

Through Waltherian analysis of the lithofacies succession of the Paradox, Honaker Trail, and lower Cutler formations exposed in the Gypsum Valley megaflap, 11 fourth-order (.1-.2my duration; Mitchum & Van Wagoner, 1991) unconformity-bound sequences are identified (Figure 6.1).The sequence stratigraphic framework presented is derived from interpretation of depositional facies stacking patterns; specifically waltherian and non-waltherian facies shifts, exposure surfaces denoting type-1 sequence boundaries (Vail, 1987), and prolonged flooding events corresponding to marine transgressions. Sequence boundaries in this field area are defined by shallow marine carbonates capped by subaerial exposure surfaces with overlying terrigenous non-marine facies; defining a non-waltherian basinward facies shift. Parasequence sets are interpreted based on methodologies defined by Van Wagoner et al. (1988) for a conformable succession of genetically related shallowing-upward facies, bound by flooding surfaces. Parasequence-sets amalgamate into the larger scale fourth-order sequences that can be subdivided into component highstand, transgressive, and lowstand systems tracts. The interpreted sequence stratigraphic framework of the Klondike Ridge megaflap is compared to previous workers sequence stratigraphic analysis of Pennsylvanian strata along the western and eastern margin of the Paradox Basin.

The megaflap lowstand systems tracts (LST) are primarily composed of laterally continuous, stacked fluvial channel and flood-plain siliciclastics. Transgressive systems tracts (TST) are composed of marine silty argillaceous mudstones and wackestones or shoreface siliciclastic successions. Highstand systems tracts (HST) contain thin laterally continuous shoaling-up parasequences of shallow marine packestones-wackestones capped by skeletal grainstones and peritidal laminated dolomites.

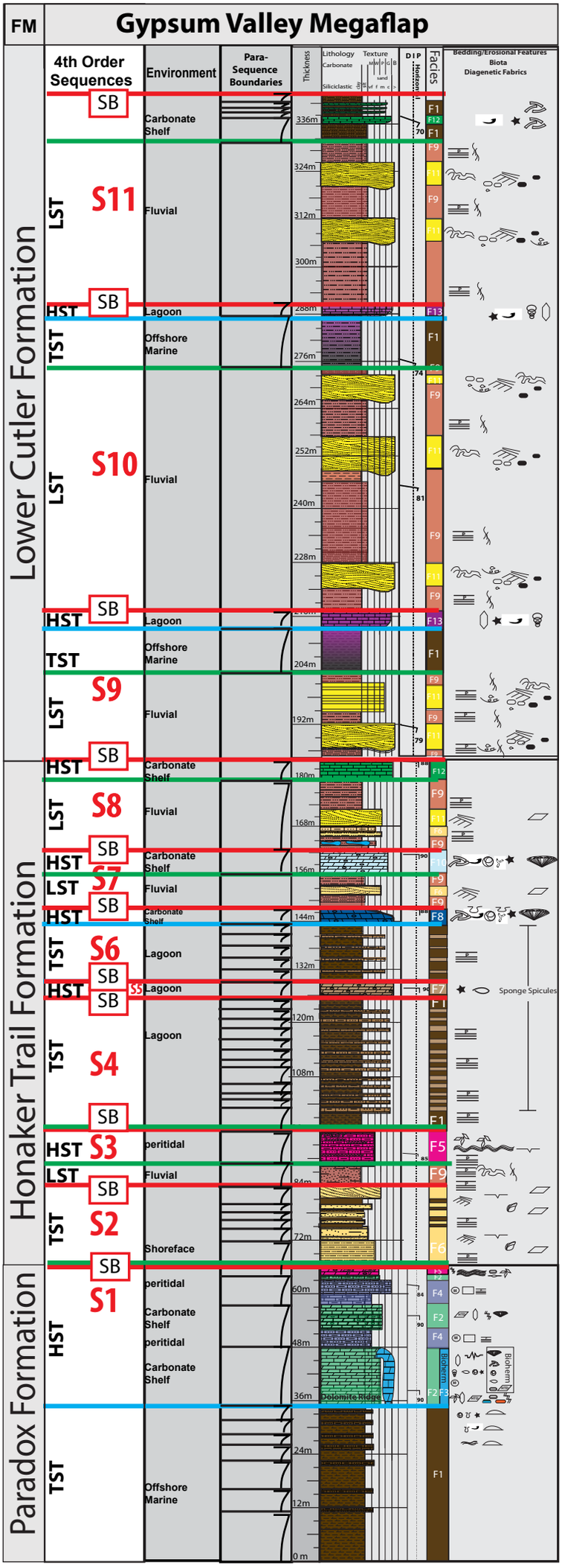

Depositional Environments

Fluvial

- F11 — Channelized Conglomeratic Sandstone
- F9 — Red Silty Micaceous Mudstones and Thin Sands

Lagoonal Limestones

- F7 — Sponge Spicule Packstone - Grainstones
- F13 — Coated Gastropod Brachiopod Mudstone-Packstone

Shelf Carbonates and Marine Sands

- F12 — Phylloid Algal Bafflestone- Wackestone
- Intermediate Facies: Bryozoan Productid Packstone-Wackestone
- F8 — Skeletal Cap Grainstone-Diverse and Crinoidal
- F6 — Ripple Cross-Laminated Calcareous Micaceous Sandstones

Sabkha to Shallow Marine / Evaporitic Environment

- F5 — Carbonate Laminites / Subariel Exposure
- F4 — Silty Micaceous Carbonate Mudstone
- F3 — Phylloid Algal Tube Fossil - Chaetidid Bioherm
- F2 — Dolomite Ridge -Carbonate Wackestone -Mudstone
- F1 — Black Laminated Muds - Silty Argillaceous Dolomitic Mudstone

Figure 6.1 – Composite Klondike Ridge megaflap stratigraphic chart with sequence stratigraphic interpretation. The chart documents sequence 1-11 and associated LST, TST and HST of the Paradox Formation, Honaker Trail Formation, and lower Cutler

6.1 Paradox Formation Sequence Stratigraphy

The Paradox Formation outcropping in the Klondike Hill Megaflap contains a single 4th-order sequence measuring 66m and bound at the top by a type-1 sequence boundary showing subaerial exposure (Figure 4.7). This Paradox Fm. 4th order sequence is likely time correlative to down-dip evaporites and black shales of the Hite (1969) cycles, as well as correlative to the limestones and algal mounds of the western shelf (Peterson and Hite, 1969; Goldhammer et al., 1994; Weber et al., 1995; Grammer et al., 1996; Matheny and Longman, 1996). The initial TST is composed of a 33m thick section of shaly dolomitic mudstones of facies F-1 representing an initial phase of flooding of the shelf producing anaerobic to dysaerobic marine bottom water conditions (Wengerd and Matheny, 1958; Goldhammer et al., 1994; Weber et al., 1995; Grammer et al., 1996). Parasequence thickness thins upward indicating progressively lower carbonate mudstone accumulation during transgressive deepening. The TST is capped by the maximum flooding surface at the base of the dolomite ridge facies F-2 and F-3. As carbonate sedimentation began to outpace sea-level rise and conditions returned to normal marine salinities, colonization by marine organisms was more pervasive thus developing a sustained carbonate factory on the shelf and forming a 30 m thick, progradational HST composed of parasequence sets of dolomitic shelf carbonates of F-2 and biohermal facies F-3, capped by peritidal silty argillaceous dolomitic mudstones of facies F-4. The latest HST is dominated by a rapid decline in accommodation space indicated by the deposition of laterally continuous cyanobacterial mats of facies F-5 in a peritidal to sabkha type environment. The upper sequence boundary of S1 is placed at the top of this bed

and shows karst collapse features as well as meteoric dissolution and precipitation of meteoric calcite cement indicative of prolonged subaerial exposure. The sequence boundary between S1 and S2 corresponds to the formational contact between the Paradox Formation and the Honaker Trail Formation (Figure 6.2).

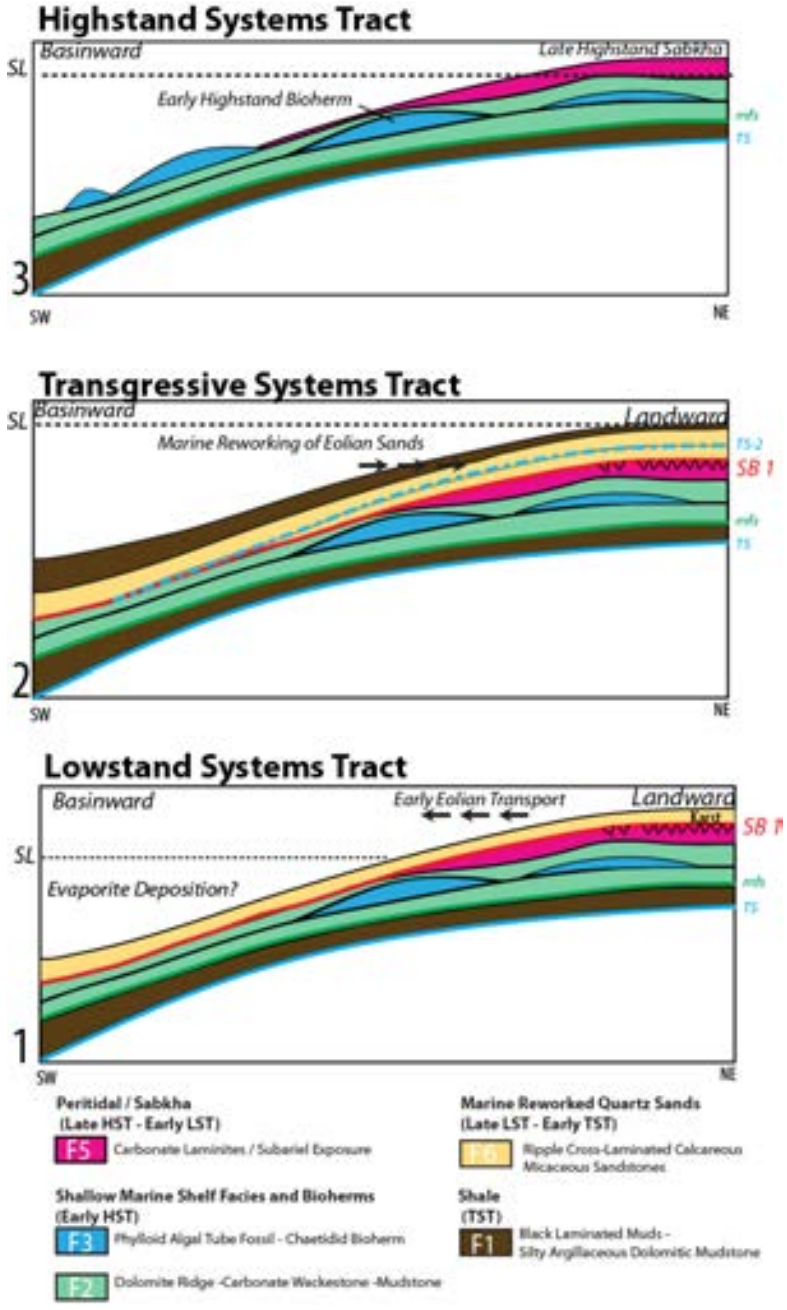

Figure 6.2- Schematic diagram illustrating the sequence stratigraphic systems tracts inferred from facies stacking patterns in the Paradox Formation. This diagram is derived from outcrop observations and shows the evolution of a 4th-order stacking pattern from basinal shale, shallow marine shelf and peritidal dolomites to marine reworked eolian sandstones.

6.2 Honaker Trail Formation and Lower Cutler Formation Sequence Stratigraphy

The Honaker Trail and lower Cutler formations description and interpretation of sequences and respective systems tracts are combined here as they represent a regionally conformable succession of Pennsylvanian stratigraphy that transitions gradationally from marine carbonate and siliciclastic dominated facies to more non-marine fluvial siliciclastics dominated facies. Sequences S2-S10 range in thickness from 12m to 45m with thinner sequences present in the Honaker Trail Formation, which thicken up into the Lower Cutler Formation.

6.2.1 Lowstand Systems Tracts

LST of the Honaker Trail and lower Cutler formations in the megaflap are dominated by laterally continuous packages of stacked braided fluvial systems and associated floodplains. They display basal type-1 sequence boundaries that truncate underlying marine strata (Figure 6.3) and are capped by transgressive marine flooding surfaces. The LST siliciclastics are deposited directly over marine limestone grainstones and packstones of the previous HST and typically show incision into the underlying carbonates as well as marked erosion of up-dip carbonates observed as black chert pebbles and limestone rip-up clasts within conglomeratic fluvial channels. Furthermore, the presence of red chert siliceous replacement fabrics of skeletal grains from the underlying shelf HSTs indicates prolonged subaerial exposure at the type-1 sequence boundary as the groundwater table dropped below the shelf margin and resulted in oxidizing pyrite inclusions within the silica cemented limestones (Loope and Watkins, 1989). . The LSTs range in thickness from 6-60 m, with progressive LST thickness increasing upward into the lower Cutler.

In general, type-1 sequence boundaries and associated LST of Pennsylvanian strata worldwide are thought to be the result of a glacio-eustatic sea-level drop below the shelf margin of the basin (Peterson and Hite, 1969; Vail et al., 1977, 1977, 1977; Heckel, 1986; Loope and Watkins, 1989). In the Paradox Basin, this produced forced regressions bringing fluvial-dominated depositional systems originating in the Uncompahgre highlands to prograde across and incise the exposed eastern shelf (Gianniny and Miskell-Gerhardt, 2009).

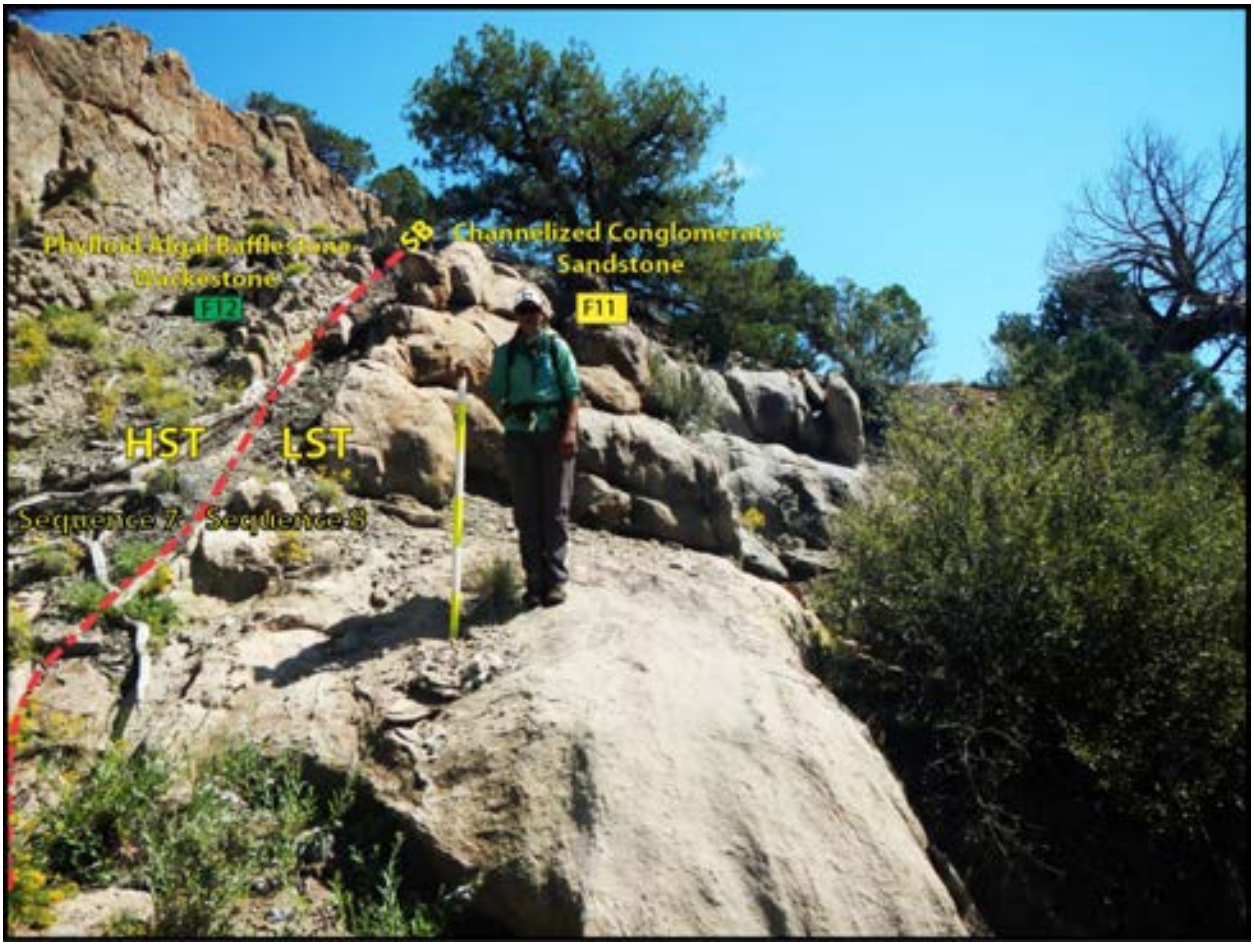

Figure 6.3: Field photograph of highstand system tract (HST) shelf carbonates represented by the phylloid algal bafflestones of facies F-12 (Left) truncated at a type-1 sequence boundary (red dotted line) with overlying lowstand systems tract (LST) represented by channelized fluvial conglomeratic sandstones of facies F-11. Photo is sequence 8 and 9 forming at the Honaker Trail Fm., lower Cutler formational contact.

6.2.2 Transgressive Systems Tract

The TST of S2 at base of the Honaker Trail Formation is composed of marine shoreface reworked eolian sandstones (facies F-6), whereas S4 and S5 contain shaly transgressive mudstones. The shaly dolomitic mudstones characterized by facies F-1 represent an initial marine transgression that transitions from anaerobic bottom water conditions that progressively become dysaerobic upwards, permitting soft-bodied siliceous sponges (facies F-7) to colonize the bottom as oxygenation levels improve (TST in Figure 6.5). Much of the TSTs in the lower Honaker Trail Formation are dominated by shoaling-upward parasequences of siliceous sponge spicule packstones- grainstones interbedded with deeper water facies of F-1.

The earliest stages of flooding are documented by facies F-1 as anaerobic hypersaline marine waters move across the shelf. The sponge facies form in highly restricted environments on a partially restricted shelf during the initial stages of flooding, however during a progressive return to normal marine salinities. These transgressive shaly dolomitic mudstones, marine reworked eolian sandstones, and siliceous sponge spicule grainstones of the TSTs are correlative to deeper water shales that are not observed here in outcrop (Goldhammer, 1991, Grammer, 1995), however may be present within the mini-basins throughout the Paradox foredeep. The initial transgression of hypersaline marine waters onto the shelf is followed by circulating oxygen-rich waters that establish a normal marine carbonate factory composed of the HST shelf limestones.

6.2.2 Highstand Systems Tracts

The megaflap HSTs are characterized by relatively thin (3-6m) shoaling up parasequences of shelf limestones (Facies; F-7, F-8, F-10, F-12), with typically sharp upper and lower depositional contacts with bounding facies (Figure 6.4). The HST typically has a sharp to wavy lower contact with the underlying TST at the maximum flooding surface or the contact is condensed and the HST directly overlies the terrigenous non-marine facies of the LST with no

TST preserved. The late stage HST contains photic zone marine fauna and are composed of skeletal grainstones to phylloid algal bafflestones that overlie early highstand wackestones. The HSTs of S4 – S9 stack to form an overall progradational carbonate shelf to lagoon system related to the progressive decrease in accommodation space in the Paradox Basin and infilling of the basin by LST siliciclastics shed from the Uncompahgre Uplift (Figure 6.5). Megaflap HSTs are very thin compared HSTs at the margins of the Paradox Basin where HSTs are dominated by thick (up to 60m) progradational shelf limestones (Goldhammer, 1991; Grammer, 1995).

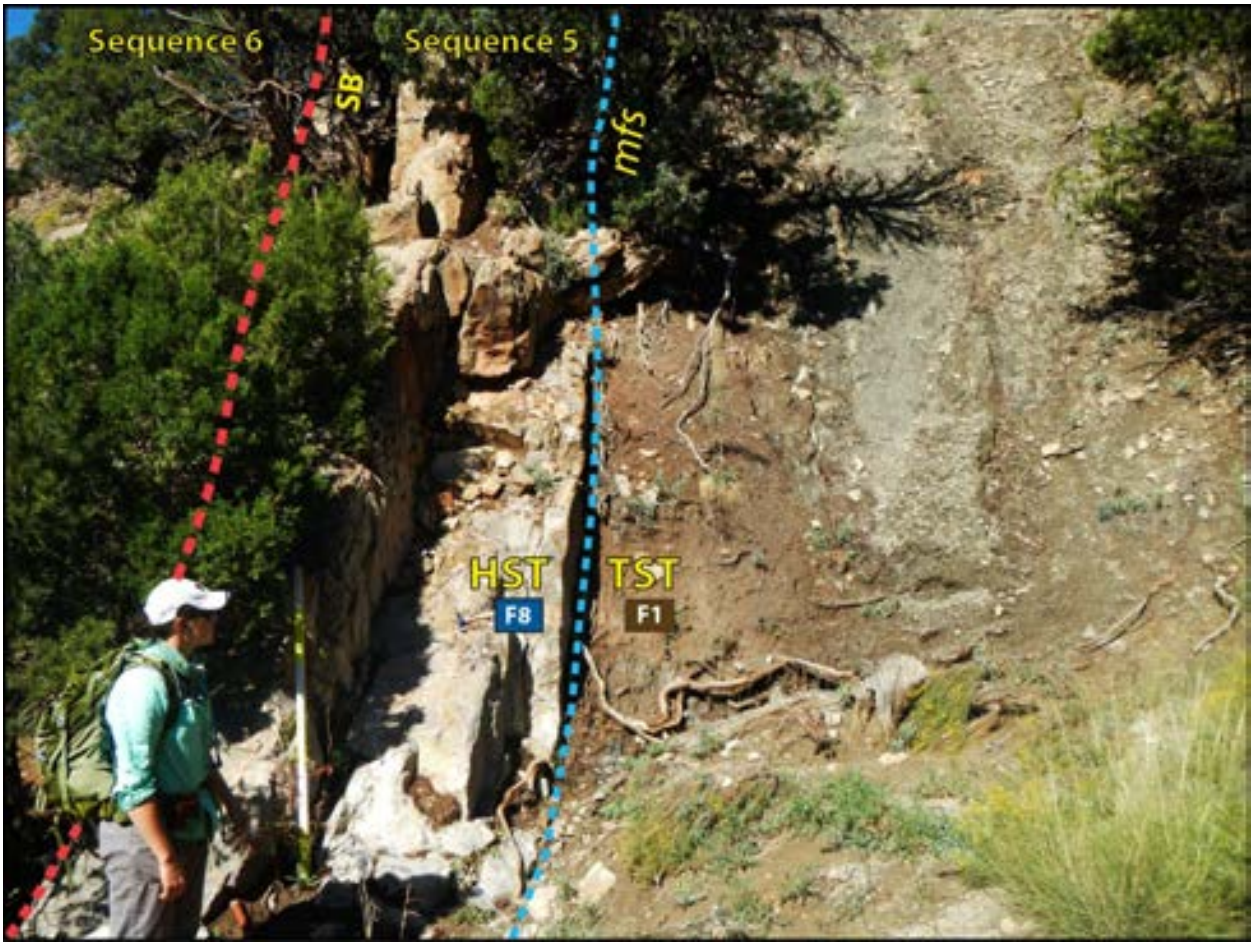

Figure 6.4- Field photograph of transgressive systems tract (TST) composed of offshore marine shales of facies F-1 and the maximum flood surface (mfs). The TST is capped by a ledge of HST wackestone to skeletal grainstone cap of facies F-8.

Highstand Systems Tract

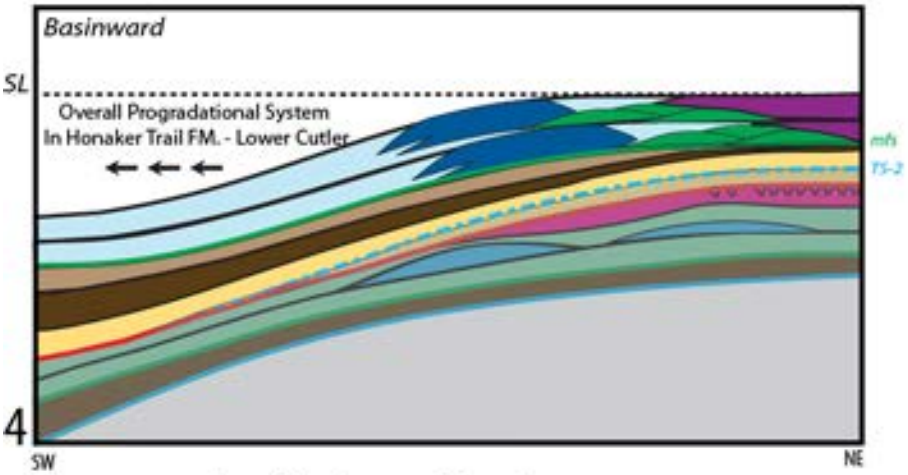

Transgressive Systems Tract

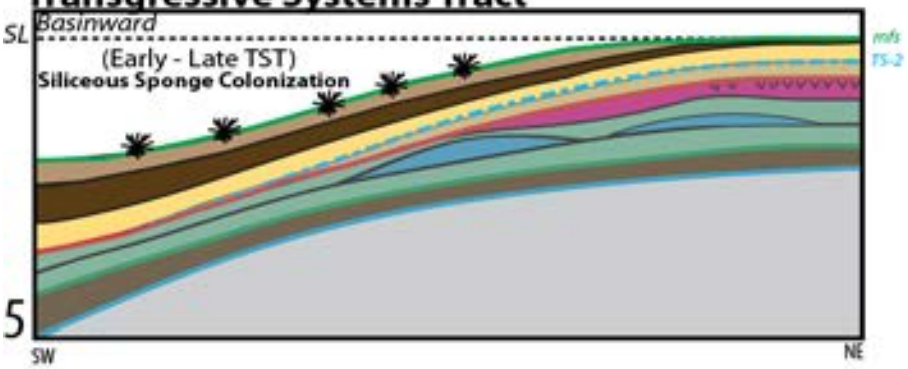

Lowstand Systems Tract

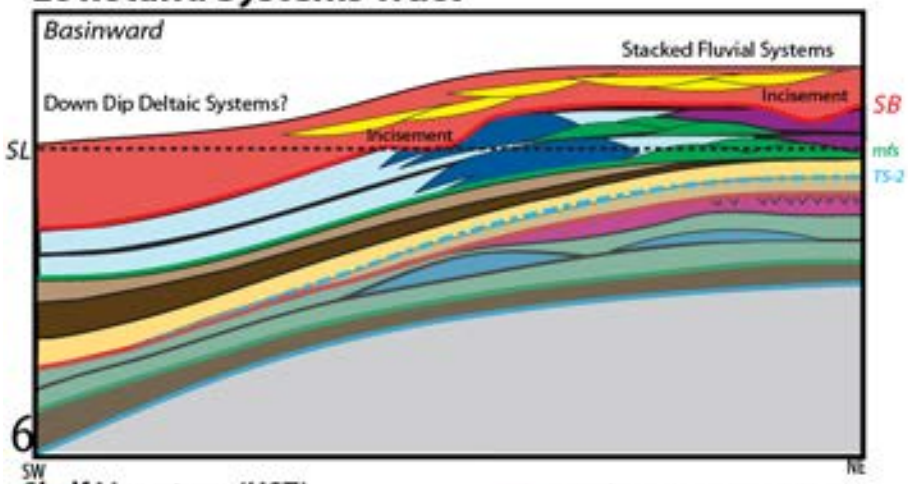

Shelf Limestone (HST)

- F12 Phylloid Algal Bafflestone- Wackestone
- Intermediate Facies:
- F10 Bryozoan Productid Packstone-Wackestone
- F8 Skeletal Cap Grainstone-Diverse and Crinoidal

Fluvial (LST)

- F11 Channelized Conglomeratic Sandstone
- F9 Red Silty Micaceous Mudstones and Thin Sands

Lagoonal Limestones (HST)

- F7 Sponge Spicule Packstone - Grainstones
- F13 Coated Gastropod Brachiopod Mudstone-Packstone

Offshore to CoastalMarine (TST)

- F1 Black Laminated Muds - Silty Argillaceous Dolomitic Mudstone
- F6 Ripple Cross-Laminated Calcareous Micaceous Sandstones

Figure 6.5- Schematic diagram illustrating the sequence stratigraphic mechanisms responsible for facies stacking patterns in the Honaker Trail Formation and lower Cutler. This diagram is derived from outcrop observations and shows the evolution of a 4th-order systems tracts.

6.3 Sequence Stratigraphic Interpretation

Mixed-clastic depositional systems and the resultant vertical stacking patterns are derived from complex interactions of glacio-eustatic sea-level fluctuations, tectonic subsidence, sediment accumulation rates, topography, compaction rates, and climatic changes (Wilson, 1975, Kendall and Schlager, 1981, Goldhammer, 1991). The most critical of which, with regards to resultant generation of sequence stratigraphic surfaces and depositional facies architecture are eustatic sea-level changes, tectonic subsidence, and sedimentation rate (Crevello et al. 1989). In most depositional settings the long-term rates of subsidence are roughly constant and slowly changing over long time scales, similarly as are sedimentation rates (Goldhammer, 1991). This leaves the eustatic, or global sea-level signal as the principal variable controlling the stratigraphic framework of coastal depositional systems. Eustatic changes in sea-level occur at high frequencies (10,000-100,000 yr) and at rapid rates (10m per 1,000 yr; Schalger, 1981) that outpace signals from subsidence and sedimentation rates. Eustatic sea-level fluctuations occur at various frequencies based on the duration of the cycle and yield a hierarchy of cyclicity ranging from first to fifth order (Vail, 1977). The Honaker Trail Formation within the study area contains 7 cycles bound by type-1 sequence boundaries. The period of deposition for the formation ranges from Missourian to Virgilian or approximately 6 million years (Gradstein and Ogg, 2004), indicating that each cycle or sequence covers a duration of 1-1.1 m.y. This cycle duration corresponds to fourth-order sequences that range from .1-1 m.y. (Sloss, 1963; Miall, 1984; Goldhammer 1991). The fourth-order sequences are composed of 31 higher-frequency parasequence sets of shorter duration

(Figure 6.1). The parasequence sets are thinner and range from 3-10 m and are recognized by shallowing upward facies successions bound by flooding surfaces.

Previous work along the western shelf of the Paradox Basin by Goldhammer et al (1991) revealed 8 4th -order sequences from the base of the Akah to top Desmoinesian, which have an average thickness of 35m. The shelf carbonates along the western margin of the basin are time correlative up-dip equivalents to the Hite (1969) cycles of the basin center, forming the layered evaporites of the Paradox Formation. These sequences along the shelf are determined to be 4^{th}-order (averaging 35m thick with an approximately 257,000 year period), and bound by type-1 sequence boundaries. 4^{th} order sequence boundaries along the western shelf of the basin are characterized by features indicating widespread and long-lived subaerial exposure surfaces, and are referred to as exposure cycles (Goldhammer, et al., 1991). These features include: karst collapse and brecciated features, caliche horizons, truncation of beds and carbonate grains, as well as notable diagenetic processes observed petrographically, such as meteoric diagenesis including dissolution and precipitation of calcite sparry cement as well as carbonate replacement by red chert. Meter-scale karst features and caliche horizons are common along the shelf and can be traced laterally for kilometers indicating a regional sea-level drop exposing the carbonate-dominated shelf (Grammer, et al., 1996). Higher frequency 5^{th} and 6^{th} order cycles consist of shallowing upward parasequences bounded by either sub-aerial exposure, marine hardgrounds, or marine transgressions. Sequence boundaries in these higher order cycles are discrete and are typically centimeter scale and cannot be regionally traced across the shelf (Grammer, et al., 1996). The fourth-order sequences studied by Goldhammer, (1991), and Grammer et al., (1996), can be partitioned into component lowstand, transgressive, and highstand systems tracts that can be

correlated in outcrop and into the subsurface. Lowstand systems tracts along the western shelf are composed of wedges of evaporites and quartz -dominated siliciclastics that are laterally restricted within intrashelf topographic lows and thin onto topographic highs. The LST contains anhydrite, siliciclastics, and mudcracked algal laminites (Golhammer, 1991). Conversely along the eastern shelf, lowstand system tracts documented by Gianniny and Miskell-Gerhardt (2009), are dominated by up-dip laterally continuous fluvial siliciclastics with deltaic systems in down-dip positions or minor evaporitic systems characteristic of sabkha type environments. Transgressive system tracts along the western shelf and eastern shelf are similar and are composed primarily of black organic-rich shales and shaly carbonate mudstones. The transgressive systems tracts along the margins of the basin are 3-12 m, and thicken toward the basin center where they become the organic-rich petroleum source rocks of the region. Transgressive system tracts along the western and eastern margin as well as the observed intervals for this study in the foredeep of the basin contain similar lithologies and thicknesses.

Highstand systems tracts show some of the most variable deposition across the basin, specifically regarding system tract thickness, facies, and depositional thicknesses. The western margin contains thick, up to 60 m packages of shoaling upward carbonate wackestone to capping grainstones and phylloid algal mounds, while along the eastern margin and central basin, these aggradational to progradational carbonates are much thinner at 3-20 meters, with the thinnest occurring in the foredeep of this study. Although previous work by Goldhammer et al. (1991), Grammer et al. (1996), and Gianniny and Miskell-Gerhardt (2009) contain concise sequence stratigraphic documentation, comparison of systems tracts is not one-to-one in that the stratigraphic sections observed cover different localities within the Paradox Basin as well as different chronostratigraphic intervals. Also as discussed by Grammer et al. (1996), comparison

of sequence thickness does not necessarily yield accurate information regarding forcing mechanisms. Furthermore, the Honaker Trail Fm. cannot be traced across the basin as it is unlikely that a single limestone extends across the basin due to the rapid lateral facies changes characteristic of the formation (Condon, 1997). However, observing the behavior of systems tracts at different localities within the basin at roughly similar ages can give some insight into the controls responsible for development of the Desmoinesian sequence stratigraphic architecture in the Paradox Basin.

Table 4: Chart describing previous workers and a summary of this studies sequence stratigraphic analysis within the Paradox Basin

Systems Tract	Western Shelf, San Juan Canyon (Goldhammer, 1991; Grammer, 1996)	Foredeep, Gypsum Valley Diapir (This study)	Eastern Shelf, Hermosa Cliffs (Gianniny and Miskell-Gerhardt, 2009)
HST	Aggradational mound growth, mound flanking skeletal wackestones and capping skeletal and ooid grainstones (HST avg. 60 m)	**Honaker Trail Fm. and Lower Cutler** Shoaling up carbonate wackestones to capping skeletal grainstone or algal biostromes (HST avg. 3 - 6 m) **Paradox Fm.** Mound growth (HST avg. 20 m)	Aggradation of fossiliferous packstones with capping grainstones (HST avg. 10-15 m)
TST	Black shales and carbonate mudstones (BLM facies) transitioning into sponge facies. Marine re-worked eolian sands. Salinity reduced enough in latest cycle to develop carbonate factory (TST range 3-12 m)	**Honaker Trail Fm. and Lower Cutler** Black shales and carbonate mudstones condensed (TST avg. 1-3 m) **Paradox Fm.** Quartz-rich marine re-worked eolian siliciclastics, algal dolomitic laminites. (TST avg. 36 m)	Thin carbonaceous siltstones or photic zone carbonates directly ontop of lowstand siliciclastics (TST avg. 5-10 m)
LST	Evaporites, cryptalgal laminite, quartz-rich siliciclastics (eolian to marine transport) (LST range 6-18 m)	**Honaker Trail Fm. and Lower Cutler** Thick packages of coarse-grained arkosic fluvial systems and flood plain mudstones (LST range 6-60 m) **Paradox Fm.** algal dolomitic laminites. (LST avg. 1-3 m)	Laterally continuous, fluvial siliciclastics and pro-delta siltstones and mudstones (LST avg 20 m)
	Upper Akah - Top Desmoinesian (Paradox Fm. to Within Honaker Trail Fm.) 400 m section 8 Fourth-Order Sequences	**Upper Paradox Fm. to Lower Cutler 339 m section 10 Fourth-Order Sequences**	**Akah (Paradox Fm.) to lower Honaker Trail Fm. 384 m section 19 Fourth-Order Sequences**

6.3.1 Glacio-Eustatic Drivers in the Pennsylvanian

The Pennsylvanian Period is well-documented throughout the world and renowned for well-preserved examples of cyclical deposition of marine and terrigenous siliciclastic and marine carbonate strata. Wanless and Shepard (1936) initially proposed that the cyclical nature of Pennsylvanian stratigraphy within the North American Midcontinent was a result of regional marine transgressions and regressions that are derived from eustatic sea-level rise and fall generated by advancing and retreating Gondwanan glaciers (Heckel, 1986). The glacial-eustatic model is supported by the presence of Gondwanan glacial deposits that span the entire Pennsylvanian (Crowell, 1978). The basic sequence of Midcontinent cyclothems consist of (1) a basal thin, transgressive marine limestone; (2) thin, offshore conodont-rich black shale; (3) thicker shoaling up cycles of limestone; and (4) nearshore to terrigenous siliciclastics (Heckel, 1986). The complete sequence represents initial marine transgression and maximum flooding surfaces of the transgressive and highstand systems tracts and subsequent regression marked by terrigenous siliciclastics advancing across the shelf.

The cycles exposed within the study area exhibit these characteristics and are an excellent example of Pennsylvanian glacio-eustatic mechanisms controlling the resultant vertical stacking pattern. Understanding the mechanisms responsible for the creation of the cyclic deposition of the Desmoinesian-Virgillian stratigraphy in the Paradox Basin was a primary goal to previous workers in the basin. The mechanism of cyclicity was interpreted by Goldhammer et al. (1992), via interpretation of depositional environments and subsequent stacking patterns as 4^{th} order sequences and associated higher and lower frequencies. These 4^{th}-order cycles are generally accepted as being controlled by eustatic sea-level fluctuations of the Pennsylvanian that were derived from the advance and retreat of glaciers on the Gondwanan supercontinent (Crowell, 1978;

Heckel, 1986). Glacio-eustatic fluctuations derived from orbital-forcing through Milankovitch cycles is generally accepted as the mechanism controlling climatic factors responsible for eustatic sea-level change throughout the Pennsylvanian. In summary the cyclic stacking pattern of Pennsylvanian stratigraphy is generally accepted to be driven by eustatic changes in sea-level that result in altering terrigenous or marine sedimentation rates, marine salinities, and oxygen levels that control the resultant depositional environment.

However, based on uncertainties regarding uplift rates, and the likelihood that Uncompaghre tectonics are not cyclical, the controls exerted by tectonics are likely reduced to overall 2nd-order foreland -basin flexural subsidence formational level sequences that record an initial deepening followed by an overall loss of accommodation space that results in the infilling of the Paradox Basin. This progressive infilling resulted in a progressive change from dominantly marine deposition in the Paradox and Honaker Trail formations to dominantly terrigenous in the Permian Cutler Formation. The proximity to the highlands in this study result in pronounced lowstand systems tracts that record the un-roofing of the Uncompaghre Uplift, however controlled primarily by glacio-eustatic sea-level changes.

6.3.3 Tectonic Controls on Pennsylvanian Cycles

Other mechanisms controlling the architecture of the sequence stratigraphic framework of the Pennsylvanian strata, especially within this study area, is syn-tectonic sedimentation and tectonic controls on accommodation space due to proximity to the Uncompaghre highlands (Baars, 1966; Giles and Dickinson, 1995; Barbeau, 2003). Development of depositional sequences and resultant vertical stacking patterns are directly related to changes in accommodation space through time and space (Giles and Dickinson, 1995). Accommodation space is directly related to tectonic

subsidence or uplift, sediment supply, and eustasy (Giles and Dickinson, 1995). However, partitioning each signal is difficult as no single mechanism acts independently of the others, making individual assessments of theses controls problematic (Giles and Dickinson, 1995). In the Paradox Basin, lithospheric flexure resulting from progressive thrust sheet loading by the Uncompahgre Uplift generated rapid subsidence adjacent to the thrust panel forming the foredeep of the basin (The location of this study) (Baars, 1966; Barbeau, 2003). Lithospheric flexure generating the characteristic geometries of foreland basins significantly alters subsidence and uplift rates through time and space and directly controls resultant accommodation space (Giles and Dickinson, 1995; DeCelles and Giles, 1996). Trending away from the rapidly subsiding foredeep generated by progressive downwarping of the lithosphere, subsidence gradually decreases, ultimately creating the asymmetrical characteristics typical of foreland basins (Giles and Dickinson, 1995; DeCelles and Giles, 1996). The western shelf of the Paradox Basin was generated by flexural uplift, an isostatic response to downwarping of the lithosphere forming the distal margin of the basin, and is referred to as the forebulge (Giles and Dickinson, 1995; DeCelles and Giles, 1996; Barbeau, 2003). The contrasting tectonic signatures impart a significant control on accommodation space across the basin ultimately controlling facies distribution as well as the sequence stratigraphic framework (Giles and Dickinson, 1995; Weber et al., 1995; DeCelles and Giles, 1996) (Figure 6.6).

Weber et al. (1995) developed an idealized facies distribution based on well-log correlations, measured sections, and seismic data that partitions the Paradox Basin into: (1) thick sequences of phylloid algal mounds along the western margin, (2) thinned distal limestones within the foredeep, and (3) a tectonically active siliciclastic front along the eastern margin (Figure 6.6). This large scale regional facies distribution is derived from tectonic controls related to foreland

basin development and the asymmetric distribution of subsidence and uplift (Baars, 1966; Goldhammer et al., 1994; Giles and Dickinson, 1995; DeCelles and Giles, 1996; Condon, 1997; Barbeau, 2003; Gianniny and Miskell-Gerhardt 2009).

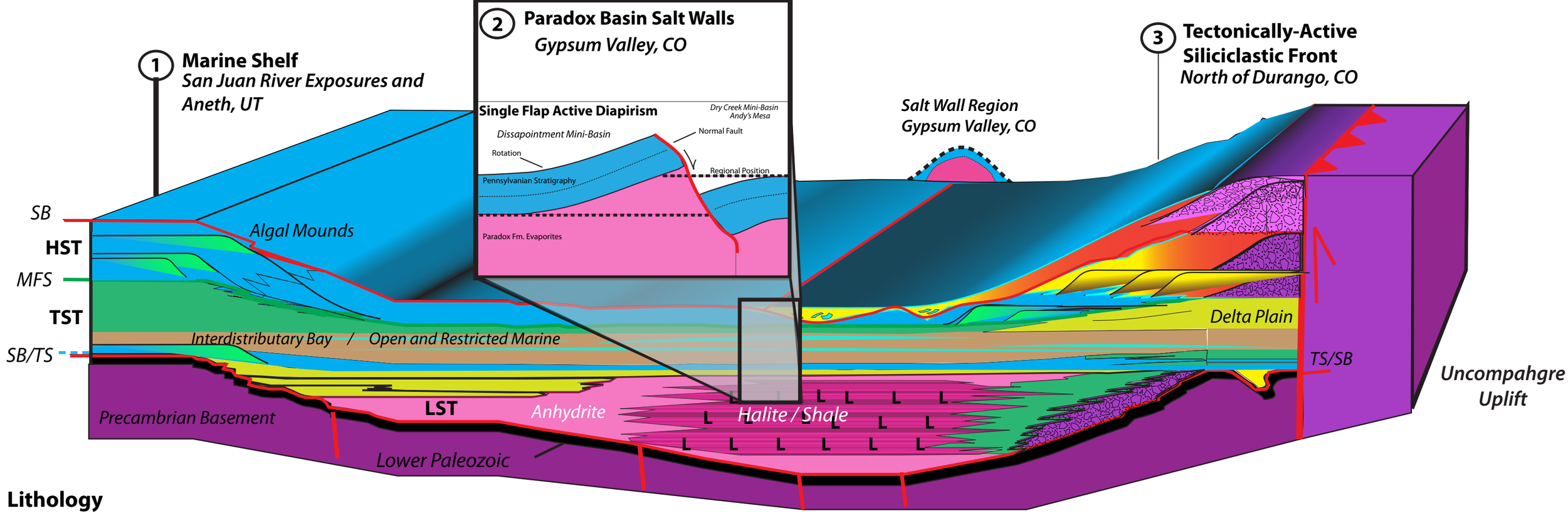

Lithology

- Halite
- Anhydrite & Gypsum
- Precambrian Basement
- Fluvial Systems
- Shale & Siltstone
- Black Laminated Mudstone "Shale"
- Dolomite
- Limestone
- Algal Mounds
- Alluvial Mega Fans
- Deltaic Systems

- Sequence Boundary
- Maximum Flooding Surface
- Transgressive Surface

*Schematic not to scale

Figure 6.6 – Facies distribution for the Paradox Basin at (1) Aneth field along the western shelf, (2) Salt tectonics of this study in the foredeep, Gypsum Valley, CO and (3) the tectonically active eastern margin near Durango, CO. (Modified from Weber et al., 1995, interpretation of the western and eastern margins).

The other mechanism that plays a role in controlling the local depositional environments and thus the observed sequence stratigraphic framework is diapir rise rate. The principal goal of this study is to interpret the Pennsylvanian and Permian strata and identify any signatures that could be related to or influenced by salt diapirism. Through analysis of the lithofacies succession in outcrop combined with any lateral variation in facies and systems tracts it can be concluded that the Paradox Fm., Honaker Trail Fm., were likely deposited on an inflated salt-pillow with moderate topographic relief. This interpretation stems from the overwhelming presence of shallow marine limestones containing abundant photosynthetic organisms such as phylloid algae and cyanobacterial mats in what should the flexurally deeper part of the basin. Previous workers of the Paradox Basin, based on outcrop and well-log data, have developed depositional models that explicitly state deeper water facies should be present within the foredeep while the margins of the basin will contain shallow marine shelf limestones (Goldhammer et al., 1994; Weber et al., 1995; Grammer et al., 1996; Gianniny and Miskell-Gerhardt, 2009). In the Klondike Hill megaflap, presence of biohermal facies containing phylloid algae as well as facies characteristic of shelf limestones deviates from the regional depositional model. The presence of a shallow marine facies assemblage within the Paradox and Honaker Trail formations is interpreted to be controlled by proximity to incipient diapirism that ultimately decreased accommodation space resulting in thinned highstand limestones as well as generating enough topography to allow for the colonization of photosynthetic marine organism. The diapir rise rate is interpreted to be too slow to impart notable changes to the sequence stratigraphic architecture at the parasequence and 4^{th} order scale, specifically because progressive angular unconformities are not developed until the Permian. The most notable feature interpreted to be related to salt diapirism is the observed angular unconformity marking the top Honaker Trail Fm., and base lower Cutler. Here it is interpreted that

the previous diapir roof transitions into a large scale pillow geometry that progressively steepens. Do to the inherent complexity of lateral facies variations of the Pennsylvanian strata as well as depositional controls of high-frequency sea-level cyclicity and local tectonics, deriving information about salt-tectonics from the Pennsylvanian strata must be looked at carefully and in the context of diapir rise rate, specifically at what stratigraphic level diapirism will impart a change (i.e., parasequence or formation level).

Chapter 7: Discussion

7.1 Gypsum Valley Megaflap Formation

Rowan et al. (2016) and Escosa et al. (2019) interpreted the Pennsylvanian and Permian stratigraphy exposed in Big Gypsum Valley to represent the unconformity-bound vertical upper reaches of a megaflap that initially developed under single flap active diapirism as a thinned horizontal roof over a moderately inflated salt pillow as opposed to halokinetic drape folding at the margin of an active steeply dipping salt-sediment interface. This interpretation is drawn from several lines of evidence established by Rowan 2016 and Escosa 2019. This interpretation of the origin of the megaflap is further supported by observations drawn from this study: (1) Progressively shallowing dips in the lower Cutler from 79° to 70° compared to the concordant vertical beds of the Paradox and Honaker Trial formations in the megaflap, which document progressive formation scale inflation of the salt pillow generating an approximately 9° to 20° structural margin in the early Permian; (2) Evidence of significant sub-aerial exposure identified through extensive diagenetic modification of shelfal marine limestones of the Pennsylvanian and Permian stratigraphy, which are interpreted regionally to be in the zone of deep water facies assemblages proximal to the Paradox Basin fore deep; (3) The abundance of shallow water, photic zone carbonates in the megaflap within the fore-deep of the Paradox Basin; documenting a lithofacies assemblage more closely related to the shelf carbonates of Aneth, Utah and the tectonically active eastern margin of the Paradox Basin in Colorado; (4) Lateral isopachous facies correlations across the megaflap, suggesting an initial pre-kinematic depositional environment; (5) Further evidence of single-flap active diapirism as the measured megaflap stratigraphy represents a thinned roof compared to the thicker units in well log measurements from Andy's Mesa field within the Dry Creek mini-basin, on the northeast flank of Gypsum Valley and finally; (6) No

evidence of diapir-derived detritus within the Pennsylvanian and Permian stratigraphy of the megaflap.

In cross-section the Gypsum Valley salt wall is bound by asymmetric flanks of Pennsylvanian and Permian stratigraphy and are composed of progressively rotated, thinned strata (117m) forming a megaflap on the northern flank of the Disappointment minibasin, and a shallowly dipping thickened (737m) sedimentary wedge on the southern margin of the Dry Creek minibasin. The exposed megaflap, when rotated back to its original near horizontal position as the roof of an inflated salt pillow, would be the lateral equivalent to the Pennsylvanian and Permian stratigraphy in the Andy's Mesa gas field in the Dry Creek minibasin. This minibasin however contains thickened Pennsylvanian and Permian stratigraphy compared to the lateral equivalent measured in the exposed megaflap (Figure 7.1a). Based on previous workers well log analysis, within Andy's Mesa, the base of the Honaker Trail Formation is is defined by by the last prominent anhydrite interval, below which are the upper Paradox Formation Hite cycles of mostly marine dolomites, calcareous to dolomitic black shale, and anhydrite (Duchene, 2009; Amador, 2009). These cycles are interpreted here to be the down-dip deep water equivalents to the Upper Paradox Formation facies exposed in the megaflap. The base Honaker Trail Formation in the Dry Creek minibasin is defined as the first continuous sandstones of the Honaker Trail at 8979 ft TVD (2.7 km deep) (Duchene, 2009, Amador, 2009). The top of the Honaker Trail Formation at Andy's Mesa is picked at the top of the highest continuous limestone observed; 6560 ft TVD (1.9 km deep). The Honaker Trail Formation within the Dry Creek minibasin therefore is approximately 2,419 ft TVD (737 m thick) (Duchene, 2009, Amador, 2009). The exposed vertical Honaker Trail Fm. within the megaflap, begins at the first laterally extensive sandstone layer that is bound at the base by a type-1 sequence boundary represented by marked subaerial exposure of dolomitic

peritidal cyanobacterial mat facies (Figure 6.1 Sequence 2). These cyanobacterial mats represent facies F-5 and within the sequence stratigraphic framework are interpreted to have an evaporite dominated down-dip lateral equivalent such as the anhydrite observed in Andy's Mesa of the Dry Creek minibasin (Duchene 2009; Amador, 2009). The top Honaker Trail Formation within the megaflap is picked at the top of the last shelf limestone bound at the top by a type-1 sequence boundary similar to Duchene and Amador (2009) top pick of the Honaker Trail within Andy's Mesa (Figure 6.1 Sequence 8). The exposure in the megaflap therefore is approximately 383 ft (117 m) thick. The exposed, vertical Honaker Trail stratigraphy consequently represent the thinned roof over an inflating salt pillow flanked by a syn-kinematic minibasin accommodating an additional 350 m of Pennsylvanian sediment as single flap active diapirism is initiated.

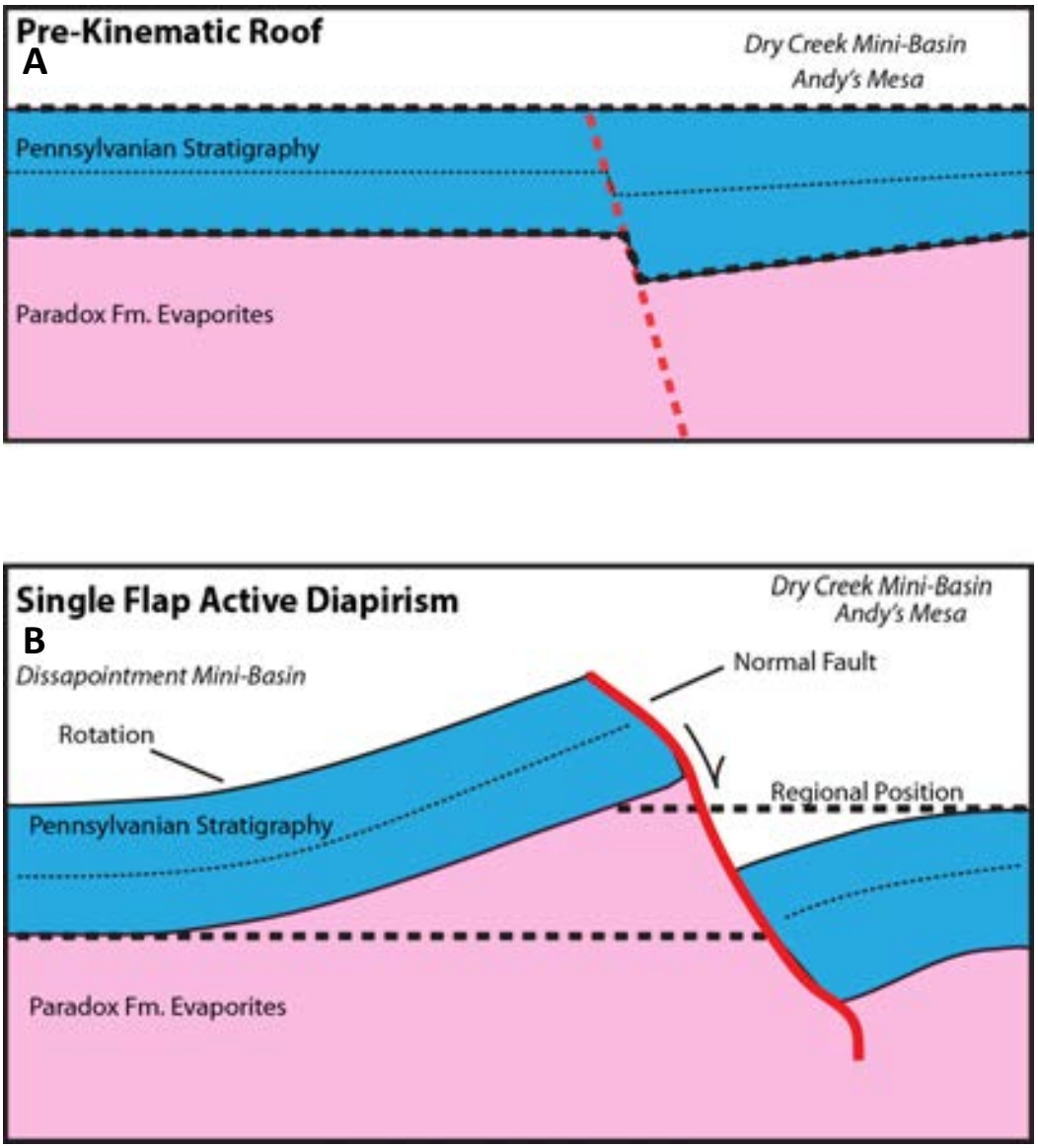

Figure 7.1 – (A) Schematic drawing of the pre-kinematic roof of Pennsylvanian mixed-clastics and thickened Andy's Mesa stratigraphy. (B) Single Flap Active Diapirism modified after Schultz-Ela et al. 1994.

7.2 Megaflap Stratigraphy within a Regional Sequence Stratigraphic Framework

The regional Pennsylvanian depositional facies models and sequence stratigraphic frameworks generated by previous workers of the Paradox Basin indicate that the stratigraphy in the fore-deep of the Paradox foreland basin and more specifically the general location of the Gypsum Valley megaflap stratigraphy would contain the down-dip, deeper water equivalents relative to the depositional environments interpreted along the shallow water shelf margins of the area near Aneth, Utah, along the western shelf and the Hermosa Cliffs along the more tectonically active eastern margin (Wengerd and Matheny, 1958; Weber et al., 1995; Grammer et al., 1996; Gianniny and Miskell-Gerhardt, 2009). However, through outcrop observations, the depositional environments and sequence stratigraphic interpretations of this study suggest that the Pennsylvanian stratigraphy of the megaflap is a condensed section, relative to the basin margins, of predominately shallow water, photic zone marine limestones and sabkha dolomites and terrigenous fluvial siliciclastic facies assemblages that lack significant deep-water components (Chapter 6 Table 1). The deeper water down-dip equivalents of the Paradox Basin shelf margins are interpreted to exist within the subsiding diapir-flanking minibasins. Based on previous workers facies models (Wengerd and Matheny, 1958; Goldhammer et al., 1994; Gianniny and Miskell-Gerhardt, 2009) as well as this study, the depositional facies of the down-dip deeper water equivalents would be dominated by more mudstone and wackestone carbonate systems that lack colonizing photic zone facies assemblages such as phylloid algae and would lack shallow water sedimentary structures in favor of more laminated textures. The down-dip facies would also contain transgressive, black, organic-rich shales as well as preserved lowstand anhydrite facies (Weber et al., 1995; Grammer et al., 1996; Matheny and Longman, 1996; Gianniny and Miskell-Gerhardt, 2009). As observed by Duchene (2009) and Amador (2009), the description of the

Pennsylvanian Honaker Trail Formation in the Andy's Mesa gas field of the Dry Creek minibasin is: "*comprised of beds of limestone and black calcareous shale and anhydrite with intercalated beds of fluvial sandstone*" (Duchene, 2009). The descriptions of black organic-rich shales and anhydrite come from Amador (2009) as well, and together represent a significant deviation from the description of the Honaker Trail Formation of this study's outcrop observations. The Pennsylvanian stratigraphy of this study would be described in contrast: beds of shallow marine grainstones to wackestones, phylloid algae biostromes, siliceous sponge lagoons, shoreface marine re-worked sands, and braided fluvial systems with prominent flood plains. The most significant deviation and requirement for down-dip facies within established facies models and sequence stratigraphic frameworks is the presence of non-sabkha type anhydrite facies and black organic-rich shales, which are conspicuously not found in the Honaker Trail in the exposed field area. The Pennsylvanian and lower Permian stratigraphy contained within the megaflap therefore likely record deposition within a shallow marine to terrigenous fluvial environment controlled by a local positive topographic relief developed by a progressively inflating salt-pillow initiated through single flap active diapirism.

7.3 Formation Scale Angular Unconformities

Along with containing numerous subaerial exposure surfaces derived from Pennsylvanian and Permian high-frequency glacio-eustatic sea-level fluctuations, the megaflap field area also records many subaerial exposure surfaces at the formational level that record the progressive rotation of the Pennsylvanian and Permian stratigraphy into a vertical position, and also suggest that the stratigraphy of the megaflap was at or near the surface until burial by the Jurassic Morrison Formation and later exposed by modern day uplift and exhumation. These exposures are

represented as angular unconformities and record progressive rotation from the earliest Permian through the Jurassic and are documented chronologically by : (1) Progressively shallowing dips and an exposed angular unconformity of the Permian lower Cutler Formation within the megaflap marking a change from predominantly vertical to approx. 79° ; (2) Triassic unconformities buried in the subsurface of the field area however observable on seismic line-drawings and exposed within radial faults of the down dropped graben observed in Escosa et al. (2019) and (3) Exposed Jurassic Entrada, Summerville, and Morrison formations angular unconformities capping wave-washed corrugated Honaker Trail Formation marine limestones. The Permian lower Cutler angular unconformity records a transition from predominately near vertical-to-vertical stratigraphy of the Honaker Trail and Paradox formations to an approximately 79° structural dip as observed today. When rotating the megaflap back to horizontal, this represents an approximate 9° rotation of the Honaker Trail strata prior to truncation (Figure 7.2). The lower Cutler extends up-section with progressively shallowing dips to 70° over 156 m before truncation beneath a second angular unconformity, onto which thin Jurassic Entrada and Summerville formations onlap. Therefore in approximately 156 m the lower Cutler records a progressively steepening salt-pillow that generates a rotation from 9-20° during the earliest Permian. This early Permian unconformity combined with the lateral syn-depositional thickening of the Honaker Trail Formation and Permian stratigraphy in the Dry Creek mini-basin sets up a transition from an early salt-pillow to an asymmetrical minibasin-flanked single-flap active diapir (Schultz-Ela et al. 1994; Rowan et al., 2016; Escosa et al., 2019) with a thinned condensed roof of shallow marine carbonates, as documented by this study. The regionally correlative mid-Cutler unconformity (buried beneath the onlapping Triassic and Jurassic stratigraphy and not exposed in this field area) is responsible for the erosion of the

domed roof that ultimately exposes the evaporite sequence of the Paradox Formation subsequently triggering passive diapirism (Rasmussen 2014; Rowan et al. 2016; Escosa et al., 2019).

Continued unroofing of the Uncompaghre Uplift throughout the Permian controls diapirism through differential loading produced by prograding asymmetrical wedges of Cutler Group alluvial megafans and fluvial systems flanking the Uncompaghre Uplift (Ge et al., 1997). From the Permian through the Triassic, rotation of the megaflap progresses quickly (Figure 7.2) and is marked by significant accumulation of diapir-derived detritus within the Triassic Chinle Formation observed in the down-dropped graben to the east of the megaflap. Although the Glen Canyon Group is not exposed in the study area, its relative position in time can be inferred from the exposure of the San Raphael Group, specifically the marine transgressive Summerville Formation.

The Jurassic Summerville Formation is exposed in the field area as an approx. 20° angular unconformity with Jurassic sediment infilling the corrugated surface of the vertical marine carbonates of the Honaker Trail, as well as infilling collapsed fabrics and radial faults within the megaflap (Figure 5.4 and Figure 5.7). The Jurassic was a unique time during megaflap formation as the megaflap stratigraphy was exposed at the surface and had already rotated to approximately 60° to 70°. It is interpreted to have been diagenetically overprinted with cements from Jurassic-aged formation waters. Figure 5.3 C and D specifically show aragonitic fibrous radial fans nucleating off botryoidal hematitic cements that line fracture walls of a silicified carbonate host (Facies 3). These aragonitic cements are interpreted to nucleate off successive generations of burial cements and are interpreted to be emplaced as a result of the marine carbonates and evaporites being exposed within a Jurassic- aged marine environment. The incipient marine environment of the Summerville Formation was short lived and environments quickly returned to fluvial dominated systems through the deposition of the Jurassic Morrison Formation.

Based on outcrop relationships with the vertical Honaker Trail Formation and the capping Morrison Formation, the fluvial sandstones capping the Paradox Formation dip slightly toward the central axis of the Gypsum Valley and the onlapping Morrison Formation overlying the lower Cutler dip away from Gypsum Valley, when restored this structure will create a synclinal geometry as the fluvial Morrison Formation siliciclastics erode into the evaporite and shale dominated diapir core. Finally as the salt budget is depleted and the Pennsylvanian carbonates weld to the underlying Mississippian Leadville Limestone overlying the Precambrian basement, passive salt diapirism is ended and the Gypsum Valley Salt Wall is buried in the Cretaceous and finally exhumed throughout the Tertiary (Figure 7.2).

Pennsylvanian
Honaker Trail Fm.
Paradox Fm.
Apprx. 300m

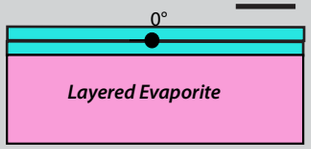

Syn-Depositional
Subaerial Exposure

Permian
Lower Cutler

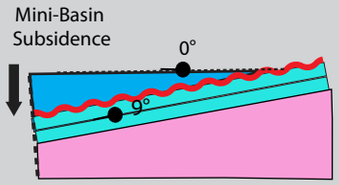

Lower-Cutler Unconformity
Subaerial Exposure

Permian
Cutler Fm.

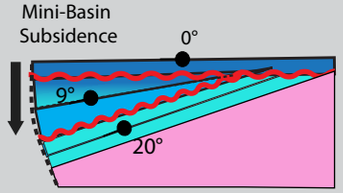

Mid-Cutler Unconformity
Regional Subaerial Exposure

Triassic
Chinle Fm.,
Moenkopi Fm.

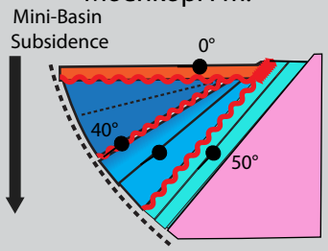

Triassic Unconformities
Subaerial Exposure

Jurassic
Glen Canyon Gp.
Wingate,
Kayenta, and
Navajo Sst.

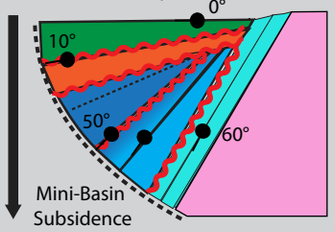

Jurassic Unconformities
Subaerial Exposure

Jurassic
San Raphael Gp.
Summerville Fm.,
Entrada Sst.

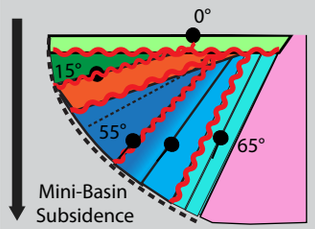

Jurassic Unconformities
Subaerial Exposure

Jurassic
Morrison Fm.
Salt Wash Member and
Brushy Basin Member

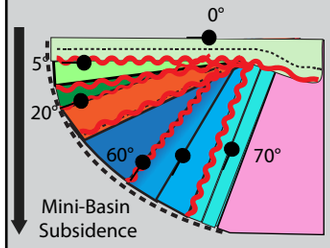

Jurassic Unconformities
Subaerial Exposure

Petroleum System
Deposition of
Paradox Fm. Source Rocks

Early Oil Generation

Peak Oil Generation

Cretaceous
Mesa Verde Gp.
Mancos Shale
Dakota Sst.

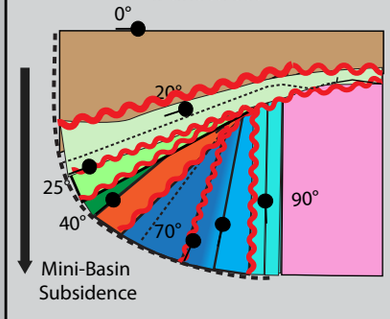

Burial - End Diapirism -Weld

Tertiary
Modern
Apprx. 300m

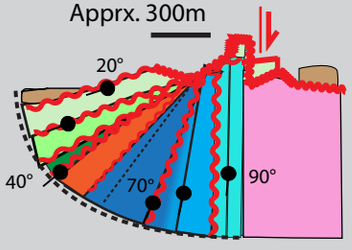

Uplift
Diapir Roof Collapse
Subaerial Exposure

Wet Gas

Dry Gas

Figure 7.2 – Schematic reconstruction of progressive formation scale unconformities determined from outcrop observations (far right) and progressively rotated back to Honaker Trail and Paradox formations, horizontal pre-kinematic positions. Oil generation overlay derived from burial thermal history plots from Duchene (2009)

References

Amador, C.M., Schurger, S.G., and Miller, B.L., 2009, Andy's Mesa Unit, San Miguel County, Colorado: Rocky Mountain Association of Geologists Special Publication, p. 497–517.

Anderson, O. J., and Lucas, S. G., 1994, Middle Jurassic Stratigraphy, Sedimentation and Paleogeography in the Southern Colorado Plateau and Southern High Plains: p. 299–314.

Andrie, J. R., Giles, K. A., Lawton, T. F., and Rowan, M. G., 2012, Halokinetic-sequence stratigraphy, fluvial sedimentology and structural geometry of the Eocene Carroza Formation along La Popa salt weld, La Popa Basin, Mexico: Geological Society, London, Special Publications, v. 363, no. 1, p. 59–79.

Aschoff, J. L., and Giles, K. A., 2005, Salt diapir-influenced, shallow-marine sediment dispersal patterns: Insights from outcrop analogs: AAPG Bulletin, v. 89, no. 4, p. 447–469.

Ashley, G. M., J. B. Southard, J. B., and Boothroyd, J. C., 1982, Deposition of climbing-ripple beds: a flume simulation: Sedimentology, v. 29, no. 1, p. 67–79.

Baars, D. L., 1966, Pre-Pennsylvanian Paleotectonics - Key to Basin Evolution and Petroleum Occurrences in Paradox Basin, Utah and Colorado: AAPG Bulletin, v. 50, no. 10, p. 2082–2111.

Baars, D. L., Parker, J. W., and Chronic, J., 1967, Revised Stratigraphic Nomenclature of Pennsylvanian System, Paradox Basin: AAPG Bulletin, v. 51, no. 3, p. 393–403.

Baars, D.L., and Stevenson, G.M., 1981, Tectonic evolution of western Colorado and eastern Utah, in Western Slope (Western Colorado), New Mexico Geological Society Guidebooks, p. 105–112.

Barbeau, D. L., 2003, A flexural model for the Paradox Basin: implications for the tectonics of the Ancestral Rocky Mountains: Basin Research, v. 15, no. 1, p. 97–115.

Borer, J. M., and Harris, P. M., 1989, Depositional Facies and Cycles in Yates Formation Outcrops, Guadalupe Mountains, New Mexico. The Society of Economic Paleontologists and Mineralogists (SEPM), p. 314

Burley, S. D., and Worden, R. H., 2003, Sandstone diagenesis: recent and ancient: Malden, MA, Blackwell Pub, Reprint series volume 4 of the International Association of Sedimentologists, p. 649

Candelaria, M. P., 1989, Shallow Marine Sheet Sandstones, Upper Yates Formation, Northwest Shelf, Delaware Basin, New Mexico.The Society of Economic Paleontologists and Mineralogists (SEPM) p. 314

Cater, F. W., and Craig, L. C., 1970, Geology of the Salt Anticline region in southwestern Colorado, with a section on stratigraphy, Report 637: Professional Paper. Prepared on behalf of the U.S. Atomic Energy Commission: A study of the stratigraphy, structure, and geomorphology of an area characterized by large salt-cored anticlines, with a discussion of the growth of the salt cores. USGS Numbered Series, United States Government Printing Office, Washington, p. 80.

Choquette, P. W., and Pray, L. C., 1970, Geologic Nomenclature and Classification of Porosity in Sedimentary Carbonates: AAPG Bulletin, v. 54, no. 2, p. 207–250.

Condon, S. M., 1997, Geology of the Pennsylvanian and Permian Cutler Group and Permian Kaibab Limestone in the Paradox Basin, Southeastern Utah and Southwestern Colorado: U.S. Government Printing Office, p. 64.

Connolly, W. M., Lambert, L. L., and Stanton, R. J., 1989, Paleoecology of lower and Middle Pennsylvanian (Middle Carboniferous) Chaetetes in North America Palökologie von Chaetetes aus dem Unter- und Mittel-Pennsylvanian (Mittleres Karbon) von Nordamerika: Facies, v. 20, no. 1, p. 139–167, doi:10.1007/BF02536860.

Cross, W., 1907, Stratigraphic Results of a Reconnaissance in Western Colorado and Eastern Utah: The Journal of Geology, v. 15, no. 7, p. 634–679.

Cross, W., and Howe, E., 1905, Red beds of southwestern Colorado and their correlation: GSA Bulletin, v. 16, no. 1, p. 447–498, doi:10.1130/GSAB-16-447.

Crowell, J. C., 1978, Gondwanan glaciation, cyclothems, continental positioning, and climate change: American Journal of Science, v. 278, no. 10, p. 1345–1372, doi:10.2475/ajs.278.10.1345.

Davies, G. R., and L. B. S. Jr, 2006, Structurally controlled hydrothermal dolomite reservoir facies: An overview: AAPG Bulletin, v. 90, no. 11, p. 1641–1690, doi:10.1306/05220605164.

DeCelles, P. G., and Giles, K. A., 1996, Foreland basin systems: Basin Research, v. 8, no. 2, p. 105–123, doi:10.1046/j.1365-2117.199.6.01491.x

D Hartman, W., and Goreau, T., 1975, A Pacific tabulate sponge, living representative of a new order of sclerosponges, p 1-21.

Dickinson, W. R., and Lawton, T. F., 2003, Sequential intercontinental suturing as the ultimate control for Pennsylvanian Ancestral Rocky Mountains deformation: Geology, v. 31, no. 7, p. 609–612, doi:10.1130/0091-7613

Doelling, H. H., Utah Geological Survey, and Geological Survey (U.S.), 2002, Geologic map of the Fishers Towers 7.5’ quadrangle, Grand County, Utah: Salt Lake City, Utah, Utah Geological Survey.

Driese, S. G., and Dott, R. H., and Jr, 1984, Model for Sandstone-Carbonate: AAPG Bulletin, v. 68, no. 5, p. 574–597.

DuChene, H. R., Cole, S. L. III, and Greenberg, N., 2009, Geology of the Double Eagle Unit, Andy's Mesa Field, San Miguel County, Colorado: Rocky Mountain Association of Geologists, p. 519–533.

Elston, D. P., Shoemaker, E. M., and Landis, E. R., 1962, Uncompahgre Front and Salt Anticline Region of Paradox Basin, Colorado and Utah: AAPG Bulletin, v. 46, no. 10, p. 1857–1878.

Enos, P., 1983, Shelf Environment: Chapter 6: v. 43, p. 267–295. in Scholle, P. A., Bebout, D. G., and Moore, C. H., 1983, Carbonate Depositional Environments: AAPG Memoir 33: AAPG, p. 694.

Escosa, F. O., Rowan, M. G., Giles, K. A., Deatrick, K. T., Mast, A. M., Langford, R. P., Hearon T. E., and Roca, E., 2018, Lateral terminations of salt walls and megaflaps: An example from Gypsum Valley Diapir, Paradox Basin, Colorado, USA: Basin Research, v. 31, no. 1, p. 191–212, doi:10.1111/bre.12316.

Esteban, M., and Wilson, J. L., 1993, Introduction to Karst Systems and Paleokarst Reservoirs, Society for Sedimentary Geology (SEPM), p.9

Lawton, T. F., Vega, J., Giles, K. A., and Rosales-Domnguez, C., 2001, AAPG Memoir 75, Chapter 9: Stratigraphy and Origin of the La Popa Basin, Nuevo Len and Coahuila, Mexico: p. 219–240.

Flügel, E., 2010, New Perspectives in Microfacies, *in* Microfacies of Carbonate Rocks: Springer, Berlin, Heidelberg, p. 1–6.

Foster, A. M., 2015, Depositional facies and interpretation of salt-sediment interaction in the lower Triassic Moenkopi formation adjacent to the Castle Valley Salt Wall, Paradox Basin, Utah, M.S.: United States -- Texas, The University of Texas at El Paso, p. 105

Friedman, G. M., Ali, S. A., and Krinsley, D. H., 1976, Dissolution of Quartz Accompanying Carbonate Precipitation and Cementation in Reefs: Example from the Red Sea: Journal of Sedimentary Research, v. 46, no. 4, p. 4.

Gannaway, C. E., 2014, Depositional and sequence stratigraphic framework of an exposed Neoproterozoic suprasalt minibasin at Patawarta Diapir, Flinders Ranges, South Australia, M.S.: United States -- Texas, The University of Texas at El Paso, p. 153.

Ge, H., and Jackson, M. P. A., 1998, Physical Modeling of Structures Formed by Salt Withdrawal: Implications for Deformation Caused by Salt Dissolution: AAPG Bulletin, v. 82, no. 2, p. 228–250.

Ge, H., Jackson, M. P. A., and and B. C. Vendeville, 1997, Kinematics and Dynamics of Salt Tectonics Driven by Progradation: AAPG Bulletin, v. 81, no. 3, p. 398–423.

Gianniny, G. L. and Miskell-Gerdardt, Kimberlee J., 2009, Progradational to aggradational mixed siliciclastic/carbonate sequence sets on the tectonically active Eastern margin of the Pennsylvanian Paradox basin, Southwestern Colorado, in Houston, W., Wray, L., and Moreland, P., eds., The Paradox basin: New developments in petroleum systems and basin analysis, Rocky Mountain Association of Geologists, Denver, p. 310-379.

Giles, K. A., and Dickinson, W. R., 1995, The Interplay of Eustasy and Lithospheric Flexure in Forming Stratigraphic Sequences in Foreland Settings: An Example From the Antler Foreland, Nevada and Utah, Stratigraphic Evolution of Foreland Basins: SEPM Special Puhlicalion No 52, SEPM Society for Sedimentary Geology, p. 25.

Giles, K. A., and Lawton, T. F., 1999, Attributes and evolution of an exhumed salt weld, La Popa basin, northeastern Mexico: Geology, v. 27, no. 4, p. 323–326.

Giles, K. A., and Rowan, M. G., 2012, Concepts in halokinetic-sequence deformation and stratigraphy: Geological Society, London, Special Publications, v. 363, no. 1, p. 7–31.

Goldhammer, R. K., Oswald, E. J., and Dunn, P. A., 1994, High-Frequency, Glacio-Eustatic Cyclicity in the Middle Pennsylvanian of the Paradox Basin: An Evaluation of Milankovitch Forcing, *in* P. L. de Boer, and D. G. Smith, eds., Orbital Forcing and Cyclic Sequences: Blackwell Publishing Ltd., p. 243–283.

Gradstein, F., and Ogg, J., 2004, Geologic Time Scale 2004 - why, how, and where next! Lethaia, v. 37, no. 2, p. 175–181, doi:10.1080/00241160410006483.

Grammer, G. M., Eberli, G. P., Buchem, F. S. P. V., Stevenson, G. M., and Homewood, P., 1996, Application of High-Resolution Sequence Stratigraphy to Evaluate Lateral Variability in Outcrop and Subsurface—Desert Creek and Ismay Intervals, Paradox Basin: p. 235–266.

Hartman, W. D., and Goreau, T. F., 1975, A Pacific tabulate sponge, living representative of a new order of sclerosponges, Postilla, p. 167, p. 1–21.

Hearon, T. E., Rowan, M. G., Lawton, T. F., Hannah, P. T., and Giles, K. A., 2015, Geology and tectonics of Neoproterozoic salt diapirs and salt sheets in the eastern Willouran Ranges, South Australia: Basin Research, v. 27, no. 2, p. 183–207.

Heckel, P. H., 1986, Sea-level curve for Pennsylvanian eustatic marine transgressive-regressive depositional cycles along midcontinent outcrop belt, North America: Geology, v. 14, no. 4, p. 330–334.

Hite, R. J., and Buckner, D. H., 1981, Stratigraphic Correlations, Facies Concepts, and Cyclicity in Pennsylvanian Rocks of the Paradox Basin. Rocky Mountain Association of Geologists, 1981 Field Conference, p. 13

Hudec, M. R., Jackson, M. P. A., and Schultz-Ela, D. D., 2009, The paradox of minibasin subsidence into salt: Clues to the evolution of crustal basins: Geological Society of America Bulletin, v. 121, no. 1-2, p. 201–221.

Kjerfve, B., 1994, Chapter 1 Coastal Lagoons, *in* B. Kjerfve, ed., Elsevier Oceanography Series: Elsevier, Coastal Lagoon Processes, p. 1–8.

Kluth, C. F., 1986, Plate tectonics of the Ancestral Rocky Mountains: Part III. Middle Rocky Mountains, in J. A. Peterson, ed., Paleotectonics and sedimentation in the Rocky Mountain region, United States: American Association of Petroleum Geologists Memoir 41, p. 353–369.

Lawton, T. F., and Buck, B. J., 2006, Implications of diapir-derived detritus and gypsic paleosols in Lower Triassic strata near the Castle Valley salt wall, Paradox Basin, Utah: Geology, v. 34, no. 10, p. 885–888, doi:10.1130/G22574.1.

Loope, D. B., and Watkins, D. K., 1989, Pennsylvanian Fossils Replaced by Red Chert: Early Oxidation of Pyritic Precursors: Journal of Sedimentary Research, v. 59, no. 3, p. 12

Mack, G. H., and Rasmussen, K. A., 1984, Alluvial-fan sedimentation of the Cutler Formation (Permo-Pennsylvanian) near Gateway, Colorado: GSA Bulletin, v. 95, no. 1, p. 109–116.

Maliva, R. G., and Siever, R., 1988, Mechanism and Controls of Silicification of Fossils in Limestones: The Journal of Geology, v. 96, no. 4, p. 387–398.

Matheny, J. P., and Longman, M. W., 1996, Lower Desert Creek Reservoirs in the Paradox Basin: Examples of Phylloid Algae Filling Depositional Lows Related to Salt Dissolution: Paleozoic Systems of the Rocky Mountain Region, SEPM p. 267–282.

Miall, A. D., 2013, The Geology of Fluvial Deposits: Sedimentary Facies, Basin Analysis, and Petroleum Geology: Springer, p. 589.

Moore, C. H., 1989, Chapter 9 Burial Diagenetic Environment, *in* Developments in Sedimentology: Elsevier, Carbonate Diagenesis and Porosity, p. 237–284.

Nuccio, V. F., and Condon, S. M., 1996, Burial and Thermal History of the Paradox Basin, Utah and Colorado, and Petroleum Potential of the Middle Pennsylvanian Paradox Formation, Bulletin 2000-O: US.S. Geological Survey, 41 p.

Peterson, J. A., and Hite, R. J., 1969, Pennsylvanian Evaporite-Carbonate Cycles and Their Relation to Petroleum Occurrence, Southern Rocky Mountains: AAPG Bulletin, v. 53, no. 4, p. 884–908.

Poprawski, Y., Basile, C., Agirrezabala, L. M., Jaillard, E., Gaudin, M., and Jacquin, T., 2014, Sedimentary and structural record of the Albian growth of the Bakio salt diapir (the Basque Country, northern Spain): Basin Research, v. 26, no. 6, p. 746–766.

Pray, L. C., and Wray, J. L., 1963, Porous Algal Facies (Pennsylvanian) Honaker Trail, San Juan Canyon, Utah, in Bass, R. O., ed., Shelf Carbonates of the Paradox Basin, Fourth Field Conference: Farmington New Mexico, Four Corners Geological Society, p. 204–234.

Prochnow, S. J., Atchley, S. C., Boucher, E., Nordt, L. C., and Hudec, M. R., 2006, The influence of salt withdrawal subsidence on palaeosol maturity and cyclic fluvial deposition in the Upper Triassic Chinle Formation: Castle Valley, Utah: Sedimentology, v. 53, no. 6, p. 1319–1345.

Rasmussen, D. L., 2014, Namakiers in Triassic and Permian Formations in the Paradox Basin (USA) with comparisons to modern examples in the Zagros fold belt Iran: Geology of Utah's Far South: Utah Geological Association Publication, v. 43, p. 689–756.

Rasmussen, L., and Rasmussen, D. L., 2009, Burial History Analysis of the Pennsylvanian Petroleum System in the Deep Paradox Basin Fold and Fault Belt, Colorado and Utah: p. 24–94.

Reineck, H.-E., and Singh, I. B., 1980, Tidal Flats, *in* Depositional Sedimentary Environments: Springer, Berlin, Heidelberg, Springer Study Edition, p. 430–456.

Ribes, C., Kergaravat, C., Bonnel, C., Crumeyrolle, P., Callot, J.-P., Poisson, A., Temiz, H., and Ringenbach, J.-C., 2015, Fluvial sedimentation in a salt-controlled mini-basin: stratal patterns and facies assemblages, Sivas Basin, Turkey: Sedimentology, v. 62, no. 6, p. 1

Riding, R., 2000, Microbial carbonates: the geological record of calcified bacterial–algal mats and biofilms: Sedimentology, v. 47, p. 179–214.

Robeck, R. C., 1960, Wingate Through Summerville Formations in the Area of Salt Anticlines, Utah-Colorado: p. 107–108.

Rowan, M. G., Giles, K. A., Hearon T. E., and Fiduk, J. C., 2016, Megaflaps adjacent to salt diapirs: AAPG Bulletin, v. 100, no. 11, p. 1723–1747.

Rowan, M. G., Lawton, T. F. and Giles, K. A. 2012, Anatomy of an exposed vertical salt weld and flanking strata, La Popa Basin, Mexico: Geological Society, London, Special Publications, v. 363, no. 1, p. 33–57.

Scholle, P. A., Bebout, D. G., and Moore, C. H., 1983, Carbonate Depositional Environments: AAPG Memoir 33: AAPG, p. 694.

Schultz-Ela, D. D., Jackson, M. P. A., and Vendeville, B. C., 1993, Mechanics of active salt diapirism: Tectonophysics, v. 228, no. 3, p. 275–312.

Shinn, E. A., 1983, Birdseyes, Fenestrae, Shrinkage Pores, and Loferites: A Reevaluation: Journal of Sedimentary Research, v. 53, no. 2.

Shinn, E. A., 1968, Burrowing in Recent Lime Sediments of Florida and the Bahamas: Journal of Paleontology, v. 42, no. 4, p. 879–894.

Shoemaker, E. M., J. E. Case, and D. P. Elston, 1958, Salt Anticlines of the Paradox Basin, in Guidebook to the Geology of the Paradox basin, Intermountain Association of Petroleum Geologists Guidebook, 9th Ann. Field Conf.; 1956, p. 39-59.

Silver, B. A., and Todd, R. G., 1969, Permian Cyclic Strata, Northern Midland and Delaware Basins, West Texas and Southeastern New Mexico: AAPG Bulletin, v. 53, no. 11, p. 2223–2251.

Stokes, W. L., and Phoenix, D. A., 1948, Geology of the Egnar-Gypsum Valley area, San Miguel and Montrose Counties, Colorado, USGS Numbered Series 93: Oil and Gas Investigation Map.

Suchy, 2001, Chaetetid Buildups in a Westphalian (Desmoinesian) Cyclothem in Southeastern Kansas: Palaios, v. 16, no. 5, p. 425–443.

Trudgill, B. D., 2011, Evolution of salt structures in the northern Paradox Basin: controls on evaporite deposition, salt wall growth and supra-salt stratigraphic architecture: Basin Research, v. 23, no. 2, p. 208–238.

Tucker, M. E., and Bathurst, R. G. C., 2009, Carbonate Diagenesis: John Wiley & Sons, p. 323.

Tucker, M. E., and Wright, V. P., 1991, Carbonate Sedimentology: Wiley, p. 502

Turner, C. E., and Peterson, F., 2004, Reconstruction of the Upper Jurassic Morrison Formation extinct ecosystem—a synthesis: Sedimentary Geology, v. 167, no. 3, p. 309–355.

Vail, P. R., 1977, Seismic Stratigraphy and Global Changes of Sea Level: Part 3. Relative Changes of Sea Level from Coastal Onlap: Section 2. Application of Seismic Reflection Configuration to Stratigrapic Interpretation: v. 165, p. 63–81.

Vogel, J. D., 1960, Geology and ore deposits of the Klondike Ridge area, Colorado, USGS Numbered Series 60-145: U.S. Geological Survey, p. 206.

Warner, L. A., 1978, The Colorado Lineament: A middle Precambrian wrench fault system: GSA Bulletin, v. 89, no. 2, p. 161–171.

Weber, L. J., (Rick) Sarg, J. F., and, Wright, F. M., 1995, Sequence Stratigraphy and Reservoir Delineation of the Middle Pennsylvanian (Desmoinesian), Paradox Basin and Aneth Field, Southwestern USA, SEPM Special Publication, p. 82.

Wengerd, S. A., and Matheny, M. L., 1958, Pennsylvanian System of Four Corners Region: AAPG Bulletin, v. 42, no. 9, p. 2048–2106.

Wengerd, S. A., and Strickland, J. W., 1954, Pennsylvanian Stratigraphy of Paradox Salt Basin, Four Corners Region, Colorado and Utah: AAPG Bulletin, v. 38, no. 10, p. 2157–2199.

Werner, W. G., 1974, Petrology of the Cutler Formation (Pennsylvanian-Permian) Near Gateway, Colorado, and Fisher Towers, Utah: Journal of Sedimentary Research, v. 44, no. 2, p. 7.

West, R. R., 1988, Temporal Changes in Carboniferous Reef Mound Communities: Palaios, v. 3, no. 2, p. 152–169.

Vita

Kyle Thomas Deatrick was born and raised in DeWitt, Michigan. The younger of two children of Dennis and Julie Deatrick. Kyle graduated from DeWitt High School in 2006 and enrolled at Western Michigan University to pursue a Bachelor of Science in Geology. While completing his degree he worked as an undergraduate research assistant at the Michigan Geologic Repository for Research and Education (MGRRE) from 2009-2012. At MGRRE he assisted a team of M.Sc. students characterizing Ordovician carbonate reservoirs in the Michigan Basin under the direction of Dr. Michael Grammer. He enrolled at The University of Texas at El Paso in 2013 to complete a Master of Science degree in the Geological Sciences. As a M.Sc. student he received the competitive Geological Society of America-ExxonMobil research grant, tuition scholarships from Marathon Oil and ConocoPhillips, as well as the E. Russell Lloyd scholarship from the West Texas Geological Foundation and the Vernon G. & Joy Hunt Award from UTEP. He participated in the AAPG Imperial Barrel Award competition where he developed, with a team, prospect and play concepts for the Australian Eromanga Basin and competed in the Southwest Section in 2014. Kyle later went to South Australia to aid in field work focusing on Neo-Proterozoic salt tectonics. He went on to complete an internship with Chevron in Midland, Texas and developed and assessed horizontal drilling prospects in the Permian Basin.

Permanent Address: 1604 Waxwing Dr.
DeWitt, MI, 48820

This thesis was typed by Kyle Deatrick